

**BOND LENGTHS AND BOND VALENCES OF IONS BONDED TO OXYGEN:
THEIR VARIABILITY IN INORGANIC CRYSTALS**

by

Olivier Gagné

A Thesis submitted to the Faculty of Graduate Studies of

The University of Manitoba

in partial fulfilment of the requirements of the degree of

DOCTOR OF PHILOSOPHY

Department of Geological Sciences

University of Manitoba

Winnipeg

Copyright © 2016 by Olivier Gagné

ABSTRACT

A large amount of information concerning interatomic distances in the solid state is available, but little has been done in recent times to comprehensively filter, summarize and analyze this information. Here, I examine the distribution of bond lengths for 135 ions bonded to oxygen, using 180,331 bond lengths extracted from 9367 refined crystal structures collected from the Inorganic Crystal Structure Database (ICSD).

The data are used to evaluate the parameterization of the bond-length—bond-valence relation of the bond-valence model. Published bond-valence parameters for 135 cations bonded to oxygen, and the various methods used in their derivation, are evaluated. New equations to model the relation are tested and the common form of the equation is found to be satisfactory. A new method (the Generalized Reduced Gradient Method, GRG method) is used to derive new bond-valence parameters for 135 cations bonded to oxygen, leading to significant improvements in fit for many of the ions.

The improved parameterization is used to gain crystal-chemical insight into the milarite structure. A literature review of 350+ published compositions is done to review the end-members of the milarite group and to identify compositions that should have been described as distinct minerals species. The *a priori* bond-valences are calculated for minerals of this structure, and are used to examine the controls of bond topology on site occupancy, notably by localizing the major source of strain of the structure (the *B* site). Examination of the compositions of all known milarite-group minerals shows that compositions with a fully occupied *B* site are less common than those with a vacant *B* site, in accord with the idea that the *B* site is a local region of high strain in the structure.

The bond-length distributions for the ions of the alkali and alkaline-earth metal families are examined. Variations in mean bond-lengths are only partly explained by the distortion theorem of the bond-valence model. I have found that bond length also correlates with the amount of vibrational displacement of the constituent ions. The validity of some uncommon coordination numbers, *e.g.*, [3]-coordinated Li^+ , [3]-coordinated Be^{2+} , is confirmed.

ACKNOWLEDGEMENTS

First and foremost, I thank my thesis advisor Frank. C. Hawthorne for his help, support, encouragement and dedication over the course of my degree, and for providing me with an environment in which I was able to flourish. I thank members of my Ph.D. thesis committee, Elena Sokolova, Norman Halden, Scott Kroeker and Peter Budzelaar for their support, positivity, and helpful commentary, and the support staff of the department of Geological Sciences at the University of Manitoba.

I thank the Natural Sciences and Engineering Research Council (NSERC) for a PGS-D3 scholarship, the University of Manitoba's Faculty of Graduate Studies for a Duff Roblin and GETS Fellowships, the Mineralogical Association of Canada for awarding me with a MAC Foundation scholarship, the C.H.R. Faculty of Environment, Earth and Resources for an Entrance and Graduate Student Initiative Scholarships, and the Department of Geological Sciences for Rita Wadien scholarships.

I thank Patrick Mercier and Yvon Lepage of the National Research Council for providing help in shaping research themes early on in the project, and Éric Martineault and Yulia Uvarova whom I could always count on for advice and entertaining discussions.

Last but not least, I thank my family members, who were always present and supportive of my (often questionable) decisions. Merci Maman, Mathieu et Amélie. Finally, I thank my friends, especially the ones that tend to jump out of airplanes and things, whom I could always count on to clear my mind in time of need. Shout out to my 4-way skydiving team, team Alphagheti.

"This is for the kids who have nowhere to turn

Who have nothing to live for

You think you haven't the will to persist

You have to search within yourself"

-Jamey Jasta

TABLE OF CONTENTS

Abstract.....	ii
Acknowledgements.....	iv
Dedication.....	v
List of Tables.....	xvi
List of Figures.....	xix
Contributions of Authors.....	xxiv
List of Copyrighted Material for which Permission was Obtained.....	xxvii
Chapter 1. Introduction.....	1
1.1 General introduction.....	2
1.1.1 Concepts of crystal chemistry.....	3
1.1.1.1 The internal structure of crystals.....	4
1.1.1.2 Interatomic distances and ionic radii.....	8
1.1.1.3 The chemical bond and chemical bonding.....	9
1.1.2 Interatomic distances in the solid state.....	11
1.1.2.1 Bond lengths for cations bonded to O^{2-}	12
1.1.3 The types of chemical bonds.....	13

1.1.3.1 Ionic bonding.....	14
1.1.3.2 Covalent bonding.....	17
1.1.3.3 Metallic bonding.....	19
1.1.3.4 Van der Waals bonding.....	19
1.1.3.5 Hydrogen bonding.....	20
1.1.4 Theories of chemical bonding.....	20
1.1.4.1 Valence-bond theory.....	21
1.1.4.2 Molecular orbital (MO) theory.....	21
1.1.4.3 Bond-valence theory.....	22
1.1.4.3.1 Theoretical basis of bond-valence theory.....	23
1.1.4.3.2 The bond-valence model.....	27
1.2 Objectives and Significance of Research.....	29
1.3 Structure of the thesis.....	31
1.4 References.....	33
Chapter 2. Comprehensive derivation of bond-valence parameters for ion pairs involving oxygen.....	41
2.1 Synopsis.....	42
2.2 Abstract.....	42
2.3 Introduction.....	43

2.4 Experimental bond-lengths used in this work.....	45
2.5 Method of evaluation of bond-valence parameters.....	46
2.6 Evaluation of published oxide bond-valence parameters.....	47
2.7 The hydrogen atom.....	49
2.8 Use of bond-valence parameters for hydrogen-oxygen bonds.....	50
2.9 Comments on fixing the B parameter.....	51
2.10 Comments on the level of fit.....	52
2.11 Parameterization.....	53
2.11.1 Methods of derivation of the bond-valence parameters.....	53
2.11.1.1 Least-squares fitting.....	53
2.11.1.2 Fixing the B parameter.....	54
2.11.1.3 Graphical method: cation and anion sums.....	55
2.11.1.2 Graphical method: cation sums.....	56
2.11.1.5 RMSD minimization.....	58
2.11.2 Generalized Reduced Gradient (GRG) method of RMSD minimization.....	59
2.11.2.1 The Generalized Reduced Gradient method.....	60
2.11.2.2 Weighting scheme.....	63
2.11.3 Comparison of the most common methods of derivation.....	63

2.12 Anion-sum verification.....	99
2.13 Improvement in fit: Cations.....	104
2.14 Deviations from the valence-sum rule.....	105
2.15 Summary.....	106
2.16 Acknowledgements.....	107
2.17 References.....	108
2.18 Appendix A: Supplementary material.....	116
Chapter 3. Chemographic Exploration of the Milarite-Type Structure.....	142
3.1 Preliminary discussion.....	143
3.1.1 <i>A priori</i> bond-valence calculations.....	143
3.1.2 Structural strain.....	145
3.1.3 References.....	146
3.2 Abstract.....	148
3.3 Introduction.....	149
3.4 Description of the milarite structure-type.....	152
3.4.1 The <i>T</i> (1) tetrahedron.....	152
3.4.2 The <i>T</i> (2) tetrahedron	153
3.4.3 The <i>A</i> octahedron.....	153

3.4.4 The <i>B</i> polyhedron.....	154
3.4.5 The <i>C</i> polyhedron.....	154
3.4.6 The <i>D</i> site.....	155
3.5 End-members and their significance.....	159
3.5.1 Root charge arrangements.....	160
3.5.2 Root charge arrangements in the milarite structure-type.....	161
3.6 Chemical compositions of milarite-group minerals.....	167
3.6.1 H ₂ O content.....	171
3.6.2 Potential new mineral species.....	174
3.7 Synthetic compounds with the milarite-type structure.....	180
3.8 The relative stability of root charge arrangements with the milarite structure.....	180
3.8.1 <i>A priori</i> bond-valence calculations.....	184
3.8.2 Calculation of <i>a priori</i> bond-valences.....	184
3.8.3 <i>A priori</i> bond-valences of the milarite structure.....	185
3.8.4 Solution of the <i>a priori</i> bond-valence equations.....	189
3.9 Induced strain in the milarite group.....	195
3.9.1 The <i>B</i> site in the milarite structure.....	196
3.9.2 Compositional implications for milarite-group minerals.....	200

3.10 Summary.....	201
3.11 Acknowledgements.....	202
3.12 References.....	203
3.13 Appendix A: Supplementary material.....	214
Chapter 4. Bond-length distributions for ions bonded to oxygen: Alkali and alkaline-earth metals.....	229
4.1 Preliminary discussion.....	230
4.1.1 Molecular-orbital approaches.....	230
4.1.2 Crystal-chemical approaches.....	231
4.1.3 References.....	233
4.2 Synopsis.....	236
4.3 Abstract.....	236
4.4 Introduction.....	237
4.5 Definitions.....	239
4.6 Coordination polyhedra.....	242
4.6.1 Coordination polyhedra with the same coordination number.....	242
4.6.2 The longest bond.....	242
4.6.3 Large coordination numbers.....	245
4.7 Methods.....	245

4.7.1 Selection criteria.....	246
4.7.2 Determination of coordination polyhedra.....	246
4.8 Shape of the bond-length distributions.....	249
4.9 Effect of sampling.....	250
4.9.1 Sample size.....	250
4.9.2 The effect of outliers.....	253
4.9.3 Non-random sampling.....	253
4.10. Results for the alkali metals.....	256
4.10.1 Observed coordination numbers.....	265
4.10.1.1 Li^+	265
4.10.1.2 Na^+	266
4.10.1.3 K^+	267
4.10.1.4 Rb^+	267
4.10.1.5 Cs^+	268
4.10.2 Grand mean bond-length as a function of coordination number.....	269
4.10.3 Range in bond length as a function of coordination number.....	269
4.10.4 Skewness and kurtosis as a function of coordination number.....	269
4.11 Results for the alkaline-earth metals.....	272

4.11.1 Observed coordination numbers.....	278
4.11.1.1 Be ²⁺	278
4.11.1.2 Mg ²⁺	278
4.11.1.3 Ca ²⁺	279
4.11.1.4 Sr ²⁺	280
4.11.1.5 Ba ²⁺	280
4.11.2 Grand mean bond-length as a function of coordination number.....	281
4.11.3 Range in bond length as a function of coordination number.....	281
4.11.4 Skewness and kurtosis as a function of coordination number.....	282
4.12 General discussion of bond-length distributions.....	284
4.12.1 Skewness.....	284
4.12.2 Kurtosis.....	284
4.12.3 Multi-modal distributions.....	287
4.12.4 Bond valences.....	291
4.12.5 Ions with coordination numbers possibly exceeding [12].....	292
4.13 Mean bond-length distributions.....	296
4.13.1 The effect of distortion.....	304
4.13.1.1 The distortion theorem.....	304

4.13.1.2 Grand mean bond-length.....	311
4.13.1.3 Mean bond-length as a function of distortion.....	312
4.13.2 Atomic displacement.....	317
4.13.3 The relation between mean bond-length and atomic displacement.....	318
4.14 Summary.....	320
4.15 Acknowledgements.....	322
4.16 References.....	322
4.17 Appendix A: Supplementary material.....	328
Chapter 5. Conclusion.....	350
5.1 Summary and significance of thesis.....	351
5.2 Future research opportunities.....	358
5.2.1 Bond-length dispersion analysis for all ion pairs.....	358
5.2.2. Reassessment of ionic radii.....	359
5.2.3 Enumeration of all possible end-member compositions of a crystal structure and materials discovery.....	360
5.2.4 Toward a better understanding of crystal-structure stability.....	361
5.3 References.....	362

LIST OF TABLES

Table 2.1 Comparison between the RMSD values of the set of best published bond-valence parameters and the values obtained for bond-valence parameters derived using common methods of derivation for the 90 multiple-coordination-number ions.....	65
Table 2.2 RMSD values for a sample of ions for 19 different two-parameter equations fitted with the GRG method.....	80
Table 2.3 RMSD values for a sample of ions for 7 different three-parameter equations fitted with the GRG method.....	84
Table 2.4 New bond-valence parameters derived with the GRG method.....	87
Table 2.5 Overall RMSD for the anion bond-valence sums of 4 large sets of bond-valence parameters.....	101
Table 2.S1 Evaluation of published bond-valence parameters.....	116
Table 2.S2 ICSD code for the structures used in the derivation of the bond-length to bond-valence equations.....	127
Table 2.S3 RMSD values for six two-parameter equations for the 90 multiple-coordination-number ions.....	130
Table 2.S4 ICSD code for the structures used in the anion bond-valence sum verification.....	135
Table 3.1 Sites and site occupancies in the milarite-group minerals.....	150

Table 3.2 Current minerals of the milarite group end-member compositions, site occupancies and root charge arrangements.....	151
Table 3.3 Selected interatomic distances in sugilite.....	156
Table 3.4 Root charge arrangements for the milarite structure-type with Si = 12 <i>apfu</i>	163
Table 3.5 Root charge arrangements for the milarite structure-type with Si \neq 12 <i>apfu</i>	165
Table 3.6 New end-member compositions corresponding to observed chemical compositions of milarite-group minerals.....	168
Table 3.7 Chemical formulae consistent with new dominant end-member compositions.....	169
Table 3.8 Compositions which may lead to new end-member compositions in the milarite-group minerals.....	175
Table 3.9 Chemical formulae corresponding to the “end members” of Table 3.8.....	176
Table 3.10 Synthetic milarite-like compositions and corresponding end-members for which crystal-structure refinements are available.....	178
Table 3.11 Synthetic compositions for which there are no crystal-structure refinements.....	179
Table 3.12 Numbers of minerals and compounds for specific root charge arrangements.....	182

Table 3.13 General bond-valence table for the milarite structure.....	187
Table 3.14 <i>A priori</i> and observed bond-valences for sugilite	
$A(\text{Mn}^{3+}_{0.11}\text{Fe}^{3+}_{0.71}\text{Al}_{1.16}\text{Na}_{0.02})^B\text{Na}_{1.81}\text{K}_{1.00}^{\tau(2)}\text{Li}_{3.02}^{\tau(1)}\text{Si}_{12.06}\text{O}_{30}$	191
Table 3.15 <i>A priori</i> and observed bond-valences for sogdianite	
$A(\text{Zr}_{1.98}\text{Hf}_{0.02})^C(\text{K}_{0.99}\text{Na}_{0.01})^{\tau(2)}\text{Li}_{2.97}^{\tau(1)}\text{Si}_{12.01}\text{O}_{30}$	192
Table 3.16 Absolute difference between <i>a priori</i> bond-valence and experimental bond-valences by bond.....	193
Table 3.17 Global instability index and bond strain index.....	194
Table 3.S1 Publications describing milarite-group minerals and synthetic milarite-group compounds used in the review.....	215
Table 4.1 Bond-length statistics for the 5 common alkali-metal ions.....	257
Table 4.2 Bond-length statistics for the 5 common alkaline-earth-metal ions.....	273
Table 4.3 Bond-valence parameters for large alkali and alkaline-earth metals calculated with and without a hard cut-off of 12 bonds.....	294
Table 4.4 Mean-bond-length statistics for the 5 common alkali-metal ions.....	297
Table 4.5 Mean-bond-length statistics for the 5 common alkaline-earth-metal ions....	300

LIST OF FIGURES

Figure 1.1 Layer arrangement in hexagonal close packing (HCP) of spheres.....	6
Figure 1.2 Layer arrangement in cubic close packing (CCP) of spheres.....	7
Figure 1.3 Potential energy diagram of the chemical bond.....	15
Figure 1.4 Electron-density map for a slice of the NaCl structure.....	16
Figure 2.1 RMSD from the valence-sum rule as a function of the bond-valence parameters for Fe^{3+}	62
Figure 2.2 Determination of the curvature of the bond-valence relation by a match of the <i>a priori</i> bond-valences to their observed bond-lengths.....	78
Figure 2.3 Bond-valence parameter R_0 as a function of mean bond-length for the 90 multiple-coordination-number ions.....	94
Figure 2.4 Relation between bond-valence parameter R_0 and (a) oxidation state, (b) ionization energy, and (c) Pauling electronegativity.....	96
Figure 2.5 Anion bond-valence sums for the parameters of Brown & Altermatt (1985) and the parameters given here.....	103
Figure 3.1 The crystal structure of milarite projected down the c axis.....	157
Figure 3.2 The crystal structure of milarite projected orthogonal to the c axis.....	158
Figure 3.3 A histogram of the H_2O content in milarite-group minerals taken from the literature.....	172

Figure 3.4 Possible compositional variation in roedderite-“Mg-merrihueite” structures.....	173
Figure 3.5 Total charge (<i>pfu</i>) at the <i>A</i> site as a function of total charge at the <i>T</i> (2) site in milarite-type structures.....	183
Figure 3.6 A fragment of the milarite structure viewed perpendicular to c , showing a loop in the topology of the structure.....	188
Figure 3.7 Comparison of experimental and <i>a priori</i> bond-valences for thirteen well-refined milarite-group minerals for which reliable chemical analyses are available.....	198
Figure 3.8 The coordination around the <i>B</i> site in sugilite.....	199
Figure 4.1 A typical distribution of bond lengths, shown for ^[6] Na ⁺ bonded to O ²⁻	241
Figure 4.2 Ratio of the gap between the (a) third- and fourth-, (b) eighth- and ninth-, (c) thirteenth and fourteenth-shortest bonded and non-bonded distances for different coordination numbers.....	244
Figure 4.3 The effect of sample size on (a) mean bond-length (b) standard deviation of the mean bond-length, (c) skewness, and (d) kurtosis.....	252
Figure 4.4 Bond-length distribution for ^[6] Cr ³⁺ bonded to O ²⁻ showing a spike of data due to extensive work done on the spinel structure.....	255
Figure 4.5 Bond-length distributions for the configurations of the alkali-metal ions bonded to O ²⁻ with a sample size of 100+ bonds.....	261
Figure 4.6 Observed coordination numbers for the alkali-metal ions.....	264

Figure 4.7 Values of (a) grand mean bond-length, (b) bond-length range, (c) skewness, and (d) kurtosis for the different coordination numbers of the alkali-metal ions.....	271
Figure 4.8 Bond-length distributions for the configurations of the alkaline-earth-metal ions bonded to O^{2-} with a sample size of 100+ bonds.....	275
Figure 4.9 Observed coordination numbers for the alkaline-earth-metal ions.....	277
Figure 4.10 Values of (a) grand mean bond-length, (b) bond-length range, (c) skewness, and (d) kurtosis for the different coordination numbers of the alkaline-earth-metal ions.....	283
Figure 4.11 Kernel-density estimation of the bond-length distributions of the coordination numbers [6] to [9] for Na^+	286
Figure 4.12 Mean bond length distribution of $^{[8]}Ca^{2+}$ bonded to O^{2-} (a). Bond-length distribution for $^{[8]}Ca^{2+}$ bonded to O^{2-} for configurations with a mean bond length (b) less or equal to 2.44 Å and (c) greater than 2.44 Å and their combined distribution (d).....	289
Figure 4.13 Bond-valence sum as a function of coordination number for the (a) alkali-metal and (b) alkaline-earth-metal ions.....	290
Figure 4.14 Mean bond-length distributions for the configurations of the alkali-metal ions bonded to O^{2-} with a sample size of 100+ coordination polyhedra.....	302
Figure 4.15 Mean bond-length distributions for the configurations of the alkaline-earth-metal ions bonded to O^{2-} with a sample size of 100+ coordination polyhedra.....	303
Figure 4.16 Bond-valence bond-length curve for Na^+ showing how the exponential shape leads to the distortion theorem of the bond-valence model.....	307

Figure 4.17 Bond-valence curve for the Na isoelectronic series, and ideal mean bond-valence and associated mean bond-length for the most common coordination number of each ion of the series.....	308
Figure 4.18 Variation in the observed bond-length ranges for the different coordination numbers of (a) Na ⁺ , (b) K ⁺ , (c) Rb ⁺ and (d) Cs ⁺ bonded to O ²⁻ as a function of the slope of the bond-valence curve at the mean bond-length corresponding to those coordinations.....	309
Figure 4.19 Observed vs predicted values of the grand mean bond-length for all observed ion configurations of the alkali-metal and alkaline-earth metal ions.....	310
Figure 4.20 The effect of bond-length distortion on mean bond-length for (a) [6]Na ⁺ , (b) [10]K ⁺ and (c) [8]Ca ²⁺	315
Figure 4.21 The effect of atomic displacement on mean bond-length.....	316
Figure 4.S1 Bond-length distributions for all configurations of the alkali-metal ions bonded to O ²⁻	328
Figure 4.S2 Bond-length distributions for all configurations of the alkaline-earth-metal ions bonded to O ²⁻	333
Figure 4.S3 Mean bond-length distributions for all configurations of the alkali-metal ions bonded to O ²⁻	336
Figure 4.S4 Mean bond-length distributions for all configurations of the alkaline-earth-metal ions bonded to O ²⁻	340

Figure 4.S5 The effect of bond-length distortion on mean bond-length for all configurations of the alkaline-earth-metal ions bonded to O^{2-} 343

Figure 4.S6 The effect of bond-length distortion on mean bond-length for all configurations of the alkaline-earth-metal ions bonded to O^{2-} 347

CONTRIBUTIONS OF AUTHORS

Chapter 2. Comprehensive derivation of bond-valence parameters for ion pairs involving oxygen

This chapter is an article published in *Acta Crystallographica Section B* in co-authorship with my thesis advisor. This chapter is based on work done for my thesis research. I was responsible for the research done, including the evaluation of published parameterizations to model the bond-length to bond-valence relation, the derivation of an improved parameterization, for drafting all figures and tables, and for writing the majority of the text. My co-author drafted parts of the text and helped in reviewing the manuscript. This article is reproduced with permission from my co-author and from The International Union of Crystallography (IUCr).

Gagné, O.C. & Hawthorne, F.C. (2015). Comprehensive derivation of bond-valence parameters for ion pairs involving oxygen. *Acta Crystallographica*, **B71**, 562-578

Chapter 3. Chemographic Exploration of the Milarite-Type Structure

This chapter is an article accepted for publication in the *Canadian Mineralogist* in co-authorship with my thesis advisor. This chapter is based on work done for my thesis research. I was responsible for the research done, including the literature review of all published milarite-type compositions, the determination of published compositions that

could have been described as new minerals, the calculation of the *a priori* bond-valences of the structure, and the determination of the relation between *B*-site occupancy and stability. I was also responsible for drafting most of the figures and tables, and for writing the majority of the text. My co-author enumerated all possible charge arrangements for this structure, drafted parts of the text and some figures, and helped in reviewing the manuscript. This article is reproduced with permission from my co-author and from the Mineralogical Association of Canada (MAC).

Gagné, O.C. & Hawthorne, F.C. (2016). Chemographic Exploration of the Milarite-Type Structure. *Canadian Mineralogist* (*accepted*)

Chapter 4. Bond-length distributions for ions bonded to oxygen: Alkali and alkaline-earth metals

This chapter is an article published in *Acta Crystallographica Section B* in co-authorship with my thesis advisor. This chapter is based on work done for my thesis research. I was responsible for the research done, including the bond-length dispersion analysis of the Inorganic Crystal Structure Database for all ions bonded to oxygen, the effects of sample size and non-random sampling, the interpretation of skewness and kurtosis values, determination of the factors that affect mean bond-length, the idea of coordination numbers greater than [12] in oxides, and for drafting all figures and tables as well as the majority of the text. My co-author verified structures for which the ions were observed in unusual coordination numbers, drafted parts of the text and helped in

reviewing the manuscript. This article is reproduced with permission from my co-author and from The International Union of Crystallography (IUCr).

Gagné, O.C. & Hawthorne, F.C. (2016). Bond-length distributions for ions bonded to oxygen: Alkali and alkaline-earth metals. *Acta Crystallographica*, **B72**, 602-625

LIST OF COPYRIGHTED MATERIAL FOR WHICH PERMISSION WAS OBTAINED

Figure 1.1, 1.2 Brittanie Harbick, Laura Suh, Jenny Fong,

http://chemwiki.ucdavis.edu/Core/Physical_Chemistry/Physical_Properties_of_Matter/States_of_Matter/Solids/Crystal_Lattice/Closest_Pack_Structures).....6, 7

Figure 1.4 Joshua Halpern, Scott Sinex and Scott Johnson,

http://chemwiki.ucdavis.edu/Textbook_Maps/General_Chemistry_Textbook_Maps/Map%3A_Chemistry%3A_The_Central_Science_%28Brown_et_al.%29/07._Periodic_Properties_of_the_Elements/7.3%3A_Sizes_of_Atoms_and_Ions).....16

Chapter 2 Gagné & Hawthorne, 2015.....41

Chapter 3 Gagné & Hawthorne, 2016a.....142

Chapter 4 Gagné & Hawthorne, 2016b.....229

Chapter 1

Introduction

1.1 General introduction

One hundred years have passed since the first crystal-structure solutions (Bragg, 1913; Bragg and Bragg, 1913), and since then we have amassed an enormous amount of information concerning crystal structures and their atomic arrangements. Yet, our understanding of the factors that control the stability of these crystal structures is still limited, as if more focus has been put toward the collection of new data than on understanding these data. This problem was epitomized by Maddox in an editorial in the journal *Nature* where he identified the general failure to make reliable crystal-structure predictions from chemical composition as a “scandal” in Crystallography (Maddox, 1988; DiSalvo, 1990; Hawthorne, 1990; Pannetier et al, 1990; Woodley & Catlow 2008; Oganov et al 2010). Today, attempts at crystal-structure prediction often combine combinatorial analysis and computational simulation with the second law of thermodynamics, the principle of minimum energy, to obtain and classify possible atomic arrangements on energy grounds (Parker et al, 1984; Pannetier et al, 1990; Lufaso & Woodward, 2001; Karamertzanis & Pantelides, 2005; Oganov & Glass 2006; Podeszwa et al, 2008; Woodley and Catlow 2008; Wang et al, 2010; Wang *et al.* 2012). Despite the variety of these computational techniques, they have had limited success and applicability, and the lack of understanding of the factors affecting crystal stability is not addressed, which is made evident by simulations that are stochastic in nature.

What factors affect the connectivity of the atoms of a structure, the symmetry of the structure, polymorphism, order/disorder, etc.? Pauling (1929) pointed out that TiO_2 has the atomic arrangements of rutile, brookite and anatase under different conditions, but more importantly, he asked “why is this the case?”. While the answer to this question is

obvious, *because it leads to the structure of minimum free energy*, this is largely unsatisfying because this provides no mechanism as to *why* that is. Pauling (1929) emphasized that we should be looking at observables (e.g., bond lengths) to try and get a mechanistic sense of what controls structure stability. The idea was pursued by Dent-Glasser (1979) who looked at silicates and asked “why do some compounds exist, whereas others do not?”. These are important questions that remain unsolved today. While it would be an understatement to say these questions are hard to answer, it is apparent that answers to these questions will come from crystal-chemical argument rather than “black-box” methods.

In this thesis, I will systematize and attempt to understand what affects the variation of bond lengths in oxide and oxysalt crystals based on crystal-chemical arguments and using the results of a large-scale bond-length dispersion analysis of the Inorganic Crystal Structure Database (ICSD).

1.1.1 Concepts of crystal chemistry

Crystal chemistry is concerned with the relation between the atomic arrangement of a crystal and its corresponding physical and chemical properties, and is at the intersection of the fields of Mineralogy, Solid-State Chemistry, Solid-State Physics, and Materials Science (Vainshtein *et al.*, 2000). Crystal chemistry was developed shortly after the first crystal-structure solutions by Bragg (1913) and Bragg and Bragg (1913), and the subsequent interpretation of these results by the same authors and others (e.g., Goldschmidt, 1926a, 1927; Pauling, 1929). They developed an understanding of crystal

structures based on interatomic distance and the idea of coordination number. Below, I discuss various concepts of crystal chemistry that are relevant to this thesis and to a basic understanding of atomic arrangements in crystals.

1.1.1.1 The internal structure of crystals

Crystals are regular arrangements of atoms that repeat in three dimensions (Vainshtein *et al.*, 2000). The unit that is repeated solely by the translational symmetry of the crystal is called the *unit cell*. The internal structure of a crystal is concerned with two types of symmetry, the point symmetry and the translational symmetry, by the application of which the full crystal is obtained from the unit cell. Point symmetry describes the invariance of a structural feature around a point, while translational symmetry describes the periodic repetition of that structural feature through space. Crystals are characterized by long-range order, or *periodicity*, in contrast to amorphous materials such as glasses and gels.

Many crystals (*e.g.*, elements, alloys, oxide and oxysalt structures) can be described as close-packed arrangements of spheres. In oxide and oxysalt structures, the spheres commonly represent anions, which are commonly larger than cations, and the cations occupy interstices within the close-packed arrangement of anions. There are two basic types of close packing: *hexagonal* and *cubic* close-packing. The type of close packing is defined by the stacking of adjacent layers, with regard to the voids between these layers. When sequentially stacking three layers of spheres (A, B, and C), layer C may either be placed directly above layer A (separated by layer B), or it can be placed in

voids that are not directly above A. This leads to the possible stacking sequences ABAB (hexagonal), and ABCABC (cubic). This is shown in Figs. 1.1 and 1.2. Note that the packing coefficient is the same for each arrangement (74.05% fill of space). Close packing plays a major role in affecting the coordination numbers of cations in oxide (and halogen) structures.

Figure 1.1 Layer arrangement in hexagonal close packing (HCP) of spheres
(chemwiki.ucdavis.edu/Closest Pack Structures CC BY-NC-SA 3.0 US)

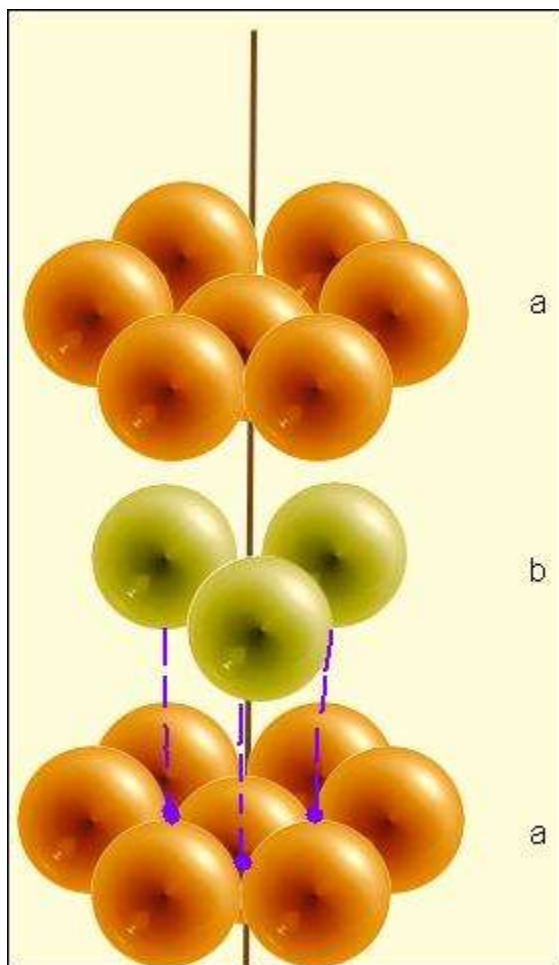
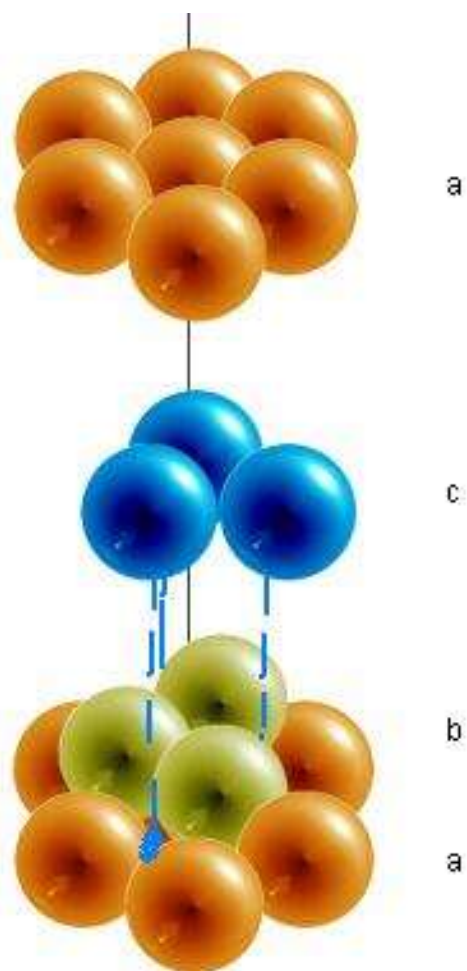


Figure 1.2 Layer arrangement in cubic close packing (CCP) of spheres
(chemwiki.ucdavis.edu/Closest Pack Structures CC BY-NC-SA 3.0 US)



1.1.1.2 Interatomic distances and ionic radii

A crystal consists of a collection of atoms, some of which are in direct contact with each other. From this results the very important concept of *interatomic distance*, from which follows the concept of *ionic radius*. Interatomic distances are a key component to this thesis, and are discussed at greater length below (section 1.1.2).

The derivation of interatomic distances naturally leads to the idea of the sizes of ions.

The sizes of ions were first determined by Landé (1920) by considering simple structures with large differences in size between the cations and anions, such as LiI. In LiI, the Li^+ ions are so small in relation to the I^- ions that I^- ions can be approximated to be in contact in the close-packed structure, allowing the determination of its radius (*i.e.*, half the I-I interatomic distance). Once the radius of I^- had been determined by Landé, the determination of other ionic radii followed by subtracting the radius of I^- from the interatomic distance of cations bonded to I^- . Wasastjerna (1923) used the relative volume of ions, derived from their electrical polarizability, to derive the radius of certain ions and to correct Landé's value for the radius of I^- from 2.14 to 2.19 Å. This work was soon expanded by Goldschmidt (1926b). Pauling (1927) used an atomic model derived from the wave mechanics of Schrödinger to develop a set of ionic radii based on quantum mechanics, and found that his model gave an ionic radius of 2.16 Å for I^- . Pauling (1960) later used the effective nuclear charge to better determine the proportion of anion/cation sizes. A major review of crystallographic data in the solid state was done by Shannon & Prewitt (1969) which led to the derivation of an empirical set of *effective* ionic radii (*i.e.*, using the value of 1.40 Å given by Pauling for the radius of O^{2-}) using a technique similar to that of Goldschmidt (1926b). This was subsequently revised and

expanded by Shannon (1976) to include more unusual oxidation states and coordinations based on new structural data. Shannon gives the ionic radii of atoms on the basis of oxidation state, coordination number, electronic coordination and spin state. The concept of a fixed ionic radius is sometimes criticized (e.g., Gibbs *et al.*, 2013), whereby ions are argued to (1) vary in size according to their environment, and (2) have a non-spherical electron density distribution. Shortcomings of the concept of ionic radius can be summarized by a quote from Pauling's seminal work on the nature of the chemical bond (1960), where he states: "*Since the electron distribution function for an ion extends indefinitely, it is evident that no single characteristic size can be assigned to it. Instead, the apparent ionic radius will depend upon the property under discussion and will differ for different properties*". Despite this, the concept of ionic radius has proven extremely useful (Shannon 1976 currently has ~35,000 citations) and simple radii remain a concept central to Crystallography and the Solid-State Sciences.

1.1.1.3 The chemical bond and chemical bonding

While atoms in crystal structures can sometimes be represented as close-packing of spheres (Smart and Moore, 2005), atoms are not to be interpreted as inert bodies that obey the laws of classical physics. Atoms commonly react with one another to form *ions*, with a charge defined by the number of electrons lost (*i.e.*, a cation) or gained (*i.e.*, an anion). The charge of the ion is its *oxidation state*. Atoms may be observed in a single oxidation state (e.g., +1 for the alkali metals) or as a series of oxidation states (e.g., most transition metals); this depends on the *ionization energy* of each charge-

state, where the ionization energy is defined as the amount of energy required for the removal of the outermost (most loosely bound) electron of the atom (or ion).

The concept of losing, gaining, or even *sharing* electrons between atoms leads to the notions of *chemical bonding* and of the *chemical bond*. There are numerous ways in which the formation of a chemical bond may be described. Certain models draw from classical mechanics, others from quantum mechanics, and together they cover a wide spectrum in terms of complexity and applicability. Despite the number of ways in which chemical bonding between atoms may be rationalized, the *chemical bond* itself eludes rigorous definition (Cortés-Guzmán & Bader, 2005), and the interpretation of what is a chemical bond is dependent on the method used in explaining its formation. The concepts of the chemical bond and of chemical bonding are discussed at greater length below (sections 1.1.3 and 1.1.4, respectively).

Another important concept of crystal chemistry is that of *coordination number*. The coordination number of an atom (or ion) was initially defined by Werner (1893) in the study of coordination compounds as *the total number of ligands bound to the metal ion*. Today, the terminology has evolved to be more inclusive (descriptive of any atom in a chemical species) and coordination number is defined as the number of atoms that are directly linked to a specific atom (*i.e.*, the number of atoms with which an atom partakes in chemical bonding). However, the problem with defining coordination number is that it relies heavily upon the definition and recognition of a chemical bond, which as discussed above, lacks rigorous definition. While the determination of which atoms are bonded to which in molecules can be straightforward, it is much less so in crystals, where the interaction between ions can be weaker and more numerous. However, it is

fortunate that in many crystal structures, there is a general consensus as to the coordination numbers observed. Thus rutile has Ti^{4+} in [6]-coordination and O^{2-} in [3]-coordination, and quartz has Si^{4+} in [4]-coordination and O^{2-} in [2]-coordination. The determination of the coordination polyhedron is usually straightforward for cations making a small number of bonds to their counterions, and this information may be used to extrapolate trends to higher coordination numbers. The issue of the determination of the coordination number will be discussed at greater length in Chapter 4.

1.1.2 Interatomic distances in the solid state

Following the discovery of X-rays by Röntgen (1895) and the successful experiment of Friedrich and Knipping of diffracting X-rays using crystals (as proposed by Max Laue; 1912), X-rays were confirmed to be electromagnetic waves, with a wavelength estimated to be of the order of magnitude of the size of atoms ($\sim 10^{-10}$ m). The experiment quickly led to a new branch of research that consisted of the application of X-ray diffraction to crystallography, and to the pioneering work of William H. Bragg and William L. Bragg who used X-rays to solve the structure of crystals (1913). Since then, we have amassed an enormous amount of information concerning crystal structures and their atomic arrangements, and the distance that separate atoms in crystal structures. Yet, little has been done in recent times to summarize and comprehensively analyze these data, and the efforts expended on understanding these data are far less than those expended on their collection. Only a handful of ion configurations have been systematically examined, and these generally involve highly-charged cations bonded to O^{2-} in low coordination numbers (e.g., $[\text{Si}^{4+}\text{-O}]$, Baur, 1971; $[\text{P}^{5+}\text{-O}]$, Baur, 1974,

Huminicki & Hawthorne, 2002; $^{[4]}\text{S}^{6+}\text{-O}$, Hawthorne *et al.*, 2000). There are several hundred ion configurations that have not yet been examined (for cations bonded to O^{2-} alone), and those that have been examined have used much smaller data sets than are now available, and can now be further examined. In an attempt to address this problem, I have done a bond-length dispersion analysis of cations bonded to oxygen that has resulted in the collection of 180,331 bond lengths from 31,514 coordination polyhedra for 135 ions bonded to oxygen in 462 ion configurations, using 9367 refined crystal structures. I will discuss some of these results in Chapters 2 and 4 of my thesis. First, I look at some of the work that has been done with regard to the analysis of bond lengths for cations bonded to O^{2-} .

1.1.2.1 Bond lengths for cations bonded to O^{2-}

Baur (1971) used 148 tetrahedra from 26 crystal structures to study bond-length variations of the silicate group ($^{[4]}\text{Si}^{4+}\text{-O}$) and to derive an expression to predict Si-O bond distances. Baur (1974) later focused on polyhedral distortion in the study of the phosphate group configuration ($^{[4]}\text{P}^{5+}\text{-O}$) by looking at 211 phosphate tetrahedra. Baur focused on the shape of the tetrahedra, and analyzed individual and mean P-O distances, O-P-O angles and O-O distances in phosphate groups. Although Baur (1971,1974) lists the data he used, he does not explicitly plot the bond-length distributions for his data.

Following the work of Baur, a series of papers describing the crystal chemistry of other important ion configurations were written for the book series *Review in Mineralogy and*

Geochemistry. These include $^{[3]}\text{B}^{3+}\text{-O}$ and $^{[4]}\text{B}^{3+}\text{-O}$ (Hawthorne *et al.*, 1996), $^{[4]}\text{S}^{6+}\text{-O}$ (Hawthorne *et al.*, 2000), $^{[4]}\text{Be}^{2+}\text{-O}$ (Hawthorne & Huminicki, 2002), $^{[4]}\text{P}^{5+}\text{-O}$ (Huminicki & Hawthorne, 2002), $^{[3]}\text{As}^{3+}\text{-O}$ and $^{[4]}\text{As}^{3+}\text{-O}$ (Majzlan *et al.*, 2014). These contributions include the bond-length distributions and their statistics as well as relevant discussions on the crystal chemistry of these ion configurations that are primarily based on this bond-length information.

Other notable contributions have been made for $^{[6]}\text{U}^{6+}\text{-O}$, $^{[7]}\text{U}^{6+}\text{-O}$, $^{[8]}\text{U}^{6+}\text{-O}$ (Burns *et al.*, 1997) and $^{[6]}\text{V}^{3+}\text{-O}$, $^{[5]}\text{V}^{4+}\text{-O}$, $^{[6]}\text{V}^{4+}\text{-O}$, $^{[5]}\text{V}^{5+}\text{-O}$, $^{[6]}\text{V}^{5+}\text{-O}$ (Schindler *et al.*, 2000) who had an in-depth look at the bonding behaviour of these ions in order to rationalize the multi-modal bond-length distributions obtained for these ion configurations. Burns *et al.* (1997) also used their data to derive new bond-valence parameters for $\text{U}^{6+}\text{-O}$ bonds. Mills & Christy (2013) recently analyzed bond-length dispersions for $\text{Te}^{4+}\text{-O}$, $\text{Te}^{6+}\text{-O}$, although their approach was primarily focused on the derivation of bond-valence parameters.

1.1.3 The types of chemical bonds

Crystals are rich in terms of their chemical composition, atomic arrangement and bond type. Chemical bonds range from ionic to covalent to metallic, plus van der Waals and hydrogen bonds. All chemical bonds are intermediate between these ideal types, and different types of bonds commonly occur in the same structure (e.g., ionic $[\text{Na-O}]$ and covalent $[\text{P-O}]$ in Na_3PO_4 , ionic, covalent and van der Waals in CdI_2). Here, I review the

more common types of bonds observed in crystals, and put special emphasis on ionic and covalent bonding due to their prevalence in oxide and oxysalt structures.

1.1.3.1 Ionic bonding

Ionic bonding describes the transfer of valence electron(s) from one atom to another that results in a positive electrostatic attraction between oppositely charged ions (West, 2014). This positive interaction results from the interplay between the Coulomb attraction and Born repulsion. The Coulomb attraction results from the interaction between ions of opposite charge. The Born repulsion is a result of the finite size of atoms, where repulsion forces are strongest at short interatomic distances.

Fig. 1.3 gives a typical plot of the potential energy of a chemical bond $V(r)$ as a function of the distance r between the ions. The Coulomb attraction is shown by the dashed line in Fig. 1.3, and the Born repulsion by the dotted line. The overall shape is given by the solid line (Fig. 1.3) where r_{eq} is the equilibrium bond distance corresponding to the minimum in the potential energy.

Figure 1.3 Potential energy diagram of the chemical bond

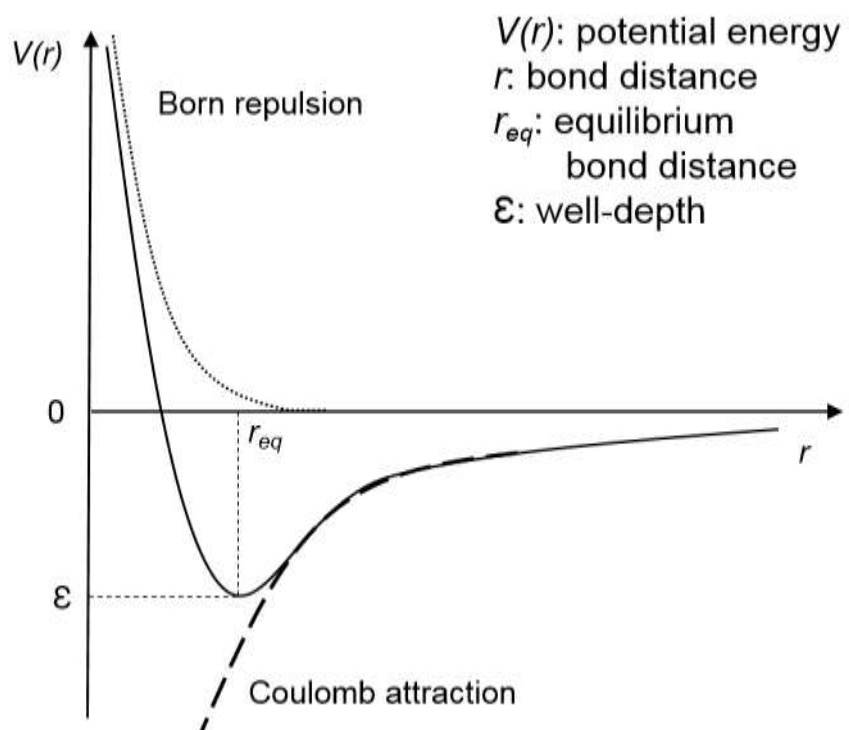
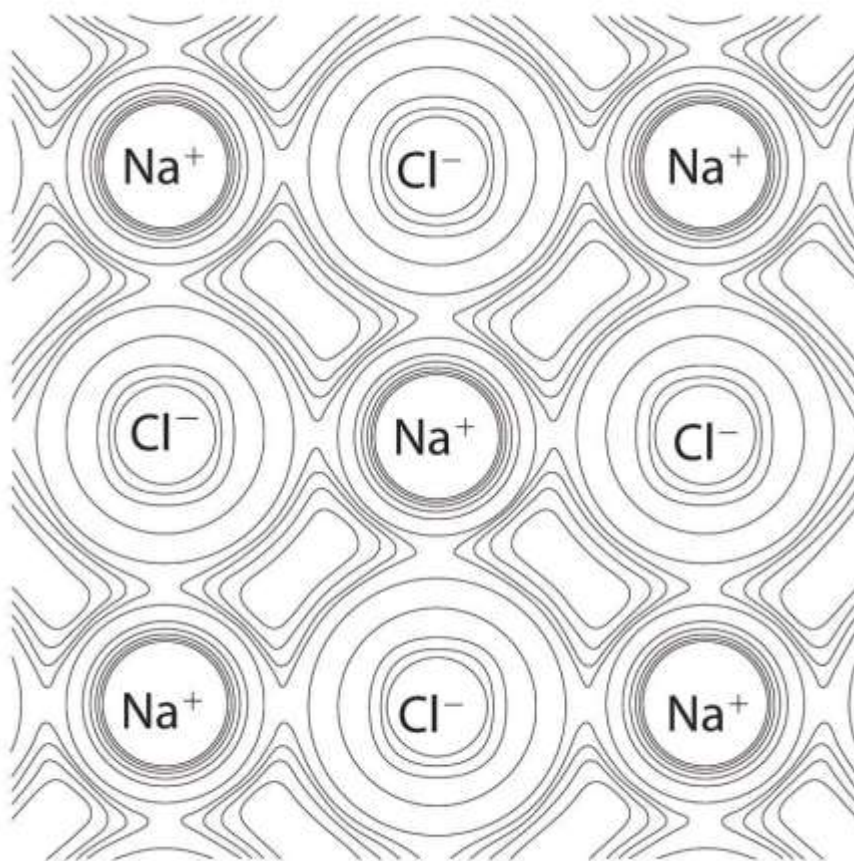


Figure 1.4 Electron-density map for a slice of the NaCl structure
([chemwiki.ucdavis.edu/Sizes of Atoms and Ions](http://chemwiki.ucdavis.edu/Sizes_of_Atoms_and_Ions) CC BY-NC-SA 3.0 US)



Thus ionic structures are held together by electrostatic forces where cations are arranged so that they are surrounded by anions and vice versa.

No structure (or bond) is truly ionic, and always has partial covalent character (West, 2014). Ideally, the single-electron transfer from the valence shell of Na to Cl results in Na^+ and Cl^- ions. However, the structure of NaCl has some covalent character, *i.e.*, the valence electron is not entirely transferred (Fig. 1.4); there is electron density that is not centered on the ions themselves, *i.e.*, there are chemical bonds between Na and Cl. Thus, the term “ionic bonding” has now evolved to describe a bond that has more ionic than covalent character. The concept of ionic bonding is extremely useful and widely applicable, and is a good starting point in describing structures that may contain other types of bonding (*e.g.*, covalent, hydrogen).

1.1.3.2 Covalent bonding

Covalent bonding involves the *sharing* of valence-electron pairs between atoms, in contrast to the transfer of one or more electrons from one atom to the other (as in ionic bonding; Smart & Moore, 2005). This sharing of electrons allows the atoms to effectively attain a stable electronic configuration (*i.e.*, octet rule) and is typical for atoms of similar electronegativity.

In a covalent bond, electron sharing is biased toward the atom of higher electronegativity, leaving partial charges on the atoms. Because of this, covalent bonds may be interpreted as forming a continuum with ionic bonds. Parallel to the discussion

of ionic bonding above, a chemical bond is described as covalent where the character of the bond is more covalent than ionic.

The lack of need to distinguish between covalent and ionic bonds has been suggested (see bond-valence theory, below). The coexistence of the two bond types is exemplified in minerals, where oxyanion groups (*e.g.*, SiO_4^{4-} , SO_4^{2-}), which are generally covalent in character, commonly bond to lower-charge cations via electrostatic interactions (*i.e.*, ionic bonding).

The simplest case of pure covalent bonding is that of H_2 , *i.e.*, two atoms of identical electronegativity. The individual H atoms have a partially filled *s* orbital (occupied by one electron), and may combine by sharing their valence electron with each other to form H_2 in which the (sigma-bonding) orbital is filled by 2 electrons.

The mechanisms of covalent bonding are rooted in quantum-mechanical arguments. The two main approaches to covalent bonding are the valence-bond (VB) theory (not to be confused with the bond-valence theory, which is unfortunately named) and molecular orbital (MO) theory (West, 2014). In VB theory, the atomic orbitals of the participating atoms overlap to form a chemical bond, where the electron of one atomic orbital is attracted by the nucleus of another atom until there is a repulsion of the electron density caused by the overlap of the atomic orbitals (Shaik & Hiberty, 2008). In molecular-orbital (MO) theory, molecules are instead treated as a collection of (unreactive) nuclei, under the influence of which electrons are considered as mobile entities from the point of view of the whole molecule (West, 2014). In MO theory, the electrons are delocalized throughout the molecule, whereas for ionic bonding, there is transfer of the electron from one atom to another.

1.1.3.3 Metallic bonding

Metallic bonding arises from the electrostatic interaction between conduction electrons and positively-charged metal ions, where the electrons move freely about the crystal and act as a glue that binds metal-ion cores into a periodic structure (Vainshtein *et al.*, 2000). In MO theory (covalent bonding), bonds are formed via delocalization of electrons into molecular orbitals that bind the atoms together. In metallic bonding, the valence-shell electrons occupy levels that are delocalized over the entire metal crystal (which can be viewed as a giant MO) and cause the structure to be a metallic conductor. These levels (atomic orbitals) are very numerous over a macroscopic metal crystal, and they are also very close in energy. This has led to the development of “band theory”, which deals with the continuous range of energies that an electron within a solid may have, and is crucial in explaining the properties of conductors, semi-conductors and insulators.

1.1.3.4 Van der Waals bonding

Van der Waals bonding originates from residual forces between neutral atoms, molecules or atomic groups that result from a momentary electrical polarization caused by the movement of electrons (Rao & Gopalakrishnan, 1997). These forces are relatively weak and only operate at a short distance. They include permanent/permanent, permanent/induced and induced/induced dipole interactions. Examples of van der Waals bonding in minerals include the weak interaction between

the sheets of carbon in graphite and between uranium-carbonate sheets in rutherfordine: $\text{UO}_2(\text{CO}_3)$ (Finch *et al.*, 1999).

1.1.3.5 Hydrogen bonding

Hydrogen bonding results from the polar interaction between the hydrogen atom $\text{H}^{\delta+}$ and other atoms or molecules $\text{X}^{\delta-}$ (δ = partial charge, X = commonly N, O, F). Hydrogen bonding is caused by a significant difference in electronegativity between bonded atoms H and X, resulting in an uneven distribution of the electron density toward X, leaving the hydrogen atom with a partial positive charge that is strong enough to attract the negative part of other ions or molecules (West, 2014). Hydrogen bonding is very common in minerals. It plays a significant role in defining the stability and properties of minerals, and is also a driving factor of mineral diversity (Hawthorne, 1992).

1.1.4 Theories of chemical bonding

There are various theories of chemical bonding with different degrees of sophistication and applicability. The most sophisticated and widely used result from quantum mechanical arguments and are the valence-bond (VB) theory and molecular orbital (MO) theory. However, many theories of chemical bonding are available and the selection of a theory is dependent on its intended use, as each theory has its own strengths and drawbacks.

1.1.4.1 Valence-bond theory

In valence-bond theory, bonds are viewed as weakly coupled orbitals where electron pairs between two bonded atoms reside in a region of overlap of the atomic orbitals. In order to rationalize the directionality of the covalent bond, atomic orbitals are sometimes mixed into *hybrid orbitals* of different shapes and energies in a process called *hybridization* (West, 2014). For example, for boron, with 3 valence electrons, the oxyanion BO_3^{3-} is formed by hybridization of the s and p orbitals of B to form a planar triangular hybrid-orbital (sp^2) which then overlaps with the half-filled valence atomic orbitals of three oxygen atoms (containing one unpaired electron) to form the oxyanion group.

1.1.4.2 Molecular-orbital (MO) theory

In molecular-orbital (MO) theory, the electrons are not assigned to individual atoms (as in valence-bond theory) but to molecular orbitals that span the entire molecule or (finite) structure. The most common way of deriving molecular orbitals is by linear combination of atomic orbitals (LCAO), where the atomic orbitals, represented by basis functions (one-electron functions), are centered on the nuclei of the constituent atoms (Vainshtein *et al.*, 2000). The combinations of the atomic orbitals may result in *bonding* interaction, where the lobes of the wavefunction describing the atomic orbitals are in phase (*i.e.*, same sign), resulting in maximum positive interaction, *antibonding*, where the wavefunctions are out of phase, resulting in a negative interaction, and *non-bonding*,

where there is no net overlap of the lobes described by the wavefunctions (e.g., an equal amount of positive and negative overlap).

Valence-bond theory and molecular-orbital theory were developed around the same time (~1920s), and have historically been observed to be in direct competition with each other; valence-bond theory was favoured up to the 1950-1960's, notably due to Pauling's endorsement (and his large influence in the field), while the use of molecular orbital theory increased thereafter following many successes at the expense of a "stalling" valence-bond theory (Shaik & Hiberty, 2008).

Today, the use of MO theory over VB theory is dependent on the kind of information sought. While VB theory generally does well at qualitatively describing the shapes of covalent compounds, it has certain drawbacks and limitations, and a popular illustration of the failure of the VB model is that it wrongfully predicts O_2 to be diamagnetic *via* spin pairing arguments (O_2 is paramagnetic). However, "failures" encountered in either valence-bond or molecular-orbital theory are usually due to the cut-off used in the expansion terms rather than problems with the theories themselves (Shaik & Hiberty, 2008); the two theories describe the same reality, starting from different elementary components, and converge towards exactly the same and complete description of a molecule. Because of this, the two approaches are now often viewed as complementary, and depending on what kind of information is sought, one is usually favourable over the other.

1.1.4.3 Bond-valence theory

There are several other theories of bonding that are wide ranging in terms of their complexity and applicability (e.g., crystal-field theory, ligand-field theory, Lewis theory), and as mentioned earlier, the selection of an appropriate model is largely dependent on the materials investigated and the kind of interpretation or understanding required. I am interested in developing a general understanding of the factors affecting the variation of bond lengths in crystals, and as will be discussed in the next chapter, I have done a bond-length dispersion analysis of cations bonded to oxygen that has resulted in the collection of 180,331 bond lengths from 31,514 coordination polyhedra for 135 ions bonded to oxygen from 9367 refined crystal structures. This is a large amount of data, and the interpretation of these crystal structures and their chemical bonding on the basis of VB or MO theory is not possible. Bond-valence (BV) theory is most suitable for the interpretation of these data, and is the most useful with regard to gaining insight into the crystal-chemical behaviour of these structures.

1.1.4.3.1 Theoretical basis of bond-valence theory

The bond-valence *method* was proposed by Brown and Shannon (1973) following the development and increasing use of equations that related the length of a bond to its strength (called bond valence) for a pair of ions (Pauling, 1947; Byström and Wilhelmi, 1951; Smith, 1953; Zachariasen, 1954; Zachariasen and Plettinger, 1959; Zachariasen, 1963; Evans and Mrose, 1960; Evans 1960; Pant and Cruikshank, 1967; Clark *et al.* 1969; Perloff, 1970; Donnay and Allmann, 1970). The bond-valence method rapidly gained popularity as a simple way of verifying the validity of crystal structures, and the success of the method was due entirely to the successful parameterization of the

relation between bond length and bond strength for ions pairs based on the valence-sum rule.

A theoretical basis for bond-valence method was developed by Preiser *et al.* (1999) and was largely based on the ionic model. They showed that by using the electric field rather than the electric potential, the bond valence can be identified with the electrostatic flux linking the cations to the anions, due to a natural partition of the Coulomb field into localized regions (the chemical bonds) between neighbouring ions of opposite charge. The idea dates back to Bragg (1930) who suggested electrostatic lines of force emanating from cations and ending on anions, in proportion to the cation charge. Preiser *et al.* (1999) argued that the energy (W) of an inorganic solid consists of two terms, one that deals with the classical electrostatic energy ($W_{\text{electrostatic}}$) determined by the distribution of electric charge, and the other one a quantum mechanical term (W_{qm}) that describes the Fermi repulsion between overlapping electron cores:

$$W = W_{\text{electrostatic}} + W_{\text{qm}} \quad (\text{eq. 1.1})$$

Preiser *et al.* go on to say that W_{qm} depends on the details of the electron density distribution, and so includes the influence of covalent bonding; in fact, they state that the ionic and covalent models of chemical bonding are not mutually exclusive, and that either the ionic or covalent model may describe bonds with partial ionic/covalent character.

There are two important theorems in bond-valence theory (Brown, 2002), and they are analogous to Kirchhoff's rules for electrical circuits: (1) the valence-sum rule, which states that *the sum of the bond-valences around an ion is equal to its formal valence*,

and (2) the equal-valence rule (or loop rule), which states that *in a closed circuit, the sum of the directed bond valences is equal to 0*. Preiser *et al.* (1999) showed that the valence-sum rule is rooted in Gauss's law, where the sum of the existent electrostatic fluxes φ_{ij} from a cation i to an anion j is equal to the formal valence Q_i of the ion

$$\sum_j \varphi_{ij} = \oint \mathbf{E}_{Monopole} \cdot d\mathbf{A} = Q_i \quad (\text{eq. 1.2})$$

where the electrostatic field $\mathbf{E}_{Monopole}$ is estimated as a monopole for a spherical atom, and where the integration is taken over any closed surface surrounding Q_i . The equal-valence rule is then explained by analogy with capacitance, where each “link” between the ions is modeled as a capacitor C_{ij} supporting a potential difference P_{ij} . The electrostatic fluxes φ_{ij} is equal to the charge q_{ij} on the ions (*i.e.*, the capacitor plates), and the potential P_{ij} across the capacitor is given by the capacitor equation

$$P_{ij} = \frac{q_{ij}}{C_{ij}} = \frac{\varphi_{ij}}{C_{ij}} \quad (\text{eq. 1.3})$$

From the law of conservation of energy, the sum of the potentials P_{ij} around any closed loop is zero, and

$$0 = \sum_{\text{loop}} P_{ij} = \sum_{\text{loop}} \frac{\varphi_{ij}}{C_{ij}} \quad (\text{eq. 1.4})$$

where the electrostatic flux is taken as positive or negative according to the direction in which it is traversed (from cation to anion and vice versa). From this result, Brown (2002) derived the network equations (discussed below) of a crystal structure by modeling the bond network as a capacitive electric circuit and assuming that when a structure is in equilibrium, all the bonds have the same capacitance C_{ij} . This allows simplification of eq. 1.4 by multiplying each side of the equation by C_{ij} , and the loop rule

is then only concerned with the summation (and cancellation) of the electrostatic fluxes ϕ_{ij} . Thus, bond-valence theory results from simple classical electrostatic arguments, and quantum effects are introduced as needed on an *ad hoc* basis. Burdett and Hawthorne (1993) have also shown that the valence-sum rule can be derived using a perturbation theory and a molecular-orbital approach.

Bond-valence theory, which is widely concerned with the connectivity of the atoms (topology), also finds roots in Graph Theory. The topology of an atomic arrangement may be described as a graph, by defining a set of *vertices* (ions) and *edges* (bonds) that connect the vertices. These vertices may be *labelled* to make them distinguishable (ion identity), and *coloured* to form different collections of vertices (cations and anions). Furthermore, the graph may be *directed* (a digraph), giving directions to the paths between adjacent vertices, and *weighted*, giving values to the vertices (corresponding to the charges of the ions) and to the edges (corresponding to the strengths, or bond valences, of the bonds). Any crystal structure may be described as a graph, and treated using the mathematics of Graph Theory.

The network equations of a crystal structure are derived from the valence-sum rule and from the loop rule, and any linearly-independent set of these equations can be solved to obtain the *a priori* bond-valences, with no knowledge other than the connectivity of the ions and their formal charges. Thus, *a priori* bond-valences are intrinsic to a crystal structure, those that site occupants must be able to satisfy in order for a crystal structure to be stable and observed. As a result, with only the knowledge of the connectivity of a crystal structure and the formal charges of the constituent ions, the bond valences for that structure may be predicted *a priori* and the associated bond

lengths may be calculated if the bond-valence—bond-length curves are known for those ions. This is a very important result of bond-valence theory, and one that has been largely ignored in the literature.

A problem that bond-valence theory currently faces is that the relation between (*a priori*) bond valences and bond length for pairs of ions, does not emerge from the theory; it is instead derived from experiment to form the basis of the bond-valence model (next).

1.1.4.3.2 The bond-valence model

A key aspect of the bond-valence model involves the relation between bond length and bond valence, which is derived from experiment and from the valence-sum rule. The valence-sum rule (Brown and Shannon, 1973) originates with Pauling's second rule, the *electrostatic valence rule* (1929), where following the investigation of a series of crystal structures, Pauling suggested that "the electric charge of each anion+ tends to compensate the strength of the electrostatic valence bonds reaching it from the cations". In other words, Pauling suggested that the sum of the bond strengths incident at an anion is approximately equal to the valence of that anion. This relation was very useful in deriving the formal valence of ions in a crystal structure (especially distinguishing between O^{2-} , OH^- and H_2O). In the 1950s and 1960s, people began to recognize that there was a relation between the deviation from Pauling's (second) rule and the bond lengths to that ion, and relations began to appear that related bond strengths to bond lengths for specific ion pairs. The first relation given for a relatively

wide variety of ions was that of Brown & Shannon (1973) where the relation between bond length and bond valence was written as

$$s = s_0 \left(\frac{R}{R_0} \right)^{-N} \quad (\text{eq. 1.5})$$

where s is the bond valence, R is the bond length, s_0 is a parameter usually set to have $R/R_0 \sim 1$, and R_0 and N are the bond-valence parameters that are fitted empirically for each pair of ions. Brown & Altermatt (1985) later proposed a new equation to model the relation:

$$S_{ij} = \exp \left(\frac{R_0 - R_{ij}}{B} \right) \quad (\text{eq. 1.6})$$

where R_{ij} is the bond length between ions i and j , S_{ij} is the bond valence, and R_0 and B are the bond-valence parameters. This equation is the one in use today, and the issue of parameterization will be discussed at much greater length in Chapter 2.

The bond-valence model has been used primarily to validate crystal structures *via* experimental verification of the valence-sum rule. However, Brown (2009) lists other uses of the model, notably involving [1] distorted ion environments, [2] valence maps and ionic conduction, [3] the valence-matching principle and structure stability, [4] the assignment of charge distributions, [5] incommensurate structures, [6] the structural effects of pressure, [7] the structural effects of temperature.

The bond-valence model is of specific interest in this thesis for three reasons: [1] it is a simple method in which the physical details are not obscured by complexities of computation; [2] it is not concerned with bond type *i.e.*, it models the three most common types of bonds in inorganic crystals, ionic, covalent, and hydrogen bonding,

with equal success, (this is especially true for oxide crystals, wherein lays the focus of this thesis); [3] it is suitable to the description of network solids.

1.2 Objectives and Significance of Research

A large amount of information concerning interatomic distances in the solid state is available. A comprehensive examination of the factors affecting the lengths of chemical bonds in (inorganic) crystals requires first the extraction of the data and subsequent assessment of its accuracy and validity. This task for cations bonded to oxygen was a major part of my thesis work in terms of time expended, and was done by way of a bond-length dispersion analysis of the Inorganic Crystal Structure Database (ICSD). This resulted in 180,331 individual bond-lengths for 135 cations with coordination numbers from [2] to [20], a total of 462 configurations (a single configuration is one ion in one coordination number (*e.g.*, $^{[4]}\text{Si}^{4+}$, $^{[10]}\text{Na}^{+}$) taken from 31,514 coordination polyhedra in 9367 crystal structures. With this amount of data available, the scope of this project goes way beyond that of a Ph.D. thesis, and I intend to make the resulting bond-length information available as a citable database that others may use to examine the origin of bond-length variations in crystals for the 462 configurations, only a few of which have been examined in the literature as yet.

Some of the specific objectives of my thesis include:

(1) to evaluate the published parameterizations of the bond-length—bond-valence relation for cations bonded to oxygen. This will be done using the data of the bond-length dispersion analysis of the ICSD and by comparing deviations between mean

bond-valence and oxidation state over the set of all coordination polyhedra for each cation bonded to oxygen;

(2) to develop a better method for the derivation of bond-valence parameters. This will be done by comparing results of the various methods of derivation used so far in the literature, examining other ways in which the parameters may be derived and deciding on the optimal method for the derivation of bond-valence parameters;

(3) to examine a wide variety of algebraic expressions in order to test for the optimal form of the bond-valence equation (*i.e.*, the one giving results most in accord with the valence-sum rule of bond-valence theory);

(4) to accumulate all published structural and chemical data on milarite-group minerals, and examine all reported compositions for the group in order to determine if any / how many compositions warrant description as new mineral species;

(5) to use *a priori* bond-valence calculations to gain insight into the control bond topology has on site occupancy, using the milarite structure. This will be done *via* comparison of *a priori* and experimental bond-valences for refined crystal structures observed in this group;

(6) to show that *a priori* bond-valence calculations can be used to locate areas of strain in crystal structures, using the milarite structure as an example. This will be done *via* a measure of the deviations from ideality for both individual bond-valences and the sum of the bond valences at each site of the structure, and by relating the frequency of observed chemical compositions to aspects of strain in the structure;

(7) examine the bond-length distributions of alkali-metal and alkaline-earth-metal ions bonded to oxygen for general trends such as variations in skewness, kurtosis and mean bond-length;

(8) to examine the validity of less-common configurations of the alkali-metal and alkaline-earth metal ions. Due to the scale of the bond-length dispersion analysis, I will be able to examine whether trends for common ion configurations extend to less-common configurations of these ions;

(9) to examine the possible factors that affect variations in mean bond-length;

1.3 Structure of the thesis

The individual chapters of this thesis were written independently as published or publishable work and have the common theme of bond distances between cations and oxygen in inorganic crystals, and their interpretation and use in the explanation of crystal-chemical phenomena. The chapters are ordered by date of acceptance and are connected by linking sections at the beginning of chapters.

In Chapter 2, I give the results of a reassessment of the parameterization of the bond-valence model. I use the data I gathered from my bond-length dispersion analysis of the Inorganic Crystal Structure Database (ICSD) to evaluate the various published parameterizations of the physical relation between bond length and bond valence and to derive a new parameterization for the model. This work was crucial to the next two chapters, which use different aspects of the bond-valence model to (1) address crystal-chemical problems, and (2) aid in the determination and interpretation of coordination

polyhedra in crystal structures. It is my intention to use the bond-valence model beyond structure verification (its most common use), and for this reason, optimal parameterization of the model is crucial.

Chapter 3 begins with a literature review of the milarite-group minerals and a clarification of its end-member compositions. The milarite structure was selected in this work because of the wide compositional variation of its constituent minerals and synthetic phases; this is of interest because (1) factors constraining the possible chemical compositions for a crystal structure, and (2) the primary controls on the stability of the structure, in general, are not well understood. I have expanded on work of Brown (1977) and Rutherford (1990), that has received little notice, by providing an easy method for the calculation of *a priori* bond-valences (the bond valences intrinsic to a crystal structure and charge arrangement) to gain insight into the control that bond topology has on site occupancy in the milarite structure. The Global Instability Index, GII (Salinas-Sanchez et al., 1992), and the Bond Strain Index, BSI (Preiser et al., 1999), are measures of the agreement between the experimental bond-valences and their ideal values. These indices are used to gain insight into strain in the milarite structure. The calculation of the *a priori* bond-valences implicit to the calculation of the BSI in principle allows one to locate strain at specific sites in the structure. This will be tested using the milarite structure. The new parameterization derived in Chapter 2 is key in this regard as deviations from the valence-sum rule need to reflect strain rather than inaccuracies in the bond-valence – bond-length parameterization.

Chapter 4 gives the bond-length distributions of the 55 observed configurations of the alkali-metal ions and the 29 observed configurations of the alkaline-earth-metal ions.

While the amount of data gathered and treated here is very large, 4859 coordination polyhedra and 38,594 bond distances for the alkali metals, and 3038 coordination polyhedra and 24,487 bond distances for the alkaline-earth metals, this chapter only scratches the surface of the question “what affects the variation of bond lengths and mean bond-lengths for alkali-metal ions and alkaline-earth-metal ions bonded to oxygen?”. In this chapter, I focus on general trends observed for the families and their constituent ions in their various coordinations, and examine factors that affect the distributions of bond lengths observed. The bond-valence model is partly used here to validate certain uncommon ion configurations (*e.g.*, [3]-coordinated Li^+ , [3]-coordinated Be^{2+}), and an optimal parameterization of the relevant bond-valence curves was crucial in this analysis. Numerous detailed studies for specific ions and ion configurations may result from this work for the alkali and alkaline-earth metals alone, which may take many investigators years to examine. Similar analysis of other families of the periodic table of elements for which I have bond-length data for ions bonded to oxygen are planned.

1.4 References

Baur, W.H. (1971). Prediction of bond length variations in silicon-oxygen bonds. *Am. Mineral.* **56**, 601-621.

Baur, W.H. (1974). The geometry of polyhedral distortions. Predictive relationships for the phosphate group. *Acta Cryst. B* **30**, 1195-1215.

Bragg, W.L. (1913). The structure of some crystals as indicated by their diffraction of X-rays. *Proc. Roy. Soc.* **89**, 248-277.

Bragg, W.H. and Bragg, W.L. (1913). The structure of the diamond. *Proc. Roy. Soc.* 89, 277–291.

Bragg, W. L. (1930). The structure of silicates. *Z. Kristallogr.* 74, 237-305.

Brown, I.D. (1977). Predicting bond lengths in inorganic crystals. *Acta Cryst. B* **33**, 1305-1310.

Brown, I.D. (2002). The Chemical Bond in Inorganic Chemistry. Oxford University Press.

Brown, I.D. (2009). Recent developments in the methods and applications of the bond valence model. *Chem. Rev.* **109**, 6858-6919.

Brown, I.D. & Shannon, R.D. (1973). Empirical bond-strength bond-length curves for oxides. *Acta Cryst. A* **29**, 266-282.

Burdett, J.K. & Hawthorne, F.C. (1993). An orbital approach to the theory of bond valence. *Am. Mineral.* **78**, 884-892.

Burns, P.C., Ewing, R.C. & Hawthorne, F.C. (1997). The crystal chemistry of hexavalent uranium: Polyhedron geometries, bond-valence parameters, and polymerization of polyhedra. *Can. Mineral.* **35**, 1551-1570.

Byström, A. & Wilhelmi, K.-A. (1951). The crystal structure of $(\text{NH}_4)_2\text{Cr}_2\text{O}_7$ - with a discussion of the relation between bond number and interatomic distances. *Acta Chem. Scand.* **5**, 1003-1010.

Clark J.L., Appleman D.E. & Papike J.J. (1969). Crystal-chemical characterization of clinopyroxenes based on eight new structure refinements. *Min. Soc. Amer. Special Paper* **2**, 31-50.

Cortés-Guzmán, F. & Bader, R.F.W. (2005). Complementarity of QTAIM and MO theory in the study of bonding in donor–acceptor complexes, *Coordination Chemistry Reviews*, **249**, 633–662

Dent Glasser, L.S. (1979). Non-existent silicates. *Z. Kristallogr.* **149**, 291-305.

DiSalvo, F.J. (1990). Solid-state chemistry: a rediscovered chemical frontier. *Science*, **247**, 4943.

Donnay G. & Allmann R. (1970). How to recognize O^{2-} , OH^- , and H_2O in crystal structures determined by X-rays. *Am. Mineral.* **55**, 1003-1015.

Evans H.T. Jr (1960). Crystal structure refinement and vanadium bonding in the metavanadates KVO_3 , NH_4VO_3 and $KVO_3 \cdot H_2O$. *Z. Kristallogr.* **114**, 257-277.

Evans H.T. Jr & Mrose M.E. (1960). A crystal chemical study of the vanadium oxide minerals, haggite and doloresite. *Am. Mineral.* **45**, 1144-1166.

Finch, R.J., Cooper, M.A. and Hawthorne, F.C. (1999). Refinement of the crystal structure of Rutherfordine. *Can. Mineral.* **37**, 929-938

Friedrich, W. Knipping, P. & Laue, M. (1912). Interferenz-Erscheinungen bei Röntgenstrahlen. *Bayerische Akad. d. Wiss. zu München, Sitzungsber. math.-phys. Kl.* **303-322**

- Gibbs, G.V., Ross, N.L., Cox, D.F., Rossoll, K.M., Iversen, B.B., Spackman, M.A. (2013). Bonded Radii and the Contraction of the Electron Density of the Oxygen Atom by Bonded Interactions. *J. Phys. Chem. A*, **117**, 1632-1640.
- Goldschmidt, V.M. (1926a). Laws of crystal chemistry. *Naturwissenschaften*, **14**, 477-485.
- Goldschmidt, V. M. (1926b). *Geochemische Verteilungsgesetze der Elemente*. Skrifter Norske Videnskaps—Akad. Oslo, (I) Mat. Natur.
- Goldschmidt, V.M. (1927). Construction of crystals. *Zeitschrift für Technische Physik*, **8**, 251-254.
- Hawthorne, F.C. (1990). Crystals from first principles. *Nature*, **345**, 297.
- Hawthorne, F.C. (1992). The role of OH and H₂O in oxide and oxysalt minerals. *Z. Kristallogr.* **201**, 183-206.
- Hawthorne, F.C. & Huminicki, D.M.C. (2002). The crystal chemistry of beryllium. *Rev. Mineral.* **50**, 333-403
- Hawthorne, F.C., Burns, P.C., Grice, J.D. (1996). The crystal chemistry of boron. *Rev. Mineral.* **33**, 41-115.
- Hawthorne, F.C., Krivovichev, S.V. & Burns, P.C. (2000). The crystal chemistry of sulfate minerals. *Rev. Mineral. Geochem.* **40**, 1-112.
- Huminicki, D.M.C. & Hawthorne, F.C. (2002). The crystal chemistry of the phosphate minerals. *Rev. Mineral. Geochem.* **48**, 123-253.

- Karamertzanis, P.G. & Pantelides C.C. (2005). *Ab initio* crystal structure prediction—I. Rigid molecules. *J. Comput. Chem.* **26**, 304–324.
- Landé A. (1920). Über die Größe der Atome. *Zeitschrift für Physik* 1, **3**, 191–197.
- Lufaso, M.W. & Woodward, P.M. (2001). Prediction of the crystal structures of perovskites using the software program SPuDS. *Acta Cryst. B* **57**, 725-738
- Maddox, J. (1988). Crystals from first principles. *Nature*, **335**, 201.
- Majzlan, J., Drahota, P. and Filippi, M. (2014). Parageneses and crystal chemistry of arsenic minerals. *Rev. Mineral.* **79**, 17-184
- Mills, S.G. & Christy A.G. (2013). Revised values of the bond-valence parameters for Te-IV-O, Te-VI-O and Te-IV-Cl. *Acta Cryst. B* **69**, 145-149.
- Oganov, A.R. & Glass, C.W. (2006). Crystal structure prediction using *ab initio* evolutionary techniques: Principles and applications. *J. Chem. Phys.* **124**, 244704.
- Oganov, A.R., Yanming, M., Lyakhov, A.O., Valle, M., Gatti, C. (2010). Evolutionary crystal structure prediction as a method for the discovery of minerals and materials. *Rev. Mineral. Geochem.* **71**, 271-298.
- Pannetier, J., Bassas-Alsina, J., Rodriguez-Carvajal, J., Caignaert, V. (1990). Prediction of crystal structures from crystal chemistry rules by simulated annealing. *Nature*, **346**, 343-345.
- Pant A.K. & Cruikshank D.W.J. (1967). A reconsideration of structure of datolite $\text{CaBSiO}_4(\text{OH})$. *Z. Kristallogr.* **125**, 286-297.

- Parker, S.C., Catlow, C.R.A., Cormack, A.N. (1984). Structure prediction of silicate minerals using energy-minimization techniques. *Acta crystallographica*, B **40**, 200-208.
- Pauling, L. (1927). The sizes of ions and the structure of ionic crystals. *J. Am. Chem. Soc.* **49**, 765-790.
- Pauling, L. (1929). The principles determining the structures of complex ionic crystals. *J. Am. Chem. Soc.* **51**, 1010-1026.
- Pauling, L. (1947). Atomic radii and interatomic distances in metals. *J. Am. Chem. Soc.* **69**, 542–553.
- Pauling, L. (1960). The nature of the chemical bond and the structure of molecules and crystals: an introduction to modern structural chemistry. Cornell University Press.
- Perloff A. (1970). Crystal structure of sodium hexamolybdochromate(iii) octahydrate, $\text{Na}(\text{CrMo}_6\text{O}_{24}\text{H}_6) \cdot 8\text{H}_2\text{O}$. *Inorg. Chem.* **9**, 2228-2239.
- Podeszwa, R., Rice, B.M., Szalewicz, K. (2008). Predicting structure of molecular crystals from first principles. *Phys. Rev. Lett.* **101**, 115503.
- Preiser, C., Lösel, J., Brown, I.D., Kunz, M., Skowron, A. (1999). Long-range Coulomb forces and localized bonds. *Acta Cryst. B* **55**, 698-711.
- Rao, C.N.R. & Gopalakrishnan, J. (1997). New Directions in Solid State Chemistry, 2nd edition, Cambridge University Press, Cambridge p 549.
- Röntgen, W.C. (1895). Ueber eine neue Art von Strahlen. Aus den Sitzungsberichten der Würzburger Physik.-medic. Gesellschaft. 1-16

Rutherford, J.S. (1990). Theoretical prediction of bond-valence networks. *Acta Cryst. B* **46**, 289-292.

Salinas-Sanchez, A., Garcia-Munoz, J.L., Rodriguez-Carvajal, J., Saez-puche, R., & Martinez, J.L. (1992) Structural characterization of R_2BaCuO_5 ($R = Y, Lu, Yb, Tm, Er, Ho, Dy, Gd, Eu$ and Sm) oxides by X-ray and neutron-diffraction, *J. Solid State Chem.* **100**, 201–211.

Schindler, M., Hawthorne, F.C. and Baur, W.H. (2000). Crystal chemical aspects of vanadium: polyhedral geometries, characteristic bond valences, and polymerization of (VOn) polyhedra. *Chem. Mater.*, **12**, 1248-1259

Shannon, R.D. (1976). Revised effective ionic radii and systematic studies of interatomic distances in halides and chalcogenides. *Acta Cryst. A* **32**, 751–767.

Shannon, R.D. & Prewitt C.T. (1969). Effective ionic radii in oxides and fluorides. *Acta Cryst. B* **25**, 925-946.

Shaik, S.S. & Hiberty, P.C. (2008). A Chemist's Guide to Valence Bond Theory, Wiley Interscience, John Wiley & Sons, Inc., Hoboken, New Jersey, p 316.

Smart, L.E. and Moore, E.A (2005). Solid State Chemistry: An Introduction, 3rd edition, CRC Press/Taylor & Francis, Boca Raton, p 407.

Smith, J.V. (1953). Reexamination of the crystal structure of melilite. *Am. Mineral.* **38**, 643-661.

Vainshtein, B.K., Fridkin, V.M. and Indenbom, V.L. (2000). Modern Crystallography series, vol.2, Springer, Berlin, p 520.

- Wang, Y., Lv, J., Li, Z., Ma, Y. (2010). Crystal structure prediction via particle swarm optimization. *Phys. Rev. B* **82**, 094116.
- Wang, Y., Lv, J., Li, Z., Ma, Y. (2012). CALYPSO: A method for crystal structure prediction. *Comput. Phys. Commun.* **183**, 2063-2070.
- Wasastjerna, J. A. (1923). On the radii of ions. *Comm. Phys.-Math., Soc. Sci. Fenn.* **1(38)**, 1-25.
- Werner, A. (1893). Beitrag zur Konstitution anorganischer Verbindungen. *Z. Anorg. Allg. Chem.* **2**, 267-330.
- West, A.R. (2014). Solid State Chemistry and its Applications, 2nd edition, Student edition, Wiley, Chichester, West Sussex, p 556.
- Woodley, S.M. & Catlow, C.R.A. (2008). Crystal structure prediction from first principles. *Nat. Mater.* **7**, 937 – 946.
- Zachariasen W.H. (1954). Crystal chemical studies of the 5f-series of elements.23. On the crystal chemistry of uranyl compounds and of related compounds of transuranic elements. *Acta Cryst.* **7**, 795-799.
- Zachariasen W.H. (1963). Crystal structure of monoclinic metaboric acid. *Acta Cryst.* **16**, 385-389.
- Zachariasen W.H. & Plettinger H.A. (1959). Crystal chemical studies of the 5f-series of elements.25. The crystal structure of sodium uranyl acetate. *Acta Cryst.* **12**, 526-530.

Chapter 2

Comprehensive derivation of bond-valence parameters for ion pairs involving oxygen

Gagné, O.C. & Hawthorne, F.C. (2015). Comprehensive derivation of bond-valence parameters for ion pairs involving oxygen. *Acta Crystallographica*, **B71**, 562-578

2.1 Synopsis

Published bond-valence parameters for cation-oxygen bonds are evaluated with regard to their agreement with the valence-sum rule, and new bond-valence parameters are derived for 135 cations bonded to oxygen.

2.2 Abstract

Published two-body bond-valence parameters for cation-oxygen bonds have been evaluated via the Root Mean-Square Deviation (RMSD) from the valence-sum rule for 128 cations, using 180,194 filtered bond-lengths from 31,489 coordination polyhedra. Values of the RMSD range from 0.033-2.451 v.u. (1.1%-40.9% per unit of charge) with a weighted mean of 0.174 v.u. (7.34% per unit of charge). The set of best published parameters has been determined for 128 ions and used as a benchmark for the determination of new bond-valence parameters in this paper. Two common methods for the derivation of bond-valence parameters have been evaluated: (1) fixing B and solving for R_0 ; (2) the graphical method. On a subset of 90 ions observed in more than one coordination, fixing B at 0.37 Å leads to a mean weighted-RMSD of 0.139 v.u. (6.7% per unit of charge), while graphical derivation gives 0.161 v.u. (8.0% per unit of charge). The advantages and disadvantages of these (and other) methods of derivation have been considered, leading to the conclusion that current methods of derivation of bond-valence parameters are not satisfactory. A new method of derivation is introduced, the GRG (Generalized Reduced-Gradient) method, which leads to a mean weighted-RMSD of 0.128 v.u. (6.1% per unit of charge) over the same sample of 90 multiple-coordination

ions. The evaluation of 19 two-parameter equations and 7 three-parameter equations to model the bond-valence—bond-length relation indicates that (1) many equations can adequately describe the relation; (2) a plateau has been reached in the fit for two-parameter equations; (3) the equation of Brown and Altermatt (1985) is sufficiently good that use of any of the other equations tested is not warranted. Improved bond-valence parameters have been derived for 135 ions for the equation of Brown and Altermatt (1985) in terms of both the cation and anion bond-valence sums using the GRG method and our complete data set.

Keywords: bond-valence parameters, bond-valence equations, the valence-sum rule

2.3 Introduction

Many people have investigated correlations between deviations from Pauling's second rule (Pauling, 1929) and bond-length variations in crystals (e.g., Baur, 1970, 1974; Donnay & Allman, 1970; Pyatenko, 1972; Brown & Shannon, 1973; Ferguson, 1974), generally developing quantitative relations between bond length and the strength of a bond. During the 1960s and early 1970s, the term 'bond strength' was used, but was later changed to 'bond valence' to distinguish these values from Pauling bond strengths. In the early 1970s, several different forms of the (inverse) relation between bond valence and bond length were used, but the equation of Brown and Altermatt (1985) was eventually accepted as the general form of the bond-valence—bond-length curve: $S = \exp[(R_0 - R)/B]$ where S is the bond valence (in valence units), R is the observed bond length, and R_0 and B are fitted constants called bond-valence parameters. Brown

& Altermatt (1985) gave values of R_0 and B for 141 pairs of ions, and Brese & O'Keeffe (1991) gave analogous values for 969 pairs of ions. Many smaller-scale studies have produced bond-valence parameters for a wide range of ion pairs that have been compiled by Brown (2002, 2009, 2013). Brown's latest list of published bond-valence parameters (2013) contains 1749 sets of bond-valence parameters for the equation of Brown & Altermatt (1985), for 1350 unique ion pairs, and counts 340 sets of bond-valence parameters for 194 cations bonded to oxygen. Several sets of bond-valence parameters are often available for unique ion pairs, and there has been little comparison between different sets of parameters available to determine which is the most suitable for a given ion pair. Here, we consider bond-valence parameters for cations bonded to oxygen. Notably, with regard to the bond-valence parameters currently available:

[1] There is no consistency between parameters from different sources; in particular, the criteria used to select the bond lengths used in the derivation of the bond-valence curves vary widely;

[2] Different fitting methods have been used by different authors to derive the bond-valence parameters (*i.e.*, there is no consensus on the best way to derive the bond-valence parameters);

[3] Very few alternative forms of the bond-valence—bond-length relation have been tested.

Here, we (1) evaluate published bond-valence parameters for 128 cations bonded to oxygen, using a very large set of bond lengths that have undergone rigorous filtering; (2) investigate many alternative algebraic forms of the bond-valence—bond-length

relation; (3) evaluate different fitting methods used in the derivation of bond-valence parameters; (4) determine new bond-valence parameters for 135 cations bonded to oxygen.

2.4 Experimental bond-lengths used in this work

As part of other work examining the dispersion of bond lengths in inorganic crystals, we have used the Inorganic Crystal Structure Database (ICSD) to extract bond lengths for all atoms of the periodic table of elements bonded to oxygen, as a function of oxidation state and coordination number. The following selection criteria were used during collection of the bond-length data: (1) Publication date ≥ 1975 ; (2) $R_1 \leq 6\%$; (3) the site of interest is fully occupied by the cation; (4) all bonds involve ions at fully occupied sites; (5) the cation and anion sites of interest show no positional disorder; (6) crystallographic data were measured at ambient conditions; (7) no data from powder, electron or synchrotron diffraction were included; (8) where there was severe ambiguity as to the correct coordination number, the data were not included to avoid error; (9) for H, only neutron-diffraction data were collected.

Following collection of the bond distances, the bond-length distributions were examined for outliers. Where outliers were identified, the original publications were examined to validate the distances or identify errors. The most common source of error involved sites which, in the ICSD, were erroneously identified as containing only one cation whereas inspection of the original paper showed that cation disorder was present (e.g., for Si, large mean distances commonly involved the presence of Al^{3+} at the Si^{4+} site,

and small distances involved the presence of B³⁺ at the Si⁴⁺ site). We note here that verified outliers that showed no apparent error were retained in our analysis. Where such analysis had been done for specific ions, we checked our results with those given previously to ensure compatibility (or confirm the validity of any differences). For example, Sidey (2013) gives the shortest [3]-coordinated B³⁺-O distance as 1.20 Å, in close accord with our value of 1.22 Å, and Mills *et al.* (2009) and Mills & Christy (2013) use maximum Sb³⁺ and As³⁺ distances of 3.5 Å, in reasonable accord with our values of ~3.4 Å (determined by examination of each individual structure rather than using a pre-determined cutoff). Use of the above criteria resulted in 180,369 bond lengths from 31,521 coordination polyhedra, for 135 ions bonded to oxygen from 9367 refined crystal structures.

2.5 Method of evaluation of bond-valence parameters

To evaluate the bond-valence parameters for an ion pair, we calculated the root-mean-square deviation (RMSD) between the bond-valence sum (using the bond-valence parameters and the experimental bond-lengths) and the valence of the constituent cation for each polyhedron, over the entire dataset of coordination polyhedra for that cation:

$$RMSD = \sqrt{\frac{\sum_n (\sum_j S_{ij} - V_i)^2}{n}} \quad (\text{eq. 2.1})$$

where S_{ij} is the bond valence between ions i and j , V_i is the valence of the i^{th} cation, and the sum is over the j bonds that cation i makes to O for the n coordination polyhedra

available from the dataset of that particular ion pair. This method evaluates deviations from the valence-sum rule (Brown 2002), and is applicable to any parameterization. From here on, any mention of RMSD in the text will imply the deviation to be from the valence-sum rule, in valence units (v.u.).

Brown & Shannon (1973) reported the *relative* RMSD (D_i), on the basis of a unit of charge:

$$D_i = \sqrt{\frac{\left(\sum_{i=1}^m \frac{(z_i - p_i)^2}{z_i^2}\right)}{m}} \times 100\% \quad (\text{eq. 2.2})$$

where z_i is the valence of ion i , p_i is the bond-valence sum, and m is the number of ions of type i . This expression has been used by many people reporting new bond-valence parameters. However, the basis of bond-valence curves is the valence-sum rule (Brown, 1980, 2002), and minimization of deviations from the valence-sum rule involves bond valences, not bond valences divided by valence, and hence a more appropriate measure of agreement with the valence-sum rule involves eq. 2.1 rather than eq. 2.2. Though eq. 2.1 is the recommended way of reporting the RMSD in the future, our results will be reported using both eq. 2.1 and 2.2 for the most part throughout this work, so that they can easily be compared with other published work.

2.6 Evaluation of published oxide bond-valence parameters

We evaluated 244 pairs of bond-valence parameters (Ro, B) for 128 ion pairs involving cations bonded to O²⁻. By and large, bond-valence parameters have been, and continue to be, derived based on the first coordination shell of ions. However, Adams (2001,

2014) used the concept of bond softness to argue for the consideration of higher coordination shells in the determination of bond-valence parameters (which he calls softBV parameters) for use in dynamic situations where the use of discrete coordination number is not continuously applicable (e.g., ionic conduction, Adams & Prasada Rao, 2014). Due to the coordination-based nature of our dataset, we did not evaluate softBV parameters.

Table 2.S1 gives the bond-valence parameters of the constituent ions and their associated RMSD obtained from eq. 2.1, listed in the same order as in Brown (2013), using the same reference codes. The RMSD values range from 0.033 to 2.451 v.u. However, the extremely large values are caused by inappropriate parameters; for example, Ce^{3+} has two published sets of parameters, with RMSD values of 1.500 and 0.161 v.u., and U^{6+} has three sets of parameters with RMSD values of 0.894, 0.699 and 0.193 v.u., respectively. The mean value of the RMSD for all published parameters using our dataset is 0.219 v.u. with a standard deviation of 0.232 v.u. and a median value of 0.241 v.u.

We note here that it is critical for bond-valence parameters to be evaluated in the same way they were derived; while this may seem intuitive, we often observed poor agreements for ions showing large gaps in their bond-length distributions (*i.e.*, ions that form “secondary bonds”), as different sets of bond-valence parameters available for the same ions were presumably derived both with and without the inclusion of secondary bonds (e.g., for I^{5+} , Te^{4+}). Following experimentation with this practice, we conclude that the inclusion of the long bonds in the first coordination shell leads to better bond-valence sums, and have therefore retained them in our dataset for this evaluation. As a

corollary, as we derive our bond-valence parameters (below) using the longer bonds where appropriate (e.g., elements of periods 4-6, typically not transition metals), the longer bonds should be included when using the parameters derived in this work.

From the results of Table 2.S1, we may identify a set of best published parameters that provides a useful benchmark for comparison in the derivation of new bond-valence parameters.

2.7 The hydrogen atom

It is necessary to treat the hydrogen atom somewhat differently from the other atoms of the periodic table for two reasons: (1) for hydrogen atoms, positional parameters derived from X-ray data show significant systematic error, as the electron density notionally associated with the hydrogen atom is partly delocalized into the O-H bond, leading to O-H distances that are systematically shorter than the O-H internuclear distances. In turn, this will lead to H...O (hydrogen-bond) distances that are systematically longer than the H...O internuclear distances; (2) some authors suggest the use of more than one pair of bond-valence parameters to model the relation for this atom. These conditions are specified in Table 2.S1 for each reference.

Grabowski (2000) used neutron-diffraction data to derive a single pair of parameters, $R_0 = 0.93 \text{ \AA}$ and $B = 0.40 \text{ \AA}$, resulting in a RMSD of 0.035 v.u. for our dataset. Also using neutron-diffraction data, Brown (2002) proposed the use of 3 pairs of parameters to model the relation over specific ranges of bond lengths (the resulting RMSD for our dataset is 0.059 v.u.) and argued that the use of different parameters over different

bond-length ranges gives better sums around the O^{2-} ions than the parameters of Alig *et al.* (1994).

Yu *et al.* (2006) argued that hydrogen requires two sets of parameters, one set for $s > 0.5$ *vu* (the donor-hydrogen bond), and another set for $s < 0.5$ *vu* (the hydrogen-acceptor bond); they also give 1.30 Å as the cut-off between stronger and weaker bonds. Although they do not specify if they used X-ray data, neutron data, or a combination of both, the reported bond lengths strongly suggest the sole use of X-ray data. As a result, their parameters are not directly compatible with our dataset, which consists of neutron-diffraction data for hydrogen. However, we decided to test their parameters on our dataset of 224 coordination polyhedra for hydrogen, to evaluate the effect of using X-ray versus neutron data for H^+ ; we used their first set of parameters ($R_0 = 0.79$ Å and $B = 0.37$ Å) with the shorter of the O-H distances and their second set of parameters ($R_0 = 1.409$ Å and $B = 0.37$ Å) with the longer of the H...O distances, which resulted in an overall RMSD of 0.181 v.u.

The lowest RMSD for bonds involving hydrogen and oxygen (0.035 v.u.) is thus obtained for the single pair of parameters of Grabowski (2000), and suggests that a single pair of parameters is sufficient to deal with bonds involving hydrogen and oxygen.

2.8 Use of bond-valence parameters for hydrogen-oxygen bonds

Bond-valence parameters derived from neutron-diffraction data (such as those we give later) are obviously not relevant to hydrogen positions from unconstrained refinement of X-ray diffraction data (for the reasons outlined above). However, most information on

hydrogen in crystal structures comes from X-ray diffraction data. The best way around this situation is to use constrained refinement in the derivation of hydrogen positions. The $O_{\text{donor}}\text{-H}$ distance may be softly constrained to an appropriate value ($\sim 0.96\text{-}0.98$ Å) for OH and H_2O groups involved in asymmetric hydrogen-bonds, and the H-H distance in H_2O groups may be constrained to ~ 1.55 Å (which gives an H-O-H angle of $\sim 105^\circ$). Of course, the result is only approximate, but the ensuing $\text{H}\dots\text{O}_{\text{acceptor}}$ distances are likely to be far closer to the analogous nucleus-nucleus distances than those derived by unconstrained X-ray refinement. This method of refinement allows the use of bond-valence parameters derived from neutron-diffraction data with bond lengths derived from X-ray diffraction data, and usually leads to good bond-valence sums.

2.9 Comments on fixing the B parameter

The results of the evaluation (Table 2.S1) give us some insight into the practice of fixing the B parameter (to 0.37 Å), an issue that has received some comment in recent years (Adams, 2001; Krivovichev & Brown, 2001; Locock & Burns, 2004; Sidey, 2008; Brown, 2009; Mills *et al.*, 2009; Sidey, 2010; Krivovichev, 2012; Brown, 2014). Many ions have bond-valence parameters to oxygen available for both fixed and refined values of B , and we may use these ions to evaluate the effectiveness of fixing B to 0.37 Å. Out of 37 instances, 12 ions have lower RMSD values for $B = 0.37$ Å whereas 25 ions have lower RMSD values for $B \neq 0.37$ Å. This comes as a surprise, as fitting with two variable parameters should give at least as good a fit as fitting with only one variable parameter. This result is probably due to the choice of method for the derivation of the bond-valence parameters, as this can greatly influence the quality of the fit; the use of a poor

method of derivation that allows refinement of both R_0 and B can easily lead to a poorer fit than the method of fixing B , as will be shown later. Nonetheless, significant improvements in fit with two variable parameters are common. A persuasive example is that of Burns *et al.* (1997). Their parameters for U^{6+} have $B = 0.519 \text{ \AA}$ and result in a RMSD value of 0.158 v.u. for our dataset (585 polyhedra), whereas the other parameters (with $B = 0.37 \text{ \AA}$) give a RMSD of 0.690 and 0.889 v.u. (Table 2.S1). Even where bond-valence parameters with $B = 0.37 \text{ \AA}$ give low RMSD values, the fit can be improved significantly by allowing B to vary. For example, Mills & Christy (2013) derive new parameters for Te^{6+} with $B = 0.56 \text{ \AA}$, resulting in a RMSD value of 0.146 v.u. compared to 0.229 v.u. for the available parameters with $B = 0.37 \text{ \AA}$). These examples suggest that both R_0 and B should be varied in the derivation of bond-valence parameters; of the 244 pairs of bond-valence parameters examined here, 191 have B fixed at 0.37 \AA .

2.10 Comments on the level of fit

The mean RMSD for the 244 pairs of bond-valence parameters evaluated here, weighted by the number of coordination polyhedra of the ions, is 0.174 v.u. (7.34% per unit of charge using the equation of Brown & Shannon (1973; eq. 2.2)). The set of best parameters available for each ion (the 128 best pairs) has a mean weighted RMSD of 0.136 v.u. (5.68% per unit of charge). These values are slightly higher than those commonly reported in the literature, and to the generally accepted “5% error margin” observed by Brown and Shannon (1973). This difference may be due to the fact that authors typically select a small subset of “high-quality” structures from the available data

to derive bond-valence parameters, the size of which strongly influences the reported RMSD value, which in turn does not necessarily reflect the fit for all data. Although the data we use here has been thoroughly filtered for errors, our derivation of the bond-valence parameters (below) foregoes this practice to reduce the possibility of such bias.

From the evaluation of the published bond-valence parameters, we conclude that the fit of the currently available parameters to the valence-sum rule is variable and can be significantly improved.

2.11 Parameterization

2.11.1 Methods of derivation of the bond-valence parameters

Bond-valence parameters have been derived using a variety of methods based on different optimization criteria for both experimental and interpolated data. Here, we discuss the most common methods used in the derivation of bond-valence parameters based on experimental data.

2.11.1.1 Least-squares fitting

The initial form of the bond-valence equation proposed by Brown and Shannon (1973) is

$$s = s_0 \left(\frac{R}{R_0} \right)^{-N} \quad (\text{eq. 2.3})$$

where s is the bond valence (called bond strength by them), R is the bond length, s_o is a parameter usually set to have $R/R_o \sim 1$, and R_o and N are the bond-valence parameters. Brown and Shannon (1973) derived their bond-valence parameters in three different ways using least-squares fitting to minimize deviations from the valence-sum rule: (1) vary R_o and N for the incident bond-valence sums around the cations; (2) fix N and vary R_o for the incident bond-valence sums around the cations; (3) vary R_o and N for the incident bond-valence sums around the cations and the anions. In principle, method (3) is best as the valence-sum rule holds around both cations and anions. However, the inclusion of the anion bond-valence sums in the optimization is quite difficult on a large scale (this issue will be discussed later). Brown & Shannon (1973) generally used methods (1) and (2) to derive their parameters. The least-squares optimization was done using the following equation:

$$Q = \sum_{i=1}^m w_i (z_i - p_i)^2 \quad (\text{eq. 2.4})$$

where Q is the sum of the residuals, m is the number of ions of type i , z_i is the valence, p_i is the bond-valence sum, and w_i is a weight set to $1/\sigma^2(p_i)$, where $\sigma(p_i)$ is the standard error on p_i . Following the optimization, Brown & Shannon (1973) evaluated the quality of their parameters by calculating root-mean-square *relative* deviations between the sums of the bond-valences of an ion, and its valence (eq. 2.2).

2.11.1.2 Fixing the B parameter

Brown & Altermatt (1985) proposed a new equation to model the bond-length to bond-valence relation:

$$S_{ij} = \exp\left(\frac{R_0 - R_{ij}}{B}\right) \quad (\text{eq. 2.5})$$

where R_{ij} is the bond length between ions i and j , S_{ij} is the bond valence, and R_0 and B are the bond-valence parameters. The valence-sum rule requires that

$$\sum S_{ij} = \sum_j \exp\left(\frac{R_0 - R_{ij}}{B}\right) = V_i \quad (\text{eq. 2.6})$$

Eq. 2.6 may be rearranged to give eq. 2.7:

$$R_0 = B \ln \frac{V_i}{\sum_j \exp\left(\frac{-R_{ij}}{B}\right)} \quad (\text{eq. 2.7})$$

Other than an improved fit, an advantage of this equation is that the B parameter adopts a narrow range of values that has a relatively low influence on the resulting bond-valence sums. This led Brown & Altermatt (1985) to give B a fixed value of 0.37 Å for all ion pairs, which allows exact solution of R_0 for individual cation coordination polyhedra. The value of R_0 for a given ion pair given by Brown & Altermatt (1985) is the geometric mean value for all cation-coordination polyhedra used in the calculation.

2.11.1.3 Graphical method: cation and anion sums

Krivovichev (1999) pointed out that oxygen ions encapsulated as OPb_4 clusters consistently show higher-than-expected bond-valence sums at the central anion, and Krivovichev & Brown (2001) attributed this problem to the choice of bond-valence parameters. They suggested a new method of derivation that refines both R_0 and B using the following equation, obtained by rearrangement of the equation of Brown & Altermatt (1985):

$$R_o = c + kB \quad (\text{eq. 2.8})$$

where c and k are fitted constants. Eq. 2.8 is refined for both the cations and the anions, and the bond-valence parameters are extracted at the intersection of these curves.

Krivovichev (2012) derived 8 pairs of bond-valence parameters using this method, but pointed out that the introduction of anion-centered coordination polyhedra into the refinement greatly limits the applicability of the method; for structures to be usable, not only must the cation make all bonds to the same anion, but the anion must also make all bonds to that same cation. This constraint is of significant importance in data collection and precludes this method being used for most cation-anion pairs.

Furthermore, eq. 2.8 only holds for $B \approx 0.30\text{-}0.60 \text{ \AA}$.

2.11.1.4 Graphical method: cation sums

Sidey (2009) proposed a variation of the method of Krivovichev and Brown (2001) that also allows simultaneous determination of R_o and B where only the bond-valence sums of the cations are optimized. This enhances the applicability of the approach, and the anion bond-valences are checked *a posteriori* to see if they are of acceptable quality.

The valence-sum rule,

$$V_i = \sum_j S_{ij} = \sum_j \exp\left(\frac{R_o - R_{ij}}{B}\right) \quad (\text{eq. 2.9})$$

may be rearranged to

$$\sum_j R_{ij} = R_o - B \sum_j \ln S_{ij} \quad (\text{eq. 2.10})$$

For coordination environments in which all bonds are of the same length, this equation simplifies to

$$\bar{R}_{ij} = R_o - B \ln \bar{S}_{ij} \quad (\text{eq. 2.11})$$

where \bar{R}_{ij} is the mean bond-length and \bar{S}_{ij} is the mean bond-valence.

Graphical representation of $\ln \bar{S}_{ij}$ as a function of \bar{R}_{ij} gives B as the slope and R_o as the y-intercept from a linear least-squares fit for many coordination polyhedra. However, the constraint of equal bond-lengths on the coordination environment greatly restricts the amount of data that can be used with this method. Moreover, the sole use of coordination environments of equal bond-length is generally not recommended in the determination of bond-valence parameters, as they cannot appropriately model the relation over the full range of bond lengths of the ion pairs.

Brown (2009) used an approximation proposed by Urusov (2003) (in dealing with the distortion theorem) in order to circumvent the constraint on the bonding environment. A Taylor expansion is applied to the mean bond-length, \bar{R}_{ij} , to obtain the adjusted mean-bond-length, R_s :

$$R_s = \bar{R}_{ij} - \frac{\delta_2}{2B} + \frac{\delta_3}{3B^2} \quad (\text{eq. 2.12})$$

where δ_2 is the mean-square deviation and δ_3 the mean-cube deviation of the bond lengths from the mean bond-length \bar{R}_{ij} . Substituting R_s for \bar{R}_{ij} in eq. 2.11 and changing the mean bond-valence \bar{S}_{ij} to its ideal value of V_i/n , where V_i is the valence of the cation and n its coordination number:

$$R_s = R_o - B \sum_j \ln \left(\frac{V_i}{n} \right) \quad (\text{eq. 2.13})$$

Solution for the bond-valence parameters then follows the same procedure as for eq. 2.11. Although the graphical method is attractive for providing a solution for both R_o and B , and having wide applicability, it suffers a major drawback in addition to the approximation introduced in eq. 2.12: rather than minimizing deviations between the sum of the bond-valences and the valence of the ion, the parameters derived by this method are based on minimization of bond-length deviations from the mean, and hence do not relate directly to the valence-sum rule. Moreover, this method assumes that variations in mean bond-lengths are solely the result of distortion, whereas variation in coordination number of the anions can also contribute in a major way to variations in mean bond-length (e.g., Shannon, 1976). The method also fails for certain ions showing very large gaps in their bond-length distributions (e.g., H^+ , Se^{4+} , I^{5+} , discussed below).

2.11.1.5 RMSD minimization

Brown (2002) proposed minimizing the squared difference between the sum of the bond valences and the valence (oxidation state) of the ion:

$$\sum_i (V_i - \sum_j S_{ij})^2 \rightarrow 0 \quad (\text{eq. 2.14})$$

Mills et al. (2009) reformulated this optimization into a minimization of the root-mean-square deviation,

$$RMSD = \sqrt{\frac{\sum_{i=1}^n (\sum_j S_{ij} - V_i)^2}{n}} \rightarrow 0 \quad (\text{eq. 2.15})$$

where the minimization is done over n cation coordination-polyhedra. They generally report their results in v.u. but also sometimes in % deviation per unit of charge (eq. 2.2). Whereas eq. 2.14 and 2.15 lead to the same result, eq. 2.15 is more appropriate for reporting these results, as the squared deviation from eq. 2.14 is extensive, *i.e.*, the resultant value is dependent on the number of coordination polyhedra used in the minimization, whereas the RMSD from eq. 2.15 is intensive, *i.e.*, it is independent of the number of coordination polyhedra used.

A significant drawback of the RMSD minimization (although not exclusive to it) is found in its weighting scheme. In this minimization, every coordination polyhedron is weighted equally, meaning that the dominant coordination number of a cation can easily dominate the optimization at the expense of others. A classic example of this failure is for Si^{4+} , with ~ 100 times more data for coordination 4 than for coordination 6. When deriving bond-valence parameters for Si^{4+} by minimizing the RMSD, we obtain stellar agreement for coordination number 4, with a mean bond-valence sum (BVS) of 3.99 v.u., and overall (mean BVS 4.00 v.u., RMSD = 0.097 v.u.), but the refined parameters yield a mean bond-valence sum of 4.54 v.u. for coordination 6. We observe this result to various degrees for all ions with multiple coordination numbers, and hence minimizing the RMSD is often not reliable. However, the minimization can be modified to become an integral part of the method of derivation of choice (next).

2.11.2 Generalized Reduced Gradient (GRG) method of RMSD minimization

To address the problem described above, we (1) use a weighting scheme that finds a balance between overall fit, and fit on the basis of coordination number, and (2) introduce the use of a new search algorithm.

2.11.2.1 The Generalized Reduced Gradient method

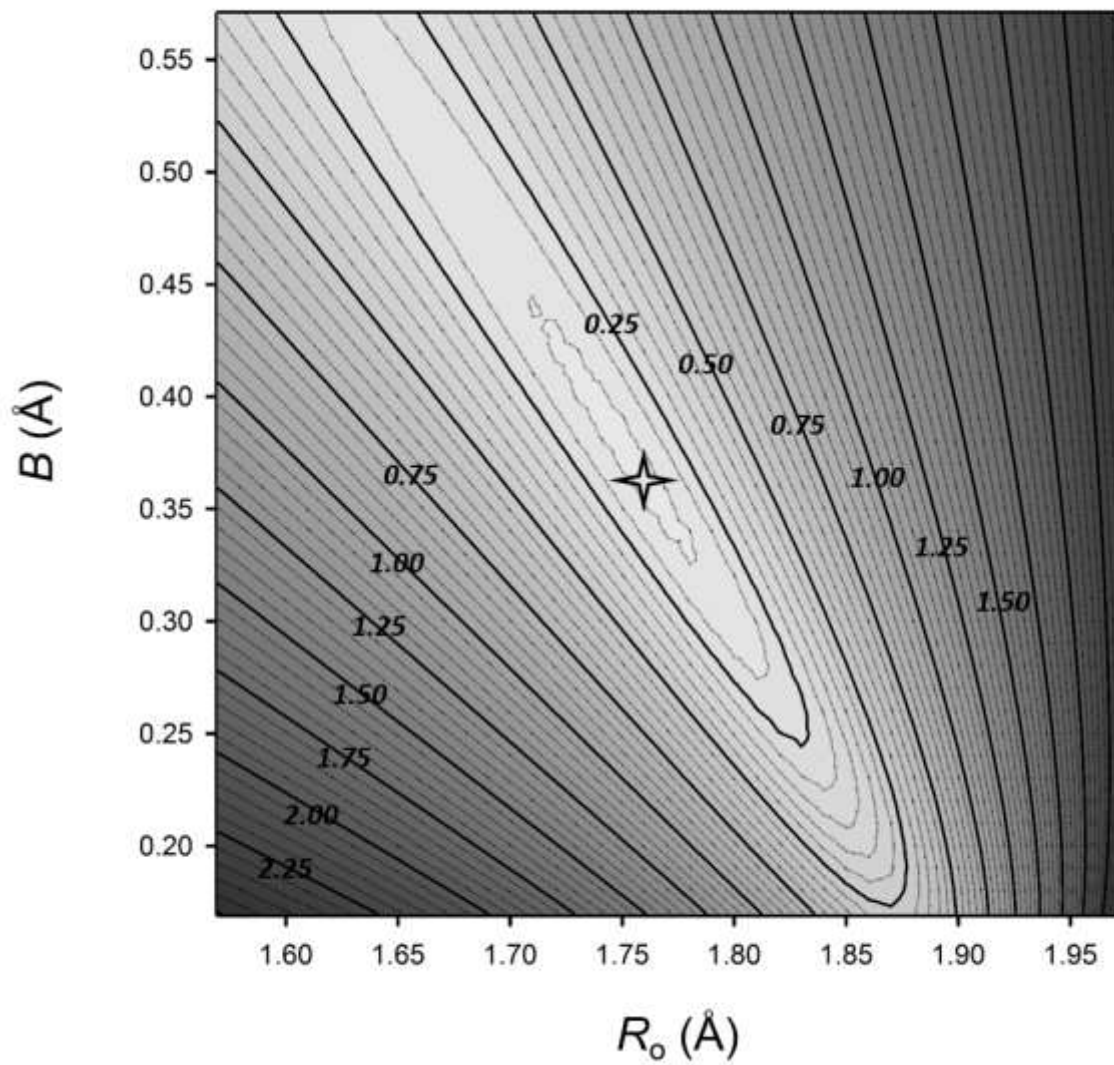
The search for the global minimum involving eq. 2.15 has so far been done iteratively, by varying the bond-valence parameters until a minimum, presumably the global minimum, was found (Mills et al., 2009; Mills & Christy, 2013). However, this method is not practicable where dealing with more than a handful of ions.

We propose using the Generalized Reduced Gradient (GRG) search algorithm (Abadie & Carpentier, 1969) in combination with the RMSD minimization. We chose this algorithm because (1) it can deal with the optimization of non-linear equations, (2) it is very efficient (convergence occurs in a matter of seconds), (3) it is very consistent, and (4) it consistently gives a better fit to the data than other search algorithms used.

While the GRG optimization has proved to be much more effective than an iterative search method, the use of a search algorithm generally raises concern as to whether the minimization obtained is a local minimum as opposed to the global minimum. Mills & Christy (2013) show that contour plots of RMSD as a function of R_0 and B for Te are smooth and concave in shape, but the plots only cover a narrow range of values around the extracted parameters. In Fig. 2.1, we show (for Fe^{3+}) that the shape remains concave over a much larger range of values, and no maxima, saddle points or other minima are observed. As a result, convergence can only lead to the global minimum.

Note that both Fig. 2.1 and the plot of Mills & Christy (2013) show that the contour lines can have a pronounced oval shape; thus different combinations of values for R_0 and B can lead to the same level of fit over a non-negligible range of values for the cations (although different parameters from one contour line may give different anion BVS), which may be deceptive in an iterative search for the global minimum.

Figure 2.1 RMSD (v.u.) from the valence-sum rule as a function of the bond-valence parameters for Fe^{3+} .



2.11.2.2 Weighting scheme

To deal with (1), we introduced a second optimization criterion where we additionally minimize the RMSD between the mean bond-valence sum of the observed coordination numbers of an ion, and the oxidation state of that ion (*i.e.*, coordination-based RMSD minimization). Following experimentation with weighting schemes, we concluded that a 2:1 ratio between overall RMSD and coordination-based RMSD gave the best results, in keeping the overall RMSD low while suppressing the dominant effect of certain coordination numbers.

Hence, the GRG method of RMSD minimization proposed here implicitly entails optimization on both the overall and coordination-based RMSD (denoted hereon as the GRG method), and addresses many shortcomings of the other methods of derivation in that it (1) refines both bond-valence parameters, (2) optimizes the appropriate quantity, (3) does not require approximations, and (4) is universally applicable. The main drawback of this new method (although it is a drawback of most methods) is that it does not optimize the anion bond-valence sums. However, as will be discussed later, optimizing the anion bond-valence sums may not be necessary, and is not practical on the scale of this study. Where using this method, the anions bond-valence sums are tested *a posteriori*.

In this work, the GRG method used a multi-start approach of 1000 random starting pairs of variables until convergence to the 4th decimal place using forward derivative.

2.11.3 Comparison of the most common methods of derivation

First, we will focus on ions that occur in more than one coordination by O^{2-} ; of the 135 ions examined here, 45 have only one coordination number and 90 have more than one coordination number. Table 2.1 compares two common methods of derivation to the GRG method for the 90 ions. The first column gives the RMSD of the set of best published parameters, taken from Table 2.S1. The second column gives the RMSD obtained using the graphical method (eq. 2.13). The third column gives the RMSD by setting $B = 0.370 \text{ \AA}$ and refining R_0 in the same way as the GRG method, and the last column gives the RMSD values for the GRG method, refining both R_0 and B .

Table 2.1 Comparison between the RMSD values (v.u.) of the set of best published bond-valence parameters and the values obtained for bond-valence parameters derived using common methods of derivation for the 90 multiple-coordination-number ions

Ion	No. of coordination polyhedra	Best published parameters	Fixing <i>B</i> at 0.370 Å	Graphical Method	GRG method (this work)
H ⁺	224	0.035	0.532	0.040	0.033
Li ⁺	690	0.092	0.091	0.115	0.077
Be ²⁺	169	0.080	0.092	0.082	0.092
B ³⁺	1572	0.069	0.069	0.068	0.069
N ⁵⁺	497	0.162	0.118	0.164	0.118
Na ⁺	1683	0.132	0.172	0.157	0.143
Mg ²⁺	469	0.120	0.119	0.121	0.110
Al ³⁺	856	0.121	0.109	0.115	0.108
Si ⁴⁺	2530	0.126	0.119	0.128	0.119
Cl ³⁺	5	0.151	0.374	0.087	0.086
K ⁺	1479	0.155	0.212	0.171	0.164
Ca ²⁺	1168	0.171	0.174	0.176	0.163
Sc ³⁺	88	0.152	0.112	0.140	0.108
Ti ³⁺	24	0.183	0.099	0.161	0.094
Ti ⁴⁺	324	0.139	0.155	0.139	0.143
V ³⁺	70	0.130	0.113	0.129	0.115
V ⁴⁺	226	0.121	0.109	0.103	0.105
V ⁵⁺	714	0.117	0.105	0.114	0.105
Cr ²⁺	17	0.090	0.064	0.060	0.060
Cr ⁴⁺	7	0.242	0.156	0.185	0.156
Mn ²⁺	392	0.124	0.124	0.126	0.116
Mn ³⁺	94	0.128	0.173	0.130	0.166

Mn ⁴⁺	21	0.122	0.120	0.122	0.120
Fe ²⁺	192	0.135	0.115	0.133	0.114
Fe ³⁺	466	0.137	0.140	0.138	0.139
Co ²⁺	304	0.102	0.099	0.099	0.100
Ni ²⁺	255	0.105	0.110	0.107	0.107
Cu ⁺	57	0.133	0.081	0.079	0.078
Cu ²⁺	716	0.084	0.103	0.085	0.085
Zn ²⁺	461	0.085	0.086	0.087	0.085
Ga ³⁺	228	0.139	0.139	0.138	0.136
Ge ⁴⁺	350	0.148	0.152	0.148	0.149
As ³⁺	28	0.127	0.485	0.086	0.065
As ⁵⁺	526	0.108	0.111	0.109	0.111
Se ⁴⁺	202	0.147	47.223	0.090	0.083
Br ⁵⁺	9	0.147	3.771	0.104	0.064
Rb ⁺	464	0.186	0.233	0.171	0.150
Sr ²⁺	377	0.222	0.225	0.221	0.189
Y ³⁺	178	0.157	0.140	0.157	0.140
Zr ⁴⁺	117	0.135	0.106	0.135	0.106
Nb ⁵⁺	251	0.161	0.162	0.157	0.157
Mo ⁵⁺	76	0.136	0.252	0.116	0.131
Mo ⁶⁺	970	0.147	0.145	0.140	0.143
Ag ⁺	200	0.088	0.085	0.080	0.081
Cd ²⁺	164	0.122	0.092	0.102	0.088
In ³⁺	125	0.200	0.113	0.143	0.111
Sn ²⁺	50	0.135	0.125	0.147	0.082
Sn ⁴⁺	38	0.195	0.158	0.196	0.158
Sb ³⁺	54	0.085	0.178	0.130	0.084

Te ⁴⁺	212	0.107	4x10 ⁴	0.108	0.104
I ⁵⁺	134	0.113	108.803	0.130	0.107
I ⁷⁺	36	0.327	0.199	0.212	0.196
Cs ⁺	544	0.138	0.176	0.143	0.135
Ba ²⁺	857	0.237	0.248	0.231	0.217
La ³⁺	182	0.162	0.159	0.153	0.155
Ce ³⁺	76	0.162	0.132	0.137	0.131
Ce ⁴⁺	28	0.176	0.124	0.154	0.122
Pr ³⁺	99	0.185	0.135	0.146	0.134
Nd ³⁺	203	0.160	0.163	0.159	0.159
Sm ³⁺	97	0.171	0.149	0.150	0.145
Eu ²⁺	3	0.071	0.028	0.047	0.024
Eu ³⁺	49	0.196	0.142	0.132	0.134
Gd ³⁺	107	0.188	0.141	0.138	0.129
Tb ³⁺	48	0.122	0.116	0.117	0.115
Dy ³⁺	70	0.174	0.134	0.134	0.129
Ho ³⁺	81	0.188	0.129	0.133	0.128
Er ³⁺	102	0.141	0.138	0.134	0.133
Tm ³⁺	44	0.184	0.146	0.143	0.140
Yb ³⁺	82	0.169	0.260	0.172	0.174
Lu ³⁺	53	0.175	0.171	0.170	0.162
Hf ⁴⁺	22	0.095	0.087	0.087	0.087
Ta ⁵⁺	162	0.214	0.183	0.185	0.195
W ⁶⁺	436	0.181	0.207	0.182	0.188
Re ⁷⁺	59	0.923	0.192	0.237	0.191
Os ⁷⁺	7	-	0.230	0.197	0.209
Os ⁸⁺	8	0.608	0.264	0.266	0.233

Ir ⁴⁺	17	0.243	0.136	0.239	0.136
Hg ²⁺	52	0.129	0.143	0.120	0.120
Tl ⁺	74	0.113	0.101	0.113	0.098
Tl ³⁺	9	0.294	0.080	0.145	0.079
Pb ²⁺	276	0.125	0.118	0.177	0.111
Pb ⁴⁺	12	0.286	0.184	0.219	0.181
Bi ³⁺	231	0.190	0.149	0.152	0.138
Bi ⁵⁺	11	0.316	0.202	0.195	0.203
Th ⁴⁺	27	0.221	0.167	0.182	0.163
U ⁴⁺	18	0.166	0.123	0.116	0.116
U ⁵⁺	4	0.239	0.089	0.214	0.030
U ⁶⁺	585	0.158	0.786	0.226	0.161
Np ⁵⁺	33	0.820	0.126	0.073	0.061
Np ⁶⁺	7	1.209	0.745	0.169	0.083
Weighted mean		0.140	*0.161	0.139	0.128
# Improvements			59	62	76

*Without the values for Se⁴⁺, Br⁵⁺, Te⁴⁺ and I⁵⁺ where the method fails

We use the set of best published parameters (Table 2.S1) as a benchmark to evaluate the other methods. Table 2.1 shows that the graphical method gives better parameters for 59 of the 90 ions with more than one coordination number, 62 for the method of fixing B at 0.37 Å, and 76 for the GRG method. One of the major problems of the graphical method is observed for ions showing large gaps in their bond-length distributions, such as Se^{4+} (RMSD = 47.223 v.u.), Te^{4+} (4×10^4 v.u.), I^{5+} (108.803 v.u.), where the approximation of the “adjusted mean bond-length (R_s)” fails, and unusual values of the bond-valence parameters are obtained (e.g., $R_0 = 2.119$ and $B = -0.052$ for Te^{4+}).

In terms of the mean weighted-RMSD (weighted by the number of coordination polyhedra), a higher value is obtained for the graphical method than for the set of best published parameters with values of 0.161 v.u. (7.96% per unit of charge) and 0.140 v.u. (6.5% per unit of charge), respectively, despite omitting the ions with RMSD > 1 v.u. in the calculation for the graphical method. The method of fixing B gives an overall fit similar to the set of best published parameters, with a mean weighted-RMSD of 0.139 v.u. (6.7% per unit of charge). In contrast, the GRG method shows significant lowering of the mean weighted-RMSD with 0.128 v.u. (6.1% per unit of charge).

These results for the GRG method are welcome improvements, and confirm our choice of a 2:1 weighting scheme between overall RMSD and coordination-based RMSD. This weighting scheme thus allows a significant improvement in overall fit for cations, without sacrificing the fit of the different coordination numbers of the cations (*i.e.*, allowing a very small increase in the RMSD leads to overwhelmingly better agreements over the entire range of coordination numbers of an ion). Moreover, we found the GRG method

to give much better bond-valence sums for the anions than a regular RMSD minimization (see below).

2.11.4 General considerations

2.11.4.1 Optimizing both cation and anion bond-valence sums

The valence-sum rule states that the sum of the bond valences for an ion is equal to the valence of that ion (Brown, 2002), and does not discriminate between cations and anions. The tendency to focus on the bond-valence sums of the cations more than those of the anions arises from the fact that cation-centered coordination polyhedra commonly involve a single type of anion, whereas anion-centered coordination polyhedra commonly do not, although exceptions such as MgO and NaCl do occur.

Modifying eq. 2.15 to include the m anions in the summation leads to:

$$RMSD = \sqrt{\frac{\sum_{i=1}^{n+m} (\sum_j S_{ij} - V_i)^2}{n+m}} \rightarrow 0 \quad (\text{eq. 2.16})$$

Eq. 2.16 can be solved in two ways to extract the bond-valence parameters. First, the optimization can be done on the basis of individual crystal structures, and the resulting parameters are averaged over all crystal structures used. However, the requirement of having at least two unique and linearly-independent coordination environments (*e.g.*, two cation environments in different coordination numbers, or 1 cation environment and 1 anion environment for the same ion pair) for every bonded pair of ions in every crystal structure renders this method practically inoperable.

The second (and more conventional) way of solving eq. 2.16 consists of optimizing the bond-valence sums on the basis of single coordination polyhedra. In this case, bonding environments are recorded for both cations and anions. A single optimization is then run for the coordination polyhedra of all crystal structures combined, to simultaneously solve for the bond-valence parameters of all pairs of ions. Whereas this removes the constraint on the bonding environments that makes the solution on the basis of individual crystal structures impractical, this method introduces a new drawback: the ensuing optimization results in a large system of (non-linear) equations, of dimension D where

$$D = 2(nm) \quad (\text{eq. 2.17})$$

where n and m are the numbers of cations and anions, respectively, and D is the minimum number of linearly-independent equations required to solve eq. 2.16 for all bond-valence parameters. Furthermore, any sensible attempt at solving eq. 2.16 using this approach necessarily entails a highly over-determined system of equations for the results to be significant. In this study, we have 135 cations bonded to a single anion (O^{2-}), and thus $D = 270$. Whereas we need a minimum of 270 equations to solve eq. 2.16 for the 135 pairs of bond-valence parameters, we derived 31,521 non-linear equations from the valence-sum rule, for the cation coordination polyhedra alone. We did not collect the bond-length data of anion-centered coordination polyhedra, but the number of resulting equations would be somewhat similar. While the simultaneous optimization of ~60,000 270-dimensional non-linear equations may not be impossible, this kind of calculation is very impractical.

A number of approximations can be made to circumvent this problem: (1) limit the number of ion environments in the refinement to only a couple of ions (e.g., Krivovichev, 2012), (2) increase the “universality” of the parameterization to lower the number of bond-valence parameters (e.g., one pair per isoelectronic series; Brown & Shannon, 1973), or (3) optimize the cation bond-valence sums only, and verify that the anion sums work *a posteriori*.

2.11.4.2 On the universality of the bond-valence equation

The universality of the bond-length to bond-valence relation is generally understood to mean the transferability of the relation between pairs of ions from structure to structure. However, it is important to realize that selection of the level of universality on the basis of pairs of ions is arbitrary, and depends on the quality of fit desired.

Bond-valence parameters can be derived with different levels of universality. Coulomb’s law, which is arguably at the core of the relation (Preiser *et al.*, 1999), offers an extreme case where only eight pairs of bond-valence parameters are required to model all ions bonding to oxygen (*i.e.*, a pair of bond-valence parameters for each cation oxidation state, 1+ to 8+). However, this parameterization would yield a very poor fit due to effects that are not transferable between ions of the same charge. Conversely, reducing the universality from ion pairs to (for example) specific coordination environments would increase the fit of the relation, though at the cost of becoming very cumbersome. Two levels of universality are compared by Brown and Shannon (1973) in their initial description of the relation. They derive parameters based on isoelectronic series,

reporting a root-mean-square *relative* deviation (eq. 2.2) of 5.4% per unit of charge for a total of 27 ion pairs, compared to 4.0% per unit of charge for parameters derived for individual ion pairs. This result led to a widespread use and derivation of parameters based on ion pairs, which today still seems like the best compromise between universality and fit.

2.11.4.3 Minimization using a priori bond-valences

A priori bond-valences (called *theoretical* by Brown, 1987; and *ideal* by Brown, 2013) are obtained by solution of the network equations of a crystal structure (see Brown, 2002). Brown (2002) suggests optimizing the bond-valence parameters on the basis of minimization of the squared difference between observed and *a priori* bond-valences. This approach has not yet been examined, and we note that it is not equivalent to the methods examined above (section 2.11.1). Aside from the method of Krivovichev (2001, 2012), the methods examined above rely on minimizing the RMSD of the bond-valence sums around the cations and omit consideration of the anions. As *a priori* bond-valences are derived from all the valence-sum-rule equations in a structure (usually augmented by loop equations), it follows that optimizing bond-valence parameters with reference to observed and *a priori* bond-valences is equivalent to optimizing the valence-sum rule for all ions (cations and anions) in a structure. However, this method faces a similar constraint as for the solution of eq. 2.16: a very large number of high-dimensional non-linear equations to solve.

2.11.5 The bond-length—bond-valence equation

We now have an effective method for the derivation of bond-valence parameters (the GRG method), and have determined that (1) the minimization should be done on the cation bond-valence sums, while the anion bond-valence sums are verified *a posteriori*, and (2) the most useful level of universality remains on the basis of ion pairs. In this section, we use these criteria to examine new potential equations to describe the bond-length—bond-valence relation.

2.11.5.1 Evolution of the bond-length—bond-valence equation

Generalization of eq. 2.15 shows that the desired optimization entails minimization of the difference between the valence of the cation V_i and some function of the independent parameter x_i , $f(x_i)$:

$$V_i - \sum f(x_i) \rightarrow 0 \quad (\text{eq. 2.18})$$

Pauling (1929) first used coordination number as the independent parameter:

$$f(x_i) = \frac{V_i}{n_i} \quad (\text{eq. 2.19})$$

where n_i is the coordination number of cation i . Taking the sum on each side of eq. 2.19,

$$\sum f(x_i) = \sum \frac{V_i}{n_i} = n_i \left(\frac{V_i}{n_i} \right) = V_i \quad (\text{eq. 2.20})$$

Eq. 2.18 (and by extension eq. 2.15) has an exact solution:

$$V_i - \sum f(x_i) = V_i - V_i = 0 \quad (\text{eq. 2.21})$$

In short, Pauling suggested an exact solution to eq. 2.15. However, with this parameterization, there is the lack of correspondence between the resulting anion bond-strength sums and the oxidation states of the anion(s).

Pauling (1947) proposed using bond length as a parameter in describing electron-sharing in metallic bonds:

$$R(1) - R(n) = 0.300 \log n \quad (\text{eq. 2.22})$$

where $R(1)$ is the length of the shortest bond in the coordination polyhedron, $R(n)$ is the length of the bond considered, and n is the bond number (the number of bonding electrons). This equation was used by Byström & Wilhelmi (1951) to show (from bond-length considerations) that the sum of the bond numbers around V in V_2O_5 is 4.96, fairly close to the vanadium oxidation state of 5. Subsequent contributions to the relation (Smith, 1953; Zachariasen, 1954; Zachariasen & Plettinger, 1959; Zachariasen, 1963; Evans & Mrose, 1960; Evans, 1960; Pant & Cruikshank, 1967; Clark *et al.*, 1969; Perloff, 1970; Donnay & Allmann, 1970) led to a major advance in the parameterization of $f(x_i)$ by Brown & Shannon (1973) who proposed a *universal* correlation between bond length and bond strength (transferrable from structure to structure) using eq. 2.2. This equation was later updated by Brown & Altermatt (1985) to eq. 2.5, which is still in use today. Other equations have been proposed (Ziółkowski, 1985; Naskar *et al.*, 1997; Valach, 1999; Mohri, 2000) that commonly attempt to give a physical justification to the bond-length—bond-valence relation, but they are of more complicated form and have not seen wide application.

Note that the choice of bond length as parameter, although well-ingrained in the bond-valence method, is not required by bond-valence *theory*, as none of the three axioms of the theory (see Brown, 2002) mention bond lengths, and it is feasible in principle that other parameters could be found in the future.

2.11.5.2 Derivation of new equations

In deriving new equations to model the relation, we must keep in mind that the number of coordination environments required to solve for the bond-valence parameters of a pair of ions is at least equal to the number of parameters of the equation used in describing the relation. In other words, the addition of parameters to increase the degree of fit is not without consequences, as many ions have few different coordination numbers. The conventional choice of a two-parameter equation to represent the bond-valence relation means that at least two distinct coordination environments are necessary to solve for the parameters of the equation. As noted above, of the 135 ions examined in this work, 45 ions occur in only one coordination, making this a common and significant problem in the derivation of bond-valence parameters.

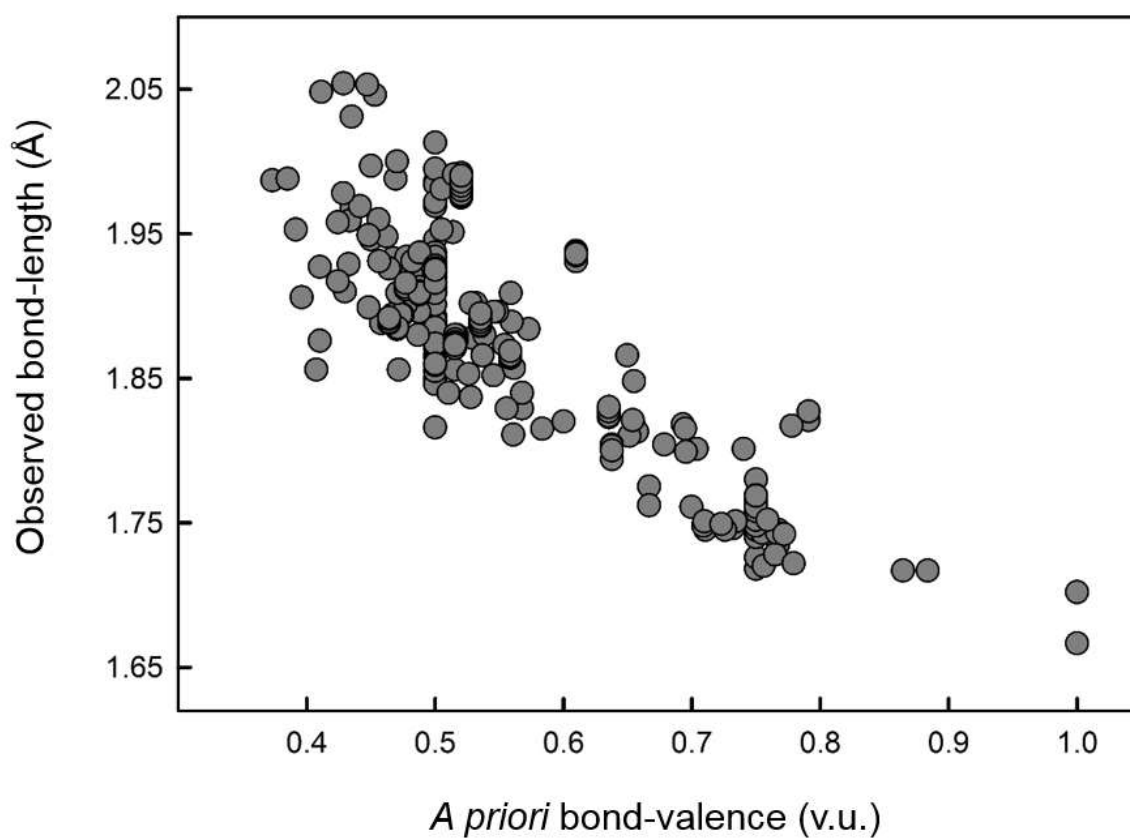
To derive new equations for the description of the bond-length to bond-valence relation, we focused on a specific ion assumed to be representative of the relation. We used Al^{3+} for this purpose as (1) it covers a wide range of bond-valences, (2) a large amount of structural data on crystals containing Al is available.

Fifty-one crystal structures containing Al^{3+} were selected from the Inorganic Crystal Structure Database (ICSD), following a strict set of filtering criteria: (1) the site of

interest is fully occupied by Al^{3+} ; (2) $R_1 < 3\%$; (3) the structure contains no H; (4) all sites in the structure are fully occupied and show no positional disorder; (5) the structure is not extensively strained; (6) the structure contains no ions showing known stereochemical electronic effects (e.g., $^{[6]}\text{Cu}^{2+}$, $^{[6]}\text{Mn}^{3+}$); (7) crystallographic data were measured at ambient conditions; (8) there is no heterovalent solid solution at any site; (9) there is no more than 10% homovalent solid-solution at any site other than that occupied by Al^{3+} . The coordination polyhedra must also be clearly defined; any doubt resulted in a discarded entry. Table 2.S2 gives the ICSD code of the resulting 51 crystal structures, their R -value (average = 1.9%), and the number of Al-centered coordination polyhedra used for each structure (for a total of 90). Note that duplicate structure types are used, as long as there is a significant change in site occupancy.

The network equations were derived for each of the 51 crystal structures to determine their *a priori* bond-valences using the method of Rutherford (1990). The *a priori* bond-valences were then compared with their respective experimental bond-lengths, for a total of 481 pairs. The resulting plot is shown in Fig. 2.2. A series of simple equations were then fitted to the data points by least-squares minimization. These equations are considered next.

Figure 2.2 Determination of the curvature of the bond-valence relation by a match of the *a priori* bond-valences to their observed bond-lengths.



2.11.5.3 Two-parameter equations: sample evaluation

The top seventeen two-parameter equations obtained in the above fitting procedure were selected for further analysis. These equations are given in Table 2.2 and are identified by the numbers in square brackets. They include the exponential equation of Brown & Altermatt (1985) as equation [1]. We group the three equations containing an external parameter (a parameter that is not a multiplier of x) as equations [15]-[17], and add two more equations: the original equation of Brown & Shannon (1973), equation [18], and an expression related to the Born-Landé equation, equation [19].

To evaluate these equations, we considered eight relatively common ions that cover different types of bonding behaviour: Na^+ , Al^{3+} , Si^{4+} , Ca^{2+} , Mn^{2+} , Mo^{6+} , La^{3+} and Pb^{2+} . We used the GRG method to derive bond-valence parameters for each of these eight ions bonded to O^{2-} for the nineteen equations of Table 2.2.

Table 2.2 RMSD values (v.u.) for a sample of ions for 19 different two-parameter equations fitted with the GRG method

	Equation	Na ⁺	Al ³⁺	Si ⁴⁺	Ca ²⁺	Mn ²⁺	Mo ⁶⁺	La ³⁺	Pb ²⁺	Mean
[1]	$y = \exp((a-x)/b)$	0.143	0.108	0.119	0.163	0.116	0.143	0.155	0.111	0.132
[2]	$y = (a+bx)^2$	0.127	0.114	0.109	0.164	0.129	0.129	0.180	0.117	0.134
[3]	$y = (a+b\ln(x))^2$	0.129	0.111	0.113	0.163	0.114	0.131	0.172	0.110	0.130
[4]	$y = (a+bx^{0.5})^2$	0.129	0.112	0.111	0.163	0.119	0.129	0.176	0.113	0.132
[5]	$y = 1/(a+bx)$	0.136	0.109	0.147	0.174	0.109	0.316	0.158	0.178	0.166
[6]	$y = 1/(a+bx^{0.5})$	0.155	0.110	0.151	0.175	0.109	0.339	0.162	0.186	0.173
[7]	$y = 1/(a+bx^{1.5})$	0.166	0.109	0.144	0.173	0.109	0.292	0.155	0.170	0.165
[8]	$y = 1/(a+bx^{0.5}\ln(x))$	0.159	0.109	0.148	0.174	0.096	0.322	0.159	0.180	0.168
[9]	$y = 1/(a+b\exp(-x))$	0.147	0.112	0.160	0.178	0.110	0.410	0.178	0.219	0.189
[10]	$y = 1/(a+b\exp(x))$	0.136	0.108	0.136	0.168	0.111	0.233	0.147	0.140	0.147
[11]	$y = \exp(a+bx^{0.5})$	0.133	0.108	0.122	0.163	0.115	0.150	0.153	0.114	0.132
[12]	$y = \exp(a+b\ln(x))$	0.135	0.107	0.125	0.164	0.114	0.159	0.151	0.118	0.134
[13]	$y = \exp(a+b\exp(-x))$	0.139	0.107	0.129	0.168	0.112	0.178	0.147	0.136	0.139
[14]	$y = (a+b\exp(-x))^2$	0.132	0.109	0.117	0.162	0.115	0.136	0.160	0.110	0.130
[15]*	$y = a+b\exp(-x)$	0.128	0.117	0.107	0.165	0.118	0.143	0.188	0.126	0.136
[16]*	$y = a+bx^{0.5}$	0.127	0.123	0.101	0.173	0.123	0.178	0.211	0.168	0.151
[17]*	$y = a+b\ln(x)$	0.127	0.120	0.104	0.170	0.121	0.165	0.206	0.157	0.146

<u>[18]</u> **	$y = s_0(a/x)^{-b}$	0.135	0.107	0.125	0.164	0.114	0.159	0.151	0.118	0.134
<u>[19]</u> **	$y = a/x^2 + b/r^3$	0.132	0.109	0.121	0.162	0.114	0.140	0.167	0.109	0.132

*Has external parameter

**Added manually

Table 2.2 gives the RMSD obtained by the GRG method for each equation, for each ion. Thus, the current form of the relation, equation [1], gives a mean RMSD of 0.132 v.u for the ions considered. Many equations give a RMSD similar to that of equation [1], and five of the nineteen equations [3, 4, 11, 14, 19] give a slightly lower mean RMSD (including the expression related to the Born-Landé equation). The original equation of Brown & Shannon (1973), equation [18], also gives reasonable results with a mean RMSD of 0.134 v.u. for the sample of ions considered. The mean RMSD of the fourteen best-fit equations with no external parameters [1-14] is 0.148 v.u. The top 3 equations with one external parameter (equations [15-17]) have a mean RMSD of 0.144 v.u., which indicates that although the presence of an external parameter removes some flexibility in the shape of the curve, it does not necessarily reduce the fit.

2.11.5.4 Two-parameter equations: full evaluation of best equations

Next, we selected six two-parameter equations that gave a similar or better fit to that of the equation of Brown and Altermatt (1985; equation [1]) on the sample of eight ions (equations [2,3,4,14,15,19]) and compared them to that equation for the 90 multiple-coordination-number ions of our bond-length dispersion analysis. Bond-valence parameters were derived for the seven equations, for each of the 90 ions, using the GRG method of derivation. The resulting RMSD for the six equations obtained for the 90 ions are given in Table 2.S3. Using the number of coordination polyhedra for each ion as a weighting factor, equations [3, 4 and 14] give a mean weighted-RMSD of 0.128 v.u., equations [2 and 19] 0.129 v.u., and equation [15] 0.130 v.u., compared to 0.128 v.u. (Table 2.1) for equation [1].

In addition to the similarity of the overall values, there is little spread in the RMSD values of the different equations of Table 2.S3 (mean standard deviation of 0.005 v.u. on the basis of ions). This leads to two conclusions: (1) many equations (and in various forms) can describe the relation, and (2) we have likely reached a plateau in the fit for two-parameter equations. It is notable that the equation of Brown & Altermatt (1985) leads to the best fit (tied here with equations [3, 4 and 14]), even though we derive the equation and its bond-valence parameters in a different way than Brown & Altermatt, and on a very different dataset. This is a welcome result, as it does not warrant update of the well-established “exponential equation”; only an improved set of bond-valence parameters is needed.

2.11.5.5 Three-parameter equations: sample evaluation

Next, we examined three-parameter equations using the same procedure as above. Six three-parameter equations were selected for evaluation over the sample of ions (above) and are given in Table 2.3 (equations [20-25]). We also add a third (external) parameter to the best two-parameter equation of Table 2.2 (equation [26]), bringing the total to seven three-parameter equations.

Table 2.3 RMSD values (v.u.) for a sample of ions for 7 different three-parameter equations fitted with the GRG method

	Equation	Na ⁺	Al ³⁺	Si ⁴⁺	Ca ²⁺	Mn ²⁺	Mo ⁶⁺	La ³⁺	Pb ²⁺	Mean
[20]	$y = \exp(a+bx+cx^2)$	0.127	0.105	0.075	0.159	0.114	0.120	0.146	0.107	0.119
[21]	$y = (a+bx+cx^2)^2$	0.127	0.104	0.075	0.159	0.110	0.125	0.147	0.108	0.119
[22]	$y = 1/(a+bx+cx^2)$	0.126	0.108	0.078	0.159	0.110	0.115	0.146	0.107	0.119
[23]	$y = (a+cx)/(1+bx)$	0.127	0.117	0.117	0.165	0.117	0.129	0.152	0.114	0.130
[24]	$y = (a+cx^2)/(1+bx^2)$	0.127	0.114	0.117	0.162	0.115	0.130	0.150	0.110	0.128
[25]	$y = (a+cx^{0.5})/(1+bx^{0.5})$	0.127	0.118	0.117	0.166	0.119	0.129	0.153	0.117	0.131
[26]*	$y = (a+b\ln(x))^2+c$	0.127	0.103	0.161	0.159	0.110	0.129	0.147	0.108	0.130

*Added manually

The lowest mean weighted-RMSD for the sample was obtained for equations [20-22] with a value of 0.119 v.u., compared to 0.130 v.u. for the best two-parameter equation (Table 2.2, equation [3]). Despite the decrease in RMSD, there are three drawbacks that make the three-parameter equations less attractive: (1) the derivation of the bond-valence parameters requires at least three coordination-environments per ion; (2) the search for the global minimum of the RMSD (for evaluation of the bond-valence parameters) becomes much less reliable as the RMSD landscape becomes more complicated; (3) the bond-valence parameters cannot be extrapolated to ions with less than three coordination numbers because of high variability, and, of the 135 ions used here, 64 ions have less than three coordination numbers. Thus three-parameter fits do not seem desirable, at least at the present time.

2.11.5.6 The bond-valence equation: conclusions

From our search for a new equation, we conclude that (1) many equations can model the bond-length—bond-valence relation adequately; (2) the loss of trends in the bond-valence parameters for three-parameter equations discourages their use; (3) the current form of the relation given by Brown & Altermatt (1985) shows the best compromise between applicability and fit.

2.11.6 New bond-valence parameters

New bond-valence parameters were derived in the same way as for the trial equations (above), that is by minimization of the difference between the sum of the bond valences of an ion and its valence using the GRG method. The bond-valence parameters of the 90 ions with more than one coordination number are given in Table 2.4 for the equation of Brown & Altermatt (1985). Table 2.4 also includes 45 additional pairs of parameters for those ions with only one coordination number, to bring the total to 135 pairs of bond-valence parameters. The parameters for the 45 additional ions are identified by a number (from 1 to 3), depending on how these parameters were derived (see below).

Table 2.4 New bond-valence parameters derived with the GRG method

Ion	No. of coordination polyhedra	R_o (Å)	B (Å)	RMSD (v.u.)	Method of derivation (1-CN ions)
H ⁺	224	0.918	0.427	0.033	
Li ⁺	690	1.062	0.642	0.077	
Be ²⁺	169	1.429	0.297	0.092	
B ³⁺	1572	1.372	0.357	0.069	
C ⁴⁺	433	1.398	0.399	0.086	3
N ⁵⁺	497	1.492	0.482	0.118	
Na ⁺	1683	1.695	0.420	0.143	
Mg ²⁺	469	1.608	0.443	0.110	
Al ³⁺	856	1.634	0.390	0.108	
Si ⁴⁺	2530	1.624	0.389	0.119	
P ³⁺	7	1.655	0.399	0.079	3
P ⁵⁺	3691	1.624	0.399	0.099	3
S ⁴⁺	30	1.643	0.399	0.087	3
S ⁶⁺	906	1.634	0.399	0.111	3
Cl ³⁺	5	1.722	0.370	0.086	
Cl ⁵⁺	9	1.703	0.428	0.068	2
Cl ⁷⁺	65	1.669	0.428	0.138	2
K ⁺	1479	2.047	0.398	0.164	
Ca ²⁺	1168	1.907	0.409	0.163	
Sc ³⁺	88	1.780	0.452	0.108	
Ti ³⁺	24	1.654	0.545	0.094	
Ti ⁴⁺	324	1.819	0.342	0.143	
V ³⁺	70	1.718	0.412	0.115	

V ⁴⁺	226	1.776	0.364	0.105	
V ⁵⁺	714	1.799	0.388	0.105	
Cr ²⁺	17	1.761	0.350	0.060	
Cr ³⁺	104	1.725	0.361	0.114	1
Cr ⁴⁺	7	1.783	0.410	0.156	
Cr ⁵⁺	1	1.777	0.375	-	2
Cr ⁶⁺	169	1.799	0.375	0.146	2
Mn ²⁺	392	1.740	0.417	0.116	
Mn ³⁺	94	1.823	0.247	0.166	
Mn ⁴⁺	21	1.750	0.374	0.120	
Mn ⁵⁺	8	1.781	0.375	0.091	2
Mn ⁶⁺	2	1.814	0.375	0.118	2
Mn ⁷⁺	7	1.819	0.375	0.121	2
Fe ²⁺	192	1.658	0.447	0.114	
Fe ³⁺	466	1.766	0.360	0.139	
Co ²⁺	304	1.698	0.376	0.100	
Co ³⁺	15	1.655	0.364	0.100	1
Co ⁴⁺	1	1.729	0.358	-	1
Ni ²⁺	255	1.689	0.347	0.107	
Ni ⁴⁺	5	1.734	0.335	0.040	1
Cu ⁺	57	1.601	0.335	0.078	
Cu ²⁺	716	1.687	0.355	0.085	
Cu ³⁺	11	1.737	0.375	0.137	2
Zn ²⁺	461	1.684	0.383	0.085	
Ga ³⁺	228	1.736	0.345	0.136	
Ge ⁴⁺	350	1.750	0.363	0.149	
As ³⁺	28	1.775	0.423	0.065	

As ⁵⁺	526	1.765	0.352	0.111	
Se ⁴⁺	202	1.805	0.401	0.083	
Se ⁶⁺	191	1.797	0.399	0.104	3
Br ⁵⁺	9	1.890	0.571	0.064	
Br ⁷⁺	2	1.850	0.428	0.052	2
Rb ⁺	464	1.993	0.478	0.150	
Sr ²⁺	377	1.958	0.479	0.189	
Y ³⁺	178	1.978	0.407	0.140	
Zr ⁴⁺	117	1.913	0.406	0.106	
Nb ⁴⁺	3	1.853	0.479	0.048	1
Nb ⁵⁺	251	1.909	0.369	0.157	
Mo ³⁺	5	1.792	0.436	0.053	1
Mo ⁴⁺	9	1.834	0.404	0.053	1
Mo ⁵⁺	76	1.888	0.314	0.131	
Mo ⁶⁺	970	1.903	0.349	0.143	
Tc ⁷⁺	6	1.915	0.375	0.070	2
Ru ³⁺	3	1.745	0.401	0.004	1
Ru ⁴⁺	8	1.833	0.366	0.121	1
Ru ⁵⁺	23	1.894	0.346	0.156	1
Rh ³⁺	11	1.769	0.369	0.162	1
Rh ⁴⁺	3	1.836	0.422	0.088	1
Pd ²⁺	29	1.749	0.375	0.104	2
Pd ⁴⁺	2	1.856	0.352	0.038	1
Ag ⁺	200	1.875	0.359	0.081	
Cd ²⁺	164	1.827	0.430	0.088	
In ³⁺	125	1.823	0.459	0.111	
Sn ²⁺	50	1.910	0.451	0.082	

Sn ⁴⁺	38	1.946	0.274	0.158	
Sb ³⁺	54	1.932	0.435	0.084	
Sb ⁵⁺	183	1.892	0.475	0.167	1
Te ⁴⁺	212	1.960	0.389	0.104	
Te ⁶⁺	155	1.922	0.387	0.208	2
I ⁵⁺	134	1.992	0.474	0.107	
I ⁷⁺	36	1.930	0.299	0.196	
Cs ⁺	544	2.296	0.411	0.135	
Ba ²⁺	857	2.223	0.406	0.217	
La ³⁺	182	2.179	0.359	0.155	
Ce ³⁺	76	2.114	0.389	0.131	
Ce ⁴⁺	28	2.046	0.416	0.122	
Pr ³⁺	99	2.071	0.411	0.134	
Nd ³⁺	203	2.103	0.371	0.159	
Sm ³⁺	97	2.049	0.404	0.145	
Eu ²⁺	3	1.943	0.490	0.024	
Eu ³⁺	49	2.068	0.359	0.134	
Gd ³⁺	107	1.988	0.433	0.129	
Tb ³⁺	48	2.020	0.379	0.115	
Tb ⁴⁺	7	2.018	0.395	0.069	2
Dy ³⁺	70	2.002	0.389	0.129	
Ho ³⁺	81	1.993	0.387	0.128	
Er ³⁺	102	1.991	0.373	0.133	
Tm ³⁺	44	1.977	0.381	0.140	
Yb ³⁺	82	1.969	0.373	0.174	
Lu ³⁺	53	1.939	0.403	0.162	
Hf ⁴⁺	22	1.923	0.375	0.087	

Ta ⁵⁺	162	1.916	0.343	0.195	
W ⁵⁺	4	1.848	0.553	0.128	1
W ⁶⁺	436	1.909	0.339	0.188	
Re ⁵⁺	3	1.834	0.557	0.033	1
Re ⁷⁺	59	1.943	0.406	0.191	
Os ⁵⁺	4	1.870	0.485	0.045	1
Os ⁶⁺	1	1.904	0.375	-	2
Os ⁷⁺	7	1.937	0.349	0.209	
Os ⁸⁺	8	1.966	0.405	0.233	
Ir ³⁺	1	1.755	0.414	-	1
Ir ⁴⁺	17	1.909	0.258	0.136	
Ir ⁵⁺	6	1.909	0.449	0.138	1
Pt ²⁺	3	1.742	0.375	0.040	2
Pt ⁴⁺	33	1.856	0.407	0.136	1
Au ³⁺	24	1.890	0.375	0.095	2
Hg ²⁺	52	1.947	0.370	0.120	
Tl ⁺	74	2.063	0.422	0.098	
Tl ³⁺	9	1.874	0.504	0.079	
Pb ²⁺	276	2.032	0.442	0.111	
Pb ⁴⁺	12	2.056	0.280	0.181	
Bi ³⁺	231	2.068	0.389	0.138	
Bi ⁵⁺	11	2.050	0.318	0.203	
Th ⁴⁺	27	2.117	0.420	0.163	
U ⁴⁺	18	2.100	0.373	0.116	
U ⁵⁺	4	2.009	0.660	0.030	
U ⁶⁺	585	2.046	0.473	0.161	
Np ⁵⁺	33	2.036	0.411	0.061	

Np ⁶⁺	7	2.022	0.523	0.083	
Np ⁷⁺	2	2.076	0.477	0.132	2
Am ³⁺	1	2.068	0.392	-	1
Cm ³⁺	1	2.034	0.412	-	1

1: R_o fixed to predicted value

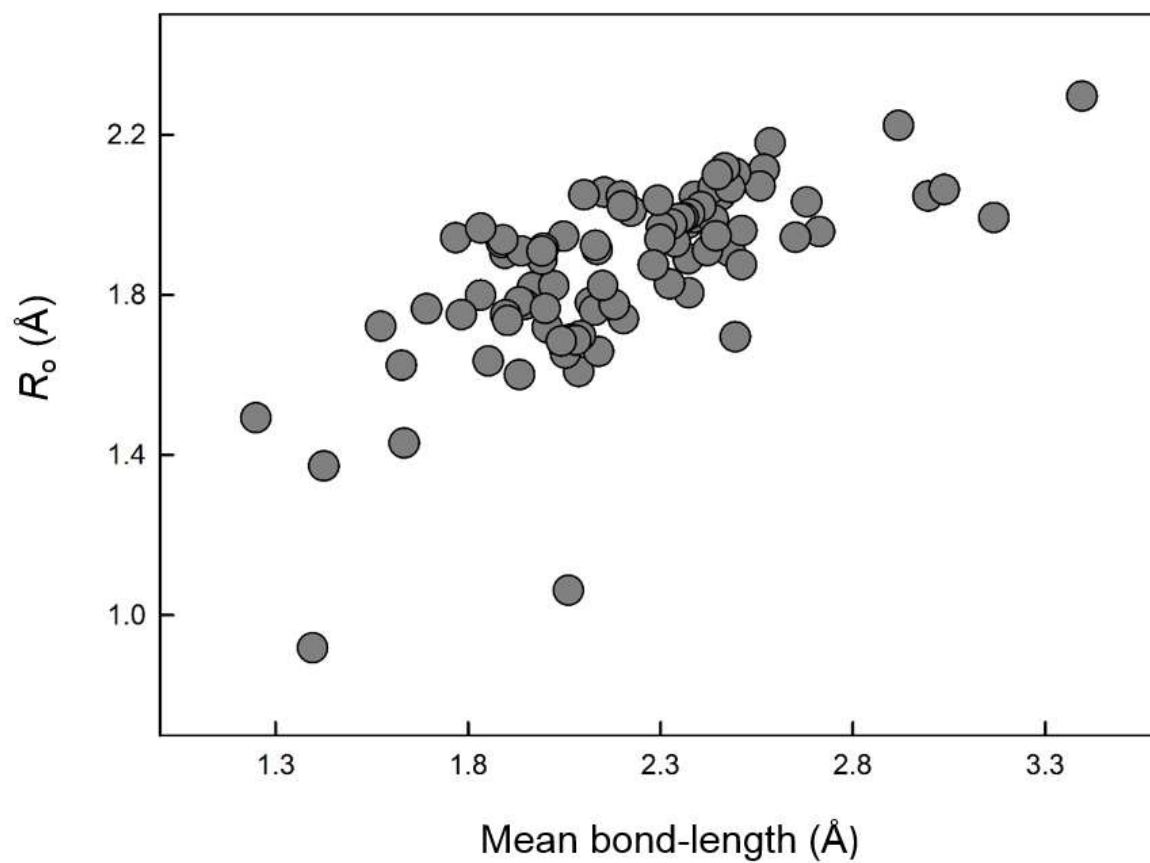
2: B fixed to family average

3: B fixed to 0.399 Å

2.11.6.1 Trends in the bond-valence parameters for ions with two or more coordination numbers

Here, we will examine trends in the bond-valence parameters derived with the GRG method for the 90 ions with two or more coordination numbers. We begin with the relation between the bond-valence parameter R_0 and the mean bond-length of a pair of ions. Fig. 2.3 shows our new values for R_0 as a function of mean bond-length. The correlation is not strong ($R^2 = 0.457$) although it changes slightly by removing the two lower outliers (H^+ , Li^+ ; $R^2 = 0.516$). Certain groups of ions of similar crystal-chemical behaviour also show significant correlation (e.g., alkali metals, $R^2 = 0.937$; alkaline-earth metals, $R^2 = 0.962$). Attempts to relate the individual parameters R_0 and B directly to other physical properties of the ions were not successful.

Figure 2.3 Bond-valence parameter R_0 as a function of mean bond-length for the 90 multiple-coordination-number ions.



On the other hand, the ratio $R_o / \langle R_{ij} \rangle$ shows significant correlation with various cation properties: (1) oxidation state, V_i ; (2) ionization energy, IE ; and to a much lesser extent (3) Pauling electronegativity, χ_i :

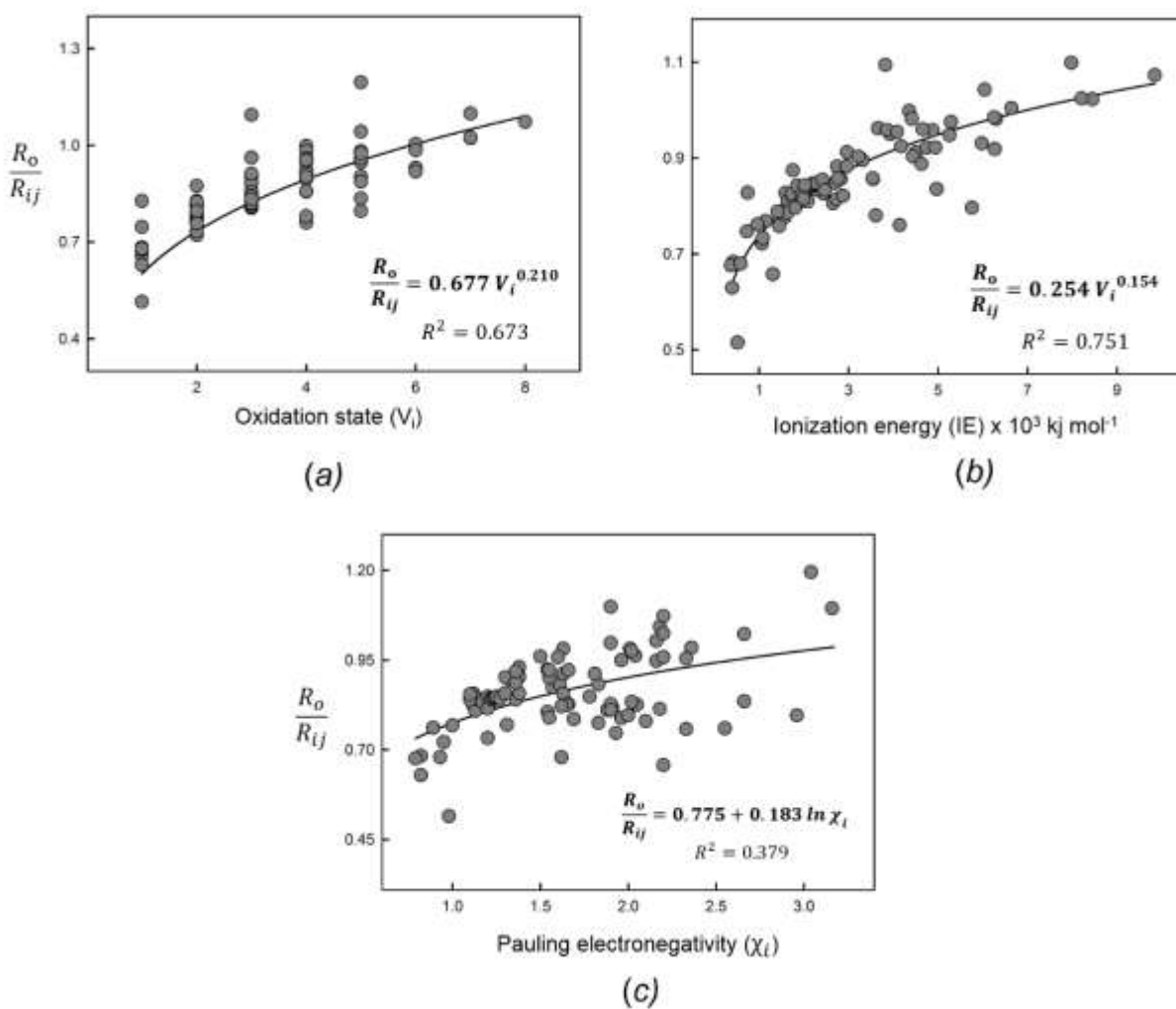
$$\frac{R_o}{\langle R_{ij} \rangle} = 0.677 \times V_i^{0.210} \quad R^2 = 0.673 \quad (\text{eq. 2.23})$$

$$\frac{R_o}{\langle R_{ij} \rangle} = 0.254 \times (IE)^{0.154} \quad R^2 = 0.751 \quad (\text{eq. 2.24})$$

$$\frac{R_o}{\langle R_{ij} \rangle} = 0.775 + 0.183 \ln \chi_i \quad R^2 = 0.276 \quad (\text{eq. 2.25})$$

These relations are shown in Fig. 2.4. We use the Pauling electronegativity scale (Pauling, 1960) as it gives a slightly better value for R^2 (0.276) compared to the scales of Allen (Allen, 1989; 0.272) and Allred-Rochow (Allred & Rochow, 1958; 0.262). Similarly, O'Keeffe & Brese (1991) derived a correlation between R_o and a combination of (Allred-Rochow) electronegativity and an empirically-derived "size parameter". To evaluate the reliability of eqs. 2.23 to 2.25, we calculate the mean absolute deviation between the values of R_o predicted by these equations, and those derived by the GRG method for all usable ions. Eqs. 2.23 to 2.25 give mean deviations of 4.89%, 4.21% and 9.00%, respectively. Even though the deviations calculated from eqs. 2.23 and 2.24 seem reasonable, one must be careful when using these equations to extrapolate values for R_o . Thus for eq. 2.24, the experimental value of R_o falls within the range of its predicted value with error for only 61 of the 90 ions. Moreover, deviations on R_o have a much larger effect on the bond-valence sums than deviations on B . As a result, it is much safer to fix B to a reasonable value (such as the mean value of 0.399 Å) rather than fixing R_o , when dealing with unfamiliar cations observed in only one coordination.

Figure 2.4 Relation between bond-valence parameter R_o and (a) oxidation state, (b) ionization energy, and (c) Pauling electronegativity.



2.11.6.2 The one-coordination-number problem

As noted above, the choice of a two-parameter equation to represent the bond-valence relation (eq. 2.5) means that at least two distinct coordination environments are required to solve for the parameters of the equation. Of the 135 ions examined here, 45 ions occur in only one coordination, resulting in a significant problem with regard to the calculation of their bond-valence parameters. Several ways around this “one-coordination-number problem” have been proposed. For example, Brown & Shannon (1973) used the bond-length information for the same cation in different coordination and bonded to other anions, and adjusted the bond lengths in proportion to the difference in ionic radius of the anions, while Brown & Altermatt (1985) fixed the B parameter to 0.37 Å, which effectively removes the factor of 2 in eq. 2.22. Other ways of dealing with this problem (e.g., Krivovichev, 2001) are applicable only to a small set of data.

2.11.6.3 Extrapolation to ions with only one coordination number

Here, we explore different options for fixing one of the bond-valence parameters for the 45 ions with only one coordination number, using the trends in the bond-valence parameters described above. We use three different methods that involve fixing either R_0 or B , and letting the other parameter refine by the GRG method.

Although the system is underdetermined, any useful solution must be physically realistic and consistent with the results obtained for the ions observed in multiple coordination numbers. Thus we have an idea of the range that calculated values of R_0 , B and of the

RMSD should occur within, based on ions showing similar crystal-chemical behaviour as well as for all ions considered. We experimented with fixing both R_0 and B , and found that ions should be treated on a case by case basis. The following three methods of derivation were used to derive the bond-valence parameters of ions observed in only one coordination:

(1) Fix R_0 to the value predicted by eq. 2.23 (ionization energy), or to the mean of the values predicted by eqs. 2.23 and 2.24). Let B refine, and see if the values for both B and the RMSD fall within a reasonable range for that family or group of ions with similar crystal-chemical behaviour. If this is not the case, move to method (2).

(2) Fix B to a reasonable value based on family (e.g., for the transition metals, the mean value of B is 0.375 Å) or group of ions with similar crystal-chemical behaviour. Let R_0 refine, and see if both R_0 and the RMSD fall within a reasonable range for that family. If this is not the case, move to method (3).

(3) Fix B to the mean value of all multiple-coordination-number ions combined (0.399 Å) and let R_0 refine. This is done where (1) and (2) fail, or where there is insufficient data available to make a reasonable estimate of B (e.g., for the non-metals).

For the 45 ions considered, we fixed R_0 for 22 ions and B for 23 ions. Parameters derived by fixing a parameter are identified by their method of derivation (1, 2 or 3) in Table 2.4.

2.11.7 Precision

Several factors affect the precision of the RMSD and bond-valence parameters calculated in this work: (1) uncertainty in the experimental bond-lengths, (2) uncertainty in the parameterization of the model, and (3) the presence of structural strain in the bond-length data. We estimated the effect of (1) by taking an average standard deviation for a bond length (~ 0.005 Å) and, using a sample of nine ions (H^+ , Na^+ , Mg^{2+} , Al^{3+} , S^{6+} , Zn^{2+} , La^{3+} , Pb^{2+} , Th^{4+}), determined the effect of varying bond lengths by ± 0.005 Å on the RMSD. The uncertainty on the bond length resulted in variations in the third decimal of the RMSD (first decimal for the relative RMSD). The error on R_0 and B was then determined by incrementally varying the value of these parameters until the same variation in the RMSD was observed. The uncertainty on both R_0 and B caused by (1) is thus determined to be in the third decimal place. On the other hand, while we strived to minimize the effect of uncertainty in the parameterization of the model in this work (2), simple factors such as the largely variable sample sizes of the ions affect the accuracy and precision of the results in ways that are arguably more important than the uncertainty on the experimental bond-lengths. As for the presence of structural strain (3), this phenomenon is structure dependent and cannot (currently) be evaluated by any method not dependent on the valence-sum rule. We thus give the values to be precise to the third decimal as a best-case scenario.

2.12 Anion-sum verification

Bond-valence parameters are usually derived on the basis of the cation bond-valence sums. However, as discussed earlier, parameters are expected to work equally well for both cations and anions according to the valence-sum rule. If a method of derivation is

selected that optimizes the bond-valence sums for cations only, it is critical that these parameters be evaluated *a posteriori* to check that they also work well for anions. As this is seldom done, here we will evaluate the anion bond-valence sums for four sets of parameters: (1) those of Brown & Altermatt (1985), (2) those of Brese & O'Keeffe (1991), (3) the set of best published parameters from Table 2.S1, and (4) the new parameters given in this paper.

We assembled a set of structures covering all pairs of bond-valence parameters derived in this paper (with at least one unique structure per cation), unless no structure could be evaluated solely with the parameters of our dataset. This resulted in a set of 128 structures (Table 2.S4). The structures were then evaluated with the 3 (smaller) sets of parameters given above, where applicable, which resulted in 4 overlapping sets of evaluated structures shown in Table 2.5 (note that the way the structure sets are assembled, less common cations become part of the evaluation as the sets get larger.). We used the program KDist (part of the Kalvados software suite; <http://www.fzu.cz/~knizek/kalvados>) to calculate the overall RMSD of the anion bond-valence sums for the different sets of parameters over the structure sets.

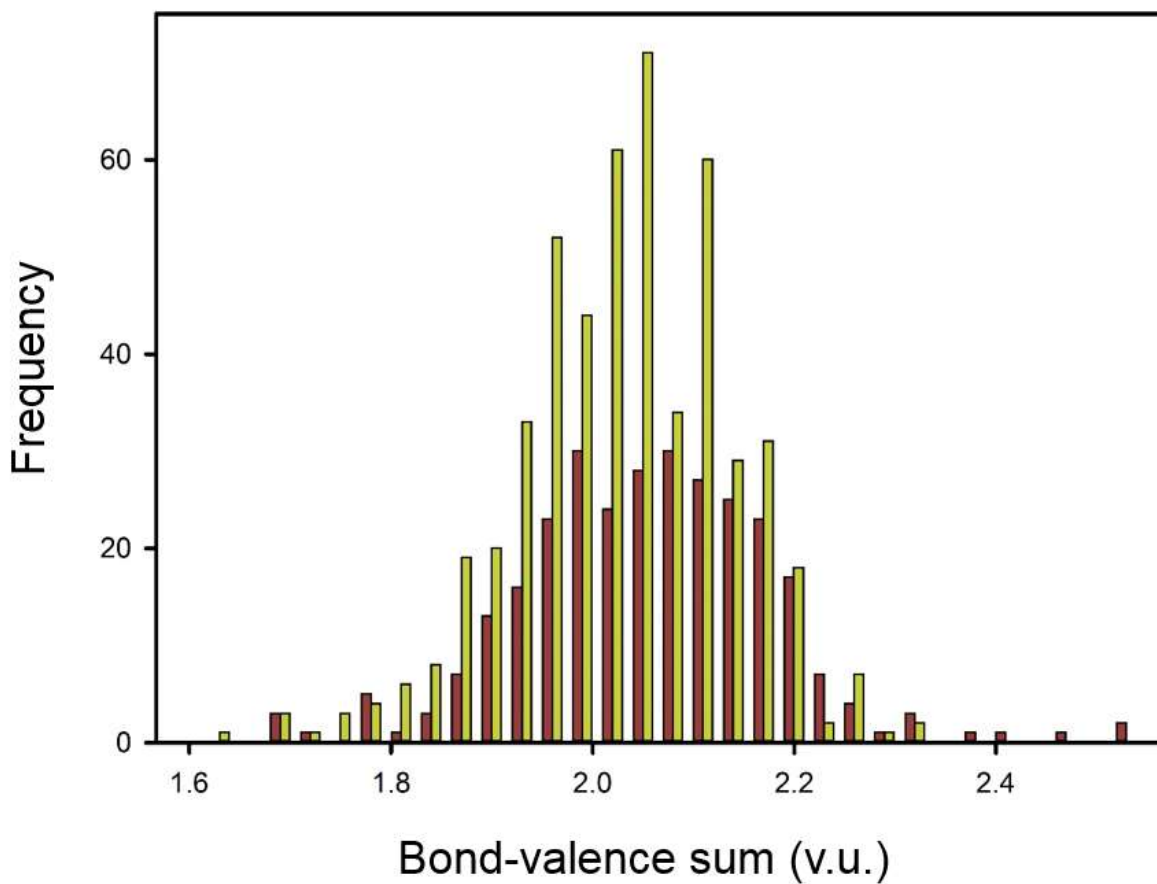
Table 2.5 Overall RMSD (v.u.) for the anion bond-valence sums of 4 large sets of bond-valence parameters

No. of structures (coordination polyhedra)	Brown & Altermatt (1985)	Brese & O'Keeffe (1991)	Best published parameters	This paper
72 (296)	0.130	0.119	0.100	0.100
100 (398)	-	0.121	0.106	0.099
122 (490)	-	-	0.120	0.103
128 (511)	-	-	-	0.104

The results are summarized in Table 2.5 together with the number of structures and the number of anion-centered coordination polyhedra used for each set. For the set of 72 structures, the set of best published parameters as well as the parameters given in this work give the best anion bond-valence sums, with an overall RMSD of 0.100 v.u. (5.0% per unit of charge), compared with 0.119 v.u. and 0.130 v.u. for the sets of Brese & O'Keeffe (1991) and Brown & Altermatt (1985), respectively. Over the set of 100 structures, the parameters of this work give the best anion bond-valence sums, with a RMSD of 0.099 (4.9% per unit of charge), compared with 0.106 v.u. and 0.121 for the set of best published parameters and the parameters of Brese and O'Keeffe, respectively. The structure set covering 122 unique ions shows even greater distinction between the parameters of this work and what we identified to be the set of best published parameters, with an overall RMSD of 0.103 v.u. (5.1% per unit of charge) compared to 0.120 v.u. Finally, the set of structures covering 128 unique ions yields an overall RMSD of 0.104 v.u. (5.2% per unit of charge) with the parameters derived here.

Fig. 2.5 shows the bond-valence sums for O^{2-} for the parameters of Brown & Altermatt (1985) and the parameters given in this paper. Although the parameters given in this paper account for more coordination polyhedra (511 vs. 296), the range of bond-valence sums is smaller (1.63-2.30) compared to that obtained from the parameters of Brown & Altermatt (1.67-2.52). The mean bond-valence sum for the parameters of this paper is 2.02 v.u., compared to 2.04 v.u. for the parameters of Brown & Altermatt, with standard deviations of 0.10 and 0.12 v.u. respectively.

Figure 2.5 Anion bond-valence sums for the parameters of Brown & Altermatt (1985; dark red) and the parameters given in this paper (yellow), with sample sizes of 296 and 511 anion coordination polyhedra, respectively.



We conclude that the parameters given in this paper give the best anion bond-valence sums of the large sets of parameters, in addition to giving the best bond-valence sums for the cations (above). Moreover, the results show that the approximation of deriving bond-valence parameters on the basis of cation coordination polyhedra is justified.

2.13 Improvement in fit: Cations

It is more difficult to compare different sets of bond-valence parameters in terms of cation bond-valence sums, as the sets of parameters often cover a wide array of cations that have different expected levels of fit. However, we can safely compare the two largest sets of parameters discussed above, which are those given in this paper and the set of best published parameters from Table 2.S1.

The parameters given in this paper yield a mean weighted-RMSD of 0.128 v.u. (6.1% per unit of charge) over 31,515 coordination polyhedra for 129 of the 135 ions (9 cations are only found in only one coordination polyhedron, for which the RMSD calculation is irrelevant). On the other hand, the set of best published parameters gives a mean weighted-RMSD of 0.136 v.u. (5.7% per unit of charge) over 31,489 coordination polyhedra for 128 ions. To put things in perspective, the mean weighted-RMSD for the anion bond-valence sums using the parameters of this paper (0.104 v.u.) is 5.2% per unit of charge, slightly lower than for the cation bond-valence sums, although this may be the result of a much smaller sample size.

In terms of specific families, we usually observe small but consistent improvements in the overall RMSD for most ions in comparison to the set of best published parameters.

Where the overall RMSD is not improved (e.g., Be^{2+}), this is usually because the GRG method gave parameters with a slightly higher overall RMSD in order to compensate for the coordination-based RMSD. The bond-valence sums for coordination numbers 3 and 4 for the best published parameters for Be^{2+} are thus 1.901 and 2.010 v.u., whereas they are 2.000 and 2.000 v.u. for the parameters of this work. Major improvements are generally associated with less common ions and are presumably the result of higher quality and/or of more data now being available. For example: for some less-common transition metals, Os^{8+} changes from 0.608 to 0.233 v.u., and Re^{7+} from 0.923 to 0.191 v.u.; for some actinide ions, Np^{5+} changes from 0.820 to 0.061 v.u., and Np^{6+} changes from 1.209 to 0.083 v.u.

The RMSD for the hydrogen ion improved slightly from 0.035 v.u. (for the parameters of Grabowski, 2000) to 0.033 v.u., which reaffirms that one pair of bond-valence parameters is sufficient to model the ion.

2.14 Deviations from the valence-sum rule

Of the 462 configurations of ions and coordination numbers examined here, 55 have overall mean bond-valence sums that deviate from the valence-sum rule by more than 0.1 v.u., 11 by more than 0.2 v.u. and 2 by more than 0.3 v.u. In terms of relative deviation from the valence-sum rule, 57 configurations have overall mean bond-valence sums that deviate by more than 2% per unit of charge, 12 by more than 5%, and 2 by more than 10%. The larger deviations are usually unavoidable by using any set of parameters, and are usually for (1) the low/high coordinations of ions observed in many

different coordination numbers (e.g., Ti^+ , alkali metal ions), (2) structure refinements of dubious quality, and (3) configurations with very little data. The deviations are significantly higher when using other sets of parameters, and show that the addition of the coordination-based RMSD minimization of the GRG method of derivation is valuable.

2.15 Summary

[1] Evaluation of 244 pairs of bond-valence parameters for 128 cations bonded to oxygen shows a wide variation in the quality of fit to the valence-sum rule, based on 180,194 (filtered) bond lengths from 31,489 coordination polyhedra from 9367 crystal-structure refinements.

[2] We have evaluated two common methods for the derivation of bond-valence parameters: (1) the graphical method, and (2) fixing B and solving for R_0 ; We conclude that both (1) fixing B at 0.37\AA , and (2) derivation of R_0 and B by the graphical method, are not ideal, and we introduce a new method of derivation, the GRG (Generalized Reduced Gradient) method, that leads to better agreement with the valence-sum rule for both cation and anion bond-valence sums.

[3] We have evaluated 19 two-parameter equations and 7 three-parameter equations to model the bond-valence—bond-length relation. We conclude that (1) several equations can describe the relation to a similar degree of accuracy; (2) we have likely reached a plateau in the degree of fit for two-parameter equations; and (3) the equation of Brown & Altermatt (1985) is best on the basis of fit and practicality.

[4] We have derived new bond-valence parameters for 135 cations bonded to O^{2-} using the GRG method. These parameters give better bond-valence sums for the cations, with a mean weighted-RMSD of 0.128 v.u. (6.1% per unit of charge) for 129 ions and 31,515 cation coordination polyhedra, compared to 0.136 v.u. (5.7% per unit of charge) for what we have determined to be the set of best published parameters over 128 ions and 31,489 coordination polyhedra.

[5] The parameter $R_o / \langle R_{ij} \rangle$ is correlated with ion valence ($R^2 = 0.673$) and ionization energy ($R^2 = 0.751$), indicating that the potential correlation between R_o and B does not adversely affect the derivation of bond-valence parameters provided an effective method of derivation is used.

[6] There are small but consistent improvements in the overall RMSD for most ions in comparison to the set of best published parameters, and excellent improvements in the coordination-based agreement between bond-valence sum and oxidation state. Moreover, some ions show a striking improvement in fit compared with published parameters, likely due to the availability of higher quality data: for example, Os^{8+} changes from 0.608 to 0.233 v.u., Re^{7+} from 1.000 to 0.276 v.u. and Np^{6+} from 1.209 to 0.078 v.u.

2.16 Acknowledgements

We thank two anonymous reviewers for their extremely helpful remarks on this paper, and we thank Dr. Karel Knížek for his help with the KDist program. This work was funded by UM Duff Roblin and GETS Fellowships, and an NSERC PGS-D3 Scholarship

to OCG, and a Canada Research Chair and a Discovery grant to FCH from the Natural Sciences and Engineering Research Council of Canada, and by Canada Foundation for Innovation grants to FCH.

2.17 References

Abadie, L. & Carpentier, J. (1969). Generalization of the Wolfe reduced gradient method to the case of nonlinear constraints. In Optimization (R. Fletcher, Ed.), Academic press, New York, Chapter 4, USA, 37-47.

Allen, L.C. (1989). Electronegativity is the average one-electron energy of the valence-shell electrons in ground-state free atoms. *J. Am. Chem. Soc.* **111**, 9003–9014.

Allred, A.L. & Rochow, E.G. (1958). A scale of electronegativity based on electrostatic force. *Journal of Inorganic and Nuclear Chemistry* **5**, 264-268.

Adams, S. (2001). Relationship between bond valence and bond softness of alkali halides and chalcogenides. *Acta Cryst.* **B57**, 278-287.

Adams, S. (2014). Practical considerations in determining bond valence parameters. *Structure and Bonding* **158**, 91-128.

Adams, S. & Prasada Rao, R. (2014). Understanding ionic conduction and energy storage materials with bond-valence methods. *Structure and Bonding* **158**, 129-160.

Alig, H., Lösel, J. & Trömel, M. (1994). Crystal-chemistry of hydrogen-oxygen bonds. *Z. Kristallogr.* **209**, 18-21.

- Baur, W.H. (1970). Bond length variation and distorted coordination polyhedra in inorganic crystals. *Trans. Am. Crystallogr. Assoc.* **6**, 129-155.
- Baur, W.H. (1974). The geometry of polyhedral distortions. Predictive relationships for the phosphate group. *Acta Cryst.* **B30**, 1195-1215.
- Born, M. & Lande, A. (1918). The absolute calculation of the crystal properties with the help of Bohr's atomic model. *Sitzungsberichte Der Koniglich Preussischen Akademie Der Wissenschaften*, 1048-1068.
- Born, M., & Mayer, J.E. (1932). Zur Gittertheorie der Ionenkristalle. *Z. Physik.* **75**, 1–18.
- Bragg, W.L. (1930). The structure of silicates. *Z. Kristallogr.* **74**, 237-305.
- Brese, N.E. & O'Keeffe, M. (1991). Bond-valence parameters for solids. *Acta Cryst.* **B47**, 192-197.
- Brown, I.D. (1974). Bond valence as an aid to understanding the stereochemistry of O and F complexes of Sn(II), Sb(III), Te(IV), I(V) and Xe(VI). *J. Solid State Chem.* **11**, 214-233.
- Brown, I.D. (1987). Recent developments in the bond valence model of inorganic bonding. *Phys. Chem. Minerals* **15**, 30-34.
- Brown, I.D. (2002). *The Chemical Bond in Inorganic Chemistry*. Oxford University Press.
- Brown, I.D. (2009). Recent developments in the methods and applications of the bond valence model. *Chem. Rev.* **109**, 6858-6919.

Brown, I.D. (2013). <http://www.iucr.org/resources/data/datasets/bond-valence-parameters>; posted 2013-10-16.

Brown, I.D. (2014). Historical introduction. *Structure and Bonding* **158**, 1-10.

Brown, I.D. & Altermatt, D. (1985). Bond-valence parameters obtained from a systematic analysis of the Inorganic Crystal-Structure Database. *Acta Cryst.*, **B41**, 244-247.

Brown, I.D. & Shannon, R.D. (1973). Empirical bond-strength bond-length curves for oxides. *Acta Cryst.*, **A29**, 266-282.

Burdett, J.K. & Hawthorne, F.C. (1993). An orbital approach to the theory of bond valence. *Am. Mineral.* **78**, 884-892.

Burns, P.C., Ewing, R.C. & Hawthorne, F.C. (1997). The crystal chemistry of hexavalent uranium: Polyhedron geometries, bond-valence parameters, and polymerization of polyhedra. *Can. Mineral.* **35**, 1551-1570.

Byström, A. & Wilhelmi, K.-A. (1951). The crystal structure of $(\text{NH}_4)_2\text{Cr}_2\text{O}_7$ - with a discussion of the relation between bond number and interatomic distances. *Acta Chem. Scand.* **5**, 1003-1010.

Cabana J., Ling, C.D., Oro-Sole, J., Gautier, D., Tobias, G., Adams, S., Canadell, E. and Palacin, M.R. (2004). Antifluorite-type lithium chromium oxide nitrides: Synthesis, structure, order, and electrochemical properties, *Inorg. Chem.* **43**, 7050-7060.

Clark J.L., Appleman D.E. & Papike J.J. (1969). Crystal-chemical characterization of clinopyroxenes based on eight new structure refinements. *Min. Soc. Amer. Special Paper* **2**, 31-50.

Donnay G. & Allmann R. (1970). How to recognize O^{2-} , OH^- , and H_2O in crystal structures determined by X-rays. *Am. Mineral.* **55**, 1003-1015.

Evans H.T. Jr (1960). Crystal structure refinement and vanadium bonding in the metavanadates KVO_3 , NH_4VO_3 and $KVO_3 \cdot H_2O$. *Z. Kristallogr.* **114**, 257-277.

Evans H.T. Jr & Mrose M.E. (1960). A crystal chemical study of the vanadium oxide minerals, haggite and doloresite. *Am. Mineral.* **45**, 1144-1166.

Ferguson, R.B. (1974). Cation-anion distance-dependent method for evaluating valence-bond distributions in ionic structures and results for some olivines and pyroxenes. *Acta Cryst.* **B30**, 2527-2539.

Filatov, S.K., Semenova, T.F. & Vergasova, L.P. (1992). Types of polymerization of $[OCu_4]^{6+}$ tetrahedra in compounds with 'additional' oxygen atoms. *Proc. USSR Academy of Sciences* **322**, 536-539. (in Russian).

Grabowski S.J. (2000). The bond valence model in analysing H-bonds of crystal structures. *J. Mol. Structure* **552**, 153-157.

Krivovichev S.V. (1999). Encapsulation effect and its influence on bond-valence parameters. *Z. Kristallogr.* **214**, 371-372.

Krivovichev S.V. (2012). Derivation of bond-valence parameters for some cation-oxygen pairs on the basis of empirical relationships between $r(o)$ and B . *Z. Kristallogr.* **227**, 575-579.

Krivovichev, S.V & Brown, I.D. (2001). Are the compressive effects of encapsulation an artifact of the bond valence parameters? *Z. Kristallogr.* **216**, 245-247.

Krivovichev, S.V. and Filatov, S.K. (1999). Structural principles for minerals and inorganic compounds containing anion-centered tetrahedra. *Am. Mineral.* **84**, 1099-1106.

Krivovichev, S.V., Filatov, S.K. & Semenova, T.F. (1998). Types of cationic complexes on the base of oxocentered tetrahedra [OM₄] in crystal structures of inorganic compounds. *Russ. Chem. Rev.* **67**, 137-155.

Locock, A.J. & Burns, P.C. (2004). Revised Tl(I)–O bond valence parameters and the structures of thallos dichromate and thallos uranyl phosphate hydrate. *Z. Kristallogr.* **219**, 259-266.

Matchatski, F. (1928). Zur Frage der Struktur und Konstitution der Feldspate. *Zentralblatt für Mineralogie Abhandlungen A*, **1928**, 97-104.

Mills, S.G. & Christy A.G. (2013). Revised values of the bond-valence parameters for Te-IV-O, Te-VI-O and Te-IV-Cl. *Acta Cryst.*, **B69**, 145-149.

Mills, S.G., Christy A.G., Chen, E.C.-C. & Raudsepp, M. (2009). Revised values of the bond valence parameters for Sb-[6](V)-O and Sb[3-11](III)-O. *Z. Kristallogr.* **224**, 423-431.

Mohri, F. (2000). A new relation between bond valence and bond distance. *Acta Cryst.*, **B56**, 626-638.

Naskar, J.P., Hati, S. & Datta, D. (1997). New bond-valence sum model. *Acta Cryst.*, **B53**, 885-894.

Pant A.K. & Cruikshank D.W.J. (1967). A reconsideration of structure of datolite $\text{CaBSiO}_4(\text{OH})$. *Z.Kristallogr.* **125**, 286-297.

Pauling, L. (1929). The principles determining the structures of complex ionic crystals. *J. Am. Chem. Soc.* **51**, 1010-1026.

Pauling, L. (1947). Atomic radii and interatomic distances in metals. *J. Am. Chem. Soc.* **69**, 542–553.

Pauling, L. (1960). The Nature of the Chemical Bond. Cornell University Press, Ithaca, New York.

Perloff A. (1970). Crystal structure of sodium hexamolybdochromate(iii) octahydrate, $\text{Na}(\text{CrMo}_6\text{O}_{24}\text{H}_6) \cdot 8\text{H}_2\text{O}$. *Inorg. Chem.* **9**, 2228-2239.

Preiser, C., Lösel, J., Brown, I.D., Kunz, M., Skworon, A. (1999). Long-range Coulomb forces and localized bonds. *Acta Cryst.*, **B55**, 698-711.

Pyatenko, Y. (1972). Unique approach to analysis of local valency balance in inorganic structures. *Kristallografiya* **17**, 773-779.

Rutherford, J.S. (1990). Theoretical prediction of bond-valence networks. *Acta Cryst.*, **B46**, 289-292.

Shannon, R.D. (1976) Revised effective ionic radii and systematic studies of interatomic distances in halides and chalcogenides. *Acta Cryst.*, **A32**, 751-767.

Sidey, V. (2008). On the correlations between the polyhedron eccentricity parameters and the bond-valence sums for the cations with one lone electron pair. *Acta Cryst.*, **B64**, 515-518.

Sidey, V. (2009). On the correlations between the polyhedron eccentricity parameters and the bond-valence sums for the cations with one lone electron pair. Addendum. *Acta Cryst.*, **B65**, 401-402.

Sidey, V. (2010). On the accurate bond-valence parameters for the $\text{Sb}^{3+}/\text{O}^{2-}$ ion pair. *Acta Cryst.*, **B66**, 307-314.

Sidey, V. (2013). On the shortest B^{III} -bonds. *Acta Cryst.*, **B69**, 86-89.

Smith, J.V. (1953). Reexamination of the crystal structure of melilite. *Am. Mineral.* **38**, 643-661.

Urusov, V.S. (2003). Theoretical analysis and empirical manifestation of the distortion theorem, *Z. Kristallogr.* **218**, 709-719.

Valach, F. (1999). A bond-valence approach to the semicoordination of copper-oxygen and copper-nitrogen complexes. *Polyhedron* **18**, 699-706.

Yu, D., Xue, D. & Ratajczak, H. (2006). Microscopic characteristics of hydrogen bonds of hydrated borates. *Physica B: Cond. Matter* **371**, 170.

Zachariasen W.H. (1954). Crystal chemical studies of the 5f-series of elements.23. On the crystal chemistry of uranyl compounds and of related compounds of transuranic elements. *Acta Cryst.* **7**, 795-799.

Zachariasen W.H. (1963). Crystal structure of monoclinic metaboric acid. *Acta Cryst.* **16**, 385-389.

Zachariasen W.H. & Plettinger H.A. (1959). Crystal chemical studies of the 5f-series of elements.25. The crystal structure of sodium uranyl acetate. *Acta Cryst.* **12**, 526-530.

Ziółkowski, J. (1985). New relation between ionic-radii, bond length, and bond strength. *J. S. State Chem.* **57**, 291-299.

Appendix A: Supplementary material

Supplementary material for

Comprehensive derivation of bond-valence parameters for ion pairs involving oxygen

Table 2.S1 Evaluation of published bond-valence parameters

Ion	No. of coordination polyhedra	Ref. code	R_o (Å)	B (Å)	RMSD (v.u.)	Special condition
Hydrogen						
H ⁺	224	bc*	0.569	0.94		1.05 Å < O-H < 1.70 Å
			0.907	0.28		O-H < 1.05 Å
			0.99	0.59	0.059	1.70 Å < O-H
		az*	0.93	0.40	0.035	
		ba†	0.79	0.37		S _{ij} > 0.5 vu; R _{ij} < 1.30 Å
Alkali metals						
Li ⁺	690	a	1.466	0.37	0.121	
		o	1.29	0.48	0.092	
Na ⁺	1682	a	1.803	0.37	0.178	
		v	1.756	0.37	0.158	
		o	1.661	0.44	0.140	
K ⁺	1478	a	2.132	0.37	0.204	

		u	2.113	0.37	0.179
		o	1.84	0.48	0.155
Rb ⁺	464	a	2.263	0.37	0.206
Cs ⁺	544	a	2.417	0.37	0.167
Alkaline-Earth metals					
Be ²⁺	169	a	1.381	0.37	0.080
Mg ²⁺	469	a	1.693	0.37	0.143
		o	1.636	0.42	0.120
Ca ²⁺	1168	a	1.967	0.37	0.183
		o	1.896	0.41	0.171
Sr ²⁺	374	a	2.118	0.37	0.222
Ba ²⁺	856	a	2.285	0.37	0.237
Metalloids					
B ³⁺	1572	a	1.371	0.37	0.069
Si ⁴⁺	2530	b	1.624	0.37	0.126
		au	1.622	0.37	0.127
		a	1.64	0.37	0.221
Ge ⁴⁺	350	a	1.748	0.37	0.148
As ³⁺	28	a	1.789	0.37	0.127
As ⁵⁺	526	a	1.767	0.37	0.108
Sb ³⁺	54	be	1.925	0.455	0.086
		bg	1.927	0.446	0.085
		bd	1.924	0.47	0.093
		an	1.955	0.37	0.13
		bj	1.885	0.53	0.147
Sb ⁵⁺	183	be	1.904	0.43	0.198
		a	1.942	0.37	0.525

		an	1.912	0.37	0.217
		aw	1.908	0.409	0.209
Te ⁴⁺	212	bd	1.955	0.44	0.120
		a	1.977	0.37	0.198
		bk	1.96	0.41	0.107
Te ⁶⁺	155	a	1.917	0.37	0.229
		bk	1.921	0.56	0.146
Non-metals					
C ⁴⁺	433	e	1.39	0.37	0.093
		au	1.407	0.37	0.211
		o	1.4	0.26	0.716
N ⁵⁺	497	a	1.432	0.37	0.162
		o	1.41	0.43	0.620
P ³⁺	7	e	1.63	0.37	0.216
P ⁵⁺	3691	a	1.617	0.37	0.107
		au	1.615	0.37	0.111
		b	1.604	0.37	0.205
S ⁴⁺	30	a	1.644	0.37	0.136
S ⁶⁺	906	a	1.624	0.37	0.124
Se ⁴⁺	202	a	1.811	0.37	0.147
Se ⁶⁺	191	a	1.788	0.37	0.119
Poor metals					
Al ³⁺	856	e	1.62	0.37	0.211
		o	1.644	0.38	0.121
Ga ³⁺	228	a	1.73	0.37	0.139
In ³⁺	125	a	1.902	0.37	0.200
Sn ²⁺	50	bd	1.849	0.5	0.144

		bh	1.859	0.55	0.135
		b	1.984	0.37	0.139
Sn ⁴⁺	38	a	1.905	0.37	0.195
Tl ⁺	74	a	2.124	0.37	0.148
		b	2.172	0.37	0.116
		af	1.927	0.5	0.113
Tl ³⁺	11	b	2.003	0.37	0.294
Pb ²⁺	276	q	1.963	0.49	0.125
		a	2.112	0.37	0.177
Pb ⁴⁺	12	a	2.042	0.37	0.286
Bi ³⁺	231	a	2.094	0.37	0.190
Bi ⁵⁺	11	b	2.06	0.37	0.316
Halogens					
Cl ³⁺	6	e	1.71	0.37	0.151
Cl ⁵⁺	9	e	1.67	0.37	0.089
Cl ⁷⁺	65	e	1.632	0.37	0.180
Br ⁵⁺	9	e	1.84	0.37	0.147
Br ⁷⁺	2	b	1.81	0.37	0.156
I ⁵⁺	134	bd	1.99	0.44	0.113
		a	2.003	0.37	0.435
I ⁷⁺	36	b	1.93	0.37	0.327
Transition metals					
Sc ³⁺	88	a	1.849	0.37	0.152
		o	1.877	0.35	0.243
Ti ³⁺	24	b	1.791	0.37	0.183
Ti ⁴⁺	324	a	1.815	0.37	0.164
		o	1.78	0.43	0.139

V ³⁺	70	a	1.743	0.37	0.130
		j	1.749	0.37	0.130
V ⁴⁺	226	a	1.784	0.37	0.149
		j	1.78	0.37	0.121
V ⁵⁺	714	a	1.803	0.37	0.139
		x	1.799	0.37	0.117
Cr ²⁺	17	b	1.73	0.37	0.090
Cr ³⁺	104	a	1.724	0.37	0.129
		w	1.708	0.37	0.136
Cr ⁴⁺	7	e	1.81	0.37	0.242
Cr ⁵⁺	1	w	1.76	0.37	0.205
		e	1.78	0.37	0.061
Cr ⁶⁺	169	a	1.794	0.37	0.157
Mn ²⁺	392	a	1.79	0.37	0.126
		j	1.765	0.37	0.163
		ap	1.762	0.40	0.124
Mn ³⁺	94	a	1.76	0.37	0.152
		j	1.732	0.37	0.188
		ap	1.762	0.35	0.128
Mn ⁴⁺	21	a	1.753	0.37	0.123
		j	1.75	0.37	0.122
		ap	1.762	0.34	0.137
Mn ⁵⁺		ap	1.762	0.30	0.119
Mn ⁶⁺	2	e	1.79	0.37	0.366
		ap	1.762	0.27	0.260
Mn ⁷⁺	7	e	1.827	0.37	0.239
		b	1.79	0.37	0.496

		ap	1.762	0.26	0.265
Fe ²⁺	192	a	1.734	0.37	0.135
		h	1.713	0.37	0.161
		j	1.7	0.37	0.205
Fe ³⁺	466	a	1.759	0.37	0.137
		h	1.751	0.37	0.138
		j	1.765	0.37	0.156
Co ²⁺	304	a	1.692	0.37	0.102
		i	1.685	0.37	0.120
Co ³⁺	15	i	1.637	0.37	0.145
		b	1.7	0.37	0.441
Co ⁴⁺	1	e	1.72	0.37	0.043
Ni ²⁺	255	e	1.675	0.37	0.131
		j	1.67	0.37	0.115
		a	1.654	0.37	0.105
Ni ⁴⁺	5	e	1.78	0.35	0.645
Cu ⁺	57	e	1.61	0.37	0.133
		l	1.504	0.37	0.185
Cu ²⁺	716	a	1.679	0.37	0.095
		j	1.649	0.37	0.172
		l	1.655	0.37	0.152
		bj	1.679	0.36	0.084
Cu ³⁺	11	t	1.735	0.37	0.141
		e	1.739	0.37	0.138
Zn ²⁺	461	a	1.704	0.37	0.101
		o	1.675	0.39	0.085
Y ³⁺	178	a	2.019	0.37	0.161

		b	2.014	0.37	0.157
		bj	2.028	0.35	0.176
Zr ⁴⁺	117	a	1.928	0.37	0.135
		b	1.937	0.37	0.149
Nb ⁴⁺	3	e	1.88	0.37	0.173
Nb ⁵⁺	251	a	1.911	0.37	0.161
		x	1.916	0.37	0.188
Mo ³⁺	5	m	1.834	0.37	0.067
Mo ⁴⁺	9	j	1.886	0.37	0.449
		m	1.856	0.37	0.114
Mo ⁵⁺	76	j	1.907	0.37	0.343
		m	1.878	0.37	0.136
Mo ⁶⁺	970	a	1.907	0.37	0.147
		x	1.915	0.41	0.183
		n	1.87	0.26	0.330
		m	1.9	0.37	0.212
Tc ⁷⁺	6	as	1.909	0.37	0.089
Ru ³⁺	3	o	1.77	0.37	0.033
Ru ⁴⁺	8	b	1.834	0.37	0.124
Ru ⁵⁺	23	o	1.9	0.37	0.219
Rh ³⁺	11	b	1.793	0.37	0.272
Pd ²⁺	29	b	1.792	0.37	0.250
Ag ⁺	200	a	1.842	0.37	0.088
		b	1.805	0.37	0.150
Cd ²⁺	164	a	1.904	0.37	0.122
		ao	1.875	0.37	0.129
Hf ⁴⁺	22	b	1.923	0.37	0.095

Ta ⁵⁺	162	a	1.92	0.37	0.214
W ⁵⁺	4	aj	1.881	0.37	0.199
W ⁶⁺	436	a	1.917	0.37	0.196
		x	1.916	0.41	0.181
		b	1.921	0.37	0.232
		aj	1.906	0.37	0.200
Re ⁵⁺	3	e	1.86	0.37	0.091
Re ⁷⁺	59	e	1.97	0.37	0.923
Os ⁶⁺	1	e	2.03	0.37	2.451
Os ⁸⁺	8	e	1.92	0.37	0.608
Ir ⁴⁺	17	e	1.87	0.37	0.243
Ir ⁵⁺	6	b	1.916	0.37	0.180
		e	2.01	0.37	1.362
Pt ²⁺	3	b	1.768	0.37	0.130
		e	1.8	0.37	0.318
Pt ⁴⁺	33	a	1.879	0.37	0.180
Au ³⁺	24	e	1.89	0.37	0.097
		b	1.833	0.37	0.446
Hg ²⁺	52	a	1.972	0.37	0.198
		b	1.93	0.37	0.139
		bj	1.924	0.38	0.129
Lanthanides					
La ³⁺	182	a	2.172	0.37	0.162
		ac	2.172	0.33	0.331
		ae	2.148	0.37	0.203
		bj	2.086	0.45	0.161
Ce ³⁺	76	b	2.151	0.37	0.208

		ab	2.121	0.37	0.162
		ae	2.116	0.37	0.186
Ce ⁴⁺	28	b	2.028	0.37	0.564
		ab	2.068	0.37	0.213
		al	2.074	0.37	0.176
Pr ³⁺	99	a	2.138	0.37	0.259
		ae	2.098	0.37	0.185
Nd ³⁺	203	a	2.105	0.37	0.160
		b	2.117	0.37	0.201
		ae	2.086	0.37	0.203
		bj	2.021	0.46	0.178
Sm ³⁺	97	b	2.088	0.37	0.171
		ae	2.063	0.37	0.188
		ai	2.055	0.37	0.232
Eu ²⁺	3	b	2.147	0.37	0.204
		al	2.102	0.37	0.071
Eu ³⁺	49	a	2.074	0.37	0.198
		ae	2.038	0.37	0.196
Gd ³⁺	107	b	2.065	0.37	0.202
		ae	2.031	0.37	0.188
Tb ³⁺	48	a	2.032	0.37	0.122
		b	2.049	0.37	0.214
		ae	2.013	0.37	0.163
Dy ³⁺	70	a	2.001	0.37	0.195
		ae	2.005	0.37	0.174
Ho ³⁺	81	a	2.025	0.37	0.188
		ae	1.992	0.37	0.188

Er ³⁺	102	a	1.988	0.37	0.141
		b	2.01	0.37	0.191
		ae	1.979	0.37	0.177
Tm ³⁺	44	b	2	0.37	0.184
		ae	1.968	0.37	0.201
		e	1.93	0.37	0.444
Yb ³⁺	82	a	1.965	0.37	0.169
		b	1.985	0.37	0.237
		ae	1.954	0.37	0.191
Lu ³⁺	53	b	1.971	0.37	0.175
		ae	1.947	0.37	0.227
Actinides					
Th ⁴⁺	27	b	2.167	0.37	0.221
		p	2.18	0.35	0.225
U ⁴⁺	18	b	2.112	0.37	0.166
		p	2.13	0.35	0.188
U ⁵⁺	4	b	2.075	0.37	0.239
		p	2.1	0.35	0.291
U ⁶⁺	585	r	2.051	0.519	0.158
		a	2.075	0.37	0.690
		p	2.08	0.35	0.889
Np ⁵⁺	33	p	2.09	0.35	0.820
Np ⁶⁺	7	p	2.07	0.35	1.209
Np ⁷⁺	2	p	2.06	0.35	0.361
Am ³⁺	1	b	2.11	0.37	0.145
		p	2.13	0.35	0.138
Cm ³⁺	1	b	2.23	0.37	1.500

p	2.12	0.35	0.161
---	------	------	-------

*Neutron-diffraction data

†*Reference not directly compatible with our dataset if X-Ray data*

Table 2.S2 ICSD code for the structures used in the derivation of the bond-length to bond-valence equations

ICSD code	R-factor	No. of Al- coordination polyhedra
1975	0.020	2
20495	0.027	1
29443	0.017	1
30521	0.015	1
30538	0.015	1
32744	0.024	1
39337	0.016	2
50618	0.011	1
60845	0.019	1
62615	0.013	2
62616	0.019	2
63185	0.024	1
64962	0.028	1
65004	0.029	1
65665	0.019	1
65666	0.016	1
68913	0.020	1
69958	0.023	1
71893	0.013	1
71894	0.011	1

71895	0.013	1
72416	0.011	2
73249	0.026	2
74860	0.029	1
74968	0.022	1
75366	0.014	1
80672	0.013	1
81358	0.017	1
83449	0.020	1
83450	0.016	4
83458	0.020	1
86785	0.024	1
92629	0.002	1
92708	0.026	2
94590	0.023	3
95408	0.027	12
96685	0.029	1
100278	0.028	1
100368	0.018	1
156658	0.023	2
156729	0.016	3
156730	0.017	3
156731	0.021	3

156732	0.021	3
156733	0.016	3
156734	0.014	3
156735	0.017	3
240475	0.015	1
280310	0.020	1
280607	0.022	2
300020	0.021	1

Table 2.S3 RMSD values for six two-parameter equations for the 90 multiple-coordination-number ions

Ion	No. of coordination polyhedra	eq.[2]	eq.[3]	eq.[4]	eq.[14]	eq.[15]	eq.[19]
H ⁺	224	0.042	0.036	0.039	0.032	0.039	0.031
Li ⁺	690	0.079	0.078	0.079	0.077	0.079	0.078
Be ²⁺	169	0.095	0.093	0.094	0.091	0.095	0.091
B ³⁺	1572	0.068	0.069	0.068	0.069	0.069	0.069
N ⁵⁺	497	0.110	0.116	0.113	0.118	0.110	0.126
Na ⁺	1683	0.142	0.143	0.142	0.144	0.142	0.143
Mg ²⁺	469	0.115	0.112	0.114	0.110	0.114	0.112
Al ³⁺	856	0.113	0.111	0.112	0.109	0.115	0.112
Si ⁴⁺	2530	0.114	0.118	0.116	0.120	0.115	0.120
Cl ³⁺	5	0.046	0.063	0.054	0.082	0.042	0.085
K ⁺	1479	0.167	0.166	0.166	0.165	0.166	0.166
Ca ²⁺	1168	0.167	0.165	0.166	0.162	0.166	0.165
Sc ³⁺	88	0.106	0.107	0.106	0.108	0.106	0.107
Ti ³⁺	24	0.087	0.092	0.089	0.098	0.089	0.094
Ti ⁴⁺	324	0.151	0.146	0.148	0.142	0.148	0.144
V ³⁺	70	0.139	0.128	0.134	0.119	0.145	0.115
V ⁴⁺	226	0.099	0.101	0.100	0.105	0.098	0.099
V ⁵⁺	714	0.096	0.099	0.097	0.103	0.098	0.100
Cr ²⁺	17	0.059	0.059	0.059	0.059	0.060	0.059
Cr ⁴⁺	7	0.164	0.160	0.161	0.156	0.164	0.160

Mn ²⁺	392	0.120	0.118	0.119	0.116	0.120	0.118
Mn ³⁺	94	0.168	0.167	0.167	0.166	0.168	0.167
Mn ⁴⁺	21	0.133	0.128	0.130	0.123	0.137	0.121
Fe ²⁺	192	0.118	0.115	0.117	0.113	0.117	0.115
Fe ³⁺	466	0.150	0.145	0.147	0.140	0.152	0.147
Co ²⁺	304	0.116	0.109	0.113	0.103	0.123	0.115
Ni ²⁺	255	0.116	0.111	0.114	0.106	0.113	0.109
Cu ⁺	57	0.079	0.079	0.079	0.078	0.080	0.079
Cu ²⁺	716	0.084	0.084	0.084	0.084	0.088	0.086
Zn ²⁺	461	0.091	0.088	0.089	0.086	0.095	0.091
Ga ³⁺	228	0.131	0.133	0.132	0.135	0.131	0.133
Ge ⁴⁺	350	0.148	0.148	0.148	0.149	0.148	0.148
As ³⁺	28	0.054	0.057	0.056	0.062	0.092	0.065
As ⁵⁺	526	0.115	0.113	0.114	0.111	0.116	0.113
Se ⁴⁺	202	0.079	0.069	0.071	0.076	0.141	0.080
Br ⁵⁺	9	0.111	0.082	0.097	0.055	0.080	0.060
Rb ⁺	464	0.151	0.150	0.150	0.150	0.150	0.151
Sr ²⁺	377	0.196	0.193	0.194	0.188	0.195	0.194
Y ³⁺	178	0.138	0.139	0.138	0.140	0.117	0.139
Zr ⁴⁺	117	0.102	0.103	0.102	0.105	0.101	0.101
Nb ⁵⁺	251	0.162	0.159	0.160	0.157	0.161	0.159
Mo ⁵⁺	76	0.142	0.143	0.142	0.146	0.134	0.143
Mo ⁶⁺	970	0.129	0.133	0.131	0.142	0.130	0.133

Ag ⁺	200	0.086	0.084	0.085	0.082	0.087	0.086
Cd ²⁺	164	0.091	0.090	0.091	0.088	0.092	0.091
In ³⁺	125	0.114	0.113	0.113	0.111	0.115	0.114
Sn ²⁺	50	0.079	0.072	0.075	0.079	0.101	0.076
Sn ⁴⁺	38	0.166	0.164	0.165	0.161	0.168	0.166
Sb ³⁺	54	0.085	0.084	0.084	0.084	0.084	0.084
Te ⁴⁺	212	0.095	0.097	0.096	0.100	0.105	0.101
I ⁵⁺	134	0.166	0.135	0.150	0.106	0.146	0.110
I ⁷⁺	36	0.242	0.226	0.234	0.213	0.276	0.215
Cs ⁺	544	0.133	0.133	0.133	0.135	0.133	0.133
Ba ²⁺	857	0.227	0.223	0.225	0.216	0.225	0.224
La ³⁺	182	0.159	0.157	0.158	0.156	0.159	0.159
Ce ³⁺	76	0.127	0.128	0.127	0.131	0.128	0.129
Ce ⁴⁺	28	0.121	0.121	0.121	0.122	0.121	0.121
Pr ³⁺	99	0.148	0.142	0.145	0.135	0.152	0.149
Nd ³⁺	203	0.175	0.169	0.172	0.161	0.181	0.178
Sm ³⁺	97	0.151	0.148	0.150	0.145	0.152	0.150
Eu ²⁺	3	0.024	0.024	0.024	0.025	0.024	0.024
Eu ³⁺	49	0.138	0.136	0.137	0.134	0.137	0.136
Gd ³⁺	107	0.136	0.133	0.134	0.130	0.137	0.135
Tb ³⁺	48	0.113	0.113	0.113	0.114	0.115	0.115
Dy ³⁺	70	0.132	0.130	0.131	0.129	0.134	0.132
Ho ³⁺	81	0.136	0.132	0.134	0.128	0.139	0.136

Er ³⁺	102	0.138	0.136	0.137	0.133	0.140	0.138
Tm ³⁺	44	0.142	0.141	0.141	0.140	0.143	0.142
Yb ³⁺	82	0.174	0.173	0.174	0.173	0.176	0.175
Lu ³⁺	53	0.165	0.164	0.165	0.163	0.169	0.167
Hf ⁴⁺	22	0.087	0.086	0.086	0.086	0.087	0.086
Ta ⁵⁺	162	0.193	0.194	0.194	0.196	0.195	0.196
W ⁶⁺	436	0.187	0.186	0.186	0.188	0.187	0.187
Re ⁷⁺	59	0.184	0.187	0.185	0.190	0.184	0.187
Os ⁷⁺	7	0.207	0.199	0.201	0.204	0.216	0.200
Os ⁸⁺	8	0.208	0.221	0.215	0.233	0.204	0.220
Ir ⁴⁺	17	0.143	0.141	0.142	0.139	0.145	0.143
Hg ²⁺	52	0.190	0.161	0.175	0.129	0.221	0.200
Tl ⁺	74	0.109	0.121	0.107	0.098	0.110	0.110
Tl ³⁺	9	0.085	0.083	0.084	0.081	0.087	0.086
Pb ²⁺	276	0.108	0.108	0.108	0.110	0.111	0.110
Pb ⁴⁺	12	0.192	0.188	0.190	0.184	0.195	0.192
Bi ³⁺	231	0.164	0.151	0.157	0.140	0.182	0.170
Bi ⁵⁺	11	0.212	0.208	0.210	0.212	0.213	0.210
Th ⁴⁺	27	0.159	0.160	0.160	0.163	0.159	0.160
U ⁴⁺	18	0.111	0.113	0.112	0.116	0.112	0.115
U ⁵⁺	4	0.016	0.024	0.020	0.035	0.021	0.027
U ⁶⁺	585	0.144	0.148	0.144	0.167	0.146	0.152
Np ⁵⁺	33	0.057	0.059	0.058	0.063	0.058	0.060

Np ⁶⁺	7	0.083	0.081	0.081	0.085	0.082	0.082
	Mean	0.128	0.126	0.126	0.125	0.130	0.127
	Wt. mean	0.129	0.128	0.128	0.128	0.130	0.129

Table 2.S4 ICSD code for the structures used in the anion bond-valence sum verification (inclusive of previous sets)

Ion	ICSD Code
<i>Brown and Altermatt (1985)</i>	
H ⁺	202360
Li ⁺	84617
Be ²⁺	54110
B ³⁺	246060
C ⁴⁺	156626
N ⁵⁺	35494
Na ⁺	84709
Mg ²⁺	31332
Al ³⁺	32744
Si ⁴⁺	30521
P ⁵⁺	79756
S ⁴⁺	15554
S ⁶⁺	95407
Cl ⁷⁺	413238
K ⁺	280999
Ca ²⁺	202245
Sc ³⁺	65010
Ti ⁴⁺	40307
V ³⁺	59244

V ⁴⁺	86775
V ⁵⁺	170714
Cr ³⁺	245275
Cr ⁶⁺	98653
Mn ²⁺	202319
Mn ³⁺	39593
Mn ⁴⁺	95653
Fe ²⁺	246811
Fe ³⁺	80140
Co ²⁺	154223
Ni ²⁺	59588
Cu ²⁺	158375
Zn ²⁺	35652
Ga ³⁺	280793
Ge ⁴⁺	67535
As ³⁺	154363
As ⁵⁺	51072
Se ⁴⁺	412998
Se ⁶⁺	280951
Rb ⁺	171137
Sr ²⁺	281299
Y ³⁺	240470

Zr ⁴⁺	89899
Nb ⁵⁺	37243
Mo ⁶⁺	158777
Ag ⁺	90414
Cd ²⁺	87937
In ³⁺	90003
Sn ⁴⁺	151591
Sb ⁵⁺	51392
Te ⁴⁺	78917
Te ⁶⁺	245054
I ⁵⁺	416691
Cs ⁺	280947
Ba ²⁺	76926
La ³⁺	95753
Pr ³⁺	92444
Nd ³⁺	412406
Eu ³⁺	84881
Tb ³⁺	240703
Dy ³⁺	412523
Ho ³⁺	79757
Er ³⁺	79758
Yb ³⁺	280936

Ta ⁵⁺	280993
W ⁶⁺	60547
Pt ⁴⁺	281475
Hg ²⁺	89685
Tl ⁺	86099
Pb ²⁺	203201
Pb ⁴⁺	36629
Bi ³⁺	39611
U ⁶⁺	280839

Brese and O'Keeffe (1991)

Ti ³⁺	8149
Cr ²⁺	280309
Mn ⁷⁺	89508
Co ³⁺	36355
Cu ⁺	61677
Se ⁶⁺	280951
Ru ⁴⁺	95715
Rh ³⁺	74726
Pd ²⁺	416619
Sb ³⁺	31996
I ⁷⁺	400552
Ce ³⁺	76608

Ce ⁴⁺	59302
Sm ³⁺	412946
Eu ²⁺	30546
Gd ³⁺	86172
Tm ³⁺	62617
Lu ³⁺	412249
Hf ⁴⁺	250391
Re ⁷⁺	416510
Ir ⁵⁺	404507
Pt ²⁺	35407
Au ³⁺	92488
Tl ³⁺	201793
Bi ⁵⁺	240975
Th ⁴⁺	64745
U ⁴⁺	201342
U ⁵⁺	170896

Best published parameters

P ³⁺	300205
Cl ³⁺	59935
Cl ⁵⁺	40285
Cr ⁴⁺	71957
Cr ⁵⁺	85055

Mn ⁶⁺	67580
Co ⁴⁺	922
Ni ⁴⁺	175
Cu ³⁺	78595
Br ⁵⁺	47173
Nb ⁴⁺	88879
Mo ³⁺	202450
Mo ⁴⁺	202860
Mo ⁵⁺	75353
Tc ⁷⁺	61
Ru ⁵⁺	96219
W ⁵⁺	203048
Re ⁵⁺	10481
Os ⁸⁺	63
Ir ⁴⁺	67826
Np ⁵⁺	66995
Np ⁶⁺	51501
<i>This work</i>	
Mn ⁵⁺	97525
Rh ⁴⁺	16448
Pd ⁴⁺	72312
Tb ⁴⁺	60768

Os^{5+}	170175
Os^{7+}	412142

Chapter 3

Chemographic Exploration of the Milarite-Type Structure

Gagné, O.C. & Hawthorne, F.C. (2016). Chemographic Exploration of the Milarite-Type Structure. *Canadian Mineralogist* (*accepted*)

3.1 Preliminary discussion

The bond-valence model is used extensively in the analysis of inorganic crystal structures, and its power is in the fact that it is a simple method in which the physical details are not obscured by complexities of computation. When this model was first introduced, it was used primarily as a method for checking the correctness of a structure, as deviations from the valence-sum rule commonly indicate errors in interatomic distances. This has continued to be the major use of the model up to the present time (e.g., Delahaye et al., 2006), and most crystallographers use bond-valence curves to examine their own structures for possible problems with the refinement, but pay no attention to the power and importance of the model itself. More recently, the number of uses of the model in crystal structures has expanded, and Brown (2009) listed the following aspects of crystal structures that have been considered from the perspective of the bond-valence model: [1] distorted ion environments, [2] valence maps and ionic conduction, [3] the valence-matching principle and structure stability, [4] assigning charge distributions, [5] incommensurate structures, [6] structural effects of pressure, [7] structural effects of temperature. However, the majority of uses still involve validation of experimental results of individual structures. I am interested in how a complicated crystal-structure arrangement responds to different chemical compositions, and this issue may be approached using the bond-valence model.

3.1.1 *A priori* bond-valence calculations

Many mineral structures show a wide range of chemical compositions for a given bond topology (arrangement of ion sites). Those structures that are quite complicated, both crystal-chemically and compositionally, are of considerable interest to examine in this regard as [1] it is often not clear what chemical compositions are distinct minerals, [2] the factors constraining the possible chemical compositions are not apparent, and [3] the primary controls on the stability of the structure in general are not clear. The milarite structure is a good example of such structure, where a wide range of cations is observed to occupy the various sites of the structures, leading to numerous minerals (Table 3.2).

There are two important theorems to Bond-Valence Theory: [1] the valence-sum rule, and [2] the loop rule. The *valence-sum rule* states that *the sum of the bond valences at each atom is equal to the magnitude of the atomic valence*. The *loop rule* states that *the sum of the directed bond-valences around any circuit (closed path) of bonds in a structure is zero*. Given a set of formal charges at the ion sites in a structure, the equations associated with the valence-sum rule and the loop rule may be solved for the bond valences (Brown 1977, Rutherford 1990). I will denote these bond valences as the *a priori* bond-valences. This approach has been used only sparingly, mostly to predict bond lengths in simple structures from the *a priori* bond-valences and the appropriate bond-valence curves for the site occupants (Brown 1977, Rutherford 1990, Urusov & Orlov 1999, Hawthorne & Sokolova 2008). However, *a priori* bond-valence calculations provide us with an ideal method for examining the control of bond topology on site occupancy in crystal structures. In this chapter, I use *a priori* bond-valence calculations to have an in-depth look at the milarite structure and its mineral constituents.

3.1.2 Structural strain

The constraint that a structural arrangement have translational symmetry and associated space-group symmetry exerts controls on the local positioning of ions, in many cases preventing them from taking up the exact position that will accord with the valence-sum rule. Deviation from the valence-sum rule is a measure of the strain in a structural arrangement: the larger the deviations the greater the strain on the structure, and too great a strain will result in the structure being unstable (*i.e.*, it does not occur). The *Global Instability Index*, GII, was introduced by Salinas-Sanchez *et al.* (1992), and is a direct measure of the deviation of the structure from the valence-sum rule; Brown (2002) suggested that a value of over 0.2 v.u. for GII usually indicates that a structure is too strained to be stable. The *Bond Strain Index*, BSI, was introduced by Preiser *et al.* (1999), and is a measure of the deviation from the valence-sum rule and the loop rule, *i.e.*, it is a measure of the mismatch between *a priori* and experimental bond valences. The index BSI is obviously a more comprehensive measure of structural strain as it depends on deviations from both the valence-sum rule and the loop rule.

The BSI has not seen very much use (compared with GII) as it requires an *a priori* bond-valence calculation on each structure for which it is used. However, the calculation of the BSI has one great advantage over GII: it leads to the specific localization of the strain in the structure. This is of considerable interest in complicated structures as this allows an assessment of the response of the strain to compositional variations by varying the charges of the ions in the structure. Strain has not been examined in a complicated structure in this way before, and in the next chapter I will do so for the

milarite structure. I use the milarite structure and the milarite-group minerals as this is a fairly complicated structure with a range of different coordination numbers and 23 minerals of different end-member chemical composition. In addition, I will use this opportunity to examine all available data on the chemical compositions of both minerals and synthetic phases with the milarite structure and assess how many minerals have been analyzed with regard to chemical composition but have not been recognized as distinct mineral species.

3.1.3 References

Brown, I.D. (1977). Predicting bond lengths in inorganic crystals. *Acta Cryst. B* **33**, 1305-1310.

Brown, I.D. (2002). *The Chemical Bond in Inorganic Chemistry. The Bond Valence Model*. Oxford University Press.

Brown, I. D. (2009). Recent developments in the methods and applications of the bond valence model. *Chem. Rev.* **109**, 6858-6919.

Delahaye, T., Boucher, F., Paris, M., Joubert, O., Caldes, M. & Piffard, Y. (2006). Some Experimental Evidence that $\text{Zn}_4\text{O}(\text{BO}_3)_2$ is $\text{Zn}_6\text{O}(\text{OH})(\text{BO}_3)$. *Angew. Chem.* **45**, 4060–4062.

Hawthorne, F.C. & Sokolova, E. (2008). The crystal chemistry of the scapolite-group minerals: II. The origin of the $I4/m \rightarrow P4_2/n$ phase transition and the non-linear variations in chemical composition. *Can. Min.* **46**, 1555-1575.

Preiser, C., Lösel, J., Brown, I.D., Kunz, M. & Skowron, A. (1999). Long-range Coulombic forces and localized bonds. *Acta Cryst. B* **55**, 698-711.

Rutherford, J.S. (1990). Theoretical prediction of bond-valence networks. *Acta Cryst. B* **46**, 289-292.

Salinas-Sanchez, A., Garcia-Munoz, J.L., Rodriguez-Carvajal, J., Saez-puche, R., & Martinez, J.L. (1992). Structural characterization of R_2BaCuO_5 ($R = Y, Lu, Yb, Tm, Er, Ho, Dy, Gd, Eu$ and Sm) oxides by X-ray and neutron-diffraction, *J. Solid State Chem.* **100**, 201–211.

Urusov V.S. & Orlov I.P. (1999). State-of-art and perspectives of the bond-valence model in inorganic crystal chemistry, *Crystallogr. rep.* **44**(4), 686-709.

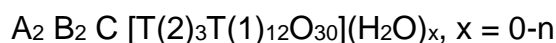
3.2 Abstract

The milarite structure-type has an uncommonly large number of distinct mineral species (twenty-three at present). Here we explore this structure type from the point of view of possible root charge arrangements and end-member compositions. Enumeration shows that there are thirty-four distinct root charge arrangements with Si = 12 *apfu* and thirty-nine distinct root charge arrangements with Si = 8-11 *apfu*. *A priori* bond-valence calculations on all root charge arrangements allows evaluation of lattice-induced strain as a function of chemical composition for all arrangements for which the detailed atomic arrangement has been refined. Analysis of localized strain indicates that the *B* site has the highest amount of strain in the structure, and in accord with this finding, milarite-group minerals with vacancies at the *B* site are more common than milarite-group minerals with fully occupied *B* sites. The *a priori* bond-valence calculations suggest that many other compositions are possible for the milarite structure-type. Examination of synthesis results reveals twenty synthetic compounds with the milarite-type structure that have distinct (dominant) end-member compositions. Examination of ~350 chemical analyses from the literature reveals twenty-nine distinct end-member compositions, six of which deserve to be described as new mineral species. Two additional analyses could lead to new minerals, but require confirmation of site populations by structure refinement.

Keywords: milarite, crystal structure, chemographic exploration, bond-valence, lattice strain.

3.3 Introduction

Milarite, ideally $K_2Ca[AlBe_2Si_{12}O_{30}](H_2O)$, was first described by Kuschel (1877) from Val Giuf, Tavetsch, Grischun, Switzerland, and a relatively large number of minerals are now known that have this specific structural arrangement. The general formula of the minerals of the milarite group (Forbes *et al.* 1972) may be written as



where the cation species corresponding the letters of the formula for all end-member compositions of approved minerals are listed in Table 3.1. Note that groups of cations are listed as regular letters whereas crystallographic sites are written in italic letters. As is apparent from Table 3.1, the milarite structure is extremely flexible with regard to its constituent cations, and a considerable number of minerals (Table 3.2) and synthetic compounds adopt this basic atomic arrangement. The value of n , the maximum amount of H_2O in the structure, is not well-characterized, and we will examine this issue here.

Table 3.1 Sites and site occupancies in the milarite-group minerals

Site	Equipoint	C.N.	Occupancy
<i>T</i> (1)	24m	4	Si, Al
<i>T</i> (2)	6f	4	Li, Be, B, Mg, Al, Si, Mn ²⁺ , Zn
<i>A</i>	4c	6	Al, Fe ³⁺ , Sn ⁴⁺ , Mg, Zr, Fe ²⁺ , Ca, Na, Y, Sc
<i>B</i>	4d	9	Na, H ₂ O, □, K
<i>C</i>	2a	12	K, Na, Ba, □
<i>D</i>	2b	18	□

Table 3.2 Current minerals of the milarite group: end-member compositions, site occupancies and root charge arrangements

Name	A ₂	B ₂	C	T(2) ₃	T(1) ₁₂	O ₃₀	Root charge arrangement	Refs
Agakhanovite-(Y)	YCa	□ ₂	K	Be ₃	Si ₁₂	O ₃₀	[21]	(1)
Almarudite	Mn ₂	□ ₂	K	Be ₂ Al	Si ₁₂	O ₃₀	[10]	(2)
Armenite	Ca ₂	□ ₂	Ba	Al ₃	(Si ₉ Al ₃)	O ₃₀	{8}	(3)
Berezanskite	Ti ₂	□ ₂	K	Li ₃	Si ₁₂	O ₃₀	[29]	(4)
Brannockite	Sn ₂	□ ₂	K	Li ₃	Si ₁₂	O ₃₀	[29]	(5)
Chayesite	Mg ₂	□ ₂	K	Mg ₂ Fe ³⁺	Si ₁₂	O ₃₀	[10]	(6)
Darapiosite	Mn ₂	Na ₂	K	LiZn ₂	Si ₁₂	O ₃₀	[24]	(7)
Dusmatovite	Mn ₂	K□	K	Zn ₃	Si ₁₂	O ₃₀	[17]	(8)
Eifelite	MgNa	Na ₂	K	Mg ₃	Si ₁₂	O ₃₀	[18]	(9)
Friedrichbeckeite	Mg ₂	Na□	K	Be ₃	Si ₁₂	O ₃₀	[17]	(10)
Klöchite	Fe ²⁺ Fe ³⁺	□ ₂	K	Zn ₃	Si ₁₂	O ₃₀	[21]	(11)
Merrihueite	Fe ²⁺ ₂	Na□	K	Fe ²⁺ ₃	Si ₁₂	O ₃₀	[17]	(12)
Milarite	Ca ₂	□ ₂	K	Be ₂ Al	Si ₁₂	O ₃₀	[10]	(13)
Oftedalite	ScCa	□ ₂	K	Be ₃	Si ₁₂	O ₃₀	[21]	(14)
Osumilite	Fe ²⁺ ₂	□ ₂	K	Al ₃	Si ₁₀ Al ₂	O ₃₀	{6}	(15)
Osumilite-(Mg)	Mg ₂	□ ₂	K	Al ₃	Si ₁₀ Al ₂	O ₃₀	{6}	(16)
Poudretteite	Na ₂	□ ₂	K	B ₃	Si ₁₂	O ₃₀	[2]	(17)
Roedderite	Mg ₂	Na□	K	Mg ₃	Si ₁₂	O ₃₀	[17]	(18)
Shibkovite	Ca ₂	K□	K	Zn ₃	Si ₁₂	O ₃₀	[17]	(19)
Sogdianite	Zr ₂	□ ₂	K	Li ₃	Si ₁₂	O ₃₀	[29]	(20)
Sugilite	Fe ³⁺ ₂	Na ₂	K	Li ₃	Si ₁₂	O ₃₀	[32]	(21)
Trattnerite	Fe ³⁺ ₂	□ ₂	□	Mg ₃	Si ₁₂	O ₃₀	[20]	(22)
Yagiite	Mg ₂	□ ₂	Na	Al ₃	Si ₁₀ Al ₂	O ₃₀	{6}	(23)

References: (1) Hawthorne *et al.* (2014), Černý *et al.* (1991); (2) Mihajlović *et al.* (2004); (3) Neumann (1941); (4) Pautov & Agakhanov (1997), Hawthorne *et al.* (2015); (5) White *et al.* (1973), Armbruster & Oberhänsli (1988b); (6) Velde *et al.* (1989); (7) Semenov *et al.* (1975), Ferraris *et al.* (1999); (8) Pautov *et al.* (1996), Sokolova & Pautov (1995); (9) Abraham *et al.* (1983); (10) Lengauer *et al.* (2009); (11) Bojar *et al.* (2011); (12) Dodd *et al.* (1965); (13) Hawthorne *et al.* (1991); (14) Cooper *et al.* (2006); (15) Miyashiro (1956), Armbruster & Oberhänsli (1988a); (16) Chukanov *et al.* (2011), Balassone *et al.* (2008); (17) Grice *et al.* (1987); (18) Fuchs *et al.* (1966), Hentschel *et al.* (1980), Armbruster (1989); (19) Pautov *et al.* (1998), Sokolova *et al.* (1999); (20) Dusmatov *et al.* (1968), Cooper *et al.* (1999), Sokolova *et al.* (2000); (21) Murakami *et al.* (1976), Kato *et al.* (1976); (22) Postl *et al.* (2004); (23) Bunch & Fuchs (1969).

3.4 Description of the milarite structure-type

Milarite is hexagonal, space group $P6/mcc$, $a \approx 10.40$, $c \approx 13.80$ Å, although various compositions can show anomalous biaxial behaviour (e.g., Goldman & Rossman 1978; Janeczek 1986). Milarite was originally considered a (double-)ring silicate, the structure of which was related to that of beryl by melding of two beryl $[\text{Si}_6\text{O}_{18}]$ rings through their apical vertices to form an $[\text{Si}_{12}\text{O}_{30}]$ double-ring. However, inclusion of other types of tetrahedra into such structural considerations (Zoltai 1960, Liebau 1985) led to the consideration of beryl and milarite as framework beryllo-alumino-silicates, and Hawthorne & Smith (1986,1988) showed that the structures of both beryl and milarite can be derived from four-connected three-dimensional nets in a similar fashion to other framework alumino-silicates. Thus the milarite structure is now considered as a framework structure. Cation-coordination polyhedra are identified by the name of the central cation site, e.g., the $T(1)$ tetrahedron.

3.4.1 The $T(1)$ tetrahedron

This tetrahedron shares O anions with two other $T(1)$ tetrahedra to form a six-membered ring with the tetrahedra all pointing in the same direction (as in beryl), and the apical anions of this ring are shared with $T(1)$ tetrahedra of another ring to form an $[\text{Si}_{12}\text{O}_{30}]$ double six-membered ring (Figs. 3.1, 3.2). The $T(1)$ tetrahedron thus shares three anions with adjacent $T(1)$ tetrahedra and one anion with a $T(2)$ tetrahedron that links the $[\text{Si}_{12}\text{O}_{30}]$ clusters into a framework (Figs. 3.1, 3.2). The $\langle T(1)\text{-O} \rangle$ distances in refined milarite structures show little variation (± 0.002 Å in the data of Černý *et al.* 1980,

and Hawthorne *et al.* 1991). However, the corresponding chemical data show a well-developed positive correlation between the Si content and the Be/(Be + Al) ratio, indicating slight replacement of Si by Al (maximum = 0.1 Al *apfu*) that is insufficient to affect significantly the size of the $T(1)$ tetrahedron.

3.4.2 The $T(2)$ tetrahedron

The $T(2)$ tetrahedron shares four anions with adjacent $T(1)$ tetrahedra and links the $[\text{Si}_{12}\text{O}_{30}]$ clusters into a framework (Figs. 3.1, 3.2). It also shares two edges with adjacent A octahedra. Refinement of several milarite samples of differing chemical composition (Hawthorne *et al.* 1991) has shown that this site is occupied by variable amounts of Be and Al, and the $\langle T(2)\text{-O} \rangle$ distance varies linearly as a function of Be/(Be + Al) ratio.

3.4.3 The A octahedron

The A octahedron lies on the threefold axis between the $[\text{Si}_{12}\text{O}_{30}]$ clusters, sharing corners with the $T(1)$ tetrahedra and further strengthening the linkage of the framework of tetrahedra. It also shares edges with three flanking $T(2)$ tetrahedra (Fig. 3.1). This site is ideally completely occupied by Ca in milarite itself. However, the A cation generally shows extremely anisotropic-displacement parameters, with the long axis of the ellipsoid oriented along the c axis; this has been modelled by a “split site” (Kimata & Hawthorne 1989, Armbruster *et al.* 1989), and the amount of splitting correlates with the Be/(Be + Al) ratio of the structure in milarite itself.

3.4.4 The *B* polyhedron

The *B* site lies on the threefold axis, between the $[\text{Si}_{12}\text{O}_{30}]$ clusters, and directly above and below the *A* octahedron (Fig. 3.2), surrounded by nine O atoms. The ideal *B* site occurs at $z = 0$, and has three O neighbors at $\sim 2.78 \text{ \AA}$ and six O neighbours at $\sim 3.30 \text{ \AA}$. The *B*-site constituents show very anisotropic-displacement behaviour (also modelled as a “split-site”). Bakakin *et al.* (1975) and Černý *et al.* (1980) showed that H_2O is an important constituent at the *B* site. However, small amounts of alkali and alkaline-earth cations also occupy this site. Armbruster *et al.* (1989) showed that the split *B* site is occupied by H_2O and that the B cations occupy the central *B* site, and went on to suggest that the *A*-site splitting in milarite is the result of $^{\text{A}}\text{Ca}-^{\text{B}}\text{H}_2\text{O}$ interaction in the *c* direction.

3.4.5 The *C* polyhedron

The *C* site occurs in the channel formed by the $[\text{Si}_{12}\text{O}_{30}]$ clusters that stack along the *c* direction (Figs. 3.1, 3.2), and is coordinated by twelve anions at a distance of $\sim 3.02 \text{ \AA}$. It is occupied primarily by K in all the milarite-group minerals except armenite, where it is occupied by Ba, and yagiite (Na). The occurrence of Ba at the *C* site in armenite is related to the occurrence of significant Al at the *T*(1) site; the divalent cation at *C* helps satisfy the local bond-valence deficiency at the O(2) anion caused by substitution of trivalent Al for Si at the *T*(1) site.

3.4.6 The *D* site

This site was identified by Forbes *et al.* (1972) and is generally mentioned in discussions of the milarite structure. However, no structure has been reported in which this site is occupied, even by small amounts of any constituent, and we will not consider it further here.

Typical interatomic distances (for sugilite) are shown in Table 3.3. In combination with Figs. 3.1 and 3.2, Table 3.3 provides important stereochemical details when considering chemical substitutions and articulation requirements of the milarite structure.

Table 3.3 Selected interatomic distances (Å) in sugilite*

<i>A</i> –O(3) x3	1.972(2)	<i>T</i> (1)–O(1)	1.625(1)
<i>A</i> –O(3)' x3	<u>2.409(1)</u>	<i>T</i> (1)–O(2)	1.620(3)
< <i>A</i> –O>	2.334	<i>T</i> (1)–O(2)"	1.615(2)
		<i>T</i> (1)–O(3)	<u>1.577(1)</u>
<i>B</i> –O(1) x3	2.420(2)	< <i>T</i> (1)–O>	1.609
<i>B</i> –O(3) x6	<u>2.733(8)</u>		
< <i>B</i> –O>	2.577	<i>T</i> (2)–O(3) x4	1.970(2)
<i>C</i> –O(2) x12	2.944(2)		

*From Armbruster & Oberhänsli (1988b)

Figure 3.1 The crystal structure of milarite projected down the **c** axis. *T*(1) tetrahedra: orange; *T*(2) tetrahedra: green; A site: small red circle; C site: yellow circle.

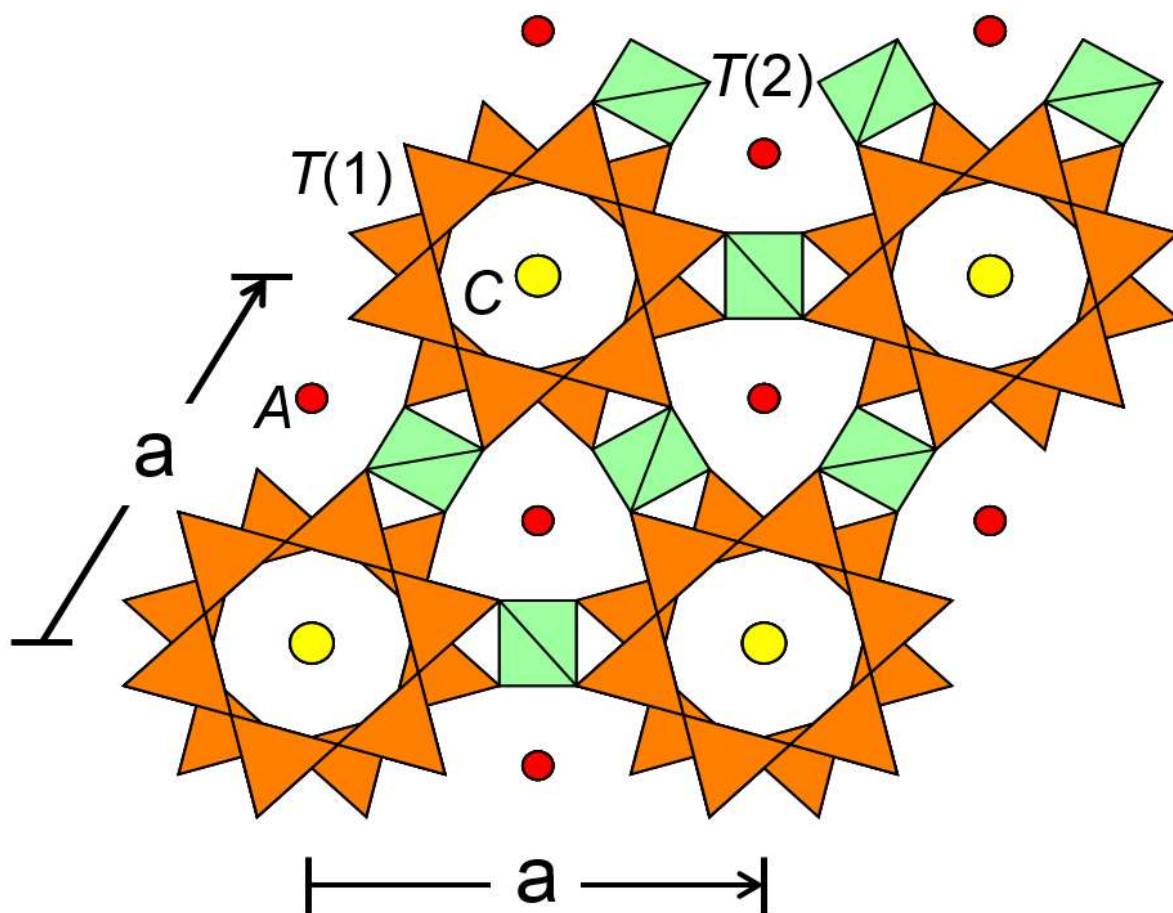
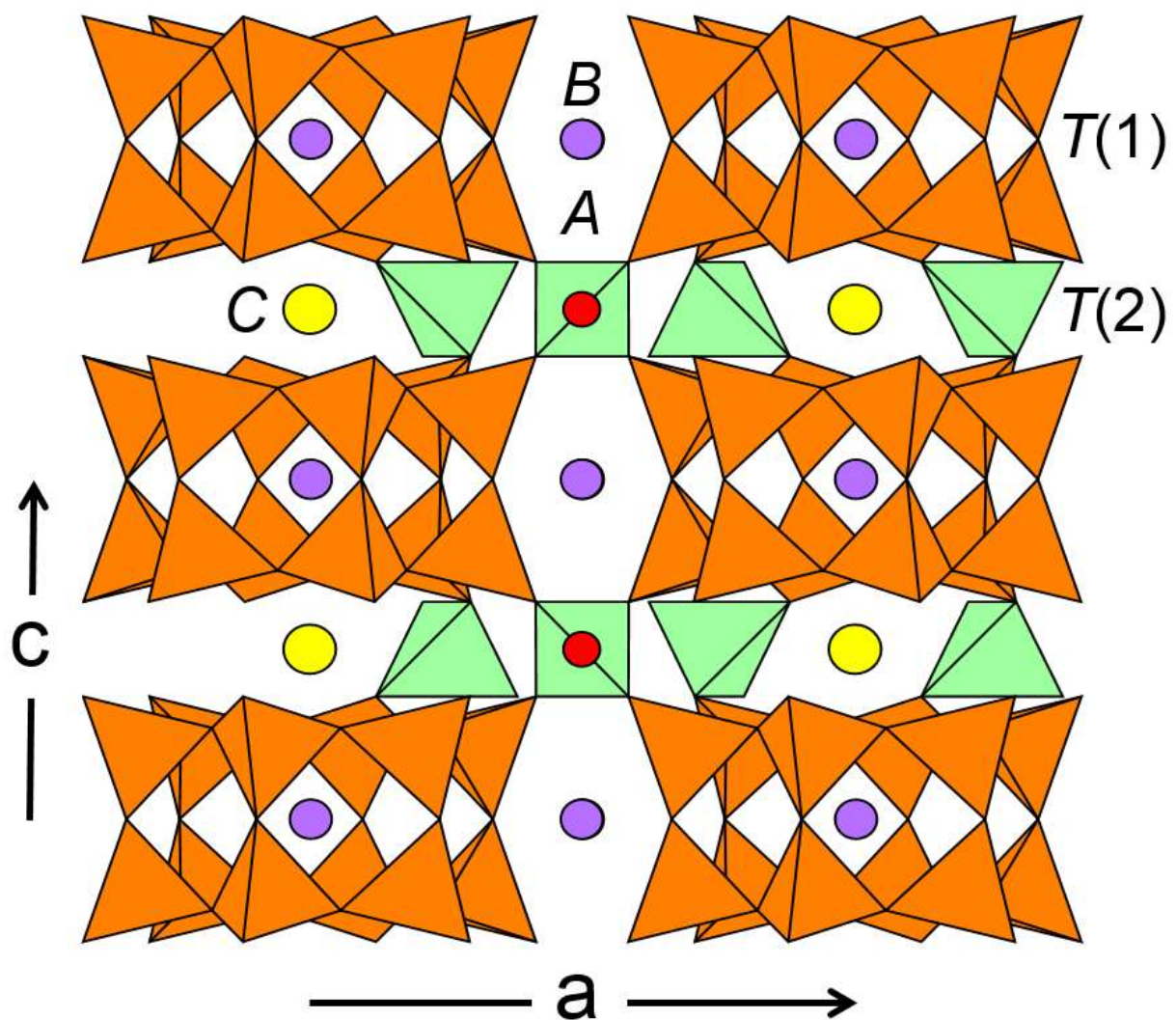


Figure 3.2 The crystal structure of milarite projected orthogonal to the **c** axis. *Legend as in Fig. 3.1; B site: mauve circle.*



3.5 End-members and their significance

From an algebraic perspective, a *chemical system* is described in terms of its components. *System components* are those (components) required to describe the chemical variability of the system and *phase components* are those components required to describe the chemical variability in individual phases (Spear 1993). Phase components must be independently variable (Gibbs 1961), *i.e.*, they must be additive, and for minerals, they must be conformable with the structure of that mineral. If we define our system as a specific crystal structure, we may define the components of this system as the smallest set of chemical formulae required to describe the composition of all minerals in the system. The definition, “the smallest set of chemical formulae required to describe the composition of all the phases in the system”, defines the components of the system as its set of end-member compositions, and the set of end-member compositions define the possible composition space occupied by that structure. End members have certain constraints (Hawthorne 2002):

- (1) they must be fixed and conformable with the crystal structure of the mineral;
- (2) they must be neutral (*i.e.*, not carry an electric charge);
- (3) they must be irreducible within the system considered (*i.e.*, they cannot be expressed as two or more simpler compositions that are compatible with the crystal structure of the system).

For the majority of atomic arrangements and chemical compositions, these constraints result in end-member formulae which have a single constituent at each site (*e.g.*, diopside: $\text{CaMgSi}_2\text{O}_6$: M1 = Mg, M2 = Ca, T = Si, O1 = O2 = O3 = O) or group of sites

(forsterite: Mg_2SiO_4 : $\text{M1} + \text{M2} = \text{Mg}$, $\text{T} = \text{Si}$, $\text{O1} = \text{O2} = \text{O3} = \text{O4} = \text{O}$) in the structure. However, Hawthorne (2002) showed that some end-members have two constituents of different valence and in a fixed ratio at one site in their structure (the remaining sites having only one constituent each). A classic example of this is milarite itself (Table 3.2), in which $\text{T}(2) = \text{Be}_2\text{Al}$ *apfu* (atoms per formula unit) in the end-member formula. Note that by definition, an end-member can have more than one species at only one site, and only two species at that site. If more than one cation or anion is introduced at another site in the structure, or a third species is introduced at a site, the resulting composition is not irreducible and may be resolved into two or more end-member compositions.

3.5.1 Root charge arrangements

In minerals, homovalent and heterovalent substitutions are very different in character. Homovalent substitutions generally introduce only minor changes in bond valences (due to relaxation of bond lengths), whereas heterovalent substitutions produce major changes in the pattern of bond valences due to the different arrangements of formal charges in the structure. Thus we may identify a set of root charge arrangements that correspond to the set of end members related only by heterovalent substitutions. A set of end members related only by homovalent substitutions between themselves will have the same root charge arrangement.

This difference between homovalent and heterovalent substitutions is embedded in the more recent classification/nomenclature schemes for minerals (*e.g.*, arrojadite, Chopin *et al.* 2006; tourmaline, Henry *et al.* 2011; amphibole, Hawthorne *et al.* 2012)

where root compositions are assigned a root name and homovalent analogues are named by adding prefixes or suffixes to the appropriate root name. The idea of root charge arrangements provides us with a very compact way to evaluate end-member arrangements, as the distinct arrangements with regard to heterovalent substitutions correspond to the distinct arrangements of the corresponding formal charges, and the distinct arrangements with regard to homovalent substitutions correspond to the distinct arrangements of homovalent cations for a specific arrangement of formal charges. We will take this approach to the milarite-type structure and derive its set of end-member compositions.

3.5.2 Root charge arrangements in the milarite structure-type

Inspection of the (ideal) site-populations listed in Table 3.2 gives us an idea of what ranges of charges to consider. For the *A* site, the formal charge varies from 2+ (e.g., *A* = Na₂ in poudretteite) to 8+ (e.g., *A* = Ti⁴⁺₂ in berezanskite). For the *B* site, the formal charge varies from 0 (e.g., *B* = □₂ in almarudite) to 2+ (e.g., *B* = Na₂ in sugilite). For the *C* site, the formal charge varies from 0 (e.g., *C* = □ in trattnerite) to 2+ (e.g., *C* = Ba in armenite). For the *T*(2) site, the formal charge varies from 3+ (e.g., *T*(2) = Li₃ in brannockite) to 9+ (e.g., *T*(2) = Al₃ in osumilite). For the *T*(1) site, the formal charge varies from 45+ (e.g., *T*(1) = Si₉Al₃ in armenite) to 48+ (e.g., *T*(1) = Si₁₂ in milarite). We note that trace amounts of Nb⁵⁺ and vacancy have been observed at the *A* site of the structure for poudretteite (Grice *et al.*, 1987) and berezanskite (Pautov & Agakhanov, 1997) respectively, and we did not discard these charges in our derivation of the root charge arrangements when they were obtained on the basis of charge balance.

Table 3.4 shows the root charge arrangements for $\text{Si} = 12 \text{ apfu}$, *i.e.*, $\text{T}(1) \text{ charge} = 48+$. The arrangements are organized in terms of increasing charge of the $\text{A} + \text{B} + \text{C}$ cations (left-hand column in Tables 3.4 and 3.5) and decreasing charge of the T cations (right-hand column in Table 3.4). It is immediately apparent on inspection of Table 3.4 that many root charge arrangements are not represented by analogous mineral species. There are thirty-four distinct root charge arrangements with $\text{Si} = 12 \text{ apfu}$, and nine of these correspond to minerals ([2], [10], [17], [18], [20], [21], [24], [29], [32]). Table 3.5 shows root charge arrangements with $\text{Si} \neq 12 \text{ apfu}$ and an aggregate $\text{T}(1) \text{ charge}$ of greater than $44+$ (Si_8Al_4). Of the thirty-nine arrangements shown, only two correspond to the structures of milarite-group minerals ({6}, {8}). We are left with a major question: are the other root charge arrangements not stable OR are there many other milarite structures with chemical compositions analogous to the as yet unrepresented root charge arrangements that we have not yet discovered or synthesized? We will consider this issue next with regard to the known chemical compositions of the milarite-group minerals.

Table 3.4 Root charge arrangements* for the milarite structure-type with Si = 12 *apfu*

Number	Charge at (A + B + C) sites	A ₂	B ₂	C	T(1) ₁₂	T(2) ₃	Charge at [T(1) + T(2)] sites
[1]	3	0 ₂	1 ₂	1 ₁	4 ₁₂	3 ₃	57
[2]	3	1₂	0₂	1₁	4₁₂	3₃	57
[3]	3	0 ₁ 1 ₁	1 ₂	0 ₁	4 ₁₂	3 ₃	57
[4]	3	1 ₂	0 ₁ 1 ₁	0 ₁	4 ₁₂	3 ₃	57
[5]	4	1 ₂	1 ₂	0 ₁	4 ₁₂	3 ₂ 2 ₁	56
[6]	4	2 ₂	0 ₂	0 ₁	4 ₁₂	3 ₂ 2 ₁	56
[7]	4	0 ₂	2 ₂	0 ₁	4 ₁₂	3 ₂ 2 ₁	56
[8]	5	0 ₂	2 ₂	1 ₁	4 ₁₂	3 ₁ 2 ₂	55
[9]	5	1 ₂	1 ₂	1 ₁	4 ₁₂	3 ₁ 2 ₂	55
[10]	5	2₂	0₂	1₁	4₁₂	3₁2₂	55
[11]	6	0 ₂	2 ₂	2 ₁	4 ₁₂	2 ₃	54
[12]	6	2 ₂	0 ₂	2 ₁	4 ₁₂	2 ₃	54
[13]	6	1 ₂	1 ₂	2 ₁	4 ₁₂	2 ₃	54
[14]	6	1 ₂	2 ₂	0 ₁	4 ₁₂	2 ₃	54
[15]	6	2₂	1₂	0₁	4₁₂	2₃	54
[16]	6	0 ₁ 1 ₁	2 ₂	1 ₁	4 ₁₂	2 ₃	54
[17]	6	2₂	0₁1₁	1₁	4₁₂	2₃	54
[18]	6	1₁2₁	1₂	1₁	4₁₂	2₃	54
[19]	6	1 ₂	1 ₁ 2 ₁	1 ₁	4 ₁₂	2 ₃	54
[20]	6	3₂	0₂	0₁	4₁₂	2₃	54
[21]	6	2₁3₁	0₂	1₁	4₁₂	2₃	54
[22]	7	3 ₂	0 ₂	1 ₁	4 ₁₂	2 ₂ 1	53
[23]	7	1 ₂	2 ₂	1 ₁	4 ₁₂	2 ₂ 1	53
[24]	7	2₂	1₂	1₁	4₁₂	2₂1	53
[25]	8	2 ₂	2 ₂	0 ₁	4 ₁₂	2 ₁ 2	52
[26]	8	3₂	1₂	0₁	4₁₂	2₁2	52
[27]	8	4 ₂	0 ₂	0 ₁	4 ₁₂	2 ₁ 2	52
[28]	9	4 ₁ 5 ₁	0 ₂	0 ₁	4 ₁₂	1 ₃	51

[29]	9	4₂	0₂	1₁	4₁₂	1₃	51
[30]	9	4 ₂	0 ₁ 1 ₁	0 ₁	4 ₁₂	1 ₃	51
[31]	9	3 ₁ 4 ₁	1 ₂	0 ₁	4 ₁₂	1 ₃	51
[32]	9	3₂	1₂	1₁	4₁₂	1₃	51
[33]	9	2 ₁ 3 ₁	2 ₂	0 ₁	4 ₁₂	1 ₃	51
[34]	9	2 ₂	2 ₂	1 ₁	4 ₁₂	1 ₃	51

*Those root charge arrangements shown in bold are the ones that correspond to observed end-member compositions of minerals, potential minerals, and synthetics

Table 3.5 Root charge arrangements* for the milarite structure-type with Si \neq 12 *apfu*

Number	Charge at (A + B + C) sites	A ₂	B ₂	C	T(1) ₁₂	T(2) ₃	Charge at [T(1) + T(2)] sites
{1}	4	1 ₂	1 ₂	0 ₁	4 ₁₁ 3 ₁	3 ₃	56
{2}	4	2₂	0₂	0₁	4₁₁3₁	3₃	56
{3}	4	0 ₂	2 ₂	0 ₁	4 ₁₁ 3 ₁	3 ₃	56
{4}	5	0 ₂	2 ₂	1 ₁	4 ₁₀ 3 ₂	3 ₃	55
{5}	5	1 ₂	1 ₂	1 ₁	4 ₁₀ 3 ₂	3 ₃	55
{6}	5	2₂	0₂	1₁	4₁₀3₂	3₃	55
{7}	6	0 ₂	2 ₂	2 ₁	4 ₉ 3 ₃	3 ₃	54
{8}	6	2₂	0₂	2₁	4₉3₃	3₃	54
{9}	6	1 ₂	1 ₂	2 ₁	4 ₉ 3 ₃	3 ₃	54
{10}	6	1 ₂	2 ₂	0 ₁	4 ₉ 3 ₃	3 ₃	54
{11}	6	2 ₂	1 ₂	0 ₁	4 ₉ 3 ₃	3 ₃	54
{12}	6	3 ₂	0 ₂	0 ₁	4 ₉ 3 ₃	3 ₃	54
{13}	7	3 ₂	0 ₂	1 ₁	4 ₈ 3 ₄	3 ₃	53
{14}	7	1 ₂	2 ₂	1 ₁	4 ₈ 3 ₄	3 ₃	53
{15}	7	2 ₂	1 ₂	1 ₁	4 ₈ 3 ₄	3 ₃	53
{16}	7	3 ₂	0 ₂	1 ₁	4 ₁₁ 3 ₁	2 ₃	53
{17}	7	1 ₂	2 ₂	1 ₁	4 ₁₁ 3 ₁	2 ₃	53
{18}	7	2₂	1₂	1₁	4₁₁3₁	2₃	53
{19}	8	2 ₂	2 ₂	0 ₁	4 ₁₀ 3 ₂	2 ₃	52
{20}	8	3 ₂	1 ₂	0 ₁	4 ₁₀ 3 ₂	2 ₃	52
{21}	8	4 ₂	0 ₂	0 ₁	4 ₁₀ 3 ₂	2 ₃	52
{22}	9	4 ₂	0 ₂	1 ₁	4 ₉ 3 ₃	2 ₃	51
{23}	9	3 ₂	1 ₂	1 ₁	4 ₉ 3 ₃	2 ₃	51
{24}	9	2 ₂	2 ₂	1 ₁	4 ₉ 3 ₃	2 ₃	51
{25}	10	2 ₂	2 ₂	2 ₁	4 ₈ 3 ₄	2 ₃	50
{26}	10	3 ₂	2 ₂	0 ₁	4 ₈ 3 ₄	2 ₃	50
{27}	10	4 ₂	1 ₂	0 ₁	4 ₈ 3 ₄	2 ₃	50
{28}	10	5 ₂	0 ₂	0 ₁	4 ₈ 3 ₄	2 ₃	50

{29}	10	2 ₂	2 ₂	2 ₁	4₁₁3₁	1 ₃	50
{30}	10	3 ₂	2 ₂	0 ₁	4₁₁3₁	1 ₃	50
{31}	10	4 ₂	1 ₂	0 ₁	4₁₁3₁	1 ₃	50
{32}	10	5 ₂	0 ₂	0 ₁	4₁₁3₁	1 ₃	50
{33}	11	5 ₂	0 ₂	1 ₁	4₁₀3₂	1 ₃	49
{34}	11	4 ₂	1 ₂	1 ₁	4₁₀3₂	1 ₃	49
{35}	11	3 ₂	2 ₂	1 ₁	4₁₀3₂	1 ₃	49
{36}	12	5 ₂	1 ₂	0 ₁	4₉3₃	1 ₃	48
{37}	12	4 ₂	2 ₂	0 ₁	4₉3₃	1 ₃	48
{38}	13	5 ₂	1 ₂	1 ₁	4₈3₄	1 ₃	47
{39}	13	4 ₂	2 ₂	1 ₁	4₈3₄	1 ₃	47

*Those root charge arrangements shown in bold are the ones that correspond to observed end-member compositions of minerals, potential minerals, and synthetics

3.6 Chemical compositions of milarite-group minerals

A literature review of over 132 publications (listed in Table 3.S1) describing milarite-group minerals and synthetic milarite-group compounds has provided us with ~350 chemical analyses. There are currently twenty-three valid mineral species with the milarite structure (Table 3.2). Among the ~350 analyses, we have identified twenty-nine distinct end-member compositions that are the dominant constituent in one or more chemical analyses, twenty-three of which correspond to the minerals of Table 3.2. The remaining six dominant distinct end-member formulae do not correspond to named mineral species. These are listed in Table 3.6, together with the dominant end-member formulae and the corresponding root charge arrangement, and the chemical compositions are listed in Table 3.7. Of course, we have made assumptions with regard to the site populations in the minerals of Table 3.6; in general, these follow the observed site-populations in Table 3.2. Where the dominant divalent cations are Mg and Fe^{2+} , there is the potential for order-disorder of these cations over the *A* and *T*(2) sites, and without crystal-structure or spectroscopic data, we cannot assign distinct site-populations. In these cases, we have written the site populations as (Mg, Fe^{2+}) or (Fe^{2+} ,Mg) according to whether Mg or Fe^{2+} is the dominant constituent (e.g., PM3, FC1 and FMM, Table 3.6).

Table 3.6 New end-member compositions corresponding to observed chemical compositions of milarite-group minerals

Sample number	A_2	B_2	C	$T(2)_3$	$T(1)_{12}$	RCA*	"Name"
PM3	$(Fe^{2+}, Mg)_2$	$K\Box$	K	$(Fe^{2+}, Mg)_3$	Si_{12}	[17]	K-merrihueite
KSR	Mg_2	Na_2	K	$(Mg, Fe^{2+})_3$	$Si_{11}Al$	{18}	New RCA
FC1	$(Mg, Fe^{2+})Fe^{3+}$	\Box_2	K	Mg_3	Si_{12}	[21]	Mg-klöchite
ALSU	Al_2	Na_2	K	Li_3	Si_{12}	[32]	Al-sugilite
MSO	Mg_2	\Box_2	\Box	Al_3	$Si_{11}Al$	{2}	New RCA
FMM	$(Fe^{2+}, Mg)Fe^{3+}$	\Box_2	K	$(Fe^{2+}, Mg)_3$	Si_{12}	[21]	Fe-klöchite

*Root charge arrangement

Table 3.7 Chemical formulae consistent with new dominant end-member compositions

	PM3	KSR	FC1	AISU	MSO	FMM
SiO ₂	62.12	68.00	68.98	71.50	63.51	61.80
TiO ₂	0.00	0.00	0.08	0.00	---	
Al ₂ O ₃	0.05	2.50	0.15	3.59	20.88	0.02
Cr ₂ O ₃	0.02	0.00	0.00	0.00		
Fe ₂ O ₃	0.00	0.00	6.70	5.48		
Mn ₂ O ₃	0.00	0.00	0.00	3.19		
FeO	25.31	0.40	5.29	0.00	6.41	23.70
MnO	0.00	0.00	0.23	0.00	----	0.50
MgO	4.18	19.00	12.85	0.00	4.53	4.40
BeO	---	---	---	---		
CaO	0.06	0.00	0.00	0.00	0.15	0.30
Li ₂ O	0.00	0.00	0.00	3.67		
Na ₂ O	0.49	5.30	0.43	6.09	0.35	2.00
K ₂ O	6.66	3.80	4.50	0.75	4.04	3.80
TOTAL	98.89	99.00	99.21	99.24	99.87	96.70
Si	11.91	11.55	11.96	12.19	10.63	12.00
Al	0.01	0.45	0.03	---	1.37	---
ΣT(1)	11.92	12.05	11.99	12.19	12.00	12.00
Li	---	---	---	2.52	---	
Be	---	---	---	---	---	
Mg+Fe ²⁺	---	2.97	3.00	---	0.25	

Fe ²⁺ +Mg	3.00	---	---	---	---	3.00
Al	---	0.03	---	0.48	2.75	
ΣT(2)	3.00	3.00	3.00	3.00	3.00	3.00
K	1.00	0.82	1.00	1.08	0.06	0.47
□	---	0.18	---	---	0.94	Na 0.36
ΣC	1.00	1.00	1.00	1.08	1.00	0.83
Na	0.18	1.75	0.15	2.01	0.10	----
K	0.63	---	---	---	---	---
□	1.19	0.25	1.85	---	1.90	2.00
ΣB	2.00	2.00	2.00	2.01	2.00	2.00
Mg + Fe ²⁺	---	1.84	0.32	---	1.74	1.27
Fe ²⁺ + Mg	2.25	0.06	0.77	---		
Mn ²⁺	---	---	0.03	---		0.08
Al	---	---	---	---		
Ca	---	---	---	0.72	0.02	0.06
Fe ³⁺	---	---	0.87	0.71		0.85
Mn ³⁺	---	---	---	0.41		
Y + REE	---	---	---	0.16		
□	---	0.10	---	---	0.26	
ΣA	2.25	2.00	2.00	2.00	2.00	2.26
References	(1)	(2)	(3)	(4)	(6)	(7)
(1) Wood & Holmberg (1994); (2) Krot & Wasson (1994); (3) Alietti <i>et al.</i> (1994); (4) Taggart <i>et al.</i> (1994); (5) Bogdanova <i>et al.</i> (1980); (6) Dodd <i>et al.</i> (1985).						

3.6.1 H₂O content

There is not a lot of reliable information on the H₂O content of milarite-group minerals, in part because of the inherent difficulties of analysing for H₂O or H, and in part because many of the milarite-group minerals are rare and have only been found in very small quantities. (H₂O) occurs at the *B* site (Table 3.1) and hence has a maximum value of 2 *apfu*. Two of the measured values exceed 2 *apfu* and must be wrong unless (H₂O) occupies another site in the structure, something that has not been confirmed by crystal-structure work. Previous work has suggested that the amount of (H₂O) does not exceed 1 *apfu*. In particular, Hawthorne *et al.* (1991) showed that for the milarite samples of Černý *et al.* (1980), there is a linear relation between the intensity of the infrared combination mode at ~5200 cm⁻¹ (**E** perpendicular to **c**) and the (H₂O) content, and the maximum amount of (H₂O) in this correlation is 1.12 *apfu*. Inspection of Fig. 3.3 shows four values significantly exceeding this value, suggesting that the (H₂O) content of the milarite structure does go up to 2 *apfu*. The crystal-chemical role of (H₂O) in the milarite structure is not clear. Hawthorne *et al.* (1991) show that the two-fold rotation axis of the (H₂O) group is parallel to the **c** axis, and the relatively short A-B distance in some milarites (*e.g.*, Černý *et al.* 1980) suggests that there could possibly be an interaction between the A-site cation and (H₂O) at the *B* site. On the other hand, many milarite-group minerals are anhydrous, suggesting that (H₂O) does not bond directly to any cation and hence belongs to the *occluded (H₂O)* category of Hawthorne (1992). This situation remains to be resolved in a convincing manner.

Figure 3.3 A histogram of the H₂O content (in molecules *pfu*) in milarite-group minerals taken from the literature. Measured values are shown in red, estimated values are shown in yellow.

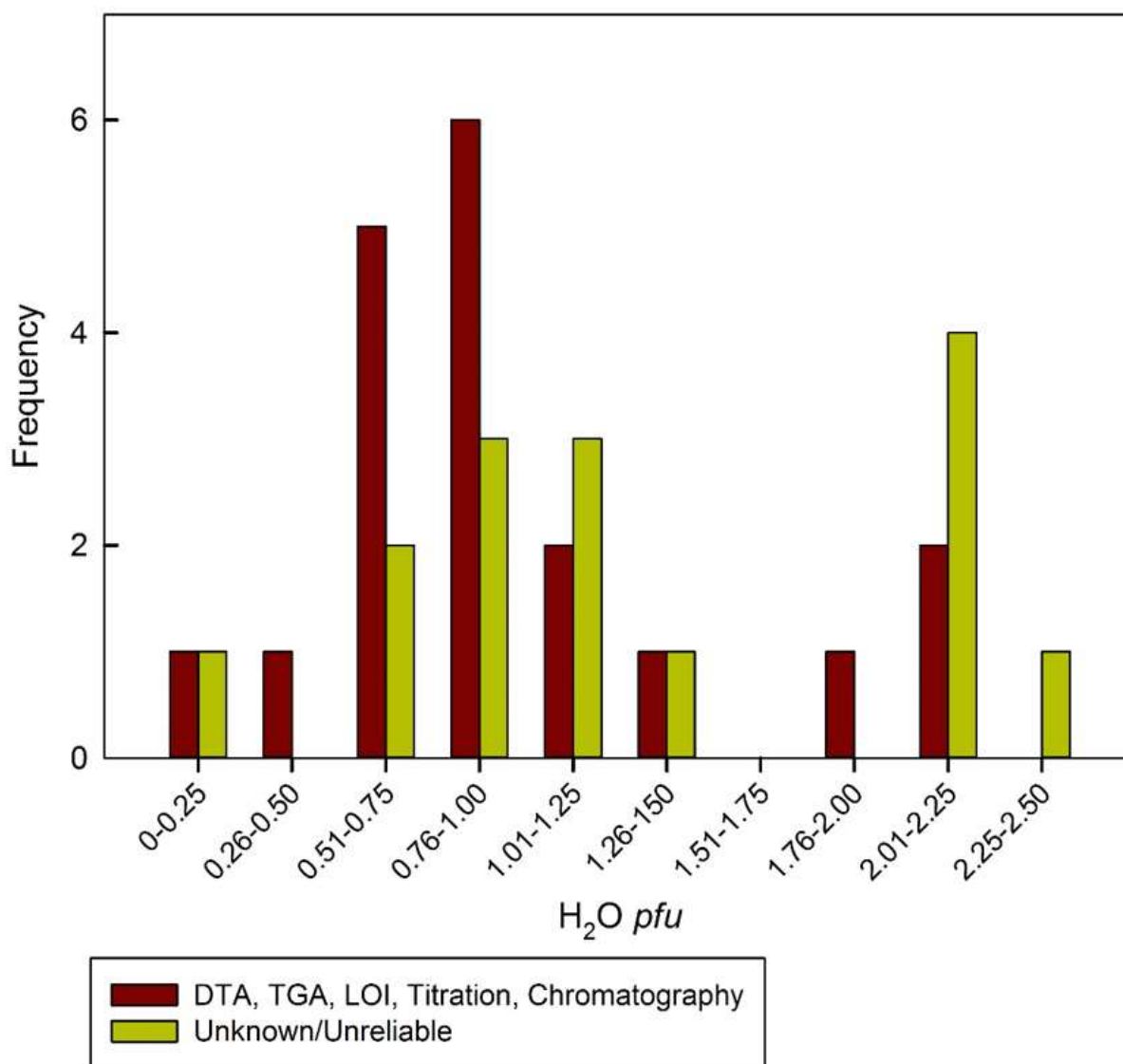
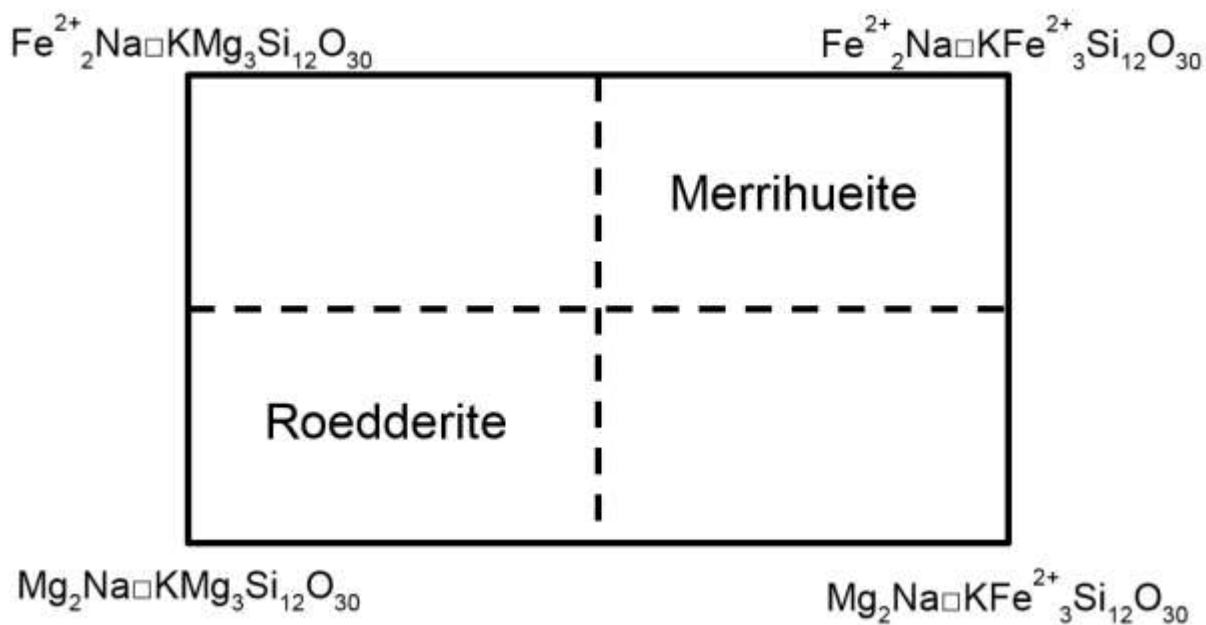


Figure 3.4 Possible compositional variation in roedderite-“Mg-merrihueite” structures. In roedderite and “Mg-merrihueite”, the *A* and *T*(2) site-populations are as follows: *A* = Mg₂, *T*(2) = Mg₃ and *A* = Fe²⁺₂, *T*(2) = Fe²⁺₃; however, order of Mg and Fe²⁺ over the *A* and *T*(2) sites can give rise to the following *A* and *T*(2) site-populations: *A* = Mg₂, *T*(2) = Fe²⁺₃ and *A* = Mg₂, *T*(2) = Fe²⁺₃, which correspond to distinct end-member compositions.



3.6.2 Potential new mineral species

There are other analyses in the literature for which the site assignments are ambiguous, and new minerals are possible if the associated site-populations can be derived experimentally. These are listed in Tables 3.8 and 3.9. The compositions have the root charge arrangement of merrihueite and roedderite (Table 3.2). In end-member roedderite, $A_2 = \text{Mg}_2$ and $T(2)_3 = \text{Mg}_3$, and in merrihueite, $A_2 = \text{Fe}^{2+}_2$ and $T(2)_3 = \text{Fe}^{2+}_3$. The possible variation in formulae along the solid solution roedderite-merrihueite is shown in Fig. 3.4. Where the A and $T(2)$ sites have the same dominant cation, the species roedderite and merrihueite are distinct. However, where Mg or Fe^{2+} is strongly ordered at A (or $T(2)$), the end members $\text{Fe}^{2+}_2\text{Na}\square\text{KMg}_3\text{Si}_{12}\text{O}_{30}$ or $\text{Mg}_2\text{Na}\square\text{KFe}^{2+}_3\text{Si}_{12}\text{O}_{30}$ can become dominant and compositions in the un-named areas of Fig. 3.4 then require distinct mineral names.

Table 3.8 Compositions which may lead to new end-member compositions in the milarite-group minerals

Sample number	A_2	B_2	C	$T(2)_3$	$T(1)_{12}$	RCA*	"Name"
MM	(Fe ²⁺ ,Mg) ₂	Na□	K	(Fe ²⁺ ,Mg) ₃	Si ₁₂	[17]	Mg-merrihueite ?
FR	(Mg,Fe ²⁺) ₂	Na□	K	(Mg,Fe ²⁺) ₃	Si ₁₂	[17]	Fe-roedderite ?

*Root charge arrangement (from Tables 3.3 & 3.4)

Table 3.9 Chemical formulae corresponding to the “end members” of table 3.8

	MM	FR
SiO ₂	65.70	67.20
TiO ₂	0.00	0.00
Al ₂ O ₃	0.08	0.09
Cr ₂ O ₃	0.03	0.00
Fe ₂ O ₃	0.00	0.00
Mn ₂ O ₃	0.00	0.00
FeO	20.10	14.40
MnO	0.00	0.19
MgO	7.00	10.60
BeO	---	---
CaO	0.02	0.00
Li ₂ O	---	0.00
Na ₂ O	1.90	3.10
K ₂ O	3.60	4.40
TOTAL	98.43	99.98
Si	12.09	11.97
Al	---	0.02
ΣT(1)	12.09	11.99
Li	---	---
Be	---	---
Mg + Fe ²⁺	---	3.00
Fe ²⁺ + Mg	2.98	---
Al	0.02	---
ΣT(2)	3.00	3.00
K	0.85	1.00
□	0.15	---
ΣC	1.00	1,00

Na	0.68	1.07
K	---	---
Ca	---	---
□	1.32	0.93
ΣB	2.00	2.00
Mg+Fe ²⁺	---	1.97
Fe ²⁺ +Mg	2.03	---
Mn ²⁺	---	0.03
Al	---	---
Ca	---	---
Fe ³⁺	---	---
Mn ³⁺	---	---
Y+REE	---	---
□	---	---
ΣA	2.03	2.00

References: (1) and (2) Krot & Wasson (1994)

Table 3.10 Synthetic milarite-like compositions and corresponding end-members for which crystal-structure refinements are available

Composition	A ₂	B ₂	C	T(2) ₃	T(1) ₁₂	Anion	RCA*	Ref.
Mg-merrihueite	Mg ₂	K□	K	Mg ₃	Si ₁₂	O ₃₀	[17]	(1)
Zn-milarite	Mn ₂	□ ₂	K	Zn ₂ Fe ³⁺	Si ₁₂	O ₃₀	[10]	(2)
Mn-milarite	Mn ₂	K□	K	Mn ₃	Si ₁₂	O ₃₀	[17]	(3)
BaMg ₂ Al ₆ Si ₉ O ₃₀	Mg ₂	□ ₂	Ba	Al ₃	Si ₉ Al ₃	O ₃₀	{8}	(4)
SrMg ₂ Al ₆ Si ₉ O ₃₀	Mg ₂	□ ₂	Sr	Al ₃	Si ₉ Al ₃	O ₃₀	{8}	(4)
Mg ₂ Al ₄ Si ₁₁ O ₃₀	Mg ₂	□ ₂	□	Al ₃	Si ₁₁ Al	O ₃₀	{2}	(4)
K ₂ Mg ₃ Zn ₂ Si ₁₂ O ₃₀	Mg ₂	K□	K	Zn ₃	Si ₁₂	O ₃₀	[17]	(5)
K ₂ Mg ₃ Fe ₂ Si ₁₂ O ₃₀	Mg ₂	K□	K	Fe ²⁺ ₃	Si ₁₂	O ₃₀	[17]	(5)
RbNaMg ₅ Si ₁₂ O ₃₀	Mg ₂	Na□	Rb	Mg ₃	Si ₁₂	O ₃₀	[17]	(5)
Na ₂ Mg ₅ Si ₁₂ O ₃₀	Mg ₂	Na□	Na	Mg ₃	Si ₁₂	O ₃₀	[17]	(5)
Na ₃ Mg ₄ LiSi ₁₂ O ₃₀	Mg ₂	Na ₂	Na	Mg ₂ Li	Si ₁₂	O ₃₀	[26]	(5)
K ₃ Mg ₄ LiSi ₁₂ O ₃₀	Mg ₂	K ₂	K	Mg ₂ Li	Si ₁₂	O ₃₀	[26]	(5)
Na ₂ Mg ₃ Cu ₂ Si ₁₂ O ₃₀	Mg ₂	Na ₂	□	Cu ₃	Si ₁₂	O ₃₀	[15]	(5)
K ₂ Mg ₃ Cu ₂ Si ₁₂ O ₃₀	Mg ₂	K□	K	Cu ₃	Si ₁₂	O ₃₀	[17]	(5)
Mg ₂ NaNaMg ₃ Si ₁₂ O ₃₀	Mg ₂	Na□	Na	Mg ₃	Si ₁₂	O ₃₀	[17]	(6)

References: (1) Khan *et al.* (1971); (2) Pushcharovskii *et al.* (1972); (3) Sandomirskii *et al.* (1977); (4) Winter *et al.* (1995); (5) Nguyen *et al.* (1980); (6) Artioli *et al.* (2013).

*Root charge arrangement (from Tables 3 and 4)

Table 3.11 Synthetic compositions for which there are no crystal-structure refinements

Number	A_2	B_2, C	$T(2)_3$	$T(1)_{12}$	RCA*	Ref.
(1)	Mg ₂	Na ₂ □	Zn ₃	Si ₁₂	[15] or [17]	(1)
(3)	Mg ₂	Na ₂ □	Fe ²⁺ ₃	Si ₁₂	[15] or [17]	(1)
(5)	Mg ₂	NaRb□	Fe ²⁺ ₃	Si ₁₂	[15] or [17]	(1)
(13)	Mg ₂	NaK□	Cu ₃	Si ₁₂	[15] or [17]	(1)
(14)	Mg ₂	NaRb□	Cu ₃	Si ₁₂	[15] or [17]	(1)

Reference : (1) Choisnet *et al.* (1981)

*Root charge arrangement

3.7 Synthetic compounds with the milarite-type structure

There are twenty synthetic compounds with the milarite-type structure that have distinct (dominant) end-member compositions. Those for which the crystal structure and site populations have been determined are listed in Table 3.10, and those for which the formulae are assumed from the starting compositions are listed in Table 3.11. In Table 3.10, “Mg-merrihueite”, “Zn-milarite” and “Mn-milarite” are the names assigned in the original studies (and hence are retained here) “Mg-merrihueite” and “Zn-milarite” are appropriately named, whereas “Mn-milarite” is actually a Mn-analogue of merrihueite. The compound $\text{BaMg}_2\text{Al}_6\text{Si}_9\text{O}_{30}$ is the Mg analogue of armenite, $\text{SrMg}_2\text{Al}_6\text{Si}_9\text{O}_{30}$ is the Sr-Mg analogue of armenite, and $\text{Mg}_2\text{Al}_4\text{Si}_{11}\text{O}_{30}$ is a new root charge arrangement: arrangement {2} in Table 3.5. Most of the remaining silicate milarite compounds have root charge arrangements [17] and [26] (Table 3.10). The compound $\text{Na}_2\text{Mg}_3\text{Cu}_2\text{Si}_{12}\text{O}_{30}$ is unusual in having root charge arrangement [15], which inspection of Tables 3.2 and 3.6 shows is the first occurrence of this arrangement.

3.8 The relative stability of root charge arrangements with the milarite structure

There are seventy-three distinct root charge arrangements with the milarite structure, as listed in Tables 3.4 and 3.5, and fifteen of these occur in minerals and synthetic compounds (Table 3.12). The obvious question arises: Can all these root charge arrangements lead to stable structures? Certainly some of the arrangements can be thought of as very stable as they occur in several minerals: for example, arrangement [17] (Table 3.4) occurs in six minerals, a further three potential minerals, and between

eight to thirteen synthetic compounds (Table 3.12), suggesting that it is a particularly stable charge arrangement.

Fig. 3.5 shows the total charge (pfu) at the A site as a function of total charge at the $T(2)$ site in milarite-type structures. Red circles are for $Si = 12\ apfu$, green triangles for $Si < 12\ apfu$, and the yellow area shows the following charge ranges: $0 \leq A_2 \leq 10$, $3 \leq T(2)_3 \leq 9$. The red dotted lines bound the range where $Si \leq 12\ apfu$. The region to the bottom left of the figure is forbidden as there is insufficient charge at the B and C sites to produce electroneutrality, and the lower red line provides a lower bound for the observed root charge arrangements. The corresponding upper limit for root charge arrangements with $Si = 12\ apfu$ (the upper red line) provides an upper bound for structures with $Si = 12\ apfu$. Above this line, all root charge arrangements (and observed structures) have $Si < 12\ apfu$. In principle, the aggregate charge at $T(2)_3$ could be 12 (or even higher if $^{T(1)}Si < 12\ apfu$); however, a completely silicate milarite structure, $^A0_2^B0_2^C0_1^{T(2)}Si_3^{T(1)}Si_{12}O_{30}$, seems unlikely because of the number of unoccupied large cavities in the structure.

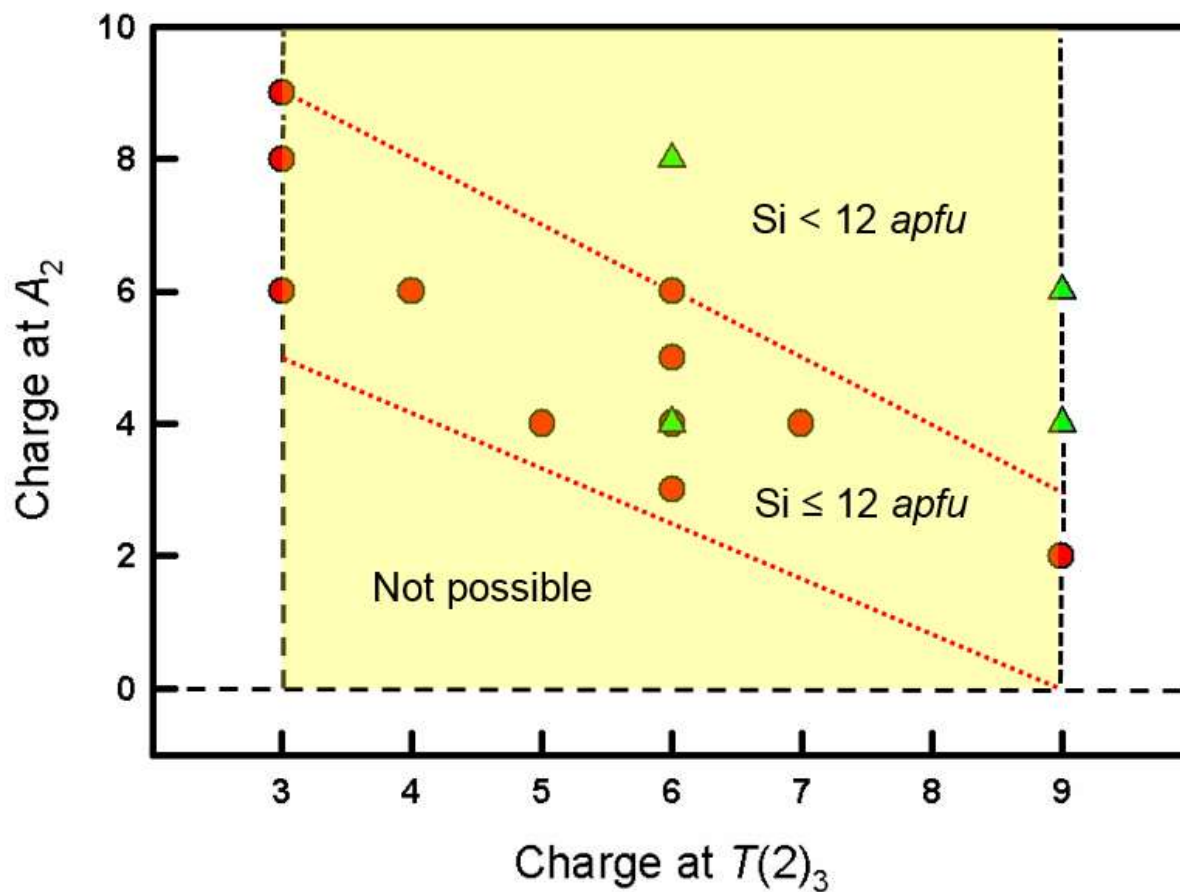
We may examine aspects of observed and algebraically possible root charge arrangements using *a priori* bond-valence calculations; this is shown next.

Table 3.12 Numbers of minerals and compounds for specific root charge arrangements

RCA*	Minerals	Potential minerals	Synthetic compounds
[2]	1	-	-
[10]	3	-	1
[15]	-	-	1 (+ up to 5)
[17]	6	3	8 (+ up to 5)
[18]	1	-	-
[20]	1	-	-
[21]	2	2	-
[24]	1	-	-
[26]	-	-	2
[29]	3	-	-
[32]	1	1	-
{2}	-	1	1
{6}	3	-	-
{8}	1	-	2
{18}	-	1	-

*Root charge arrangement

Figure 3.5 Total charge (*pfu*) at the *A* site as a function of total charge at the *T*(2) site in milarite-type structures; red circles are have $\text{Si} = 12 \text{ apfu}$, green triangles have $\text{Si} < 12 \text{ apfu}$, the yellow area shows the following charge ranges: $0 \leq A_2 \leq 10$, $3 \leq T(2)_3 \leq 9$, the red dotted lines bound the range where $\text{Si} \leq 12 \text{ apfu}$.



3.8.1 *A priori* bond-valence calculations

There are two important theorems in bond-valence theory (Brown 2002): [1] the valence-sum rule, and [2] the loop rule. The *valence-sum rule* states that *the sum of the bond valences at each atom is equal to the magnitude of the atomic valence*. The *loop rule* states that *the sum of the directed bond-valences around any circuit (closed path) of bonds in a structure is zero*. The equations associated with the valence-sum rule and the loop rule result in an exactly determined system with regard to the bond valences; these are called the *a priori* bond-valences, *i.e.*, the bond valences calculated from the formal valences of the ions at each site and the bond-topological characteristics of the structure (Brown 1977, Rutherford 1990). This approach has been used only sparingly, mostly to predict bond lengths of simple structures, based on the solution of the network equations (see below) by extraction and conversion of the *a priori* bond-valences (Brown 1977, Rutherford 1990, Urusov & Orlov 1999, Hawthorne & Sokolova 2008).

An aspect of considerable interest with regard to the milarite structure is the wide range of cations that can occur in this structure type, forming numerous minerals (Table 3.2). *A priori* bond-valence calculations provide us with an ideal method for examining the control of bond topology on site occupancy in the milarite structure and in the minerals of the milarite group.

3.8.2 Calculation of *a priori* bond-valences

The equations involved in the valence-sum rule may be written as follows:

$$\sum s_{ij} = V_i \quad (i = 1-n) \quad (\text{eq. 3.1})$$

where the summation involves all bonds to the j coordinating ions from the central ion i for all n ions in the structure.

The equations for the loop rule may be written as follows:

$$\sum s_{ij} = 0 \quad (\text{eq. 3.2})$$

where the summation is over the directed bond valences around any circuit in the digraph (directed graph) of the bond network of the structure.

3.8.3 *A priori* bond-valences of the milarite structure

A general bond-valence table for the milarite structure is shown in Table 3.13. The bond valences are represented by the variables a-h. The formal charges of the cations at the various cation sites are written as ^{site}V and the charges of the anions are constrained to equal to their formal valence. This means that there are eight unknowns (the bond valences a-h) and we need eight independent equations to solve for these unknowns.

The valence-sum rule for the cations gives us the following equations:

$$6a = {}^AV$$

$$3b + 6c = {}^BV$$

$$12d = {}^CV \quad (\text{eq. 3.3})$$

$$e + 2f + g = {}^{T(1)}V$$

$$4h = {}^{T(2)}V$$

The valence-sum rule for the anions gives us the following equations:

$$b + 2e = 2$$

$$d + 2f = 2 \quad (\text{eq. 3.4})$$

$$a + c + g + h = 2$$

These eight equations are constrained by charge balance, and hence there are only seven independent equations. In order to be able to solve for the bond valences, we need an additional equation, linearly independent of the other equations, and this is provided by the loop rule (see above). There are two (equivalent) ways in which we may derive loop equations: (1) by inspection of the crystal structure, and (2) *via* the bond-valence table. Fig. 3.6 shows a fragment of the milarite structure. A convenient loop is shown in red in Table 3.13: $B \rightarrow O(1) \rightarrow T(1) \rightarrow O(3) \rightarrow B$, resulting in the following loop equation:

$$b - e + g - c = 0 \quad (\text{eq. 3.5})$$

This loop may also be constructed in the structure itself (Fig. 3.6) by tracing out the loop indicated in Table 3.13.

Note that the sites A , C and $T(2)$ are each coordinated by only one crystallographically distinct anion and all bonds to each cation are equivalent. This means that none of these cations can (usefully) participate in loop equations as the directed bond-valences involving each of these cations always sum to zero. On the other hand, their *a priori* bond-valences are calculated directly from the valence-sum equations: $a = {}^AV/6$; $d = {}^CV/12$; $h = {}^{T(2)}V/4$ v.u.

Table 3.13 General bond-valence table for the milarite structure, showing a loop in the bond topology

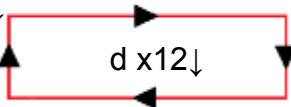
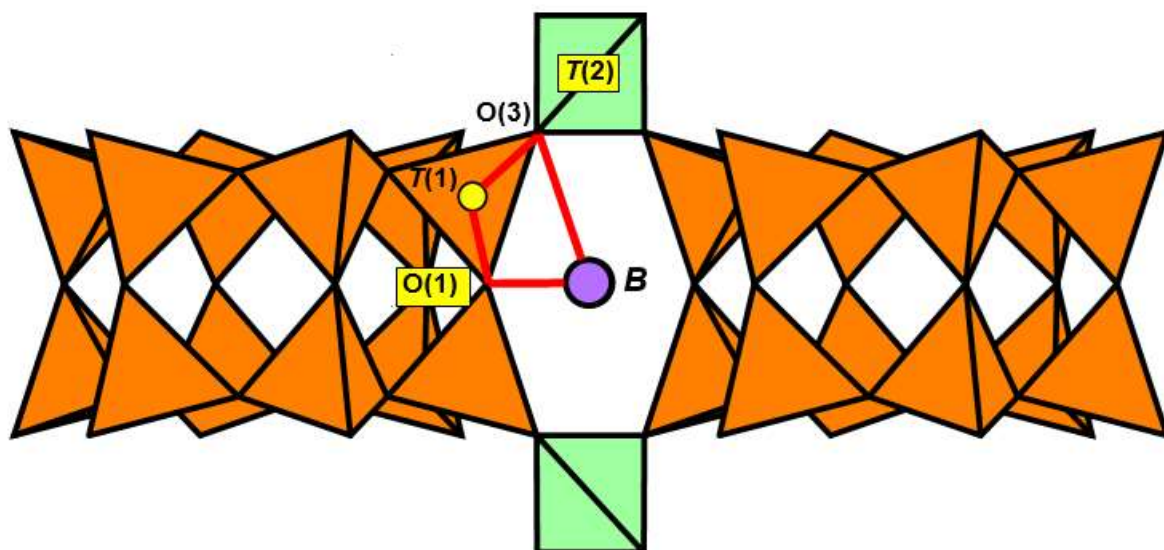
	A_2	B_2	C	$T(1)_{12}$	$T(2)_3$	Σ
O(1)		b x3↓		e x2→		2
O(2)				f x2↓ x2→		2
O(3)	a x6↓	c x6↓		g	h x4↓	2
Σ	A_V	B_V	C_V	T_1V	T_2V	

Figure 3.6 A fragment of the milarite structure viewed perpendicular to **c**, showing the loop that is outlined in Table 3.13 and discussed in the text.



3.8.4 Solution of the *a priori* bond-valence equations

We may write the system of equations in matrix form as shown below:

$$\mathbf{A} \cdot \mathbf{B} = \mathbf{C}$$

$$\begin{bmatrix} 6 & 0 & 0 & 0 & 0 & 0 & 0 & 0 \\ 0 & 3 & 6 & 0 & 0 & 0 & 0 & 0 \\ 0 & 0 & 0 & 12 & 0 & 0 & 0 & 0 \\ 0 & 0 & 0 & 0 & 1 & 2 & 1 & 0 \\ 0 & 0 & 0 & 0 & 0 & 0 & 0 & 4 \\ 0 & 1 & 0 & 0 & 2 & 0 & 0 & 0 \\ 0 & 0 & 0 & 1 & 0 & 2 & 0 & 0 \\ 1 & 0 & 1 & 0 & 0 & 0 & 1 & 1 \\ 0 & 1 & -1 & 0 & -1 & 0 & 1 & 0 \end{bmatrix} \begin{bmatrix} a \\ b \\ c \\ d \\ e \\ f \\ g \\ h \end{bmatrix} = \begin{bmatrix} 3 \\ 1 \\ 1 \\ 4 \\ 1 \\ 2 \\ 2 \\ 2 \\ 0 \end{bmatrix} \quad (\text{eq. 3.6})$$

where the **A** matrix contains the coefficients of the above equations, the first column vector (**B**) contains the *a priori* bond-valences (unknown) and the second column vector (**C**) contains the formal charges of the ions at the sites, together with the zero associated with the loop equation. Thus, we may solve this system of equations to obtain the *a priori* bond-valences.

Table 3.14 shows the results of this calculation for the charge arrangement

$A_3B_2C_1T^{(1)}_4T^{(2)}_3O_{30}$ corresponding to sugilite: $\text{Fe}^{3+}_2\text{Na}_2\text{KSi}_{12}\text{Li}_3\text{O}_{30}$, together with

the bond valences calculated from the structure of Armbruster & Oberhänsli (1988b) and the bond-valence parameters of Gagné & Hawthorne (2015). By-and-large, the *a priori* bond-valence calculations reproduce the observed bond-valences quite closely.

The principal deviations between the two occur where there are obvious steric constraints on the adoption of specific bond-lengths. Thus the major significant difference involves the *B*-O(1) bond.

Where the *B* site is vacant, what are other sources of structural strain in the milarite structure? Let us consider the structure of sogdianite (Cooper *et al.* 1998; Sokolova *et al.* 2000), where the *B* site is vacant (Table 3.2). Table 3.15 shows the calculation for the charge arrangement $A_4B_0C_1T(1)_4T(2)_1O_{30}$ corresponding to sogdianite: $Zr_2\Box_2KSi_{12}Li_3O_{30}$, together with the bond valences calculated from the structure of Sokolova *et al.* (2000) and the bond-valence parameters of Gagné & Hawthorne (2015). The unoccupied *B* site in this structure emphasizes the second significant mismatch between the *a priori* and observed bond-valences in the milarite structure, that which occurs at the *T*(1) site: the bond valences *T*(1)-O(1) and *T*(1)-O(2) are both too large by approximately 0.04 v.u. While the origin of these slightly high bond-valences is not clear, we note that this mismatch is a lot less important where the *B* site is occupied.

A summary of the mismatch between the *a priori* and observed bond-valences for all observed milarite-group minerals is given in Table 3.16.

Table 3.14 *A priori* (upper) and observed (lower) bond-valences (v.u.) for sugilite*:

^A(Mn³⁺_{0.11}Fe³⁺_{0.71}Al_{1.16}Na_{0.02})^BNa_{1.81}^CK_{1.00}^{T(2)}Li_{3.02}^{T(1)}Si_{12.06}O₃₀

	<i>A</i> ₂	<i>B</i> ₂	<i>C</i>	<i>T</i> (1) ₁₂	<i>T</i> (2)	Σ
O(1)		0.019 x3↓		0.991 x2→		2
O(2)			0.0833 x12↓	0.958 x2↓→		2
O(3)	0.497 x6↓	0.141 x6↓		1.113	0.252 x4↓	2
Σ	2.980	0.905	1	4.020	1.007	
O(1)		0.178 x3↓		0.997 x2→		2.172
O(2)			0.0924 x12↓	1.010 1.023		2.125
O(3)	0.479 x6↓	0.0844 x3↓ 0.0363 x3↓		1.128	0.243 x4↓	1.971
Σ	2.872	0.896	1.108	4.158	0.973	

*Ref: Armbruster & Oberhänsli (1988)

Table 3.15 *A priori* (upper) and observed (lower) bond-valences (v.u.) for sogdianite*:

$A(\text{Zr}_{1.98}\text{Hf}_{0.02})$ $C(\text{K}_{0.99}\text{Na}_{0.01})$ $T^{(2)}\text{Li}_{2.97}$ $T^{(1)}\text{Si}_{12.01}\text{O}_{30}$

	A_2	B_2	C	$T(1)_{12}$	$T(2)$	Σ
O(1)		---		1.000 x2→		2
O(2)			0.083 x12↓	0.958 x2↓→		2
O(3)	0.667 x6↓	---		1.083	0.248 x4↓	2
Σ	4	0	1	4.003	0.99	
O(1)		---		1.044 x2→		2.088
O(2)			0.0800 x12↓	1.000 1.002		2.100
O(3)	0.667 x6↓	---		1.077	0.252 x4↓	1.996
Σ	4.004		0.960	4.123	1.008	

*Ref: Sokolova *et al.* (2000)

Table 3.16 Absolute difference between *a priori* bond-valence and experimental bond-valences (v.u.) by bond

	A-O(3) (1)	A-O(3) (2)	B-O(1)	B-O(3) (1)	B-O(3) (2)	C-O(2)	π (1)-O(1)	π (1)-O(2) (1)	π (1)-O(2) (2)	π (1)-O(3)	π (2)-O(3)
Almarudite	0.005		0.034	0.037	0.042	0.005	0.027	0.083	0.077	0.024	0.014
Darapiosite	0.037		0.088	0.076	0.076	0.002	0.027	0.050	0.034	0.018	0.018
Dusmatovite	0.080		0.081	0.041	0.041	0.002	0.030	0.026	0.042	0.034	0.026
Eifelite	0.084		0.102	0.062	0.110	0.000	0.029	0.047		0.039	0.069
Friedrichbeckeite	0.003		0.075	0.054	0.069	0.009	0.023	0.083	0.080	0.026	0.069
Milarite	0.019	0.087	0.033	0.016	0.018	0.002	0.013	0.058	0.050	0.025	0.029
Oftedalite	0.031					0.002	0.053	0.082	0.066	0.006	0.007
Osumilite	0.016					0.016	0.021	0.050	0.034	0.041	0.015
Osumilite-Mg	0.021					0.015	0.021	0.044	0.028	0.039	0.007
Poudretteite	0.020					0.006	0.045	0.084	0.064	0.027	0.009
Shibkovite	0.018		0.072	0.054	0.054	0.004	0.023	0.047	0.034	0.018	0.017
Sogdianite	0.002					0.003	0.048	0.045	0.043	0.002	0.004
Sugilite	0.017		0.134	0.062	0.100	0.007	0.012	0.074	0.058	0.031	0.008
Average deviation	0.031		0.077	0.057		0.006	0.029	0.055		0.025	0.022

Table 3.17 Global instability index and bond strain index (v.u.)

	Global	Bond Strain	Root charge
	Instability Index	Index	arrangement
Almarudite	0.13	0.028	[10]
Berezanskite	0.10	0.024	[29]
Darapiosite	0.09	0.040	[24]
Dusmatovite	0.16	0.040	[17]
Eifelite	0.26	0.062	[18]
Friedrichbeckeite	0.13	0.037	[17]
Milarite	0.10	0.019	[10]
Oftedalite	0.13	0.029	[21]
Osumilite	0.07	0.013	{6}
Osumilite-Mg	0.06	0.014	{6}
Poudretteite	0.12	0.026	[2]
Shibkovite	0.09	0.032	[17]
Sogdianite	0.08	0.017	[29]
Sugilite	0.12	0.052	[32]
Average	0.12	0.031	

3.9 Induced strain in the milarite group

The bond-valence model offers two *a posteriori* checks on the stability of crystal structures: the *Global Instability Index* (GII, Salinas-Sanchez *et al.* 1992), and the *Bond Strain Index* (BSI, Preiser *et al.* 1999). The bond strain index (BSI) is a measure of the lattice-induced strain that causes bonds to violate the network equations (Brown 2002), which results in a mismatch between the *a priori* and experimental bond valences:

$$\text{BSI} = \left(\frac{\sum_i (w_i (s_{ij} - s_{ij}^{\text{exp}})^2)}{\sum w_i} \right)^{1/2} \quad (\text{eq. 3.7})$$

where s_{ij} is the *a priori* bond-valence, s_{ij}^{exp} is the corresponding experimental bond-valence, and where the average is taken over all bonds of the bond-topology table. The global instability index (GII) is a complementary measure of the lattice strain, evaluating the difference between the bond-valence sums at the sites of the structure compared to their ideal values:

$$\text{GII} = \left(\frac{\sum_i (w_i (\sum_j s_{ij} - V_i)^2)}{\sum w_i} \right)^{1/2} \quad (\text{eq. 3.8})$$

where s_{ij} are the experimental bond valences, V_i the valence of the ion, and where the average is taken over all ions of the structure. Brown (2002) states that a value of over 0.2 v.u for GII usually indicates a structure so strained as to be unstable. Table 3.17 shows the BSI and GII of fourteen minerals of the milarite group for which both a reliable chemical analysis and refined crystal-structure is available. The GII varies from 0.06 (osumilite-Mg) to 0.26 v.u (eifelite), with an average value of 0.12 v.u, whereas the BSI varies from 0.013 (osumilite) to 0.062 v.u (eifelite), with an average value of 0.031 v.u. These indexes are useful to gauge the relative stability of members of the group.

For example, the five highest BSI values involve five minerals with partial or total occupancy of the *B* site: darapiosite, dusmatovite, eifelite, friedrichbeckeite and sugilite. These minerals are also on the higher end of the GII values for the group, confirming the relative instability of milarite-group minerals with an occupied *B* site. There is a correlation coefficient of 0.79 between GII and BSI for the group, meaning that a high BSI does not always equate a high GII or vice versa (e.g., darapiosite). Table 3.17 also shows that milarite and osumilite have low values of GII and BSI, which could be one of the reasons for their relatively common occurrence compared to that of other minerals of the group.

3.9.1 The *B* site in the milarite structure

Fig. 3.7 compares the *a priori* bond-valences with the experimental bond-valences for thirteen well-refined milarite-group minerals for which reliable chemical analyses are available. Inspection of Fig. 3.7 shows that the maximum deviation from concordance of the *a priori* and experimental bond-valences occurs for the *B* site, with the *B*-O(1) bond showing the largest positive deviations and the *B*-O(3) bond showing the largest negative deviations. In the milarite structure, the *B* site occupies a cavity within the framework, and the dimensions of that cavity are primarily controlled by the detailed positions of the surrounding polyhedra (Fig. 3.6). The observed bond-lengths in sugilite are shown in Fig. 3.8a: *B*-O(1) = 2.42, *B*-O(3) = 2.73 Å; the ideal bond-lengths corresponding to the *a priori* bond-valences of Table 3.14 are *B*-O(1) = 3.07, *B*-O(3) = 2.51 Å. These are extremely large differences [up to 0.65 Å for O(1)], and we may understand why the structure cannot adjust to these distances by comparing Figs. 3.8a

and 3.8*b*. The [Si₁₂O₃₀] units of the milarite structure encapsulate K in [12]-coordination at the C site. The valence-sum rule requires an incident observed bond-valence of 1 v.u at the C site, with an *a priori* bond-valence of $1/12 = 0.083$ v.u per (symmetry equivalent) bond. This gives a C-O(2) distance of 3.05 Å, close to 2.99 Å observed in sugilite and ~3.05 Å observed in brannockite (Armbruster & Oberhänsli 1988*b*), sogdianite (Cooper & Hawthorne 1999, Sokolova *et al.* 2000) and berezanskite (Hawthorne *et al.* 2015). It is apparent that the [Si₁₂O₃₀] groups act as rigid units, buttressed by the central K at the C site. The B-O(1) distance may increase by increasing the distances between the [Si₁₂O₃₀] units in the **a** direction, but this also increases the B-O(3) distance which is already too long and needs to be shortened, not lengthened. The B-O(3) distance may be shortened by bringing the [Si₁₂O₃₀] units closer together; however, this will shorten the B-O(1) distance which needs to be lengthened, and will also further flatten the T(2) tetrahedron which is already very flat (see Fig. 3.8*b*). The only way that B-O(1) may be lengthened and B-O(3) may be shortened is by displacement of the B cation away from the 4*d* site parallel to the **c** axis. Although this mechanism is not very effective, it is the only one available, and most milarite minerals have the B-site cation “split” up and down the channel direction (*e.g.*, Kimata & Hawthorne 1989).

Figure 3.7 Comparison of experimental and *a priori* bond-valences for thirteen well-refined milarite-group minerals for which reliable chemical analyses are available.

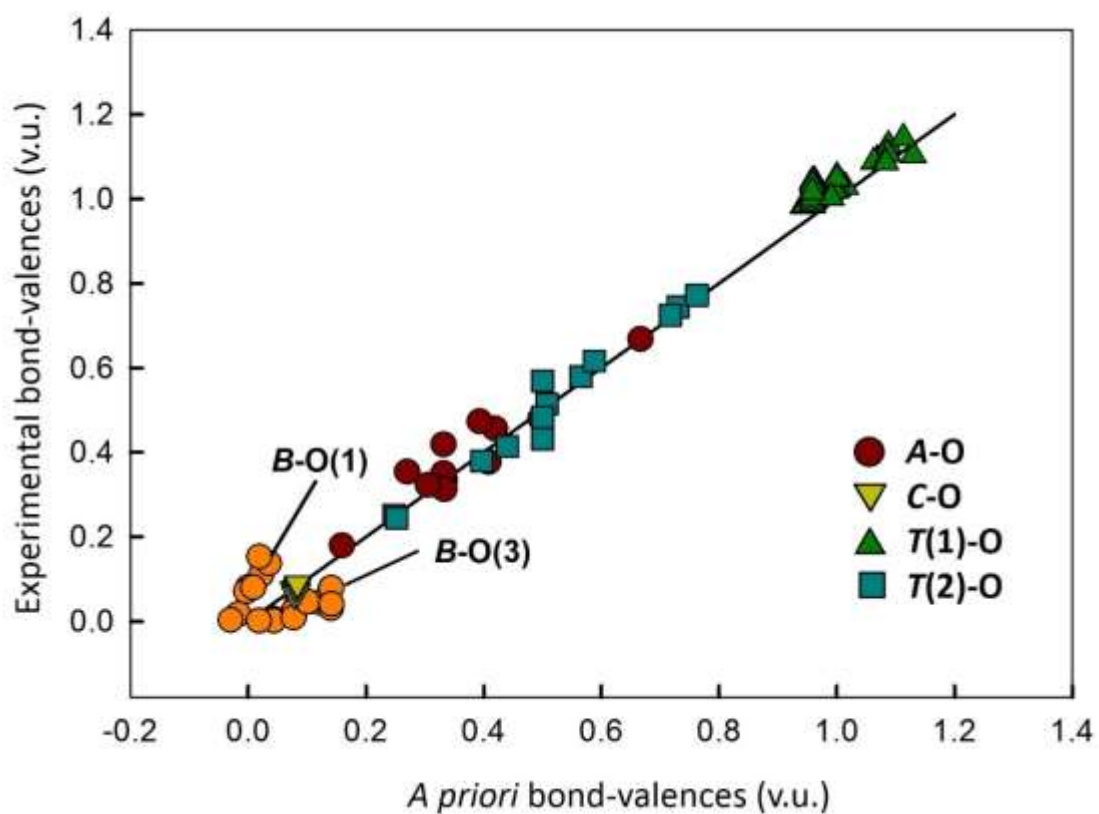
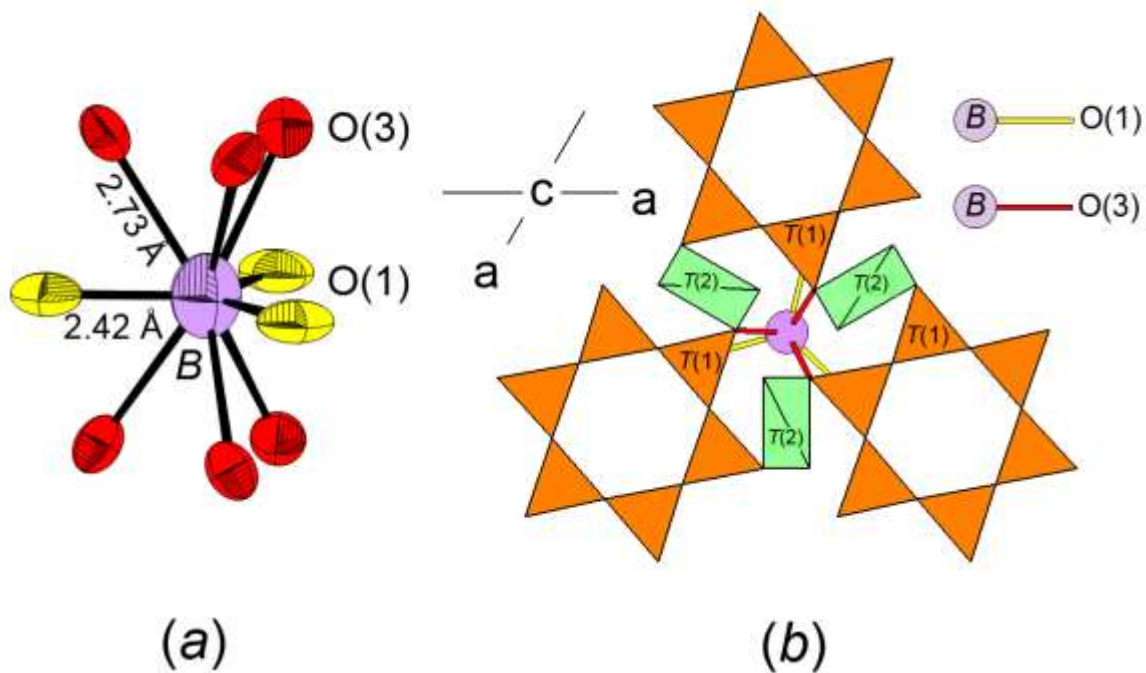


Figure 3.8 The coordination around the *B* site in sugilite; (a) ball-and-stick view with the atom-displacements shown; the *B* site has been moved to its ideal position at $z = 0$ to simplify the figure; (b) the polyhedra around the *B* site, with the *B*-O(1) and *B*-O(3) separations shown in yellow and red lines, respectively. Legend as in Figs. 3.1 and 3.2.



3.9.2 Compositional implications for milarite-group minerals

The fact that the largest deviations between the *a priori* and observed bond-valences occur at the *B* site suggests that minerals with an occupied *B* site will tend to be less stable than those with a vacant *B* site. In accord with this, of the twenty-three milarite-group minerals listed in Table 3.2, fifteen have a vacant *B* site, five have a half-occupied *B* site, and only three have a fully occupied *B* site. Moreover, the more common and widespread milarite-group minerals: armenite, milarite and osumilite have vacant *B* sites.

Of the thirty-four possible root charge arrangements for the milarite structure with $\text{Si} = 12 \text{ apfu}$ that are listed in Table 3.4, twenty-one have a fully occupied *B* site; three of these arrangements ([18], [24], [32]) are known in minerals and two are suspected in synthetic compounds ([15], [26]); three have a half-occupied *B* site and one of these arrangements ([17]) is known in minerals; ten have a vacant *B* site; six of these arrangements ([2], [10], [17], [20], [21], [29]) are known in minerals.

Of the thirty-nine possible root charge arrangements for the milarite structure with $\text{Si} \neq 12 \text{ apfu}$ that are listed in Table 3.5, twenty-eight have a fully occupied *B* site, and one of these arrangements ({18}) is known in a potential new species identified here; none have a half-occupied *B* site (these arrangements are not possible as they violate the requirements of an end member as one site, $T(1)$, is already occupied by two cation species); eleven have a vacant *B* site, two arrangements ({6}, {8}) are known in minerals and one potential new species identified here has another arrangement ({2}).

We note here that most (49) root charge arrangements of the milarite structure have a fully-occupied *B* site, and are therefore less likely to lead to minerals compared to their counterparts. This inventory of distinct root charge arrangements provides many targets for synthesis of materials with the milarite structure, especially with regard to *B* site occupancy.

3.10 Summary

- (1) All possible end-member root charge arrangements for the milarite structure-type have been derived using the criteria of Hawthorne (2002);
- (2) Examination of ~350 chemical analyses from the literature has led to the identification of six examples that definitely deserve the status of new minerals; moreover, there are two additional compositions that may also deserve this status, pending experimental determination of their patterns of cation order;
- (3) Examination of synthesis results reveals twenty synthetic compounds with the milarite-type structure that have distinct (dominant) end-member compositions;
- (4) The inventory of distinct root charge arrangements provides many targets for synthesis of materials with the milarite structure;
- (5) *A priori* bond-valence calculations allow evaluation of lattice-induced strain as a function of chemical composition for all arrangements for which the detailed atomic arrangement has been refined;

(6) Analysis of localized strain indicates that the *B* site has the highest amount of strain in the structure; and in accord with this finding, species with vacant *B* site tend to be more common;

(7) The inventory of root charge arrangements of the milarite structure shows that out of a total of 73 plausible root charge arrangements, 49 have a fully-occupied *B* site, and in accord with (6), are less likely to lead to minerals than the root charge arrangements with a vacant *B* site.

3.11 Acknowledgements

We thank Yulia Uvarova and Ed Grew for their very helpful comments on this paper.

This work was funded by UM Duff Roblin and GETS Fellowships, by a MAC Foundation Scholarship, and by a PGS-D3 Scholarship from the Natural Sciences and Engineering Research Council of Canada to OCG, by a Canada Research Chair in Crystallography and Mineralogy, by a Natural Sciences and Engineering Research Council of Canada Discovery grant, and by Innovation grants from the Canada Foundation for Innovation to FCH.

3.12 References

- Abraham, K., Gebert, W., Medenbach, O., Schreyer, W., & Hentschel, G. (1983). Eifelite, $\text{KNa}_3\text{Mg}_4\text{Si}_{12}\text{O}_{30}$, a new mineral of the osumilite group with octahedral sodium. *Contributions to Mineralogy and Petrology* **82**, 252-258.
- Agakhanov, A.A., Pautov, L.A., Uvarova, Y.A., Sokolova, E.V., Hawthorne, F.C., & Karpenko, V.Y. (2005). Senkevichite, $\text{CsKNaCa}_2\text{TiO}[\text{Si}_7\text{O}_{18}(\text{OH})]$, a new mineral. *New Data on Minerals* **40**, 17-22.
- Alietti, E., Brigatti, M. F., Capedri, S., & Poppi, L. (1994). The roedderite-chayesite series from spanish lamproites; crystal-chemical characterization. *Mineralogical Magazine* **58**, 655-662.
- Armbruster, T. (1989). Crystal chemistry of roedderite at 100 and 300 K. *European Journal of Mineralogy* **1**, 715-718.
- Armbruster, Th. & Oberhänsli, R. (1988a). Crystal chemistry of double-ring silicates: Structural, chemical and optical variation in osumilites. *American Mineralogist* **73**, 585-593.
- Armbruster, Th. & Oberhänsli, R. (1988b). Crystal chemistry of double-ring silicates: Structures of sugilite and brannockite. *American Mineralogist* **73**, 594-600.
- Armbruster, Th., Bermanec, Y., Wenger, M., & Oberhiinsli, R. (1989). Crystal chemistry of double-ring silicates: Structure of natural and dehydrated milarite at 100 K. *European Journal of Mineralogy* **1**, 353-362.

- Artioli, G., Angelini, I., & Nestola, F. (2013). New milarite/osumilite-type phase formed during ancient glazing of an Egyptian scarab. *Applied Physics A*, **110**, 371-377.
- Bakakin, V.V., Balko, V.P. & Solovyeva, L.P. (1975). Crystal structures of milarite, armenite, and sogdianite. *Soviet Physics Crystallography* **19**, 460-462.
- Balassone, G., Mormone, A., Rossi, M., Bernardi, A., Fisch, M., Armbruster, T., Malsy, A.K., & Berger, A. (2008). Crystal chemical and structural characterization of an Mg-rich osumilite from Vesuvius volcano (Italy). *European Journal of Mineralogy* **20**, 713-720.
- Bogdanova, N.G., Troneva, N.V., Zaborovskaya, N.B., Sukhanov, M.K., & Berkhin, S.I. (1980). The first find of metamorphic osumilite in the USSR. *Doklady Akademii Nauk SSSR*, **250(3)**, 690-693 (In Russian).
- Bojar, H.-P., Walter, F., Hauzenberger, C., & Postl, W. (2011). Klöchite, $K_2(Fe^{2+}Fe^{3+})Zn_3[Si_{12}O_{30}]$, a new milarite-type mineral species from the Klöch volcano, Styria, Austria. *Canadian Mineralogist* **49**, 1115-1124.
- Brown, I.D. (1977). Predicting bond lengths in inorganic crystals. *Acta Crystallographica* **B33**, 1305-1310.
- Brown, I.D. (2002). *The Chemical Bond in Inorganic Chemistry*. Oxford University Press
- Bunch, T.E. & Fuchs, L.H. (1969). Yagiite, a new sodium-magnesium analogue of osumilite. *American Mineralogist* **54**, 14-18.
- Černý, P., Hawthorne, F.C., and Jarosewich, E. (1980). Crystal chemistry of milarite. *Canadian Mineralogist* **18**, 41-57.

- Černý, P., Hawthorne, F.C., Jambor, J.L., & Grice, J.D. (1991). Yttrian milarite. *Canadian Mineralogist* **29**, 533-541.
- Choisnet, J., Cornet, D., Hemidy, J.-F., Guyen, N., & Dat, Y. (1981). Etude spectroscopique des ions cuivre (II) en coordinence tétraédrique dans les silicates synthétiques de type milarite. *Journal of Solid State Chemistry* **40**, 161-169.
- Chopin, C., Oberti, R., & Cámara, F. (2006). The arrojadite enigma: II. Compositional space, new members, and nomenclature of the group. *American Mineralogist* **91**, 1260-1270.
- Chukanov, N.V., Pekov, I.V., Rastsvetaeva, R.K., Aksenov, S.M., Belakovskiy, D.I., Schüller, W., & Ternes, B. (2012). Osumilite-(Mg). IMA 2011-083.
- Cooper, M.A., Hawthorne, F.C., & Grew, E.S. (1999). The crystal chemistry of sogdianite, a milarite-group mineral. *American Mineralogist* **84**, 764–768.
- Cooper, M.A., Hawthorne, F.C., Ball, N.A., Černý, P., & Kristiansen, R. (2006). Oftedalite, $(\text{Sc, Ca, Mn}^{2+})_2\text{K}(\text{Be,Al})_3\text{Si}_{12}\text{O}_{30}$, a new member of the milarite group from the Heftetjern pegmatite, Tørdal, Norway: description and crystal structure. *Canadian Mineralogist* **44**, 943–949.
- Dodd, R.T, van Schmus, W.R., & Marvin, U.B. (1965). Merrihueite, a new alkali ferro-magnesian silicate from the Mezo-Madaras chondrite. *Science* **149**, 972-974.
- Dusmatov, V.D., Efimova, A.F., Kataeva, Z.T., Khoroshilova, L.A., & Yanulov, K.P. (1968). Sogdianite, a new mineral. *Doklady Akademii Nauk SSSR* **182**, 1176-1177 (in Russian).

Ferraris, G., Prencipe, M., Pautov, L.A., & Sokolova, E.V. (1999). The crystal structure of darapiosite and comparison with Li- and Zn-bearing minerals of the milarite group. *Canadian Mineralogist* **37**, 769-774.

Forbes, W.C., Baur, W.H., & Khan, A.A. (1972). Crystal chemistry of milarite-type minerals. *American Mineralogist* **57**, 463-472.

Fuchs, L.H., Frondel, C., & Klein, C., Jr. (1966). Roedderite, a new mineral from the Indarch meteorite. *American Mineralogist* **51**, 949-955 .

Gagné, O.C. & Hawthorne, F.C. (2015). Comprehensive derivation of bond-valence parameters for ion pairs involving oxygen. *Acta Crystallographica* **B71**, 562-578.

Gibbs, J.W. (1961): The Scientific Papers of J. Willard Gibbs. Volume One. Thermodynamics. Dover Publications, New York.

Goldman, D.S. & Rossman, G.R. (1978). The site distribution of iron and anomalous biaxiality in osumilite. *American Mineralogist* **63**, 490-498.

Grew, E.S. (1982). Osumilite in the sapphirine-quartz terrane of Enderby Land, Antarctica: Implications for osumilite petrogenesis in granulite facies. *American Mineralogist* **67**, 762-787.

Grice, J.D., Ercit, T.S., Van Velthuisen, J., & Dunn, P.J. (1987). Poudretteite $\text{KNa}_2\text{B}_3\text{Si}_{12}\text{O}_{30}$, a new member of the osumilite group from Mont Saint-Hilaire, Quebec, and its crystal structure. *Canadian Mineralogist* **25**, 763-766.

Hawthorne, F.C. (1992): The role of OH and H₂O in oxide and oxysalt minerals. *Zeitschrift für Kristallographie* **201**, 183-206.

Hawthorne, F.C. (2002). The use of end-member charge-arrangements in defining new mineral species and heterovalent substitutions in complex minerals. *Canadian Mineralogist* **40**, 699-710.

Hawthorne, F.C. & Smith, J.V. (1986). Enumeration of 4-connected 3-dimensional nets and classification of framework silicates. 3D nets based on insertion of 2-connected vertices into 3-connected plane nets. *Zeitschrift für Kristallographie* **175**, 15-30.

Hawthorne, F.C. & Smith, J.V. (1988). Enumeration of 4-connected 3-dimensional nets and classification of framework silicates. Combination of zigzag and saw chains with 6^3 , 3.12_2 , 4.8^2 and $(5^2.8)_2(5.8^2)_1$. *Zeitschrift für Kristallographie* **183**, 213-231.

Hawthorne, F.C. & Sokolova, E. (2008). The crystal chemistry of the scapolite-group minerals: II. The origin of the $I4/m \rightarrow P4_2/n$ phase transition and the non-linear variations in chemical composition. *Canadian Mineralogist* **46**, 1555-1575.

Hawthorne, F.C., Kimata, M., Černý, P., Ball, N., Rossman, G.R., & Grice, J.D. (1991). The crystal chemistry of the milarite-group minerals. *American Mineralogist* **76**, 1836-1856.

Hawthorne, F.C., Oberti, R., Harlow, G.E., Maresch, W.V., Martin, R.F., Schumacher, J.C., & Welch, M.D. (2012). Nomenclature of the amphibole supergroup. *American Mineralogist* **97** (in press).

Hawthorne, F.C., Abdu, Y.A., Ball, N.A., Černý, P., & Kristiansen, R. (2014). Agakhanovite-(Y), ideally $(YCa)\square_2KBe_3Si_{12}O_{30}$, a new milarite-group mineral from the Heftetjern Pegmatite, Tørdal, Southern Norway: Description and crystal structure. *American Mineralogist* **99**, 2084-2088.

Hawthorne, F.C., Sokolova, E., Pautov, L.A., Agakhanov, A.A., & Karpenko, V.Yu.

(2015). Refinement of the crystal structure of berezanskite, $\text{Ti}_2\text{KLi}_3(\text{Si}_{12}\text{O}_{30})$.

Mineralogical Magazine (submitted).

Henry, D.J., Novák, M., Hawthorne, F.C., Ertl, A., Dutrow, B.L., Uher, P., & Pezzotta, F.

(2011). Nomenclature of the tourmaline super-group minerals. *American Mineralogist*

96, 895-913.

Hentschel, G., Abraham, K., & Schreyer, W. (1980). First terrestrial occurrence of

roedderite in volcanic ejecta of the Eifel, Germany. *Contributions to Mineralogy and*

Petrology **73**, 127-130.

Janeczek, J. (1986). Chemistry, optics, and crystal growth of milarite from Strzegom,

Poland. *Mineralogical Magazine* **50**, 271-277.

Kato, T., Miura, Y., & Murakami, N. (1976). Crystal structure of sugilite. *Mineralogical*

Journal **8**, 183-192.

Khan, A.A., Baur, W.H., & Forbes, W.C. (1972). Synthetic magnesium merrihueite, a

dipotassium pentamagnesium dodecasilicate: A tetrahedral magnesiosilicate framework

crystal structure. *Acta Crystallographica* **B28**, 267-272.

Kimata, M. & Hawthorne, F.C. (1989). The crystal chemistry of milarite: Two split-site

model. *Annual Report of the Institute of Geosciences, University of Tsukuba* **15**, 92-95.

Krot, A. N. & Wasson, J. T. (1994). Silica-merrihueite/roedderite-bearing chondrules and

clasts in ordinary chondrites; new occurrences and possible origin. *Meteoritics* **29**, 707-

718

Kuschel, H. (1877). Mitteilung an Prof. G. Konhard. Milarit. *Neues Jahrbuch für Mineralogie, Geologie und Palaeontologie*, 925-926.

Lengauer, C.L., Hrauda, N., Kolitsch, U., Krickl, R., & Tillmanns, E. (2009):

Friedrichbeckeite, $K(\square_{0.5}Na_{0.5})_2(Mg_{0.8}Mn_{0.1}Fe_{0.1})_2(Be_{0.6}Mg_{0.4})_3[Si_{12}O_{30}]$, a new milarite type mineral from the Bellerberg volcano, Eifel area, Germany. *Mineralogy and Petrology* **96**, 221–232.

Liebau, F. (1985). *Structural Chemistry of Silicates*. Springer-Verlag, Berlin.

Mihajlović, T., Lengauer, C.L., Ntaflos, T., Kolitsch, U., & Tillmanns, E. (2004). Two new minerals, rondorfite, $Ca_8Mg[SiO_4]_4Cl_2$, and almarudite, $K(\square,Na)_2(Mn,Fe,Mg)_2(Be,Al)_3[Si_{12}O_{30}]$, and a study on iron-rich wadalite, $Ca_{12}[(Al_8Si_4Fe_2)O_{32}]Cl_6$, from the Bellerberg volcano, Eifel, Germany. *Neues Jahrbuch für Mineralogie, Abhandlungen*. **179**, 265–294.

Miyashiro, A. (1956). Osumilite, a new silicate mineral and its crystal structure. *American Mineralogist* **41**, 104-116.

Murakami, N., Kato, T., Miura, Y., & Kirotatari, F. (1976). Sugilite, a new silicate mineral from Iwagi Islet, southwest Japan. *Mineralogical Journal* **8**, 110-121.

Neumann, H. (1941). Armenite, a water-bearing barium-calcium-aluminosilicate. *Norsk Geologisk Tidsskrift* **21**, 19-24.

Nguyen, N., Choisnet, J., & Raveau, B. (1980). Silicates synthétiques à structure milarite. *Journal of Solid State Chemistry* **34**, 1-9.

- Pautov, L.A. & Agakhanov, A.A. (1997). Berezanskite $\text{KLi}_3\text{Ti}_2\text{Si}_{12}\text{O}_{30}$, a new mineral. *Zapiski Vsesoyuznogo Mineralogicheskogo Obshchestva* **126(4)**, 75–80 (in Russian).
- Pautov, L.A., Agakhanov, A.A., & Sokolova, E.V. (1998). Shibkovite, a new mineral of milarite group. *Zapiski Vsesoyuznogo Mineralogicheskogo Obshchestva* **127(4)**, 89–94 (in Russian).
- Pautov, L.A., Agakhanov, A.A., Sokolova, E.V. & Ignatenko, K.I. (1996). Dusmatovite, a new mineral of milarite group. *Vestnik Moskovskogo Universiteta, Series 4, Geologicheskaya* **N2**, 54–60 (in Russian).
- Pautov, L.A., Agakhanov, A.A., Uvarova, Y.A., Sokolova, E.V., & Hawthorne, F.C. (2004). Zeravshanite, $\text{Cs}_4\text{Na}_2\text{Zr}_3(\text{Si}_{18}\text{O}_{45})(\text{H}_2\text{O})_2$, a new cesium mineral from Dara-i-Pioz massif (Tajikistan). *New Data on Minerals* **39**, 20-25.
- Postl, W., Walter, F., Ettinger, K., Hauzenberger, C., & Bojar, H.P. (2004). Trattnerite, $(\text{Fe,Mg})_2(\text{Mg,Fe})_3[\text{Si}_{12}\text{O}_{30}]$, a new mineral of the milarite group: mineral data and crystal structure. *European Journal of Mineralogy* **16**, 375-380.
- Preiser, C., Lösel, J., Brown, I.D., Kunz, M., Skowron, A. (1999). Long-range Coulombic forces and localized bonds. *Acta Crystallographica* **B 55**, 698-711.
- Pushcharovskii, D.Yu., Baataryn, T., Pobedinskaya, E.A., & Belov, N.V. (1972). The crystal structure of the zinc analogue of milarite. *Soviet Physics Crystallography* **16**, 628-630.
- Rutherford, J.S. (1990). Theoretical prediction of bond-valence networks. *Acta Crystallographica* **B46**, 289-292.

Salinas-Sanchez, A., Garcia-Munoz, J.L., Rodriguez-Carvajal, J., Saez-puche, R., & Martinez, J.L. (1992). Structural characterization of R_2BaCuO_5 ($R = Y, Lu, Yb, Tm, Er, Ho, Dy, Gd, Eu$ and Sm) oxides by X-ray and neutron-diffraction, *Journal of Solid State Chemistry* **100** 201–211.

Sandomirskii, P.A., Simonov, M.A., & Belov, N.V. (1977). Crystal structure of synthetic Mn-milarite $K_2Mn_5[Si_{12}O_{30}].H_2O$. *Physics Doklady* **22**, 181-183.

Semenov, E.I., Dusmatov, V.D., Khomyakov, A.P., Voronkov, A.A., & Kazakova, M. (1975). Darapiosite, a new mineral of the milarite group. *Zapiski Vserossiiskogo Mineralogicheskogo Obshchestva* **104**, 583-584 (in Russian).

Shannon, R.D. (1976). Revised effective ionic radii and systematic studies of interatomic distances in halides and chalcogenides. *Acta Crystallographica* **A32**, 751-767.

Sokolova, E.V. & Pautov, L.A. (1995). Crystal structure of dusmatovite. *Physics Doklady* **40**, 607–610.

Sokolova, E.V., Rybakov, V.B., & Pautov, L.A. (1999). Crystal structure of shibkovite. *Doklady Akademia Nauk* **369(3)**, 378–380 (in Russian).

Sokolova, E.V., Hawthorne, F.C., & Pautov, L.A. (2000). The crystal chemistry of Li-bearing minerals with the milarite-type structure: the crystal structure of end-member sogdianite. *Canadian Mineralogist* **38**, 853-859.

Spear, F.S. (1993). *Metamorphic Phase Equilibria and Pressure-Temperature-Time Paths*. Mineralogical Society of America, Washington DC, 799 pages.

Taggart, J. E., Jr., Foord, E. E., & Shigley, J. E. (1994). Chemical composition and structural formula of manganoan sugilite from the Wessels mine, Republic of South Africa. *Mineralogical Magazine* **58**, 679-681.

Urusov V.S. & Orlov I.P. (1999). State-of-art and perspectives of the bond-valence model in inorganic crystal chemistry, *Crystallography reports* **44**(4), 686-709.

Uvarova, Y.A., Sokolova, E., Hawthorne, F.C., Pautov, L.A., & Agakhanov, A.A. (2004). A novel $[\text{Si}_{18}\text{O}_{45}]_{18\text{B}}$ sheet in the crystal structure of zeravshanite, $\text{Cs}_4\text{Na}_2\text{Zr}_3[\text{Si}_{18}\text{O}_{45}](\text{H}_2\text{O})_2$. *Canadian Mineralogist* **42**, 125-134.

Uvarova, Y.A., Sokolova, E., Hawthorne, F.C., Agakhanov, A.A., Pautov, L.A., & Karpenko, V.Y. (2006). The crystal chemistry of senkevichite, $\text{CsKNaCa}_2\text{TiO}[\text{Si}_7\text{O}_{18}(\text{OH})]$, from the Dara-i-Pioz Alkaline Massif, Northern Tajikistan. *Canadian Mineralogist* **44**, 1341-1348.

Velde, D., Medenbach, O., Wagner, C., & Schreyer, W. (1989). Chayesite, $\text{K}(\text{Mg}, \text{Fe}^{2+})_4\text{Fe}^{3+}[\text{Si}_{12}\text{O}_{30}]$: A new rock-forming silicate of the osumilite group from the Moon Canyon (Utah) lamproite. *American Mineralogist* **74**, 1368-1373.

White, J.S.Jr., Arem, J.E., Nelen, J.A., Levens, P.B., & Thomssen, R.W. (1973). Brannockite, a new tin material. *Mineralogical Record* **4**, 73-76.

Winter, W., Armbruster, T., & Lengauer, C.L. (1995). Crystal structure refinement of synthetic osumilite-type phases: $\text{BaMg}_2\text{Al}_6\text{Si}_9\text{O}_{30}$, $\text{SrMg}_2\text{Al}_6\text{Si}_9\text{O}_{30}$ and $\text{Mg}_2\text{Al}_4\text{Si}_{11}\text{O}_{30}$. *European Journal of Mineralogy* **7**, 277–286.

Wood, J. A. & Holmberg, B. B. (1994). Constraints placed on the chondrule-forming process by merrihueite in the mezoe-madaras chondrite. *Icarus (Online)*. **108(2)**, 309-324.

Zoltai, T. (1960). Classification of silicates and other minerals with tetrahedral structures. *American Mineralogist* **45**, 960-973.

3.13 Appendix A: Supplementary material

Supplementary material for Chemographic Exploration of the Milarite-Type Structure

Table 3.S1 Publications describing milarite-group minerals and synthetic milarite-group compounds used in the review.

Minerals

Almarudite

Mihajlović, T., Lengauer, C. L., Ntaflos, T., Kolitsch, U., Tillmanns, E. (2004) Two new minerals rondorfite, $\text{Ca}_8\text{Mg}[\text{SiO}_4]_4\text{Cl}_2$, and almarudite, $\text{K}(\text{Na})_2(\text{Mn,Fe,Mg})_2(\text{Be,Al})_3[\text{Si}_{12}\text{O}_{30}]$, and a study of iron-rich wadalite, $\text{Ca}_{12}[(\text{Al}_8\text{Si}_4\text{Fe}_2)\text{O}_{32}]\text{Cl}_6$, from the Bellerberg (Bellberg) volcano, Eifel, Germany, *Neues Jahrbuch für Mineralogie, Abhandlungen*, **179**, 265-294

Armenite

Hetherington, C.J., Mullis, J., Graeser, S., and Gieré, R. (2003): Formation of armenite in the Berisal Complex, Simplon Region, Switzerland. *Schweizerische Mineralogische und Petrographische Mitteilungen* 83, 243-259

Armbruster, T. (1999) Si, Al ordering in the double-ring silicate armenite, $\text{BaCa}_2\text{Al}_6\text{Si}_9\text{O}_{30} \cdot 2\text{H}_2\text{O}$: A single-crystal X-ray and ^{29}Si MAS NMR study, *American Mineralogist*, 84, 92–101

Frau, F., & Stara, P. (1996) A new occurrence of armenite in Sardinia, Italy, *Mineralogica et petrographica acta*, 39, 271-274

Armbruster, T., Czank, M. (1992) H_2O ordering and superstructures in armenite, $\text{BaCa}_2\text{Al}_6\text{Si}_9\text{O}_{30} \cdot 2\text{H}_2\text{O}$: A single-crystal X-ray and TEM study, *American Mineralogist*, 77, 422-430

Fortey, N. J., Nancarrow, P. H. A., Gallagher, M.J. (1991) Armenite from the Middle Dalradian of Scotland, *Mineralogical Magazine*, 55, 135-138

Zak, L., Obst, P. (1989) Armenite-feldspar veins in basic volcanic rocks from Chvaletice (Czechoslovakia), *Casopis Pro Mineralogii A Geologii*, 34, 337-41

Balassone, G., Boni, M., Di Maio, G., Franco, E. (1989) Armenite in southwest Sardinia: first recorded occurrence in Italy, *Neues Jahrbuch für Mineralogie*, 2, 49-58

Mason, B. (1987) Armenite from Broken Hill, Australia, with comments on calciocelsian and barium anorthite, *Mineralogical Magazine*, 51, 317-18.

Semenenko, N.P., Litvin, A.L., Sharkin, O.P., Boiko, V.L., Egorova, L.N., Shurdin, G.S., Terets, G.Y., Savitskaya, A.B., and Ilovaishkaya, S.V. (1987) Armenite from northern Dneiper region, *Mineralogicheskii Zhurnal*, 9, 83–90 (in Russian).

Pouliot, G., Trudel, P., Valiquette, G., Samson, P.N. (1984) Armenite-thulite-albite veins at Remigny, Quebec; the second occurrence of armenite, *Canadian Mineralogist*, 22, 453-464

Bakakia, V.V., Balko, V.P., and Solovyeva, L.P. (1975) Crystal structures of milarite, armenite, and sogdianite, *Soviet Physics Crystallography*, 19, 460-462.

Neumann, H. (1941): Armenite, a water-bearing barium-calcium-alumo-silicate, *Norsk Geologisk Tidsskrift*, 21, 19-24

Neumann, H. (1940): Armenite, a new mineral. Preliminary note, *Norsk Geologisk Tidsskrift*, 19, 21-22

Berezanskite

Pautov, L.A., Agakhanov, A.A. (1997) Berezanskite $\text{KLi}_3\text{T}_2\text{Si}_{12}\text{O}_{30}$, a new mineral, *Zapiski Vserossiyskogo Mineralogicheskogo Obshchestva*, 126 (4), 75-80 (in Russian)

Brannockite

Armbruster, T., Oberhänsli, R (1988) Crystal chemistry of double-ring silicates: Structures of sugilite and brannockite, *American Mineralogist*, 73, 595-600

White, J.S., Arem, J.E., Nelen, J.A., Leavens, P.B., and Thomssen, R.W. (1973) Brannockite, a new tin mineral, *Mineralogical Record*, March-April, 73-76

Chayesite

Alietti, E., Brigatti, M.F., Capedri, S., and Poppi, L. (1994) The roedderite-chayesite series from Spanish lamproites: crystal chemical characterization, *Mineralogical Magazine*, 58, 655–662

Velde, D., Medenbach, O., Wagner, E., Schreyer, W. (1989) Chayesite, $K(\text{Mg}, \text{Fe}^{+2})_4\text{Fe}_3\text{Si}_{20}\text{O}_{30}$: a new rock forming silicate mineral of the osumilite group from the Moon Canyon (Utah) lamproite, *American Mineralogist*, 74, 1368-73.

Darapiosite

Ferraris, G., Prencipe, M., Pautov, L.A., & Sokolova, E.V. (1999): Crystal structure of darapiosite and comparison with Li- and Zn-bearing minerals of the milarite group, *Canadian Mineralogist*, 37, 769-774

Semenov, E.I., Dusmatov, V.D., Khomyakov, A.P., Voronkov, A.A., Kazakova, M.Y. (1976) Darapiosite, a new mineral of the milarite group, *International Geology Review*, 18 (7), 853-855 --- see also: Semenov, E.I., Dusmatov, V.D., Khomyakov, A.P., Voronkov, A.A., Kazakova, M.Y. (1975): Darapiosite, a new mineral of the milarite group, *Zap. Vses. Mineral. Obshchest.* 104, 583-585 (in Russian)

Dusmatovite

Sokolova, E. V. & Pautov, L. A. (1995) Crystal structure of dusmatovite, *Doklady Akademii Nauk*, 344, 607-610 (in Russian)

Eifelite

Abraham, K., Gebert, W., Medenbach, O., Schreyer, W., Hentschel, G. (1983) Eifelite, $\text{KNa}_3\text{Mg}_4\text{Si}_{12}\text{O}_{30}$, a New Mineral of the Osumilite Group with Octahedral Sodium, *Contribution to Mineralogy and Petrology*, 82, 252-258

Friedrichbeckeite

Lengauer, C.L., Hrauda, N., Kolitsch, U., Krickl, R., Tillmanns, E. (2009) Friedrichbeckeite, $\text{K}(\square_{0.5}\text{Na}_{0.5})_2(\text{Mg}_{0.8}\text{Mn}_{0.1}\text{Fe}_{0.1})_2(\text{Be}_{0.6}\text{Mg}_{0.4})_3[\text{Si}_{12}\text{O}_{30}]$, a new milarite-type mineral from the Bellerberg volcano, Eifel area, Germany, *Mineralogy and Petrology*, 96, 221-232

Klöchite

Walter, F. (2009) Das Steirisch-Burgenländische Vulkangebiet – Eine Quelle Seltener Und Neuer Mineralarten, Der Steirische Mineralog, Jg. 18, H. 23, 8-13 (in German)

Merrihueite

Krot, A. N. & Wasson, J. T. (1994) Silica-merrihueite/roedderite-bearing chondrules and clasts in ordinary chondrites: New occurrences and possible origin, Meteoritics, 29 (5), 707-718

Wood, J.A. and Holmberg, B.B. (1994) Constraints placed on the chondrule-forming process by merrihueite in the Mezo-Madras chondrite. Icarus, 108, 309-324.

Dodd, R.T. Jr, Van Schmus, W. R., Marvin, U. B. (1966) Significance of iron-rich silicates in the mezo-madaras chondrite, American mineralogist, 51, 1177-91

Dodd, R.T. Jr, Van Schmus, W. R., Marvin, U. B. (1965) Merrihueite, A New Alkali-Ferromagnesian Silicate from the Mezö-Madaras Chondrite, Science, 149, No. 3687, 972-974

Milarite

Cooper, M.A., Hawthorne, F.C., Ball, N.A., Cerny, P., Kristiansen, R. (2006) Oftedalite, $(\text{Sc}, \text{Ca}, \text{Mn}^{2+})_2 \text{K}(\text{Be}, \text{Al})_3 \text{Si}_{12} \text{O}_{30}$, a new member of the milarite group from the heftetjern pegmatite, Tørdal, Norway: Description and crystal structure, Canadian Mineralogist, 44, 943-949

Nysten, P. (1996) Paragenetic setting and crystal chemistry of milarites from Proterozoic granitic pegmatites in Sweden, Neues Jahrbuch für Mineralogie: Monatshefte, 12, 564-576

Hawthorne, F.C., Kimata, M., Cerny, P., Ball, N., Rossman, G.R., Grice, J.D. (1991) The crystal chemistry of the milarite-group minerals, American Mineralogist, 76, 1836-1856

Cerny, P., Hawthorne, F.C., Jambor, J.L., Grice, J.D. (1991) Yttrian milarite, Canadian Mineralogist, 29, 533-541

Kimata, M., Hawthorne, F.C. (1989) The crystal structure of milarite: two split-models, Annual report of the institute of geoscience, the university of tsukuba, 15, 92-95

Armbruster, T., Bermanec, V., Wenger, M., Oberhansli, R. (1989) Crystal chemistry of double-ring silicates: structure of natural and dehydrated milarite at 100 K, European Journal of Mineralogy, 1, 353-362

Janeczek, J. (1986) Chemistry, Optics, and crystal growth of milarite from Strzegom, Poland, Mineralogical Magazine, 50, 271-277

Conference abstract: Milarita do pegmatito de jaguaraçu, estado de minas gerais, Anais de academia brasileira de ciencias, 56, 108

Cerny, P., Hawthorne, F.C., Jarosewich, E. (1980) Crystal chemistry of milarite, Canadian Mineralogist, 18, 41-57

Bakakia, V.V., Balko, V.P., and Solovyeva, L.P. (1975) Crystal structures of milarite, armenite, and sogdianite, Soviet Physics Crystallography, 19, 460-462.

Raade, G. (1966) A new norwegian occurrence of milarite, Norsk Geologisk Tidsskrift, 46(1), 122-123

Iovcheva, E. (1966) Milarite from central asia, Doklady Akademii Nauk SSSR, 170(6), 1394-1397 (in russian)

Chistyakova, M. (1964) Milarite from central kazakhstan, Doklady Akademii Nauk SSSR, 159(6), 1305-1308 (in russian)

Sosedko, T. (1962) Chemical composition of milarite, Doklady Akademii Nauk SSSR, 146(2), 437-439 (in Russian)

Sosedko, T. (1960) Finding milarite on kola, Doklady Akademii Nauk SSSR, 131(3), 643-646 (in Russian)

Ito, T., Morimoto, N., Sadanaga, R. (1952) The crystal structure of milarite, Acta crystallographica, 5, 209

Belov, N.V. (1949) Kristallicheskaya struktura milarita, Doklady Akademii Nauk SSSR, 69(3), 365-368 (in Russian)

Palache, C. (1931) On the presence of beryllium in milarite, American Mineralogist, 16(10), 469-470

Oftedalite

Cooper, M.A., Hawthorne, F.C., Ball, N.A., Cerny, P., Kristiansen, R. (2006) Oftedalite, $(\text{Sc, Ca, Mn}^{2+})_2 \text{K}(\text{Be, Al})_3 \text{Si}_{12} \text{O}_{30}$, a new member of the milarite group from the heftetjern pegmatite, Tørdal, Norway: Description and crystal structure, *Canadian Mineralogist*, 44, 943-949

Osumilite (Osumilite-(Mg))

Balassone, G., Mormone, A., Rossi, M., Bernardi, A., Fisch, M., Armbruster, T., Malsy, A. K., Berger, A. (2008) Crystal chemical and structural characterization of an Mg-rich osumilite from Vesuvius volcano (Italy), *European Journal of Mineralogy*, 20, 713-720

Seryotkin, Y. V., Sokol, E. V., Bakakin, V. V., Likhacheva, A. Y. (2008) Pyrometamorphic osumilite: occurrence, paragenesis, and crystal structure as compared to cordierite, *European Journal of Mineralogy*, 20, 191-198

Kalman, T. (2007) Osumilite in a buchite xenolith from badacsony - a new mineral in Hungary, *Földtany Kozlony*, 137(3), 359-368 (in Hungarian)

Conference abstract. Westphal, M., Schumacher, J.C. (1997) Compositions of osumilite and quartz-cordierite pseudomorphs of a possible low-K osumilite from Rogaland, Southwestern Norway, 29(6), 397

Sokol, E.V. (1997) New genetic type of osumilite occurrence, *Zapiski Vserossiiskogo mineralogicheskogo obshchestva*, 126(4), 43-53 (in Russian)

Nowicki, T. E., Frimmel, H. E., Waters, D. J. (1995) The occurrence of osumilite in pelitic granulites of the Namaqualand metamorphic complex, South Africa, *South African Journal of Geology*, 98(2), 191-201

Carrier, G., Lorand, J.-P., Kineats, J.-R. (1994) Magmatic osumilite in an ultrapotassic dyke, southern Peru: first occurrence, *European Journal of Mineralogy*, 6, 657-665

Carrier, G., Kineast, J.-R., Audebaud, E. (1992) La osumilita del cerro morojatahua, hacienda chili palca, departamento de Puno, Peru; occurencia, quimica y condicion de formacion, *Boletín - Sociedad Geológica Boliviana*, 27, 48-51

-
- Arima, M., Gower, C.F. (1991) Osumilite-bearing Granulites in the Eastern Grenville Province, Eastern Labrador, Canada: Mineral Parageneses and Metamorphic Conditions, *Journal of Petrology*, 32, 29-61
- Kirov, G.K., Petrov, O.E. (1990) An osumilite group mineral in the hydrothermal crystallization of quartz, *Comptes rendus de l'academie bulgare des sciences*, 43(7), 49-52
- Katsuki, K., Hiromi K., Yoshimi F. (1990) Finding of osumilite and andalusite from the Pliocene subaqueous ash layer in Niigata Prefecture, central Japan, *Journal of Mineralogy, Petrology and Economic Geology*, 85, 495-501
- Parodi, G.C., Ventura, G. D., Lorand, J.-P. (1989) Mineralogy and petrology of an unusual osumilite + vanadium-rich pseudobrookite assemblage in an ejectum from the vico volcanic complex (Latium, Italy), *American Mineralogist* (December 1989), 74, 1278-1284
- Armbruster, T., Oberhänsli, R. (1988) Crystal chemistry of double-ring silicates: Structural, chemical, and optical variation in osumilites, *American Mineralogist*, 73, 585-594
- Shreyer, W., Blumel, P., MARESCH, W.V. (1986) Cordierit und Osumilith aus den Buchiten der Blauen Kuppe bei Eschwege, *Der Aufschluß*, 37, 353-367 (in German)
- Shreyer, W., Hentschel, G., Abraham, K. (1983) Osumilite in the eifel and the usage of this mineral as a petrogenetic indicator, *Tschermaks Mineralogische und petrographische mitteilungen*, 31, 215-234 (in German)
- Grew, E.S. (1982) Osumilite in the sapphirine-quartz terrane of Enderby Land, Antarctica: implications for osumilite petrogenesis in the granulite facies, *American Mineralogist*, 67, 762-787
- Hesse, K.-F., Seifert, F. (1982) Site occupancy refinement of osumilite, *Zeitschrift für Kristallographie*, 160, 179-186
- Koga, S. (1981) Osumilite of the lava of Chiyoshichiro-yama, Akagi volcano, Gunma, Japan, *Journal of Mineralogy*, 15, 10-17 (in Japanese)
- Bogdanova, N. (1980) On the 1st occurrence of metamorphic osumilite in the USSR, *Doklady Akademii Nauk SSSR*, 250(3), 690-693 (in Russian)
- Conference abstract: Grew, E.S. (1978) Osumilite at Gage ridge, Enderby Land, Antarctica, *Transactions - American Mineralogical Society*, 62, 10-11
-

geophysical union, 59(12), 1216

Goldman, D. S., Rossman, G. R. (1978) Site distribution of iron and anomalous biaxiality in osumilite, American Mineralogist, 63, 490-498

Yokomizo, H., Miyachi, S. (1978) Chemical composition of osumilite in haneyama lava, oita prefecture, Journal of Mineralogy, Petrology, and Economic Geology, 73, 180-182 (in Japanese)

Miyachi, S., Miyachi, M. (1978) New occurrence of a magnesian "Osumilite" from iriki, kagoshima prefecture, japan, ???, 20, 1-8 (In Japanese)

Maijer, C. Hansen, J.B.H., Wever, J., Poorter R.P.E. (1977) Osumilite, a mineral new to norway, Norsk Geologisk Tidsskrift, 57(2), 187-188

Berg, J. H., Wheeler, E.P. II (1976) Osumilite of deep-seated origin in the contact aureole of anorthositic nain complex, labrador, American Mineralogist, 61, 29-37

Chinner, G.A., Dixon, P.D. (1973) Irish osumilite, Mineralogical Magazine, 39, 189-192

Olsen, E., Bunch, T.E. (1970) Compositions of natural osumilites, American Mineralogist, 55, 875-879

Brown, G.E. (1969) . The Crystal Structure of Osumilite. M.S. Thesis, Virginia Polytechnic Institute.

Bunch, T.E., Fuchs, L.H. (1969) Yagiite, a new sodium-magnesium equivalent of osumilite, American Mineralogist, 54, 14-18

Brown, G.E., Gibbs, G.V. (1969) Refinement of the crystal structure of osumilite, American Mineralogist, 54, 101-116

Miyashiro, A. (1956) Osumilite, a new silicate mineral, and its crystal structure, American Mineralogist, 41, 104-116

Miyashiro, A. (1953) Osumilite, a new mineral, and cordierite in volcanic rocks, Proceedings of the Japan Academy, 29, 321-323

Poudretteite

Smith, C.P., Bosshart, G., Graeser, S., Hanni, H., Gunther, D., Hametner, K., Gubelin, E.J. (2003) Poudretteite: a rare gem species from the mogok valley, *Gems and Gemology*, 39(1), 24-31

Grice, J.D., Ercitt, T.S., Van Velthuisen, J., Dunn, P. J. (1987) Poudretteite, $\text{KNa}_2\text{B}_3\text{Si}_{12}\text{O}_3$, a new member of the osumilite group from mont saint-hilaire, quebec, and its crystal structure, *Canadian Mineralogist*, 25, 763-766

Roedderite

Conference paper. Joswiak, D.J, Matrajt, G., Brownlee D.E., Westphal, A.J., Snead, C.J. (2007) A Roedderite-Bearing Terminal Particle from Stardust Track 56: Comparison with Rare Peralkaline Chondrules in Ordinary Chondrites, *Lunar and Planetary Science XXXVIII Abstract*, 38, 2142

Conference abstract. Fogel, R.A. (2002) The composition of roedderite in aubrites, *Meteoritics and Planetary Science*, 37(7), A48

Conference abstract. Feher, B., Szakall, S. (2002) Roedderite(?) from the nagy hill, Tarpa, NE Hungary: a problem with the classification based on electron microprobe analyses in the roedderite-merrihueite subgroup of the milarite group, *General Meeting of the Mineralogical Association of International Mineralogical Association Abstract*, 18, 141

Hsu, W. (1998) Geochemical and petrographic studies of oldhamite, diopside, and roedderite in enstatite meteorites, *Meteoritics and Planetary Science*, 33, 291-301

Alietti, E., Brigatti, M.F., Capedri, S., and Poppi, L. (1994) The roedderite-chayesite series from Spanish lamproites: crystal chemical characterization. *Mineralogical Magazine*, 58, 655–662

Krot, A. N. & Wasson, J. T. (1994) Silica-merrihueite/roedderite-bearing chondrules and clasts in ordinary chondrites: New occurrences and possible origin, *Meteoritics* , 29 (5), 707-718

Armbruster, T. (1989) Crystal chemistry of double-ring silicates: strcuture of roedderite at 100K and 300K, *European Journal of Mineralogy*, 1, 715-718

Rambaldi, E.R., Rajan, R.S., Housley, R.M. (1986) Roedderite in the Qingzhen (EH3) chondrite, *Meteoritics*, 21, 141-149

Rambaldi, E.R., Rajan, R.S., Housley, R.M., Wang, D. (1984) Oxidized, refractory and alkali-rich components in Qingzhen enstatite chondrite: implications about their origin, *Lunar and Planetary Science Abstract*, 15, 661-662

Abraham, K., Gebert, W., Medenbach, O., Shreyer, W., Hentschel, G. (1983) Eifelite, $\text{KNa}_3\text{Mg}_4\text{Si}_{12}\text{O}_{30}$, a New Mineral of the Osumilite Group with Octahedral Sodium, *Contribution to Mineralogy and Petrology*, 82, 252-258

Hentschel, G., Abraham, K., Schreyer, W. (1980) First Terrestrial Occurrence of Roedderite in Volcanic Ejecta of the Eifel, Germany, *Contributions to Mineralogy and Petrology*, 73, 127-130

Olsen, E. (1967) A new occurrence of roedderite and its bearing on osumilite-type minerals, *American Mineralogist*, 52, 1519

Fuchs, L.H. (1966) Roedderite, a new mineral from the indarch meteorite, *American Mineralogist*, 51, 949-955

Shibkovite

Sokolova, E. (1999) Crystal structure of shibkovite, *Doklady Akademii Nauk*, 369, 378-380 (in Russian)

Pautov, L.A., Agakhanov, A.A., Sokolova, E.V. (1998) Shibkovite $\text{K}(\text{Ca}, \text{Mn}, \text{Na})_2(\text{K}_{2-x}\text{x})_2\text{Zn}_3\text{Si}_{12}\text{O}_{30}$ - The new mineral from the milarite group, *Proceedings of the Russian Mineralogical Society*, 127(4) 89-94 (in Russian)

Sogdianite

Park, S.-H., Hoelzel, M., Boysen, H., Schmidbauer, E. (2007) Lithium conductivity in an Li-bearing double-ring silicate mineral, sogdianite, *Journal of Solid State Chemistry*, 180, 1306-1317

Sokolova, E.V., Hawthorne, F.C., Pautov, L.A. (2000) The crystal chemistry of Li-bearing minerals with the milarite-type structure: the crystal structure of end-member sogdianite, *Canadian Mineralogist*, 38, 853-859

Cooper, M.A., Hawthorne, F.C., Grew, E.S. (1999) The crystal chemistry of sogdianite, a milarite-group mineral,

American Mineralogist, 84, 764-768

Kabalov, Y. (1993) Rietveld refinement of the sogdianite structure, Doklady Akademii Nauk, 332, 571-574 (in Russian)

Boggs, R.C. (1987) Sogdianite-Zetkzerite intergrowths and their bearing on structural relationships between the osumilite and tuhualite groups, Geological Society of America Meeting Abstract, 19(7), 594

Bakakia, V.V., Balko, V.P., and Solovyeva, L.P. (1975) Crystal structures of milarite, armenite, and sogdianite, Soviet Physics Crystallographia, 19, 460-462

Dusmatov, V. (1968) A new mineral - sogdianite, Doklady Akademii Nauk SSSR, 182(5), 1176-1177 (in Russian)

Sugilite

Geiger, C. A. (2009) A ^{57}Fe Mossbauer spectroscopic study of sugilite, $\text{KNa}_2(\text{Fe}^{3+}, \text{Mn}^{3+}, \text{Al})_2\text{Li}_3\text{Si}_{12}\text{O}_{30}$, Canadian Mineralogist, 47, 927-931

Perchiazzi, N., Biagioni, C. (2005) Sugilite e serandite dei diaspri auctt. di vagli (alpi apuane), Atti Della Societa Toscana Di Scienze Naturali. Memorie, 110, 67-71

Taggart, J.E.Jr., Foord, E.E., Shigley, J.E. (1994) Chemical composition and structural formula of manganoan sugilite from the weissel mine, republic of south africa, Mineralogical Magazine, 58, 679-681

Kawachi, Y., Ashley, P.M., Vince, D., Goodwin, M. (1994) Sugilite in manganese silicate rocks from the hoskins mine and woods mine, new south wales, australia, Mineralogical Magazine, 58, 671-677

Cabella, R., Lucchetti, G., Palenzona, A. (1990) Al-rich, Fe-poor manganoan sugilite in a pectolite-bearing assemblage from cerchiara mine (northern apennines, italy), Neues Jahrbuchfur Mineralogie Monatshefte, 1990(10), 443-448

Armbruster, T., Oberhansli, R (1988) Crystal chemistry of double-ring silicates: Structures of sugilite and brannockite, American Mineralogist, 73, 595-600

Dixon, R.D. (1985) Sugilite and associated minerals from wessels mine, kalahari manganese field, Transaction of the

Geological Society of South Africa, 88(1), 11-17

Olivier, C., Gihwala, D., Peisach., Pineda, C.A., Pienaar, H.S. (1983) Determination of lithium in the gem mineral sugilite, Journal of Radioanalytical Chemistry, 76(1), 241-248

Sunagawa, I. (1982) Nambulite and sugilite; two new minerals found in japan and later found as gem materials, Hoseki Gakkai Shi, 9, 19-24 (in Japanese)

Clark, A.M., Bearne, G.S., Fejer, E.E., Din, V.K., Couper, A.G. (1980) Additional data on sugilite, Mineralogical Magazine, 43, 947-949

Dunn, P.J., Brummer, J.J., Belsky, H. (1980) Sugilite, a second occurrence: wessels mine, kalahari manganese field, republic of south africa, Canadian Mineralogist, 18, 37-39

Kato, T., Miura, Y. Murakami, N. (1976) Crystal structure of sugilite, Mineralogical journal, 8(3), 184-192

Murakami, N., Kato, T., Miura, Y., Hirowatari, F. (1976) Sugilite, a new silicate mineral from iwagi islet, southwest japan, Mineralogical journal, 8(2), 110-121

Trattnerite

Postl, W., Walter, F., Ettinger, K., Hauzenberger, C., Bojar, H.-S. (2004) Trattnerite, $(\text{Fe,Mg})_2(\text{Mg,Fe})_3(\text{Si}_{12}\text{O}_{30})$, a new mineral of the milarite group: mineral data and crystal structure, European Journal of Mineralogy, 16, 375-370

Yagiite

Bunch, T.E., Fuchs, L.H. (1969) Yagiite, a new sodium-magnesium equivalent of osumilite, American Mineralogist, 54, 14-18

Synthetics

Eifelite

Bruckmann, P., Chatterjee, N.D., Rammensee, W., Bielefeld, K. (1993) An Equation of State for Roedderites, (K, Na)₂Mg₅[Si₁₂O₃₀], Based on Knudsen Cell Mass Spectrometry and Synthesis of Eifelite-Roedderite Crystalline Solutions, *Physics and Chemistry of Minerals*, 20, 362-368

Merrihueite

Khan, A.A., Baur, W.H., Forbes, W.C. (1972) Synthetic Magnesian Merrihueite, Dipotassium Pentamagnesium Dodecasilicate: a Tetrahedral Magnesiosilicate Framework Crystal Structure, *Acta Crystallographica*, B28, 267-272

Seifert, F., Schreyer, W. (1969) Stability Relations of K₂Mg₅Si₁₂O₃₀, and End Member of the Merrihueite-Roedderite Group of Meteoritic Minerals, *Contributions to Mineralogy and Petrology*, 22, 190-207

Milarite

Pushcharovskii, D. Y., Baataryn, T., Pobedinskaya, E.A., Belov, N.V. (1972) The crystal structure of the zinc analog of milarite, *Soviet Physics, Crystallography*, 16(4), 629-630

Osumilite

Kobayashi, Y., Takeda, T. (2004) Dense ceramics of single-crystalline-phase osumilite synthesized by solid-state reaction, *Ceramics International*, 30, 689–695

Winter, W., Armbruster, T., Lengauer, C. (1995) Crystal structure refinement of synthetic osumilite phases: BaMg₂Al₆Si₉O₃₀, SrMg₂Al₆Si₉O₃₀, Mg₂Al₄Si₁₁O₃₀, *European Journal of Mineralogy*, 7, 277-286

Olesch, M., Seifert, F. (1981) The Restricted Stability of Osumilite Under Hydrous Conditions in the System K₂O - MgO - Al₂O₃ - SiO₂ - H₂O, *Contributions to Mineralogy and Petrology*, 76, 362-367

Schreyer, W., Seifert, F. (1967) Metastability of an Osumilite End Member in the System K₂O-MgO-Al₂O₃-SiO₂-H₂O and its Possible Bearing on the Rarity of Natural Osumilites, *Contributions to Mineralogy and Petrology*, 14, 343-358

Roedderite

Bruckmann, P., Chatterjee, N.D., Rammensee, W., Bielefeld, K. (1993) An Equation of State for Roedderites, (K, Na)₂Mg₅[Si₁₂O₃₀], Based on Knudsen Cell Mass Spectrometry and Synthesis of Eifelite-Roedderite Crystalline Solutions, *Physics and Chemistry of Minerals*, 20, 362-368

Winter, W., Muller, G., Pannhorst, W. (1991) Roedderite-type solid solutions (Na,K)₂Mg₅Si₁₂O₃₀ : thermal stability, lattice constants and thermal expansion, *Neues Jahrbuch fur Mineralogie Monatshefte*, 9, 397-407

Other

Choisnet, J., Cornet, D., Hemidy, J.-F., Nguyen, N., Dat, Y. (1981) Spectroscopic study of copper (II) ions in tetrahedral coordination in milarite synthetic silicates, *Journal of Solid State Chemistry*, 40(2), 161-169

Nguyen, N., Choisnet, J., Raveau, B. (1980) Silicates synthetiques a structure milarite, *Journal of Solid State Chemistry*, 34, 1-9 (in French)

Note: The publications are organized in reverse chronological order. Publications covering multiple milarite-group minerals are given for each mineral

Chapter 4

Bond-length distributions for ions bonded to oxygen:

Alkali and alkaline-earth metals

Gagné, O.C. & Hawthorne, F.C. (2016). Bond-length distributions for ions bonded to oxygen: Alkali and alkaline-earth metals. *Acta Crystallographica*, **B72**, 602-625

4.1 Preliminary discussion

The two most important types of data that result from crystal-structure solution and refinement are [1] interatomic distances, and [2] bond topology (the pattern of chemical bonding in a structure). Virtually every paper on crystal structure discusses the variation of bond lengths in the crystals examined, and two general approaches to examining these variations are commonly used: (1) molecular-orbital approaches; (2) crystal-chemical arguments.

4.1.1 Molecular-orbital approaches

In the period 1960-1985, there was a lot of work on rationalizing observed bond lengths and bond angles in crystals in terms of molecular-orbital arguments and calculations on molecular groups that were intended to simulate the structure fragment under consideration. This work tended to focus on strongly bonded clusters, particularly oxyanions, as the arguments and calculations were easier to develop than for weakly-charged species with high coordination numbers. Influential in this regard was the work of Cruickshank (1961) which rationalized relations between bond lengths and bond angles in simple oxyanions and corresponding crystal structures. The first calculations done were simple extended Hückel calculations (*e.g.*, Gibbs *et al.*, 1972) in which the crystal environment was simulated by attaching H atoms to the peripheral anions to neutralize the total charge of the cluster. These calculations led to semi-quantitative understanding of variation in bond angles in silicates. *Ab initio* calculations of increasing sophistication rapidly followed (*e.g.*, Newton & Gibbs, 1980), and calculated distances

showed reasonable agreement with observed values in crystal structures for a few oxyanions, notably the silicate group. This type of agreement for a few oxyanion groups showed that *ab initio* calculations on small molecules are reasonable first approximations for reproducing bond lengths in crystals. However, they cannot address bond-length variations that are characteristic of the same groups in different crystal structures as they are only molecular calculations and lack the constraints of space-group symmetry. Pisani *et al.* (1988) incorporated periodicity into *ab initio* Hartree-Fock calculations by expressing the orbitals as Bloch functions (e.g., Ziman, 1964) which enabled sophisticated calculation for crystal structures and overcame the constraints associated with a molecular approach. Application of this method has led to better reproduction of bond lengths by calculation of specific structures, and fairly accurate calculation of many physical properties of crystals. However, it has not led to a general understanding of what factors control the detailed variation of bond lengths in crystals.

4.1.2 Crystal-chemical approaches

Crystal-chemical approaches to the interpretation of structure and their bond-length variations arose very early in the development of crystal-structure work, and were a major factor in actually solving the crystal structures of more complicated solids once the more simple structures had been solved. During the 1920s, Goldschmidt in particular developed the ideas of coordination number and ionic radius, and much of this information was summarized by Pauling (1929, 1960). Various sets of ionic radii were used in crystal chemistry, culminating in the seminal paper of Shannon (1976) which lists ionic radii for a wide variety of ions and coordination numbers, and which

currently has ~35,000 citations. Initially, the idea was to reproduce bond lengths by adding the radii of the constituent ions, but this only works very approximately. Much greater reproducibility of bond lengths can be produced by correlating variations in bond length as a function of constituent ion radii in specific groups of structures; the reasons for the lack of transfer of these relations from one structure type to another are much less well-understood.

The development of the bond-valence model (Brown, 2002, 2009) has led to further insight into factors that control variations in bond length. Bond-valence curves are non-linear, and this leads to a relation between the degree of dispersion of bond lengths in a specific coordination polyhedra (often called “bond-length distortion”) and the observed mean bond-length. There has been much written on this issue (*e.g.*, Brown & Shannon, 1973; Urusov, 2003, 2006, 2014), but this work has ignored some other factors that are also known to affect bond lengths. For example, Shannon (1976) lists coordination numbers for O^{2-} from [2] to [8] with a range of 0.07 Å, indicating that this factor should significantly affect mean bond-lengths and cannot be ignored. Furthermore, Shannon (1971) and Hawthorne & Faggiani (1979) have shown significant correlations between $\langle [4]Ge-O \rangle$ and $\langle [4]V^{5+}-O \rangle$ distances and the electronegativity of the other cations bonded to the complex anion, suggesting an effect of the relative covalency of the surrounding cations on mean bond-length.

It is significant that no work on the variation in mean bond-lengths has examined the effect of more than one of these factors on the data considered. Moreover, the size of the datasets considered has usually been small and focused on the structures of interest to the author(s). I have established a very large dataset of bond lengths that can

be the basis of a much more comprehensive examination of the variation in both individual and mean bond-lengths than has been done in the past. Data have been gathered for 462 cation configurations, *i.e.*, for 135 cations in all their observed coordination numbers. There seems to be a disproportionate amount of time spent on determining crystal structures and the understanding of the general factors that drive their atomic arrangement and stability. Only a handful of configurations have been examined, and these generally involve highly-charged cations in low coordination numbers (*e.g.*, $^{[4]}\text{Si}^{4+}\text{-O}$, Baur 1971; $^{[4]}\text{P}^{5+}\text{-O}$, Baur 1974, Huminicki & Hawthorne, 2002; $^{[3]}\text{B}^{3+}\text{-O}$ and $^{[4]}\text{B}^{3+}\text{-O}$, Hawthorne *et al.*, 1996; $^{[4]}\text{S}^{6+}\text{-O}$, Hawthorne *et al.*, 2000). Several hundred configurations have not yet been examined, and those that have been examined have used smaller data sets than are now available, and can now be further examined.

Obviously the amount of work involved here is huge and is not feasible to be done in this thesis. In the next chapter, I examine bond lengths for alkali-metal and alkaline-earth-metal ions bonded to O^{2-} , a total of 84 configurations. The work in the next chapter is only a preliminary examination of the data, but it is immediately apparent that the factors affecting variations in bond lengths and mean bond-lengths are more complicated than has hitherto been realized.

4.1.3 References

Baur, W.H. (1971). Prediction of bond length variations in silicon-oxygen bonds. *Am. Mineral.* **56**, 601-621.

Baur, W.H. (1974). The geometry of polyhedral distortions. Predictive relationships for the phosphate group. *Acta Cryst. B* **30**, 1195-1215.

Brown, I.D. & Shannon, R.D. (1973). Empirical bond-strength bond-length curves for oxides. *Acta Cryst.*, A **29**, 266-282.

Brown, I.D. (2002). *The Chemical Bond in Inorganic Chemistry*. Oxford University Press.

Brown, I.D. (2009). Recent developments in the methods and applications of the bond valence model. *Chem. Rev.* **109**, 6858-6919.

Cruickshank, D.W.J. (1961). The role of 3 d-orbitals in π -bonds between (a) silicon, phosphorus, sulphur, or chlorine and (b) oxygen or nitrogen. *J. Am. Chem. Soc.* **1961**, 5486-5504.

Gibbs, G.V., Hamil, M.M., Louisnathan, S.J., Bartell, L.S. & Yow, H. (1972). Correlations between Si-O bond length, Si-O-Si angle and bond overlap populations calculated using extended Huckel molecular orbital theory. *Am. Min.* **57**, 1578-1613.

Hawthorne, F.C. & Faggiani, R. (1979). Refinement of the structure of descloizite. *Acta Cryst. B* **35**, 717-720.

Huminicki, D.M.C. & Hawthorne, F.C. (2002). The crystal chemistry of the phosphate minerals. *Rev. Mineral. Geochem.* **48**, 123-253.

Hawthorne, F.C., Burns, P.C., Grice, J.D. (1996). The crystal chemistry of boron. *Rev. Mineral.* **33**, 41-115.

- Hawthorne, F.C., Krivovichev, S.V. & Burns, P.C. (2000). The crystal chemistry of sulfate minerals. *Rev. Mineral. Geochem.* **40**, 1-112.
- Newton, M.D. & Gibbs, G.V. (1980) *Ab initio* calculation of interatomic force constants in H_6SiO_7 and the bulk modulus of α -quartz and α -cristobalite. *Phys. Chem. Miner.* **6**, 305-312.
- Pauling, L. (1929). The principles determining the structures of complex ionic crystals. *J. Am. Chem. Soc.* **51**, 1010-1026.
- Pauling, L. (1960). The nature of the chemical bond and the structure of molecules and crystals: an introduction to modern structural chemistry. Cornell University Press.
- Pisani, C., Dovesi, R. & Roetti, C. (1988). *Hartree-Fock Ab Initio Treatment of Crystalline Systems*. Springer, Berlin.
- Shannon, R.D. (1971). Effects of covalency on average interatomic distances in germanates. *J. Chem. Soc. D*, **1971**, 881-882.
- Shannon, R.D. (1976). Revised effective ionic radii and systematic studies of interatomic distances in halides and chalcogenides. *Acta Cryst. A* **32**, 751–767.
- Urusov, V.S. (2003). Theoretical analysis and empirical manifestation of the distortion theorem, *Z. Kristallogr.* **218**, 709-719.
- Urusov, V.S. (2006). New formulation of the distortion theorem and distortion of Mn^{3+}O_6 octahedra in inorganic crystals. *Dokl. Phys. Chem.* **408**, 137–141.

Urusov, V.S. (2014). Terms of parity and distortion of coordination polyhedra in inorganic crystal chemistry. *J. Struct. Chem.* **55**, 1277-1292

Ziman, J.M. (1964). Principles of the Theory of Solids. Cambridge University Press

4.2 Synopsis

Bond-length distributions have been examined for 55 configurations of alkali-metal and 29 configurations of alkaline-earth-metal ions, for 4859 coordination polyhedra and 38,594 bond distances (alkali metals) and for 3038 coordination polyhedra and 24,487 bond distances (alkaline-earth metals).

4.3 Abstract

Bond-length distributions have been examined for 55 configurations of alkali-metal ions and 29 configurations of alkaline-earth-metal ions bonded to oxygen, for 4859 coordination polyhedra and 38,594 bond distances (alkali metals) and for 3038 coordination polyhedra and 24,487 bond distances (alkaline-earth metals). Bond lengths generally show a positively-skewed Gaussian distribution that originates from the variation in Born repulsion and Coulomb attraction as a function of interatomic distance. The skewness and kurtosis of these distributions generally decrease with increasing coordination number of the central cation, a result of decreasing Born repulsion with increasing coordination number. We confirm the following minimum coordination numbers: $^{[3]}\text{Li}^+$, $^{[3]}\text{Na}^+$, $^{[4]}\text{K}^+$, $^{[4]}\text{Rb}^+$, $^{[6]}\text{Cs}^+$, $^{[3]}\text{Be}^{2+}$, $^{[4]}\text{Mg}^{2+}$, $^{[6]}\text{Ca}^{2+}$, $^{[6]}\text{Sr}^{2+}$ and $^{[6]}\text{Ba}^{2+}$, but note that some reported examples are the result of extensive dynamic and/or positional

short-range disorder and are not ordered arrangements. Some distributions of bond lengths are distinctly multi-modal. This is commonly due to the occurrence of large numbers of structure refinements of a particular structure type in which a particular cation is always present, leading to an over-representation of a specific range of bond lengths. Outliers in the distributions of mean bond-lengths are often associated with anomalous values of atomic displacement of the constituent cations and/or anions. For a sample of $^{[6]}\text{Na}^+$, the ratio $U_{\text{eq}}(\text{Na})/U_{\text{eq}}(\text{bonded anions})$ is partially correlated with $\langle ^{[6]}\text{Na}^+-\text{O}^{2-} \rangle$ ($R^2 = 0.57$), suggesting that the mean bond-length is correlated with vibrational/displacement characteristics of the constituent ions for a fixed coordination number. Mean bond-lengths also show a weak correlation with bond-length distortion from the mean value in general, although some coordination numbers show the widest variation in mean bond-length for zero distortion, e.g., Li^+ in [4]- and [6]-coordination, Na^+ in [4]- and [6]-coordination. For alkali-metal and alkaline-earth-metal ions, there is a positive correlation between cation coordination number and the grand mean incident bond-valence sum at the central cation, the values varying from 0.84 v.u. for $^{[5]}\text{K}^+$ to 1.06 v.u. for $^{[8]}\text{Li}^+$, and from 1.76 v.u. for $^{[7]}\text{Ba}^{2+}$ to 2.10 v.u. for $^{[12]}\text{Sr}^{2+}$. Bond-valence arguments suggest coordination numbers higher than [12] for K^+ , Rb^+ , Cs^+ and Ba^{2+} .

Keywords: bond lengths, coordination number, alkali metals, alkaline-earth metals.

4.4 Introduction

Many crystal structures have been refined in the past 100 years, and a large amount of information concerning interatomic distances in the solid state is available. There are

many studies of bond-length distributions for specific pairs of ions, notably for cations bonded to oxygen (e.g., Baur, 1971 (Si); Burns *et al.*, 1997 (U); Hawthorne *et al.*, 2000 (S); Schindler *et al.*, 2000 (V); Hawthorne & Huminicki, 2002 (Be); Huminicki & Hawthorne, 2002 (P); Mills & Christy, 2013 (Te); Majzlan *et al.*, 2014 (As)). However, many of these studies have focused on subsets of the available information, both with regard to the number of ions and coordination numbers, and to the amount of data available for each example. We have examined the distribution of bond lengths for 135 ions bonded to oxygen in 462 configurations using 180,331 bond lengths extracted from 9367 refined crystal structures; these data involve most ions of the periodic table and all coordination numbers in which they occur. Here, we report the bond-length distributions for 10 ions, the common alkali-metal ions (Li^+ , Na^+ , K^+ , Rb^+ and Cs^+) and alkaline-earth-metal ions (Be^{2+} , Mg^{2+} , Ca^{2+} , Sr^{2+} and Ba^{2+}) in all observed coordination numbers where bonded to O^{2-} for a total of 63,081 bond lengths in 7897 polyhedra from 4258 refined crystal structures. An advantage of working with a large number of ion pairs and a large amount of data is that it allows examination of subtle differences between the shapes of various distributions (e.g., bond-length distributions, mean-bond-length distributions) for various configurations of ions, which reflect differences in their bonding behaviour. These differences typically arise from either structural and/or electronic effects, and are well known for extreme examples such as [6]-coordinated Cu^{2+} and [6]-, [7]- and [8]-coordinated U^{6+} ; however, more subtle deviations from unimodality could be expected for the bond-length distributions of other ion configurations that are involved in related electronic or structural effects. Our motivation for this work is twofold: (1) The factors that affect bond distances are of continuing interest to all who work on crystal structures

and their properties, and a comprehensive analysis of all the data should lead to increased understanding of those factors. Here, we give a preliminary examination of the alkali-metal ions and alkaline-earth-metal ions in all observed coordination numbers where bonded to O^{2-} , and make our complete dataset available for future more detailed work. (2) A comprehensive knowledge of the observed variation in bond lengths is critically important in assessing the validity of computational results on possible atomic arrangements (e.g., Richardson, 2013) and identifying unusual stereochemical features in newly solved or refined crystal structures.

4.5 Definitions

In the interest of clarity, we define certain terms that we use in the following text. We make no claims of generality; these are merely working definitions.

Chemical bond: There is no rigorous definition of a chemical bond that is useful in the context of the present work, which deals with some hundreds of thousands of observed interatomic distances. The decision on whether or not a specific interatomic distance corresponds to a chemical bond is made in terms of the local environment of the constituent atoms, e.g., is the distance consistent with a specific coordination number of the central ion, and is the valence-sum rule (Brown, 2002) reasonably well-satisfied for the constituent ions? These are the criteria that are generally used for the listing of bond lengths in crystal-structure papers.

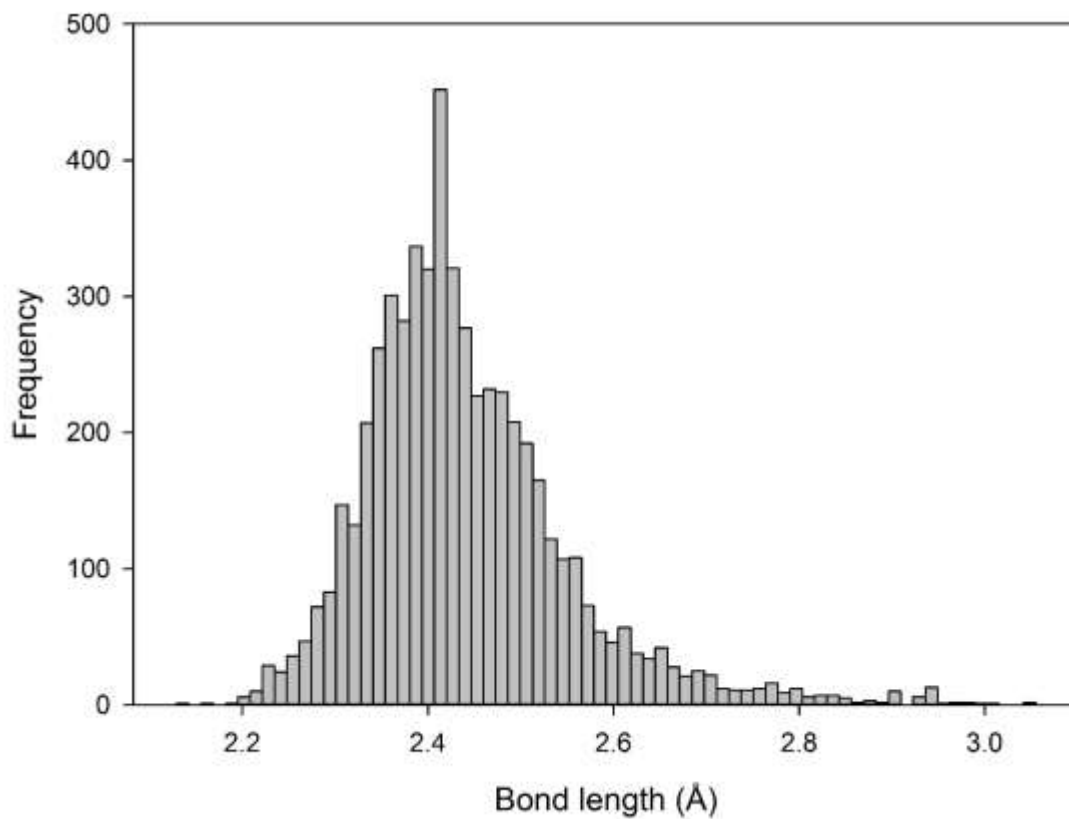
Coordination number: the number of monoatomic counterions bonded to an ion.

Coordination polyhedron: The solid figure defined by the positions of the monoatomic counterions directly attached to a central ion.

Ion configuration: A unique arrangement of ion type and coordination number.

Typical distribution: A distribution that is smooth and positively skewed, as for $^{[6]}\text{Na}^+$ (Fig. 4.1).

Figure 4.1 A typical distribution of bond lengths, shown for $^{6}\text{Na}^{+}$ bonded to O^{2-} ($n = 5532$).



4.6 Coordination polyhedra

4.6.1 Coordination polyhedra with the same coordination number

Most coordination numbers may show more than one coordination polyhedron. For example, [4]-coordination may be tetrahedral or square planar, [5]-coordination may be trigonal bipyramidal or square pyramidal, [6]-coordination may be octahedral or trigonal prismatic. However, within the bond-valence model (Brown, 2002), differences in angular arrangement of counterions have no effect on the valence sums, and hence we do not differentiate between different spatial configurations of coordination polyhedra with the same coordination number.

4.6.2 The longest bond

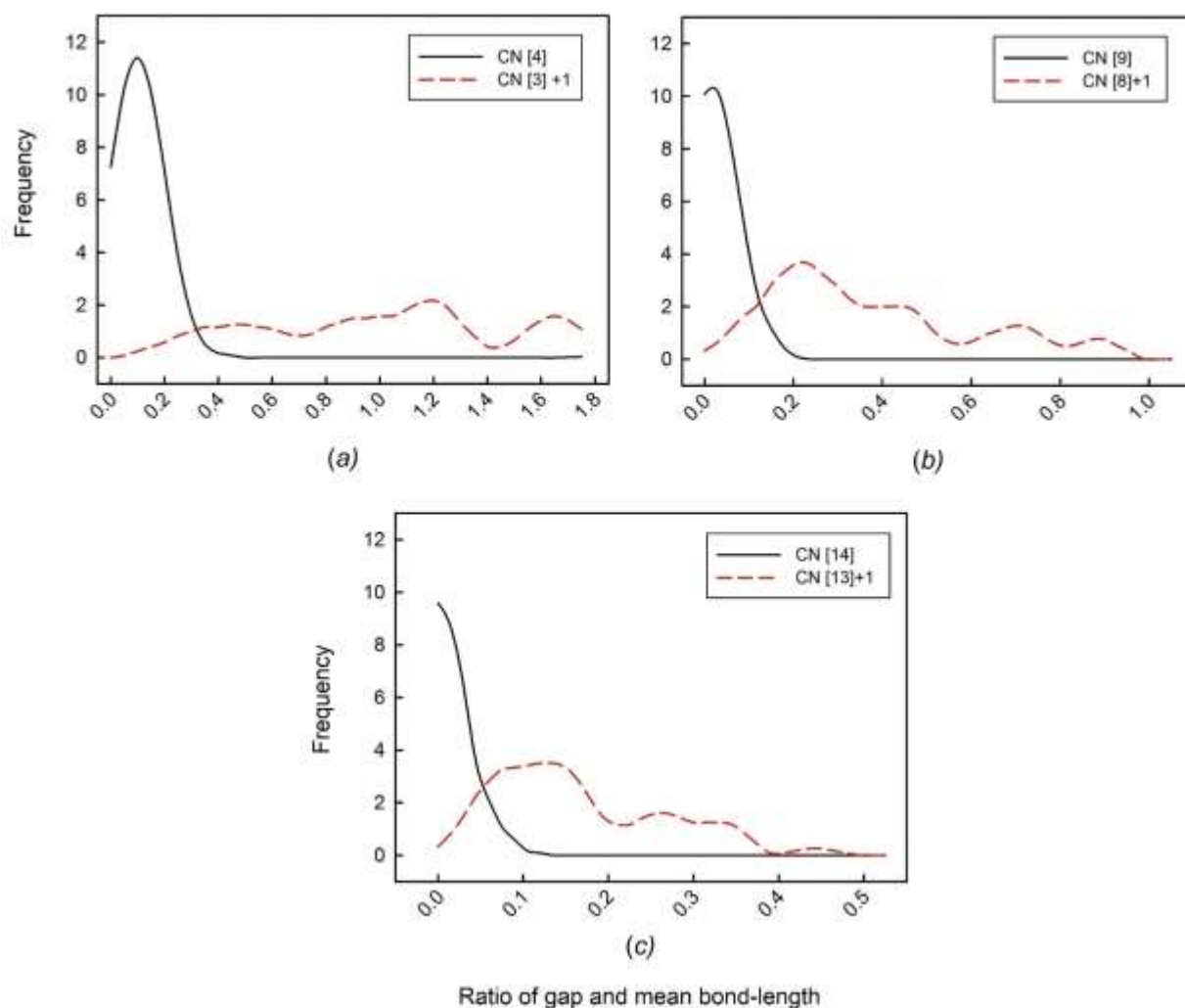
The determination of coordination number depends on how one defines a chemical bond (see “definitions” section). It is fortunate that for many (if not most) crystal structures, there is a general consensus as to the coordination numbers observed. Thus rutile has Ti^{4+} in [6]-coordination and O^{2-} in [3]-coordination, and quartz has Si^{4+} in [4]-coordination and O^{2-} in [2]-coordination. For cations making a small number of bonds to their counterions, the determination of the coordination polyhedron is usually straightforward, and the coordination number can be assumed with confidence (*e.g.*, for Mg^{2+} , Fe^{2+} , Si^{4+}). However, making a decision on what is the longest bond for cations making a large number of bonds to their counterions is often less straightforward.

We examined the bond-length distributions for [3] + 1 (the latter being the fourth-shortest distance) and [4]-coordinated Li^+ , Be^{2+} , B^{3+} , Na^+ and S^{6+} to get a sense of the

gap between the three shortest distances and the fourth distance for the coordination numbers [3] and [4]. Fig. 4.2a shows the ratio of the gap between the third- and fourth-shortest distances, and the mean bond-length for the three shortest distances: $(l_4 - l_3)/[(l_1 + l_2 + l_3)/3]$ as a kernel density plot¹. For the coordination polyhedra we defined as [4], we observe a regular distribution with a mean value of 0.104 and minimum and maximum values of 0.000 and 0.333, respectively. For [3] + 1, the mean ratio is 1.056 and the minimum and maximum values are 0.198 and 2.521, respectively. The distributions of the data are strikingly different, and for [3]- and [4]-coordinated Li^+ , Be^{2+} , B^{3+} , Na^+ and S^{6+} , suggest that the fourth-longest interatomic distance can be considered as bonded if $(l_4 - l_3)/[(l_1 + l_2 + l_3)/3] < 0.333$ (Fig. 4.2a). We give analogous data for coordination numbers [8]+1 and [9] in Fig. 4.2b and [13]+1 and [14] in Fig. 4.2c; in Fig. 4.2b, we see a slight increase in the overlap between the distributions for [8]+1 and [9], a trend that continues for [13]+1 and [14] in Fig. 4.2c. Fig. 4.2 shows that, for higher coordination numbers, the determination of the longest bond is somewhat more ambiguous, but still fairly reliable in most cases.

¹ A kernel-density estimate shows the same distribution as a histogram. A histogram assigns an exact value to a piece of data, whereas a kernel-density estimate associates a variance with each piece of data and produces a much simpler plot. We use kernel-density estimates in this paper where we want to show several distributions on one figure, as several overlapping histograms are difficult to compare, whereas overlapping kernel-density estimates are visually more simple and much more easily compared.

Figure 4.2 Ratio of the gap between the (a) third- and fourth-, (b) eighth- and ninth-, (c) thirteenth and fourteenth-shortest interatomic distance and the mean bond-length of the (a) three, (b) eight, (c) thirteen shortest interatomic distances for coordination numbers (a) [3] and [4], (b) [8] and [9] and (c) [13] and [14]. Ions used are (a) Li^+ , Be^{2+} , B^{3+} , Na^+ and S^{6+} ; (b) Na^+ , Ca^{2+} , Y^{3+} , Te^{4+} , La^{3+} ; (c) K^+ , Rb^+ , Cs^+ , Ba^{2+} . The lack of overlap between the two distributions of Fig. 4.2a suggests that the 4th shortest distance for ions described as [3] is non-bonding. In Figs. 4.2b-c, the increasing overlap between the two distributions shows that the determination of the exact coordination number for larger coordination polyhedra is more ambiguous. Sample sizes are (a) $n_{[3]+1} = 41$ and $n_{[4]} = 58$ coordination polyhedra; (b) $n_{[8]+1} = 50$ and $n_{[9]} = 50$ coordination polyhedra; (c) $n_{[13]+1} = 50$ and $n_{[14]} = 47$ coordination polyhedra.



4.6.3 Large coordination numbers

What large coordination numbers can we encounter in crystal structures? In terms of oxygen-based structures, Shannon (1976) lists ionic radii for coordination numbers up to [12], except for Rb^+ which he lists up to [14]. In different types of crystals, higher coordination numbers are common, particularly in Frank-Kasper phases. For example, A15 intermetallic alloys of the form A_3B consist of [12]-coordinated B atoms and [14]-coordinated A atoms, and Laves AB_2 intermetallic phases involve [12]- and [16]-coordinated atoms. In terms of oxygen-based structures, it is probable that only the alkali-metal and alkaline-earth-metal ions may have coordination numbers exceeding [12], and we will pay special attention to structures in which such coordination numbers may be possible. For these cations, attempting to determine the coordination number from a list of nearest-neighbour anions is usually ambiguous. Some cations form ill-defined coordination polyhedra and require special attention. To this effect, we describe the procedure whereby we assign the coordination polyhedron of a cation, below (section 4.7.2).

4.7 Methods

The DVD-ROM version of the ICSD with FindIt, version 2010-2, was used for data collection for all ions bonded to oxygen. The collection of bond-length data was done on the basis of coordination polyhedra for all cations of the periodic table. A set of structures containing each ion pair of interest was accumulated for each cation. In these structure sets, only the coordination polyhedra of the cation of interest were evaluated.

The bonds in each coordination polyhedron were calculated and individually examined to ensure that only suitable entries were included. Valid coordination polyhedra were not discarded due to problems elsewhere in the structure that have no effect on the coordination polyhedron of interest.

4.7.1 Selection criteria

The following criteria were used to select structure refinements:

(1) Publication date ≥ 1975 ; (2) $R_1 \leq 6\%$; (3) the site of interest is fully occupied by the cation; (4) all bonds involve ions at fully occupied sites; (5) the cation and anion sites of interest show no positional disorder; (6) crystallographic data were measured at ambient conditions; (7) no data from powder, electron or synchrotron diffraction were included.

4.7.2 Determination of coordination polyhedra

The following guidelines were used to decide on the coordination polyhedron (and thus coordination number) of each cation treated. For most cations, the first few points were sufficient for a clear determination of the coordination number:

(1) The cation is bonded only to O^{2-} .

- (2) In general, we assumed that all cation-anion bonds are shorter than the shortest cation-cation distance for the coordination number of interest².
- (3) The ordered list of distances was examined for a hiatus in the increasing distances.
- (4) We examined the effect of different cation-coordination numbers on the anion coordination.
- (5) We compared the bond lengths with and without potential bonds to the data already gathered for the cation to see if the behaviour resembled that of one coordination number more than other.
- (6) After ~10% of the structures had been processed for a specific ion pair, we examined the files for different coordination numbers of the same cation for potential trends and inconsistencies.
- (7) We examined the chemical formula for the presence of unrefined hydrogen atoms. This was mostly relevant in locating weak bonds between the cation of interest and the O atom of an (H₂O) group. Where hydrogen atoms were not located in the refinement, and such bonds seemed plausible, the data were discarded.
- (8) We plotted the structure to get a visual sense of any ambiguity.

² There are notable exceptions to this criterion. For example, in the structure of RbLiO (Sabrowsky and Vogt, 1987), Rb⁺ is surrounded by six O²⁻ ions with distances 2.897, 2.927 x2, 3.247 x2 and 3.488 Å, but the shortest Rb-Li distance is 2.916 Å, shorter than five of the six shortest Rb⁺-O²⁻ distances. Another example occurs in RbNaO (Sabrowsky *et al.*, 1985a); Rb⁺ is surrounded by six O²⁻ ions with distances 2.905, 3.066 x4 and 3.589 Å, but the shortest Rb-Na distance is 3.089 Å x4, very similar to the four intermediate length Rb⁺-O²⁻ distances. Similar behaviour is shown by KNaO (Sabrowsky and Schroer 1982). However, this behaviour appears to be confined to mixed alkali-metal oxides.

(9) Very sparingly, we used bond-valence curves to determine whether the inclusion or omission of bonds gave better bond-valence sums. However, little weight was given to this method because (1) it is circular, and (2) some published bond-valence parameters were doubtful at the time of this evaluation.

We plotted the bond-length frequency distributions for all ion configurations to identify obvious outliers that originated from (1) gross errors in the refinement, (2) errors in the ICSD entry, and/or (3) collection errors on our part. Arbitrary (often dynamic) limits were set for the lower and upper tails of the distribution of each ion configuration, whereby every entry with at least one bond below the former or above the latter was either (1) verified and confirmed in the original publication, or (2) discarded as an error. In particular, minerals may show considerable chemical zoning within individual grains and also significant grain-to-grain compositional differences, depending on details of paragenesis. Where this is the case, there may be significant differences between the actual composition of the crystal and that assumed for the crystal used to collect the X-ray intensity data. Thus errors regarding site occupancy may occur (unless the composition of that grain is analyzed by electron- and ion-microprobe), leading to apparently anomalous bond-lengths. For entries with abundant data (*e.g.*, Si^{4+} with over 10,500 bond distances), the entries were verified in terms of increasing bond lengths for the lower cut-off, and decreasing bond lengths for the upper cut-off, until a reliable series of entries were confirmed with those bond lengths. For configurations with very little data (~ 3 or less coordination polyhedra), all entries were verified.

Taking into account the large amount of crystal structures examined, it was generally safer to discard a doubtful entry than it was useful to have its bond-length information

included with reliable data, except where there was a paucity of bond lengths for the cation and coordination number(s) of interest.

Gagné & Hawthorne (2015) found that the agreement with the valence-sum rule of Brown (2002) is better when including the longer bonds in higher coordination polyhedra. As we shall see later, this is the case for the alkali and alkaline-earth metals, and also for configurations involving lone-pair-stereoactive cations (ms. in prep.). Thus long bonds obtained from the collection procedure described above were included.

This procedure resulted in 55 configurations involving 4859 coordination polyhedra and 38,594 individual bond-lengths for the alkali metals, and 29 configurations involving 3038 coordination polyhedra and 24,487 individual bond-lengths for the alkaline-earth metals. We make our complete dataset available for future more detailed work.

4.8 Shape of the bond-length distributions

Bond-length distributions commonly resemble a positively-skewed Gaussian distribution. The shape originates from the variation in Born repulsion and Coulomb attraction as a function of interatomic distance. Two useful statistical measures used to describe the shape of these distribution are skewness and kurtosis. Skewness is a measure of the asymmetry of the distribution about its mean, and can be positive (as in Fig. 4.1 for $^{[6]}\text{Na}^+$) or negative. Kurtosis is a measure of the distribution of data between the peak and the tails of the distribution: a high kurtosis indicates that the distribution has a sharper maximum and larger tails, and a low kurtosis indicates that the distribution has a rounder maximum and smaller tails. Thus important data that we

derive from the bond-length distributions determined here are *mean bond-length*, *skewness* and *kurtosis*. Deviations from this typical shape are frequent, and can be the result of structural and/or electronic effects that result in emergent bond-length constraints. Hence, we can gain insight into the reasons underlying the bonding behaviour of atoms from a visual inspection of their bond-length distributions, *e.g.*, the familiar (4 + 2) bimodal distribution of bond lengths for octahedrally coordinated Cu^{2+} from the Jahn-Teller effect (Jahn & Teller, 1937), associated with the degenerate electronic ground-state of a d^9 metal in a holosymmetric octahedral field.

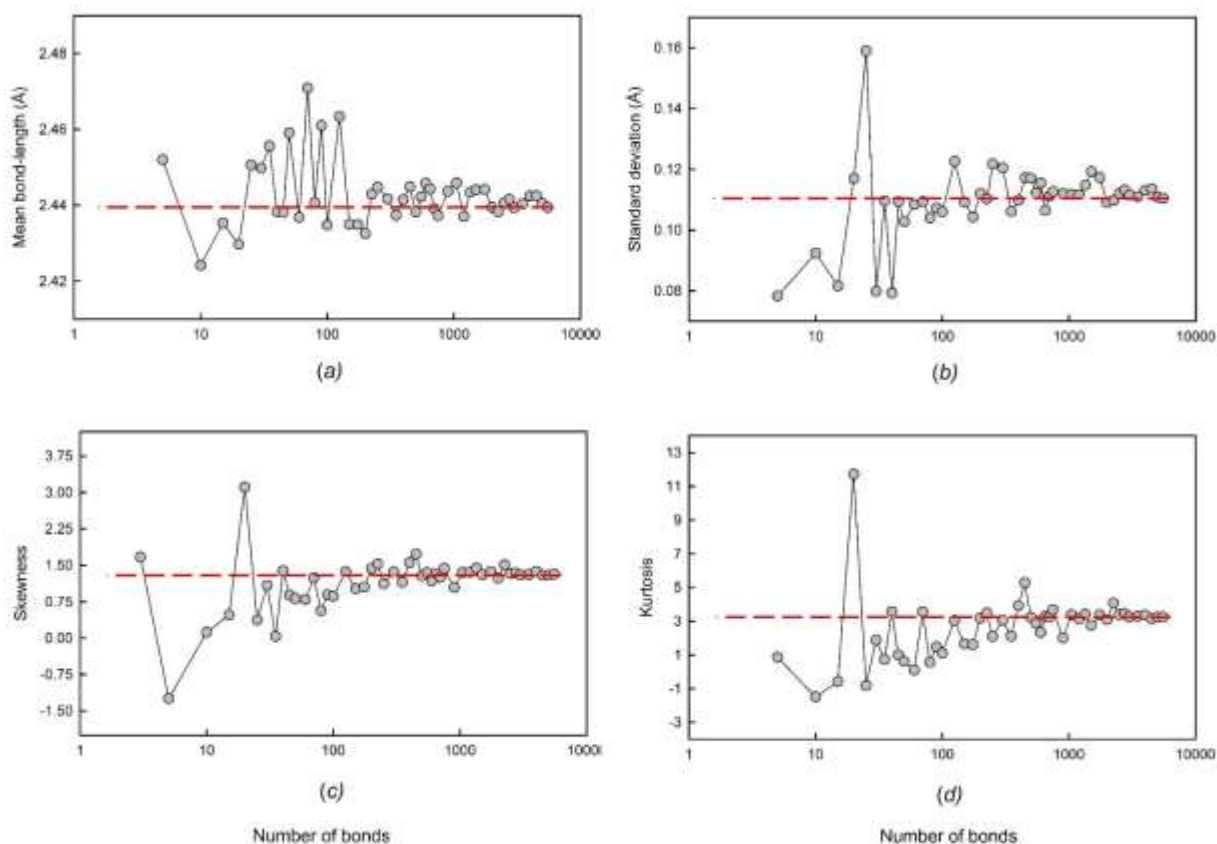
4.9 Effect of sampling

4.9.1 Sample size

A critical issue involved in the calculation of mean bond-length, skewness and kurtosis is whether the sample size (number of bond lengths) is sufficiently large to ensure a representative distribution. We examined this issue using the data of Fig. 4.1, calculating the mean bond-length, skewness and kurtosis for many different sample sizes and examining the values as a function of sample size compared with the values for the parent distribution (mean bond-length = 2.441 with a standard deviation of 0.112 Å; skewness = 1.32, kurtosis = 3.25). The results are shown in Fig. 4.3. In the range 5500 to 1000 bonds, the values of mean bond-length (Fig. 4.3a) and its standard deviation (Fig. 4.3b), skewness (Fig. 4.3c) and kurtosis (Fig. 4.3d) varied between 2.437-2.444 and 0.109-0.119 Å, 1.23-1.51 and 2.75-4.08, respectively; in the range 1000 to 100, the values of mean bond-length and its standard deviation, skewness and

kurtosis varied between 2.433-2.446 and 0.104-0.122, 1.02-1.73 and 1.60-5.28, respectively; below 100, the values of skewness and kurtosis varied from 2.424-2.471 and 0.078-0.159 Å, from -1.24 to 3.11 and from -1.49 to 11.72, respectively. Similar results were obtained (scaled by a factor of 6) by using polyhedra rather than individual bond-lengths. As a result of these large variations, we do not list skewness and kurtosis values for sample sizes of less than 100 bonds in this work, and we note that the values for sample sizes up to 1000 bonds may be associated with non-negligible error. We do list mean bond-lengths as this is important information for ongoing work on these materials, but we emphasize that the values listed may be adversely affected by small sample size.

Figure 4.3 The effect of sample size on (a) mean bond-length (b) standard deviation of the mean bond-length, (c) skewness, and (d) kurtosis. The dashed line shows the value for the parent distribution.



4.9.2 The effect of outliers

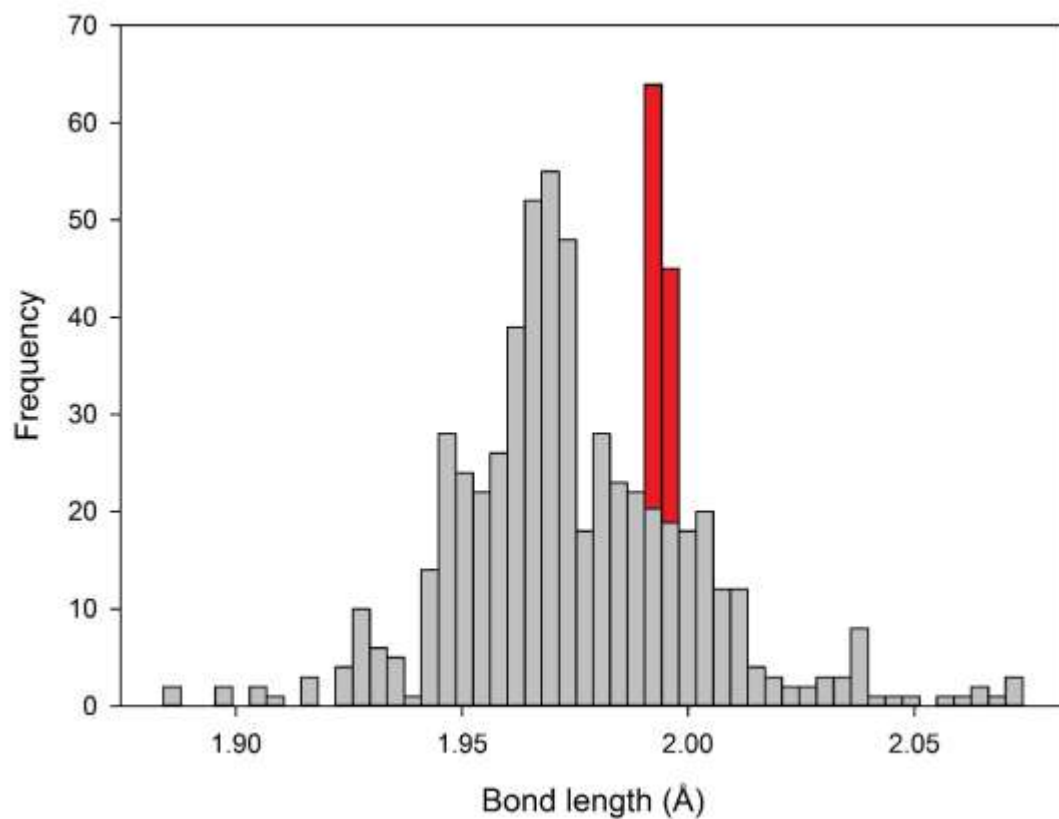
Values of skewness and kurtosis are very sensitive to the presence of outliers. For example, our dataset for $^{[7]}\text{Cs}^+$ (Fig. 4.S1aq) contains two coordination polyhedra with bonds longer than 3.75 Å, while the longest bond for the 8 other polyhedra varies in the range 3.3-3.5 Å. Calculating the skewness and kurtosis with and without the two polyhedra with bonds longer than 3.75 Å, we get values of skewness and kurtosis of 1.51 and 3.04 (with) and 0.62 and -0.31 (without), respectively. Careful evaluation of the structure and of the probable longest bond (see section 4.6.2) has greatly reduced the adverse effect of outliers on skewness and kurtosis in our analyses, but one must be careful of this issue as a single errant data point for a confirmed structure can change the values considerably.

4.9.3 Non-random sampling

Another issue that can affect skewness and kurtosis is the occurrence of spikes in the distribution of bond lengths due to extensive work on specific structure types. A prominent example is shown in Fig. 4.4: the bond-length distribution for $^{[6]}\text{Cr}^{3+}$. There is a fairly typical distribution except for a prominent spike at 1.99 Å where ~70 distances lie above the trend of the general distribution. Examination of the data shows that these distances originate from Lenaz *et al.* (2004); these authors refined structures from the solid solution $(\text{Mg},\text{Fe}^{2+})\text{Cr}^{3+}_2\text{O}_4$ with the spinel structure, and these contributed 11 structures in which the $\text{Cr}^{3+}\text{-O}^{2-}$ distances are symmetry-constrained to be identical in

each structure, providing 66 distances of ~ 1.99 Å and accounting for the spike in the distribution of Fig. 4.4.

Figure 4.4 Bond-length distribution for $^{[6]}\text{Cr}^{3+}$ bonded to O^{2-} ($n = 624$). A spike of data is observed at 1.99 Å due to extensive work done on the spinel structure.



Thus, sections 4.9.1 to 4.9.3 emphasize that the numerical values for skewness and kurtosis must be interpreted with care. While the presence of trends in skewness and kurtosis gives us structural information, the absence of such trends may be due to sampling issues.

4.10 Results for the alkali metals

Our collection and filtering criteria resulted in a combined sample size of 38,594 bonds and 4859 coordination polyhedra. Table 4.1 gives the 55 observed configurations, the mean bond-length and standard deviation, the minimum and maximum bond-length (and range), the skewness and kurtosis (where justified by sample size), and the number of bonds and coordination polyhedra for the 5 common alkali-metal ions. Fig. 4.S1 gives all the bond-length distributions for the alkali metals; those with adequate sample sizes (as discussed above) are shown in Fig. 4.5. An important issue is the reliability of the data at the limits of its distribution, *i.e.*, at the lowest and highest observed coordination numbers for each ion, and below we examine the data at the lower and upper limits of these distributions.

Table 4.1 Bond-length statistics for the 5 common alkali-metal ions

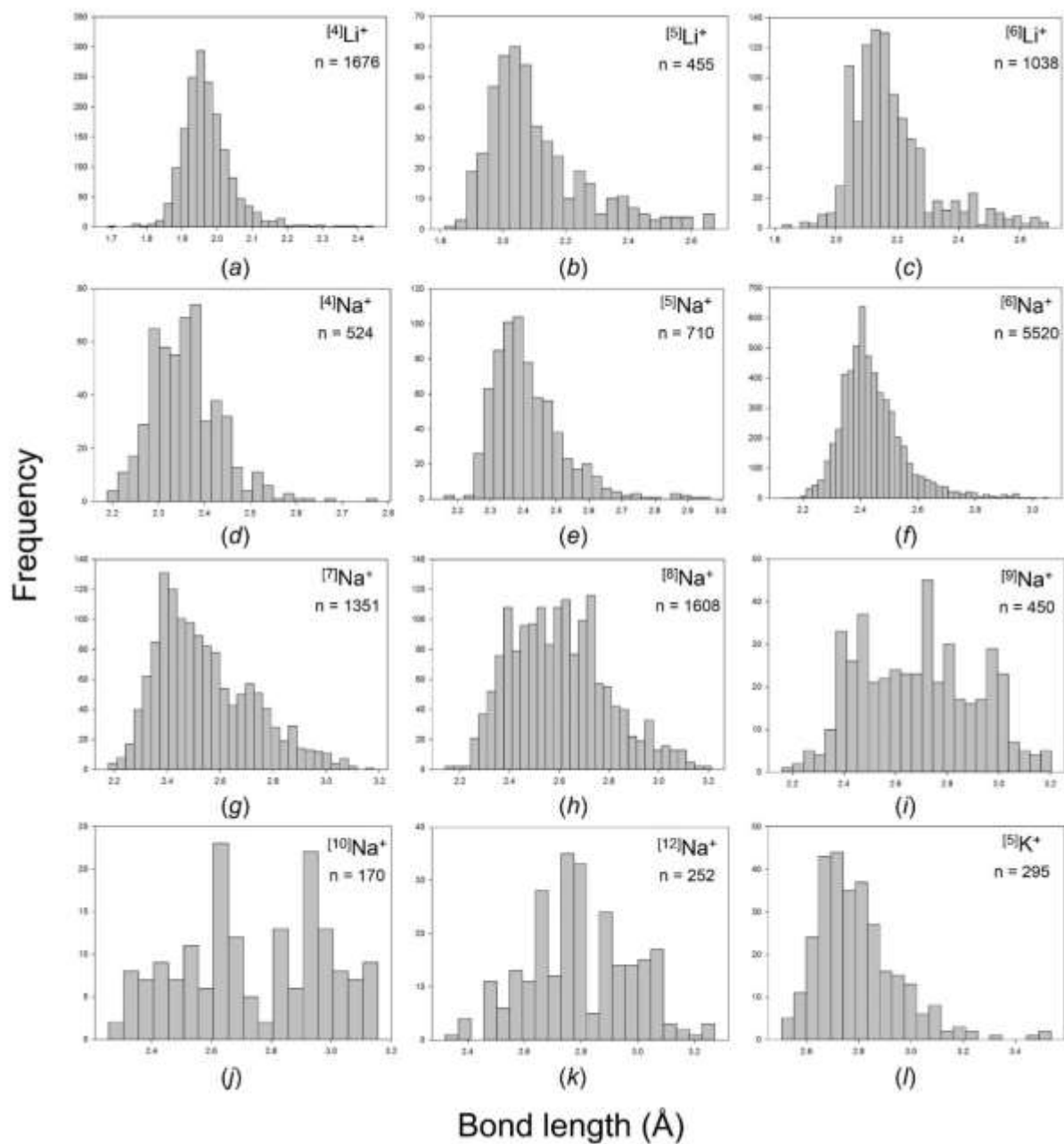
Ion	Coordination number	Number of bonds	Number of coordination polyhedra	Mean bond-length (Å)	Standard deviation (Å)	Range (Å)	Maximum bond-length (Å)	Minimum bond-length (Å)	Skewness	Kurtosis
Li ⁺	3	12	4	1.913	0.040	0.113	1.984	1.871	--	--
	4	1676	419	1.972	0.075	0.754	2.444	1.690	1.563	6.273
	5	455	91	2.108	0.161	0.858	2.673	1.815	1.265	1.362
	6	1038	173	2.178	0.137	0.866	2.692	1.826	1.293	1.996
	7	14	2	2.331	0.244	0.728	2.658	1.930	--	--
	8	8	1	2.513	0.000	0.000	2.513	2.513	--	--
	Total	3203	690							
Na ⁺	3	21	7	2.307	0.045	0.153	2.367	2.214	--	--
	4	524	131	2.359	0.076	0.586	2.775	2.189	0.878	2.032
	5	710	142	2.413	0.108	0.808	2.968	2.160	1.455	3.522
	6	5520	920	2.441	0.112	0.926	3.055	2.129	1.317	3.246
	7	1351	193	2.541	0.180	1.002	3.180	2.178	0.723	-0.020
	8	1608	201	2.599	0.192	1.069	3.211	2.142	0.461	-0.197
	9	450	50	2.686	0.224	1.044	3.204	2.160	0.121	-0.879
	10	170	17	2.741	0.240	0.899	3.156	2.257	-0.063	-1.075
	12	252	21	2.795	0.182	0.950	3.272	2.322	0.053	-0.295

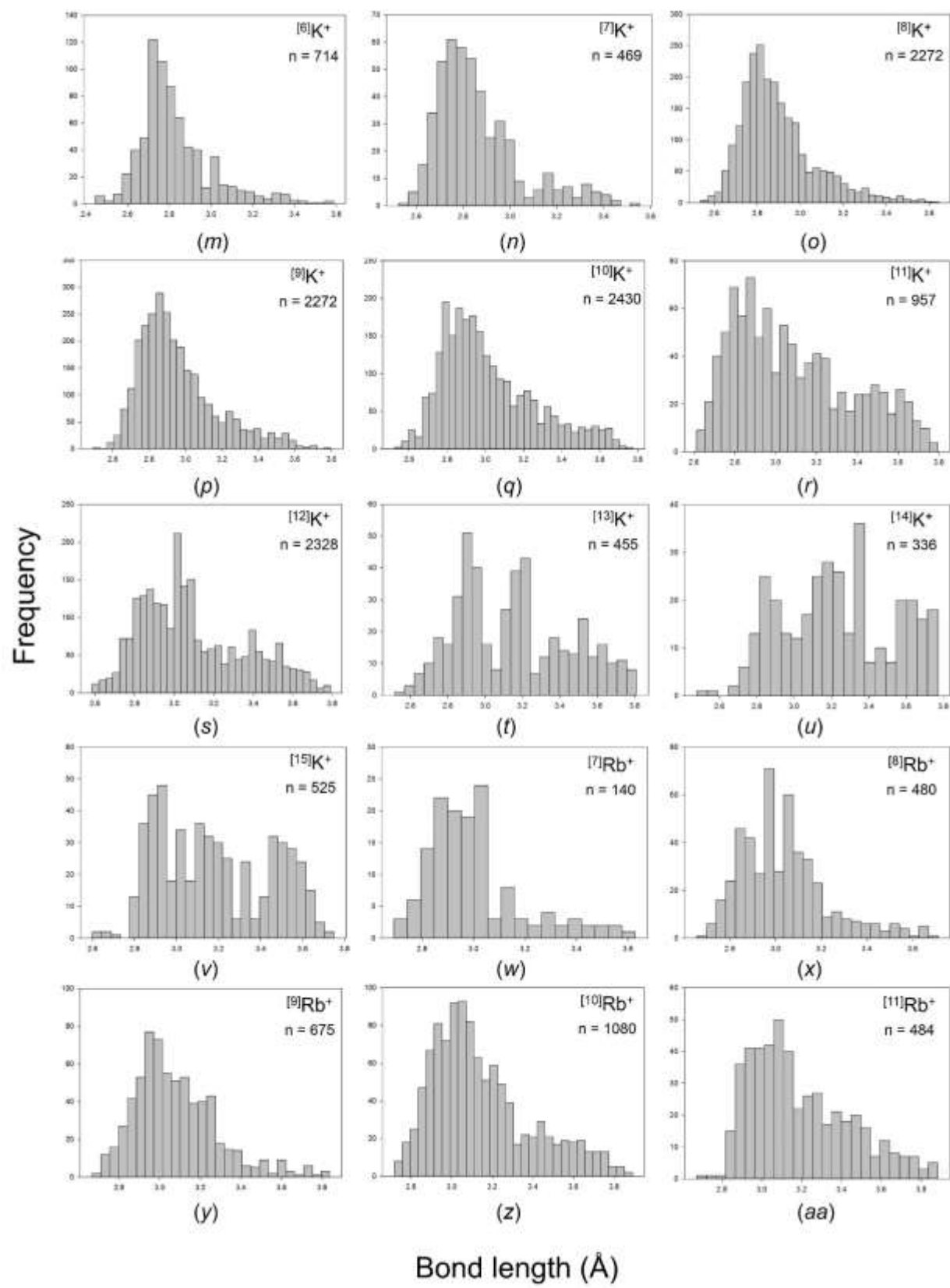
	Total	10606	1682							
K ⁺	4	96	24	2.708	0.078	0.365	2.892	2.527	--	--
	5	295	59	2.796	0.162	1.032	3.537	2.505	1.404	3.349
	6	714	119	2.828	0.177	1.140	3.587	2.447	1.299	2.268
	7	469	67	2.861	0.179	1.030	3.554	2.524	1.269	1.474
	8	2272	284	2.894	0.172	1.107	3.644	2.537	1.195	1.642
	9	2772	308	2.955	0.214	1.306	3.797	2.491	1.079	0.917
	10	2430	243	3.013	0.246	1.248	3.773	2.525	0.839	0.084
	11	957	87	3.089	0.290	1.181	3.793	2.612	0.550	-0.763
	12	2328	194	3.095	0.264	1.204	3.790	2.586	0.578	-0.535
	13	455	35	3.149	0.298	1.290	3.808	2.518	0.364	-0.834
	14	336	24	3.239	0.296	1.292	3.771	2.479	0.057	-0.929
	15	525	35	3.182	0.265	1.148	3.748	2.600	0.257	-1.164
	Total	13649	1479							
Rb ⁺	4	48	12	2.951	0.160	0.706	3.360	2.654	--	--
	5	15	3	2.864	0.078	0.236	2.976	2.740	--	--
	6	84	14	2.989	0.148	0.734	3.488	2.754	--	--
	7	140	20	3.002	0.186	0.937	3.628	2.691	1.283	1.554
	8	480	60	3.033	0.190	1.055	3.711	2.656	1.030	1.236
	9	675	75	3.079	0.204	1.172	3.839	2.667	0.980	1.192

	10	1080	108	3.146	0.244	1.171	3.890	2.719	0.858	0.081
	11	484	44	3.188	0.248	1.211	3.884	2.673	0.725	-0.242
	12	840	70	3.228	0.288	1.181	3.896	2.715	0.545	-0.663
	13	247	19	3.293	0.314	1.148	3.932	2.784	0.376	-1.163
	14	280	20	3.301	0.291	1.151	3.895	2.744	0.332	-0.938
	15	195	13	3.338	0.278	1.065	3.945	2.880	0.485	-0.934
	17	17	1	3.456	0.336	1.009	3.939	2.930	--	--
	18	90	5	3.478	0.239	0.695	3.771	3.076	--	--
	Total	4675	464							
Cs ⁺	6	102	17	3.124	0.139	0.702	3.568	2.866	0.922	1.040
	7	70	10	3.193	0.166	0.858	3.806	2.948	--	--
	8	200	25	3.244	0.189	1.017	3.911	2.894	0.863	0.708
	9	432	48	3.251	0.181	1.052	3.882	2.830	0.656	0.186
	10	930	93	3.304	0.208	1.257	3.986	2.729	0.696	0.174
	11	748	68	3.333	0.226	1.136	4.023	2.887	0.630	-0.106
	12	1080	90	3.377	0.250	1.162	4.072	2.910	0.670	-0.437
	13	520	40	3.426	0.276	1.256	4.130	2.874	0.480	-0.571
	14	714	51	3.444	0.297	1.242	4.169	2.927	0.528	-0.764
	15	705	47	3.503	0.301	1.253	4.157	2.904	0.241	-0.953
	16	224	14	3.550	0.321	1.276	4.199	2.923	0.341	-0.870

17	68	4	3.530	0.326	1.069	4.060	2.991	--	--
18	648	36	3.570	0.277	1.243	4.195	2.952	-0.010	-0.807
20	20	1	3.723	0.419	0.855	4.065	3.210	--	--
Total	6461	544							

Figure 4.5 Bond-length distributions for the configurations of the alkali-metal ions bonded to O^{2-} with a sample size of 100+ bonds: (a) $[4]Li^+$, (b) $[5]Li^+$, (c) $[6]Li^+$, (d) $[4]Na^+$, (e) $[5]Na^+$, (f) $[6]Na^+$, (g) $[7]Na^+$, (h) $[8]Na^+$, (i) $[9]Na^+$, (j) $[10]Na^+$, (k) $[12]Na^+$, (l) $[5]K^+$, (m) $[6]K^+$, (n) $[7]K^+$, (o) $[8]K^+$, (p) $[9]K^+$, (q) $[10]K^+$, (r) $[11]K^+$, (s) $[12]K^+$, (t) $[13]K^+$, (u) $[14]K^+$, (v) $[15]K^+$, (w) $[7]Rb^+$, (x) $[8]Rb^+$, (y) $[9]Rb^+$, (z) $[10]Rb^+$, (aa) $[11]Rb^+$, (ab) $[12]Rb^+$, (ac) $[13]Rb^+$, (ad) $[14]Rb^+$, (ae) $[15]Rb^+$, (af) $[6]Cs^+$, (ag) $[8]Cs^+$, (ah) $[9]Cs^+$, (ai) $[10]Cs^+$, (aj) $[11]Cs^+$, (ak) $[12]Cs^+$, (al) $[13]Cs^+$, (am) $[14]Cs^+$, (an) $[15]Cs^+$, (ao) $[16]Cs^+$, (ap) $[18]Cs^+$.





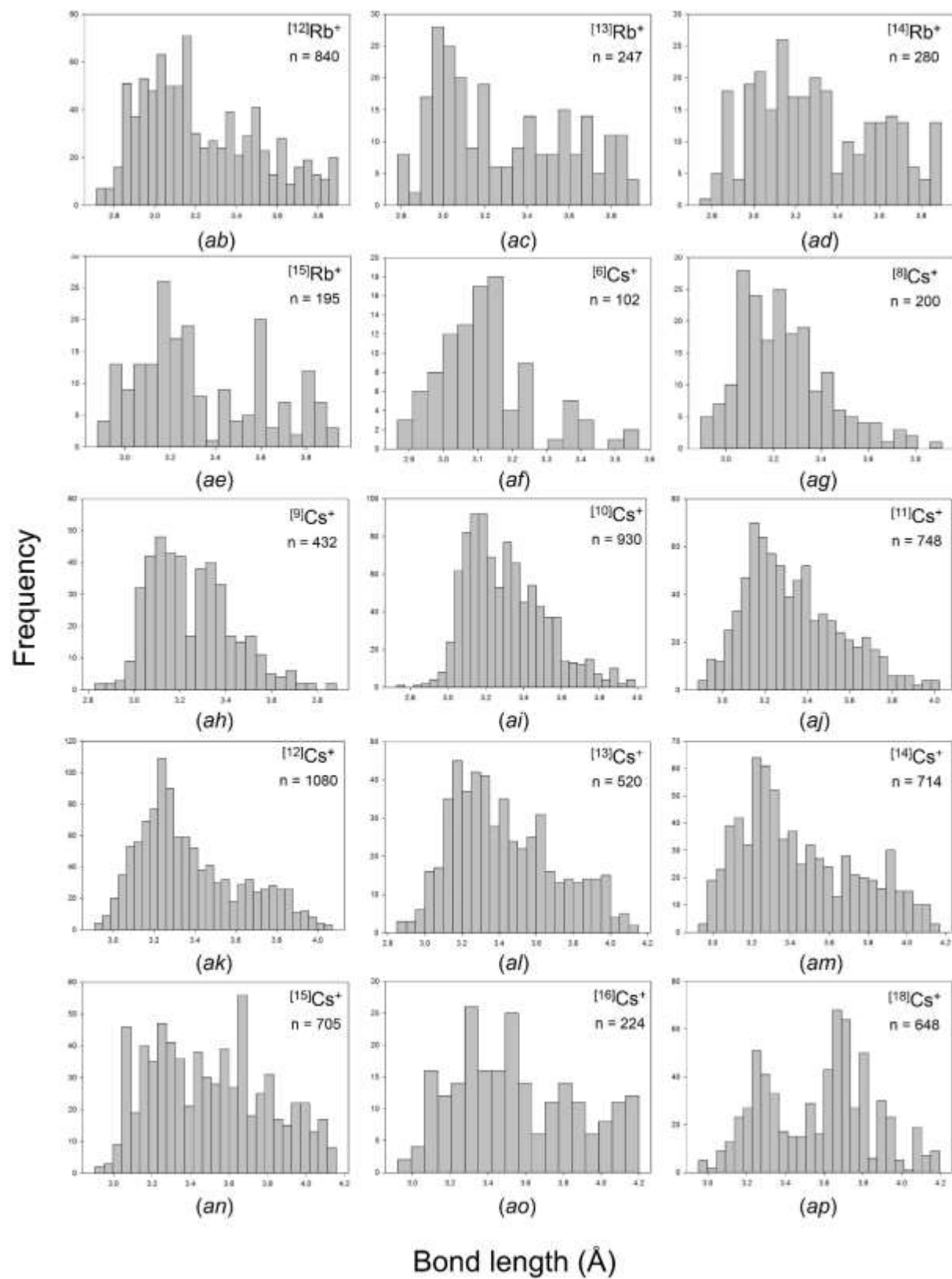
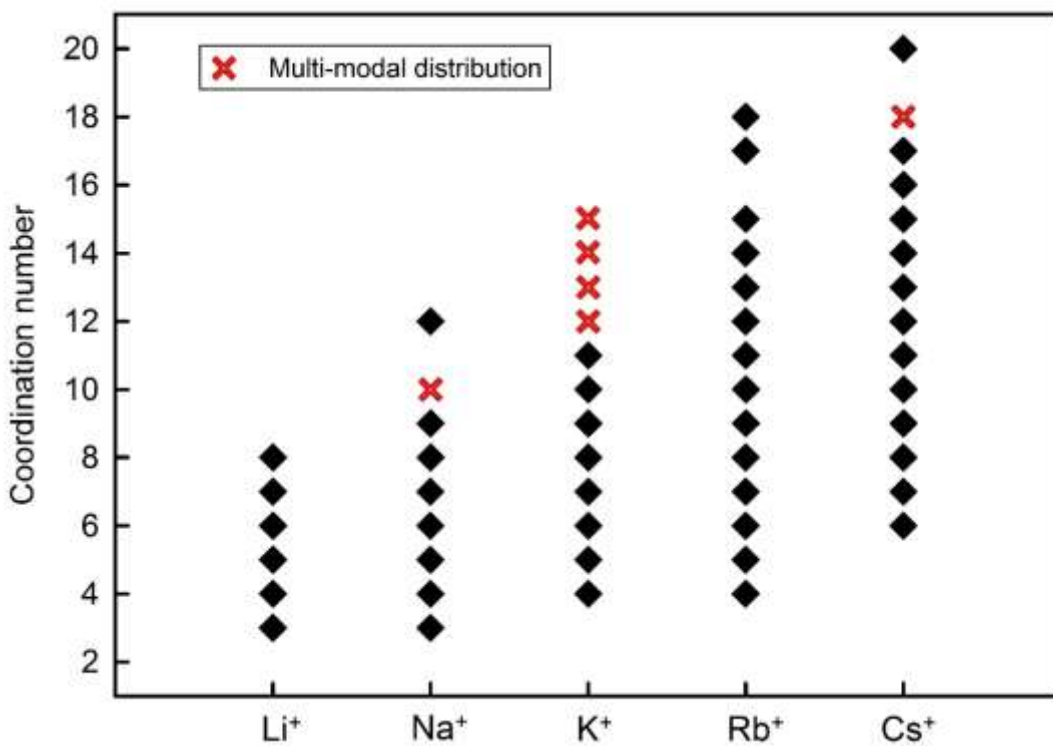


Figure 4.6 Observed coordination numbers for the alkali-metal ions. Multi-modal distributions are identified.



4.10.1 Observed coordination numbers

Fig. 4.6 shows the variation of the coordination numbers for the alkali-metal ions. The minimum coordination number increases from [3] for Li^+ and Na^+ to [4] for K^+ and Rb^+ to [6] for Cs^+ , and there is a corresponding increase in the maximum coordination number from [8] to [20]. The number of coordination numbers also increases along the series, from 6 for Li^+ to 15 for Rb^+ and Cs^+ .

4.10.1.1 Li^+

Li^+ has 6 coordination numbers from [3] to [8], with a strong preference for coordination number [4] ($n = 419$ coordination polyhedra). $^{[3]}\text{Li}^+$ is observed in only 4 coordination polyhedra in 4 structures: $\text{Li}_2\text{Yb}_5\text{O}_4(\text{BO}_3)_3$ (Jubera *et al.*, 2001); KLiO (Sabrowsky *et al.*, 1985b); RbLiO , Sabrowsky & Vogt, 1987); and $\text{LiBa}(\text{B}_9\text{O}_{15})$ (Pushcharovskii *et al.* 2002). The observed mean bond-lengths are 1.958, 1.891, 1.915 and 1.888 Å, respectively, and the incident bond-valence sums (using the parameters of Gagné & Hawthorne, 2015) are 0.744, 0.825, 0.797 and 0.829 v.u., respectively. The displacement parameters for $^{[3]}\text{Li}^+$ in $\text{Li}_2\text{Yb}_5\text{O}_4(\text{BO}_3)_3$ are an order of magnitude larger than those for Yb^{3+} and twice that of $^{[4]}\text{Li}^+$. Similarly, in $\text{LiBa}(\text{B}_9\text{O}_{15})$, U_{eq} for $^{[3]}\text{Li}^+$ is ~8 times U_{eq} for both the $^{[3]}\text{B}^{3+}$ and $^{[4]}\text{B}^{3+}$ cations (and the O^{2-} anions). These results suggest significant (dynamic or static) positional disorder. However, in KLiO , U_{eq} for $^{[3]}\text{Li}^+$ is similar to the U_{eq} values for K^+ and O^{2-} , and there is no reason to question the [3]-coordination of Li^+ in this structure.

$^{[7]}\text{Li}^+$ was found in only 2 coordination polyhedra (from two different structures) and $^{[8]}\text{Li}^+$ was found in only 1 coordination polyhedron. $^{[8]}\text{Li}^+$ was reported in $\text{Rb}_6\text{LiPr}_{11}\text{Cl}_{16}[\text{SeO}_3]_{12}$ (Lipp & Schieid, 2006) with 8 symmetrically equivalent bonds of length 2.513 Å giving an incident bond-valence sum of 0.835 v.u. with the parameters of Gagné & Hawthorne (2015). The U_{eq} value is 5 times that of its nearest-neighbour anions, all of which are equivalent, and twice that of the Rb^+ cations in the structure. $^{[7]}\text{Li}^+$ has been reported in $\text{LiGd}_6\text{O}_5(\text{BO}_3)_3$ (Chaminade *et al.*, 1999) and $\text{Li}_2(\text{Mg,Cu})\text{Cu}_2[\text{Si}_2\text{O}_6]_2$ (Horiuchi *et al.*, 1997), with mean bond-lengths of 2.337 and 2.325 Å and incident bond-valence sums of 1.021 and 1.067 v.u., respectively. Moreover, there are no significant hiati in the list of increasing bond-distances for each structure. In $\text{LiGd}_6\text{O}_5(\text{BO}_3)_3$, U_{eq} for Li^+ is 3-4 times the values of the other atoms. In $\text{Li}_2(\text{Mg,Cu})\text{Cu}_2[\text{Si}_2\text{O}_6]_2$, U_{eq} for Li^+ is 5 times the values of the other metal atoms and 3 times the values of the anions; moreover, the displacements for Li^+ are very anisotropic. There is no alternative to Li^+ in [7]- and [8]-coordination in these structures, but it is apparent from the very large U_{eq} values that Li^+ is “rattling around” in overly large holes in these structures (the cation is significantly displaced from the centre of the polyhedron). Although one might argue that the resultant observed mean bond-lengths are thus anomalous, U_{eq} values are generally correlated with coordination number and it is difficult to refute the suggestion that what we observe for [7]- and [8]-coordinated Li^+ is just a (non-linear) extrapolation of behaviour at lower coordination numbers. This issue is discussed further in section 4.13.3.

4.10.1.2 Na^+

Na⁺ is observed in 9 coordinations, from [3] to [12] excluding [11]. ^[6]Na⁺ is by far the most common coordination (n = 920), followed by ^[8]Na⁺ (n = 201) and ^[7]Na⁺ (n = 193). ^[3]Na⁺ (n = 7) has a very small spread in bond lengths, from 2.214 to 2.367 Å, but this is a common feature we observe for all [3]-coordinated cations. The incident bond-valence sums are very low (0.70 v.u. on average); for example, in Na₆CoO₃ (Möller, 1998), the $\langle^{[3]}\text{Na}^+-\text{O}^{2-}\rangle$ distance is 2.255 Å (the shortest of the 8 coordination polyhedra), and the incident bond-valence sum is 0.804 v.u. In this structure, the coordination of ^[3]Na⁺ is triangular with a $\langle\text{O}^{2-}-\text{Na}^+-\text{O}^{2-}\rangle$ angle of 117.2 and a slight pyramidal character, and the next-nearest O²⁻ anion is at 3.57 Å, far beyond any significant bond-valence interaction. Thus the occurrence of Na⁺ in [3]-coordination seems established. For [12] coordination, the central cation and the coordinating anions generally show similar values of U_{eq} with no anomalous disorder.

4.10.1.3 K⁺

K⁺ is observed in 12 different coordinations, from [4] to [15], with a preference for coordination numbers 9 (n = 308), 8 (n = 284) and 10 (n = 243). There are 24 coordination polyhedra for ^[4]K and the central cation and the coordinating anions generally show similar values of U_{eq} with no anomalous disorder. The grand mean incident bond-valence for ^[4]K is 0.77 v.u. with a range of 0.53-0.92 v.u.

4.10.1.4 Rb⁺

Rb⁺ is observed in 14 coordinations from [4] to [18], excluding [16]. It favourably adopts coordination number 10 (n = 108), followed by coordination numbers 9 (n = 75) and 8 (n = 60). Despite little data, [4]Rb⁺ (n = 12) shows a typical distribution and the constituent atoms are well-behaved in most of the structure refinements. The grand mean incident bond-valence for [4]Rb⁺ is 0.57 v.u. with a range of 0.49-0.65 v.u. The following coordination numbers [15] (n = 13), [17] (n = 1), and [18] (n = 5) have mean incident bond-valence sums of 0.947, 1.002 and 0.912 v.u., respectively. The U_{eq} values tend to be very high for the central cations in these structures. For example, in Rb₅VONb₁₄O₃₈ (Haddad & Jouini, 1997), U_{eq} of [18]Rb⁺ is 5-7 times those of the coordinating anions; in Rb₁₀Ta_{29.2}O₇₈ (Fallon & Gatehouse, 1980), U_{eq} of [18]Rb⁺ is 15-20 times those of the coordinating anions; in Rb₂V₃P₄O₁₇ (Lii *et al.*, 1990), U_{eq} of [17]Rb⁺ is ~3 times those of the coordinating anions.

4.10.1.5 Cs⁺

Cs⁺ is observed in 14 coordinations, from [6] to [20] excluding [19], with a preference for coordination numbers 10 (n = 94) and 12 (n = 90). [6]Cs⁺ (n = 18) and [7]Cs⁺ (n = 10) show regular distributions despite limited data, and the central cations and the coordinating anions generally show similar values of U_{eq} with no anomalous disorder. For [20]Cs⁺, there are distances 3.210 Å ×8 and 4.064 Å ×12 with incident bond-valence sums of 0.886 v.u. for [8] and 1.029 v.u. for [20], and the U_{eq} value of the central Cs⁺ is ~5 times those of the coordinating anions.

4.10.2 Grand mean bond-length as a function of coordination number

Fig. 4.7a shows the variation in mean bond-length as a function of coordination number, and is given for all configurations regardless of sample size. The correlation is positive, and is surprisingly regular. Minor anomalies (e.g., $^{[5]}\text{Rb}^+$) can be attributed to a small sample size. We note that the slope of the variation for each ion in Fig. 4.7a decreases slightly with the increasing size of the cations.

4.10.3 Range in bond length as a function of coordination number

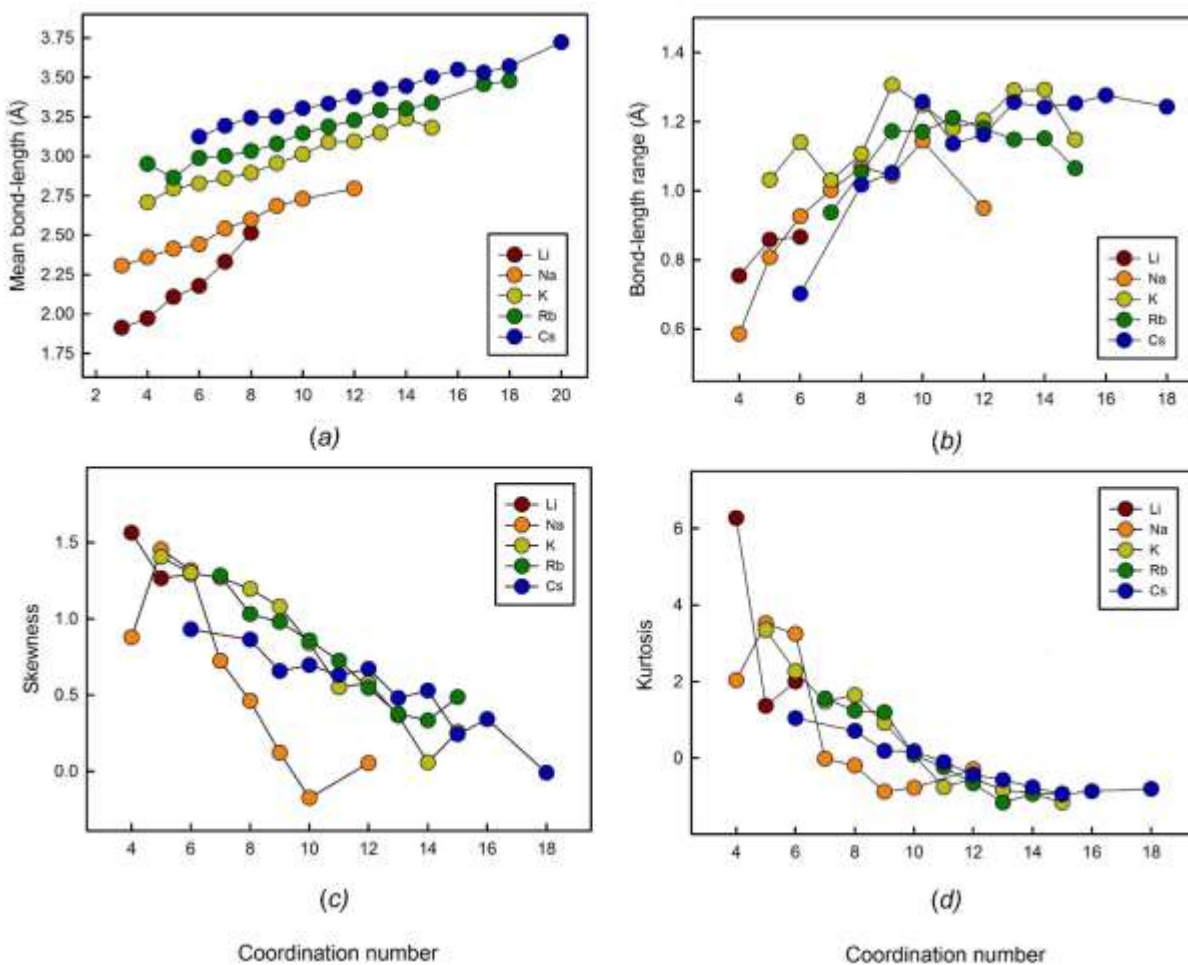
Fig. 4.7b shows the variation in the range of bond lengths as a function of coordination number. As the ranges are strongly dependent on sample size, we omitted data for configurations of less than 100 bonds. Although this criterion is sufficient to remove major outliers, the value for $^{[12]}\text{Na}^+$ is $\sim 0.22 \text{ \AA}$, smaller than expected from the general trend of Fig. 4.7b; the reason for this difference is not clear. There is a strong non-linear trend in Fig. 4.7b; the range in bond lengths is positively correlated with coordination number, and the range increases more rapidly at lower coordination numbers, and flattens out at higher coordination numbers.

4.10.4 Skewness and kurtosis as a function of coordination number

Figs. 4.7c and 4.7d show skewness and kurtosis as a function of coordination number, respectively, for the five alkali-metal ions. As skewness and kurtosis are highly influenced by the amount of data used in their calculation, the graphs only show values

for configurations with 100 bonds or more, as discussed above. Fig. 4.7c shows a more-or-less linear decrease in skewness with increasing coordination number. Na^+ shows a lower skewness for coordination [4] than would be expected from the trend, for reasons that are not clear, and the rate of decrease in kurtosis with increasing coordination number is greater than that for the other alkali-metal ions which show a surprisingly consistent trend (considering the sensitivity of skewness to sample size and outliers). Fig. 4.7d shows a well-developed trend of non-linear decrease in kurtosis as a function of coordination number for all the alkali-metal ions. The trend for Na^+ is again somewhat less consistent than for the other ions, and the shape is similar to that exhibited for skewness (Fig. 4.7c).

Figure 4.7 Values of (a) grand mean bond-length, (b) bond-length range, (c) skewness, and (d) kurtosis for the different coordination numbers of the alkali-metal ions.



4.11 Results for the alkaline-earth metals

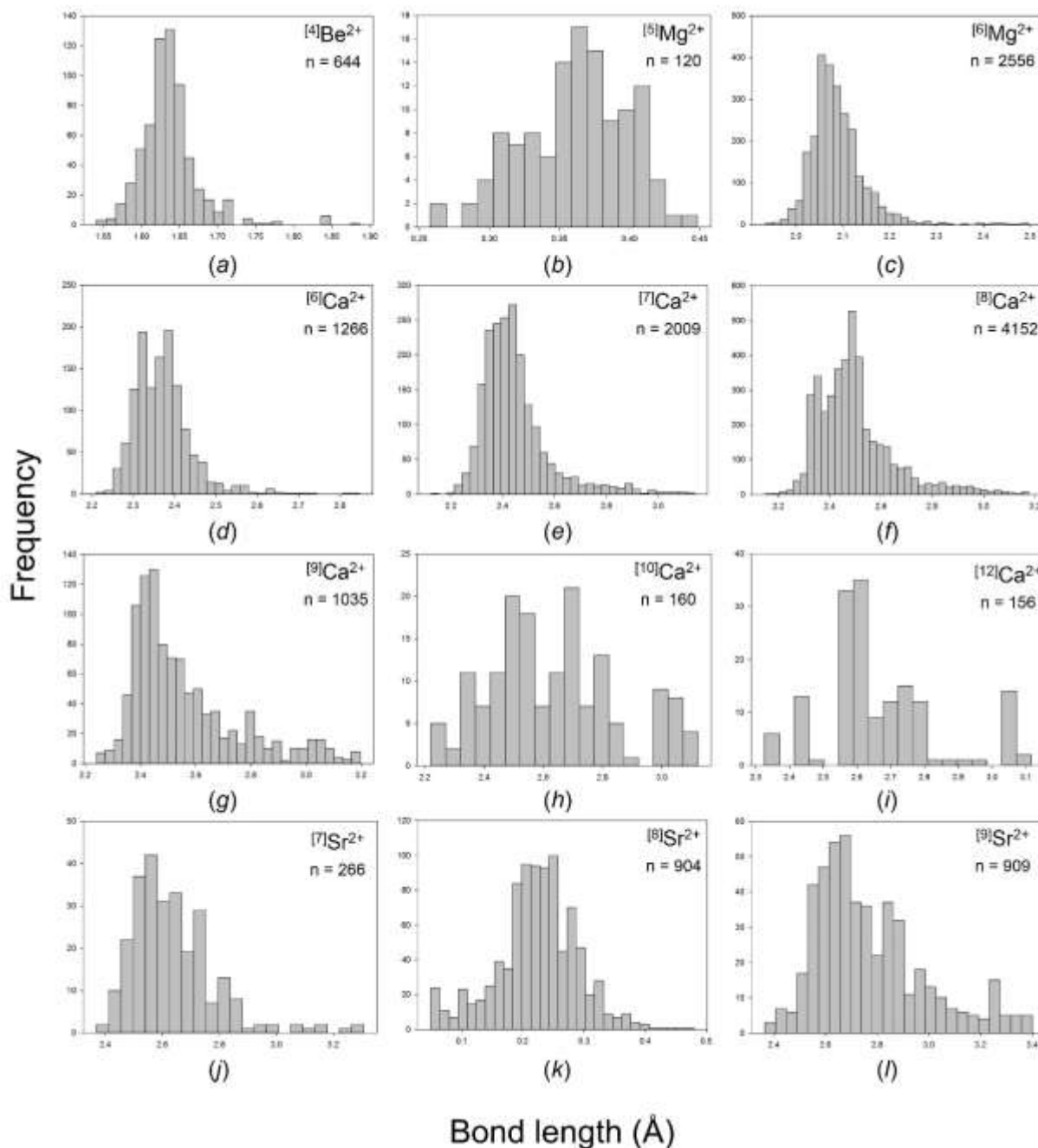
Our collection and filtering criteria resulted in a combined sample size of 24,487 bonds and 3038 coordination polyhedra. Table 4.2 gives the 29 observed configurations, the mean bond-length and standard deviation, the minimum and maximum bond-length (and range), the skewness and kurtosis (where justified by sample size), and the number of bonds and coordination polyhedra for the 5 common alkaline-earth-metal ions. Fig. 4.S2 gives all the bond-length distributions for the alkaline-earth metals; those with adequate sample sizes (as discussed above) are shown in Fig. 4.8. These ions are found in slightly more than half the number of configurations observed for the alkali metals (55), primarily because these ions are not observed in coordinations higher than [12], with the exception of Ba^{2+} (observed as [13] and [14]).

Table 4.2 Bond-length statistics for the 5 common alkaline-earth-metal ions

Ion	Coordination number	Number of bonds	Number of coordination polyhedra	Mean bond-length (Å)	Standard deviation (Å)	Range (Å)	Maximum bond-length (Å)	Minimum bond-length (Å)	Skewness	Kurtosis
Be ²⁺	3	24	8	1.550	0.018	0.081	1.587	1.506	--	--
	4	644	161	1.637	0.040	0.346	1.887	1.541	1.988	8.529
	Total	668	169							
Mg ²⁺	4	48	12	1.939	0.020	0.068	1.977	1.909	--	--
	5	120	24	2.044	0.066	0.342	2.249	1.907	0.643	0.271
	6	2556	426	2.089	0.059	0.562	2.497	1.935	1.976	8.608
	8	56	7	2.255	0.122	0.568	2.582	2.014	--	--
	Total	2780	469							
Ca ²⁺	6	1266	211	2.371	0.069	0.637	2.847	2.210	1.636	5.908
	7	2009	287	2.448	0.133	1.016	3.140	2.124	1.828	4.607
	8	4152	519	2.498	0.151	1.027	3.176	2.149	1.430	2.739
	9	1035	115	2.559	0.196	0.956	3.197	2.241	1.247	0.939
	10	160	16	2.632	0.215	0.902	3.122	2.220	0.478	-0.400
	11	77	7	2.614	0.177	0.686	2.965	2.279	--	--
	12	156	13	2.668	0.175	0.791	3.117	2.326	0.724	0.379
	Total	8855	1168							

Sr ²⁺	6	78	13	2.477	0.050	0.244	2.591	2.347	--	--
	7	266	38	2.638	0.151	0.937	3.306	2.369	1.553	3.693
	8	904	113	2.656	0.163	1.019	3.368	2.349	1.711	3.740
	9	909	101	2.704	0.178	1.088	3.397	2.309	1.545	3.094
	10	500	50	2.769	0.213	1.033	3.399	2.366	0.962	0.456
	11	88	8	2.798	0.198	0.837	3.319	2.482	--	--
	12	636	53	2.825	0.181	0.953	3.358	2.405	0.744	0.613
	Total	3381	376							
Ba ²⁺	6	126	21	2.689	0.094	0.400	2.866	2.466	-0.404	-0.665
	7	147	21	2.792	0.135	0.855	3.369	2.514	1.133	2.916
	8	704	88	2.816	0.129	0.846	3.376	2.530	0.962	1.273
	9	1278	142	2.860	0.154	1.074	3.554	2.480	1.000	1.330
	10	1930	193	2.915	0.155	1.014	3.498	2.484	0.783	1.072
	11	902	82	2.944	0.181	1.023	3.612	2.589	0.667	0.074
	12	3624	302	2.965	0.152	0.988	3.624	2.636	1.239	1.951
	13	78	6	3.010	0.206	0.922	3.463	2.541	--	--
	14	14	1	3.080	0.242	0.879	3.553	2.674	--	--
	Total	8813	856							

Figure 4.8 Bond-length distributions for the configurations of the alkaline-earth-metal ions bonded to O^{2-} with a sample size of 100+ bonds: (a) $[4]Be^{2+}$, (b) $[5]Mg^{2+}$, (c) $[6]Mg^{2+}$, (d) $[6]Ca^{2+}$, (e) $[7]Ca^{2+}$, (f) $[8]Ca^{2+}$, (g) $[9]Ca^{2+}$, (h) $[10]Ca^{2+}$, (i) $[12]Ca^{2+}$, (j) $[7]Sr^{2+}$, (k) $[8]Sr^{2+}$, (l) $[9]Sr^{2+}$, (m) $[10]Sr^{2+}$, (n) $[12]Sr^{2+}$, (o) $[6]Ba^{2+}$, (p) $[7]Ba^{2+}$, (q) $[8]Ba^{2+}$, (r) $[9]Ba^{2+}$, (s) $[10]Ba^{2+}$, (t) $[11]Ba^{2+}$, (u) $[12]Ba^{2+}$.



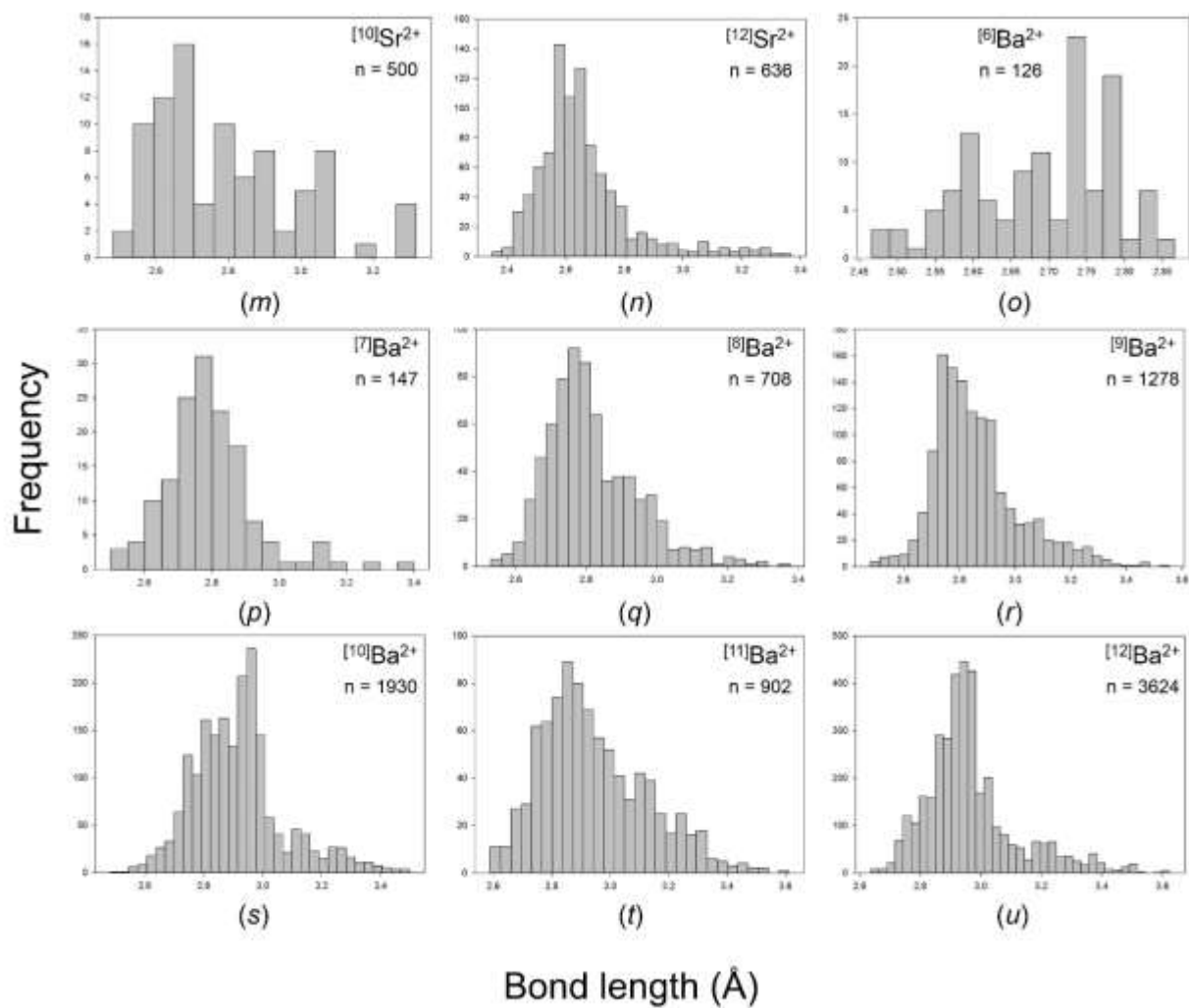
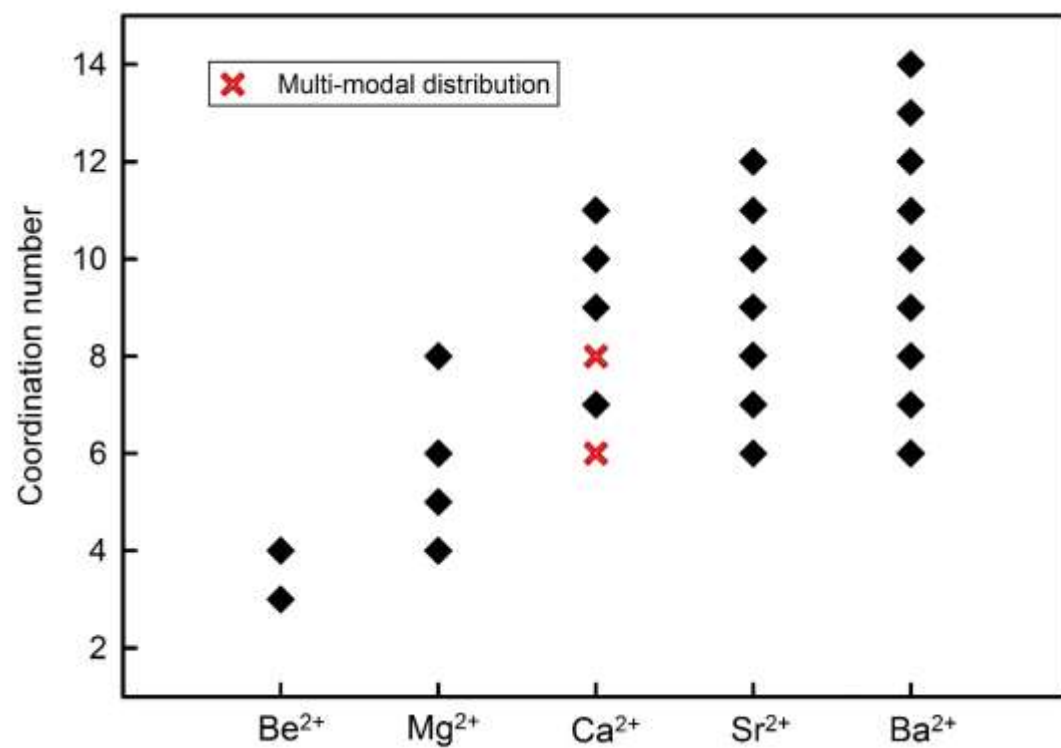


Figure 4.9 Observed coordination numbers for the alkaline-earth-metal ions. Multi-modal distributions are identified.



4.11.1 Observed coordination numbers

Fig. 4.9 shows the variation of the coordination numbers for the alkaline-earth-metal ions. The minimum and maximum coordination numbers increase with size, [3] and [4] for Be^{2+} , [4] and [8] for Mg^{2+} , [6] and [12] for Ca^{2+} and Sr^{2+} , and [6] and [14] for Ba^{2+} . The number of coordination numbers also increases along the series, from 2 for Be^{2+} to 4 for Mg^{2+} , 7 for Ca^{2+} , 8 for Sr^{2+} and 9 for Ba^{2+} .

4.11.1.1 Be^{2+}

Be^{2+} occurs in two coordination numbers, with a clear preference for coordination number [4] ($n = 161$) compared to its 3-coordinated form $^{[3]}\text{Be}^{2+}$ ($n = 8$). However, the coordination of [3] seems well-established for Be. For example, Leoni *et al.* (2005) report the structure of $\text{Ba}_3[\text{Be}_5\text{O}_8]$ with a Be atom [3]-coordinated at distances of 1.545(9) and 1.561(5) Å $\times 2$ with well-behaved U_{eq} values for both the central cation and the coordinating anions, and an incident bond-valence sum of 1.96 v.u.

4.11.1.2 Mg^{2+}

Mg^{2+} occurs in 4 different coordination numbers from [4] to [8], excluding [7]. $^{[6]}\text{Mg}^{2+}$ is by far the most common coordination with $n = 426$ coordination polyhedra. $^{[4]}\text{Mg}^{2+}$ ($n = 12$) has an apparent bimodal distribution, which is clearly an artifact of a small number of bond lengths that show little spread. However, the coordination [4] must be considered as well-established for Mg^{2+} as structure refinements show well-behaved

cations and anions. The grand mean incident bond-valence for $^{[8]}\text{Mg}$ is 1.93 v.u. with a range of 1.78-2.20 v.u. The structures containing $^{[8]}\text{Mg}^{2+}$ look well-refined, although U_{eq} values are usually somewhat higher than those of the anions, suggesting significant displacement. This effect was also suggested by Shannon & Rossman (1992) with regard to deviations of measured and calculated dielectric constants for $^{[8]}\text{Mg}^{2+}$.

4.11.1.3 Ca^{2+}

Ca^{2+} occurs in 7 different coordinations from [6] to [12] with a preference for coordination number [8] ($n = 519$). [6]-coordinated Ca^{2+} is well-established ($n = 211$). The lowest observed $\langle^{[6]}\text{Ca}^{2+}\text{-O}\rangle$ distance is 2.254(4) Å in $\text{Ba}_3\text{CaRu}_2\text{O}_9$ (Wilkins & Müller-Buschbaum, 1991); this seems very short compared to the grand $\langle^{[6]}\text{Ca}^{2+}\text{-O}\rangle$ distance of 2.371(69) Å (Table 4.2), but there is no reason to reject this value based on the structure refinement. There are few examples of the higher coordination-numbers: $^{[10]}\text{Ca}$ ($n = 16$), $^{[11]}\text{Ca}$ ($n = 7$) and $^{[12]}\text{Ca}$ ($n = 13$). The grand mean incident bond-valence for $^{[12]}\text{Ca}$ is 2.03 v.u. with a range of 1.43-2.50 v.u. The lowest values are for $\text{Ca}_3\text{Zn}_4\text{Ti}_{16}\text{O}_{38}$ (Gatehouse & Grey, 1983) and $\text{CaMg}_2\text{Al}_{16}\text{O}_{27}$ (Iyi *et al.*, 1995). $\text{Ca}_3\text{Zn}_4\text{Ti}_{16}\text{O}_{38}$ has Ca-O distances 2.762(5) ×6 and 2.792 (5) ×6 Å with a mean value of 2.777 Å and a displacement parameter that is 3-10 times those of the other atoms in the structure. $\text{CaMg}_2\text{Al}_{16}\text{O}_{27}$ has Ca-O distances 2.773(8) ×6 and 2.799 (21) ×6 Å with a mean value of 2.786 Å and a displacement parameter that is 2-6 times those of the other atoms in the structure. Thus the low incident bond-valence sums are associated with central cations that show very large displacements. The highest values are for $\text{CaCu}_3\text{Ge}_4\text{O}_{12}$ (Ozaki *et al.*, 1977) and $\text{CaCu}_3\text{Ge}_4\text{O}_{12}$ (Chenevas *et al.*, 1975).

CaCu₃Ge₄O₁₂ has Ca-O distances of 2.549(4) ×12 Å and a displacement parameter that is similar to those of the other atoms in the structure. CaCu₃Ge₄O₁₂ has Ca-O distances of 2.562(3) ×12 Å and a displacement parameter that is similar to those of the other atoms in the structure. Thus the high incident bond-valence sums are associated with central cations that show displacements similar to those of the other atoms in the structure.

4.11.1.4 Sr²⁺

Sr²⁺ occurs in 7 different coordinations from [6] to [12] with a preference for coordination numbers [8] (n = 113) and [9] (n = 101). An unusual coordination for Sr occurs in the crystal structure of β-Sr₁₀Ga₆O₁₉ (Kahlenburg, 2002), where one of 11 crystallographically distinct Sr atoms has bond lengths of 2.425(8) ×2, 2.471(9) ×2 and 3.350(9) ×2 Å; is Sr²⁺ [4]- or [6]-coordinated? For [4]-coordination, the four anions do not form a tetrahedron and the Sr²⁺ cation lies between the two closest anions with an O²⁻-Sr²⁺-O²⁻ angle of 175.4°. For [6]-coordination, the Sr²⁺ cation lies almost in the plane of four of the anions that form a face of the polyhedron. The sums of the incident bond-valences are ~1.5 v.u. for both [4]- and [6]-coordination. The two next-nearest anions are 3.519 Å away from the central Sr²⁺, but there are two Ga³⁺ atoms at 3.410 Å. Thus the coordination in this particular case is uncertain, and the coordination polyhedron was omitted from the data for Sr²⁺.

4.11.1.5 Ba²⁺

Ba²⁺ occurs in 9 different coordinations from [6] to [14] with a clear preference for coordination number [12] (n = 302). There are few examples of coordination numbers > [12]: ^[13]Ba²⁺ (n = 6) and ^[14]Ba²⁺ (n = 1). For ^[13]Ba²⁺, the sums of the incident bond-valences are in the range 1.85-2.37 v.u., and for ^[14]Ba²⁺, the sum of the incident bond-valences is 1.98 v.u.

4.11.2 Grand mean bond-length as a function of coordination number

Fig. 4.10a shows the variation in mean bond-length as a function of coordination number, and is given for all configurations regardless of sample size. The correlation is positive and very regular. The slope of the variation for each ion of Fig. 4.10a decreases slightly with the increasing size of the cations, although less than is the case for the alkali-metal ions.

4.11.3 Range in bond length as a function of coordination number

Fig. 4.10b shows the variation in the range of bond lengths as a function of coordination number, omitting data for configurations of less than 100 bonds. There is a strong non-linear trend in the data; the range increases more rapidly at lower coordination numbers, [4]-[7], but levels out at ~[8] ($\sim 0.95 \pm 0.1$ Å) and is fairly constant thereafter, aside from a decrease for the higher coordination of Ca²⁺ (probably due to few data). The initial increase in range for smaller coordination numbers is steeper for the alkaline-earth metals than for the alkali metals (Fig. 4.7b) with mean slopes of 0.37 for Mg²⁺, Ca²⁺ and Ba²⁺ up to [7], compared to ~ 0.15 for Na⁺ and Cs⁺ up to [8]

4.11.4 Skewness and kurtosis as a function of coordination number

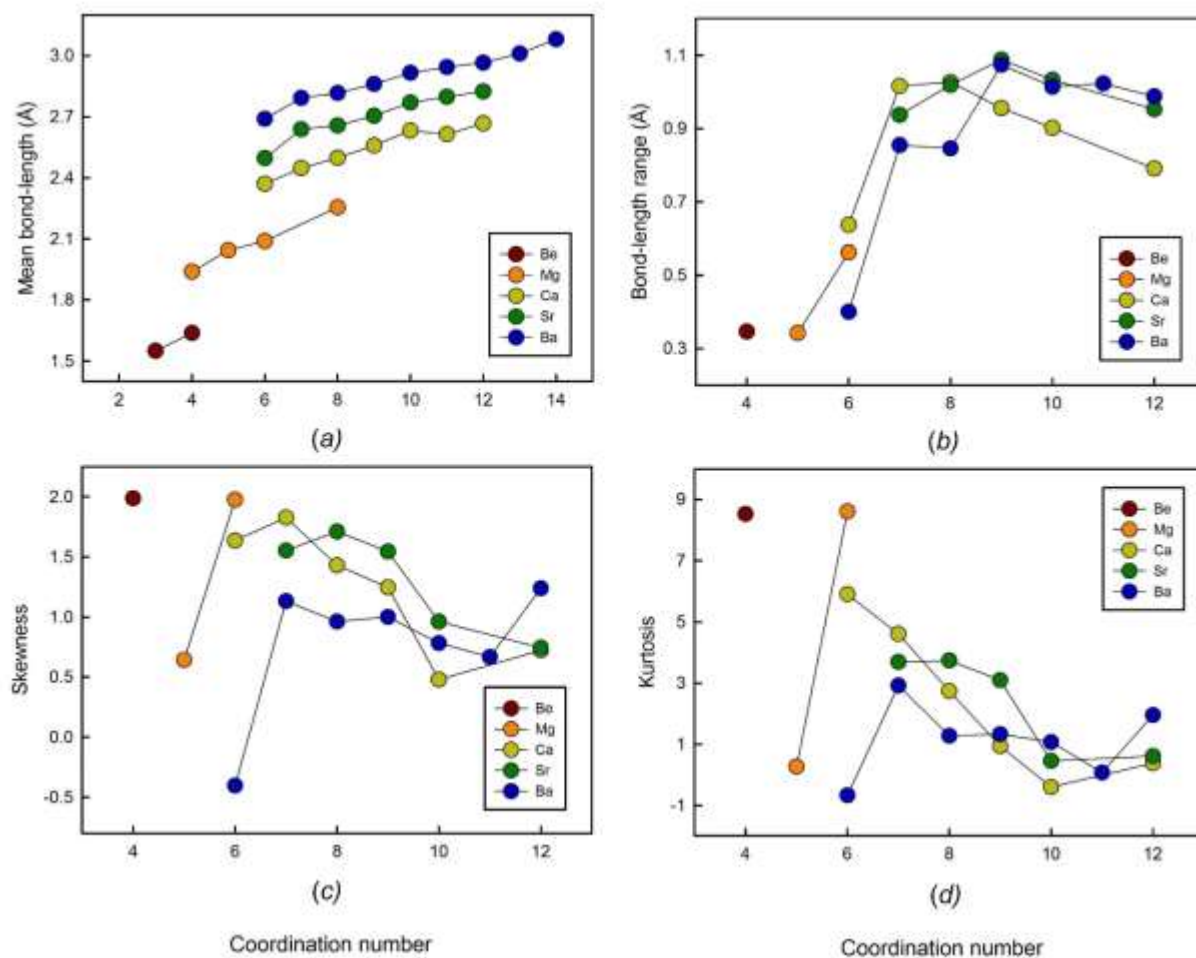
Figs. 4.10c and 4.10d summarize the variation of skewness and kurtosis as a function of coordination number for the common alkaline-earth-metal ions, respectively. There is a more-or-less linear decrease in skewness with increasing coordination number.

Abnormally low values of skewness (and kurtosis) are obtained for the bond-length distributions of $^{[5]}\text{Mg}^{2+}$ and $^{[6]}\text{Ba}^{2+}$, but are likely due to insufficient data. The slopes of these graphs are generally steeper for the alkaline-earth metals than for the alkali metals, meaning that the progressive “flattening” of the distributions described for the alkali metals is less developed for the alkaline-earth metals.

There is a systematic decrease in kurtosis with coordination number for the alkaline-earth-metal ions (Fig. 4.10d), with the same anomalies as for skewness (Fig. 4.10c).

The resemblance of the trends for skewness and kurtosis is striking, as is the case for the alkali-metal ions (Figs. 4.7c and 4.7d). The values of skewness and kurtosis arising from the bond-length distributions of each family are strongly correlated (alkali metals: $R^2 = 0.75$; alkaline-earth metals: $R^2 = 0.74$).

Figure 4.10 Values of (a) grand mean bond-length, (b) bond-length range, (c) skewness, and (d) kurtosis for the different coordination numbers of the alkaline-earth-metal ions.



4.12 General discussion of bond-length distributions

4.12.1 Skewness

As noted in section 4.8, bond-length distributions are expected to resemble a positively-skewed Gaussian distribution, and this shape originates from the variation in Born repulsion and Coulomb attraction as a function of interatomic distance. In particular, as the coordination number of a cation increases, the mean bond-length increases and the slope of the Born repulsion curve decreases as the mean cation-anion distances increase. This makes the potential energy curve more symmetrical about the mean bond-length and hence the skewness of the distribution of bond lengths should decrease with increasing coordination number. Inspection of Figs. 4.7c and 4.10c shows that this is generally the case for the alkali metals and the alkaline-earth metals.

4.12.2 Kurtosis

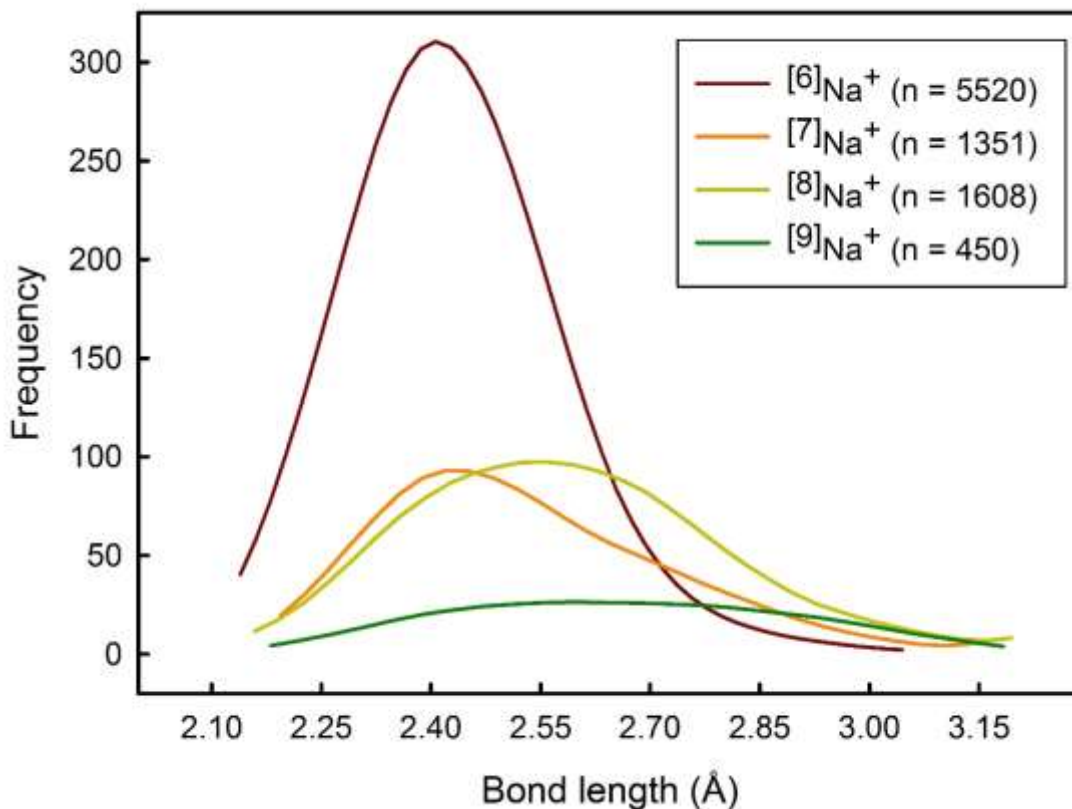
As noted above, kurtosis is a measure of the distribution of data between the peak and the tails of the distribution: a high kurtosis indicates that the distribution has a sharper maximum and larger tails, and a low kurtosis indicates that the distribution has a rounder maximum and smaller tails. Fig. 4.11 shows a kernel-density estimation of the bond-length distributions of coordination numbers [6] to [9] for Na^+ . This example shows decreases in both kurtosis and skewness from coordination [6] to [9]: kurtosis values are 1.317, 0.723, 0.461 and 0.121, and skewness values 3.246, -0.020, -0.197 and -0.879, respectively. Fig. 4.11 shows that the major contributor to kurtosis is the shape of the maximum of the distribution, rather than the length of the tail, as the tails and the

minimum and maximum bond-lengths are fairly similar for all coordination numbers, but the flattening of the distribution is very notable with increasing coordination number.

Figs. 4.7d and 4.10d show that kurtosis decreases with increasing coordination number for the alkali metals and the alkaline-earth metals; note that the main deviations from this trend are the same as those for the skewness plots, reinforcing the suggestion that small sample size may be the cause of these deviations.

For low coordination numbers, a change in bond valence corresponds to a relatively small change in bond length because of the steepness of the bond-valence—bond-length curve at short bond-lengths. For high coordination numbers, a change in bond valence corresponds to a large change in bond length because of the shallowness of the bond-valence—bond-length curve at long bond-lengths. Thus ions with low coordination numbers show a lower range in bond lengths whereas ions with high coordination numbers show a much greater range in bond lengths (Figs. 4.7b, 4.10b), leading to much flatter distributions (i.e., with lower kurtosis) at higher coordination numbers.

Figure 4.11 Kernel-density estimation of the bond-length distributions of the coordination numbers [6] to [9] for Na^+ . The plot shows that changes in skewness and kurtosis values are primarily due to a change in the shape of the maximum of the bond-length distribution.



4.12.3 Multi-modal distributions

Several cations show multi-modal distributions of their bond lengths. The most prominent bimodal distribution is for $^{[8]}\text{Ca}^{2+}$ and shows in both the distribution of individual bond-lengths (Fig. 4.8f) and mean bond-lengths (Fig. 4.12a). For the distribution of individual bond-lengths, there is an intense maximum at 2.49 Å and a less-intense maximum at 2.35 Å; for the distribution of mean bond-lengths, there is an intense maximum at 2.49 Å and a less-intense maximum at 2.42 Å. Inspection of the data with $\langle^{[8]}\text{Ca}^{2+}\text{-O}^{2-}\rangle$ less than 2.44 Å (79 polyhedra) shows that there are 33 garnet structures and 27 vesuvianite structures in this range. The distribution of individual $^{[8]}\text{Ca}^{2+}\text{-O}^{2-}$ distances from polyhedra with a mean bond-length of 2.44 Å or less are shown in Fig. 4.12b, and the distribution individual $^{[8]}\text{Ca}^{2+}\text{-O}^{2-}$ distances from polyhedra with a mean bond-length greater than 2.44 Å are shown in Fig. 4.12c. Fig. 4.12b also shows the kernel density estimation of the mean bond-length distribution of its constituent polyhedra. Removal of the data of Fig. 4.12b from the overall distribution of $^{[8]}\text{Ca}^{2+}\text{-O}^{2-}$ distances gives a single-mode distribution (Fig. 4.12c). The kernel density estimations for all three distributions are shown in Fig. 4.12d, and indicate how the bimodal distribution of Fig. 4.8f arises. In the garnet and vesuvianite structures, the bond lengths are split into two equal populations, four larger than the mean and four smaller than the mean. As shown in Fig. 4.12d, the population of larger distances merges with the overall distribution of bond lengths and does not materially alter its overall shape, whereas the population of smaller distances lies toward the lower edge of the overall distribution and gives rise to a shoulder on that distribution.

Multi-modal distributions are observed for the following configurations: $^{10}\text{Na}^+$, $^{12}\text{K}^+$, $^{13}\text{K}^+$, $^{14}\text{K}^+$, $^{15}\text{K}^+$, $^{18}\text{Cs}^+$, $^6\text{Ca}^{2+}$ and $^8\text{Ca}^{2+}$. Other configurations may show deviations from unimodal behaviour, although this is often unclear, possibly due to too few data and/or significant overlap: $^4\text{Na}^+$, $^{15}\text{Rb}^+$, $^9\text{Cs}^+$, $^{10}\text{Cs}^+$, $^{12}\text{Cs}^+$, $^{10}\text{Ba}^{2+}$. What the example of $^8\text{Ca}^{2+}$ makes clear is that one must examine the effects of non-random sampling (by large numbers of data on a specific structure type) before ascribing such an effect to any crystal-chemical mechanism.

Figure 4.12 Mean bond length distribution of $^{81}\text{Ca}^{2+}$ bonded to O^{2-} (a). Bond-length distribution for $^{81}\text{Ca}^{2+}$ bonded to O^{2-} are shown for configurations with a mean bond length (b) less or equal to 2.44 Å (superimposed with its mean bond-length kernel-density estimation) ($n = 568$), and (c) greater than 2.44 Å ($n = 3584$). The effect of the former on the aggregate bond-length distribution is shown via kernel-density estimation (d).

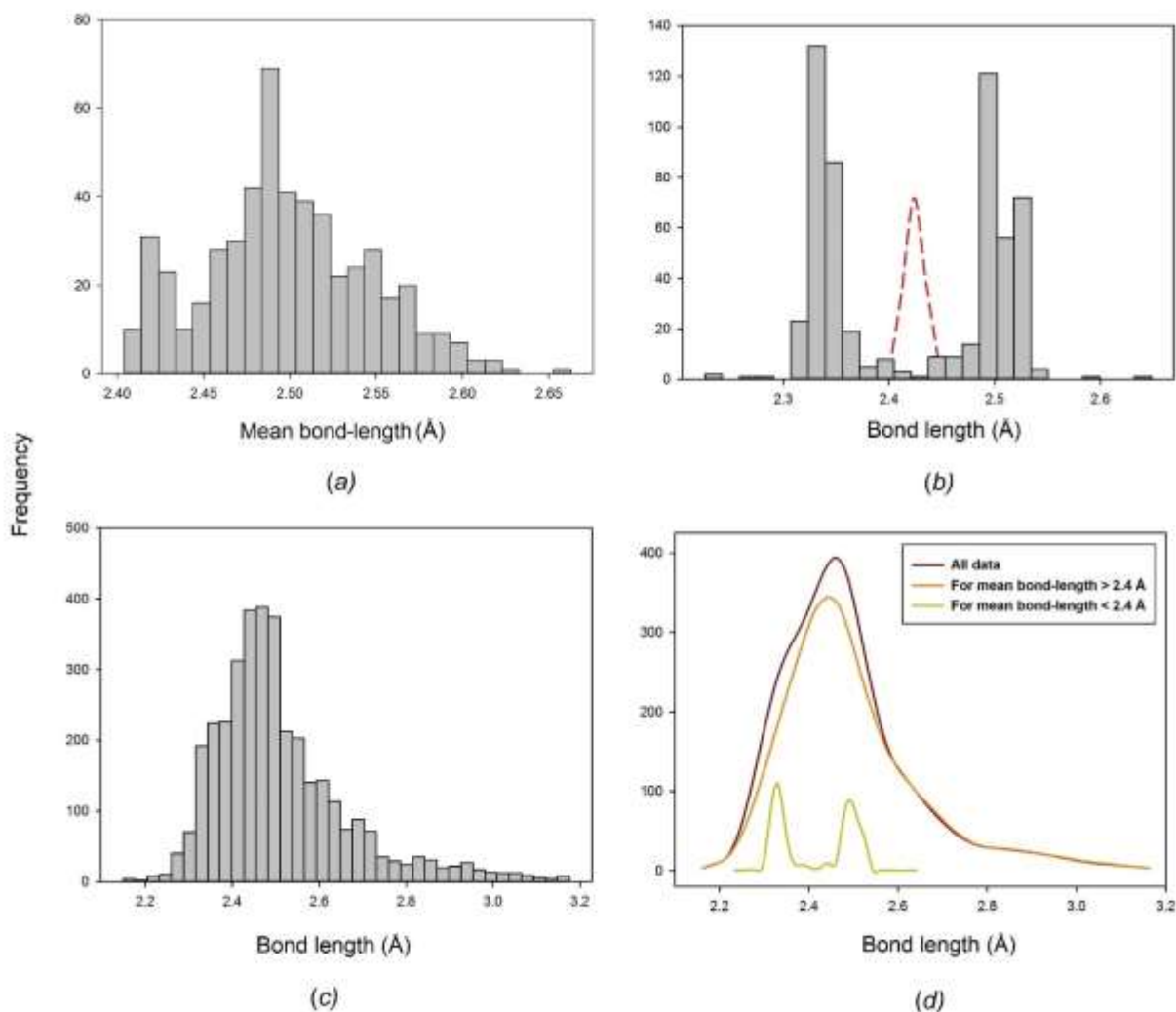
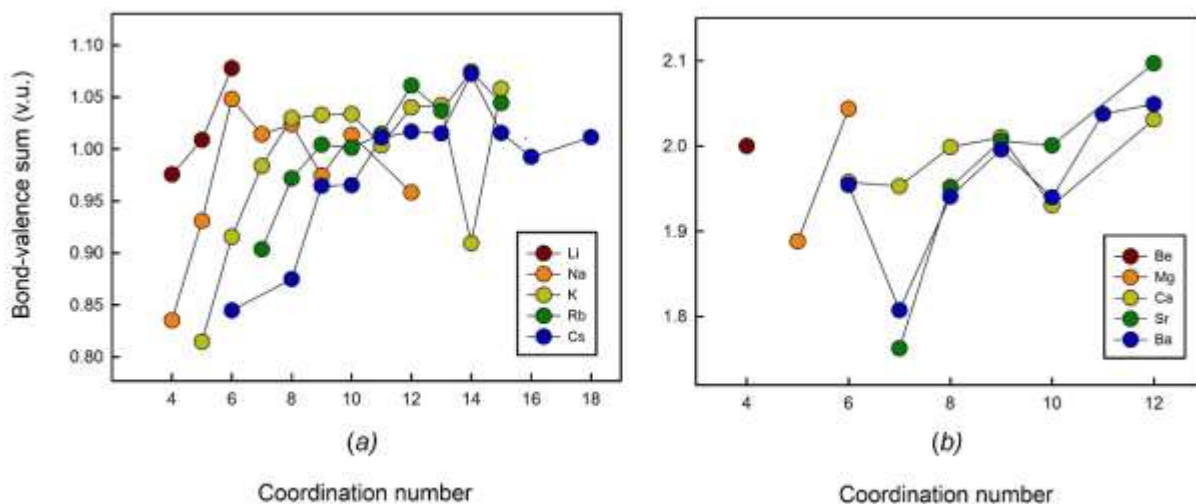


Figure 4.13 Bond-valence sum as a function of coordination number for the (a) alkali-metal and (b) alkaline-earth-metal ions using the parameters of Gagné & Hawthorne (2015).



4.12.4 Bond valences

Figs. 4.13a,b show the mean bond-valence sum as a function of coordination number, using the parameters of Gagné & Hawthorne (2015) for those alkali-metal and alkaline-earth metal configurations of 100 bonds or more. There is a general increase in mean bond-valence sum with increasing coordination number. This increase is much larger with smaller coordination numbers and tends to level off at larger ($> [9]$) coordination numbers. In the bond-valence model, the incident bond-valence sum for any ion is (approximately) equal to the ion valence, and there should be no correlation between incident bond-valence sum and coordination number of the ion. As indicated in Fig. 4.13, this is not the case. Moreover, this correlation is much more exaggerated when using the bond-valence parameters of other authors, as Gagné & Hawthorne (2015) added a coordination-based optimization factor in their method of derivation of bond-valence parameters. However, they were not able to eliminate the correlation between mean bond-valence sum and coordination number for all ions. Correlations of the type shown in Fig. 4.13 have been noted in the past, but have always been attributed to a limitation in the form of the bond-valence equation used. In particular, it has been suggested (*e.g.*, Wander *et al.*, 2015) that the exponential equation of Brown & Altermatt (1985) has too shallow a slope at both short and long bond distances, resulting in short (long) bonds seeming weaker (stronger) than they are. However, this effect is not limited to the equation of Brown and Altermatt (1985). Gagné & Hawthorne (2015) tested a series of two- and three-parameter equations, and found that any equation that gives a good fit to the data suffers from the same “curvature problem” at short and long bond-distances. Although the origin of this problem is not clear, this

shows that the problem may not lay in the parameterization of the relation, but possibly in a breakdown of the model itself in structures with unusual coordinations. This issue requires further investigating.

4.12.5 Ions with coordination numbers possibly exceeding [12]

Gagné & Hawthorne (2015) give bond-valence parameters for 4 ions to which they assign coordinations higher than [12]: K⁺, Rb⁺, Cs⁺ and Ba²⁺. Table 4.3 lists their values of the RMSD from the valence-sum rule obtained from their dataset for each ion and calculated using the equation of Brown & Altermatt (1985):

$$S_{ij} = \exp[(R_o - R_{ij})/B] \quad (\text{eq. 4.1})$$

where R_{ij} is the bond length between ions i and j , S_{ij} is the corresponding bond valence, and R_o and B are the bond-valence parameters. Here, we derive new bond-valence parameters using a hard cut-off of 12 bonds for those configurations we observe in coordination numbers greater than [12]. These are also listed in Table 4.3 with their associated RMSD values. There are minor changes in the R_o parameter for K⁺ and Ba²⁺ (2.047 to 1.985, and 2.223 to 2.208 Å, respectively) but there are major differences for Rb⁺ and Cs⁺ (1.993 to 1.780 and 2.305 to 1.966 Å, respectively). In all cases, the B parameter increases to offset the decrease in R_o : for K⁺, 0.398 to 0.425 Å; for Rb⁺ 0.478 to 0.577 Å; for Cs⁺ 0.411 to 0.561 Å; and for Ba²⁺ 0.406 to 0.417 Å. It is no surprise that R_o decreases as some of the longer distances are left out, as Gagné & Hawthorne (2015) showed that R_o is correlated with the mean bond-length of an ion (as

well as other physical observables such as ionization energy). To compensate for the decrease in R_0 , the B parameter adjusts to higher values.

Table 4.3 Bond-valence parameters for large alkali and alkaline-earth metals calculated with and without a hard cut-off of 12 bonds

Ion	R_0 (Å)	B (Å)	RMSD (v.u.)
K ⁺	2.047	0.398	0.164
K ⁺ (cn ≤ 12)	1.985	0.425	0.157
Rb ⁺	1.993	0.478	0.150
Rb ⁺ (cn ≤ 12)	1.780	0.577	0.148
Cs ⁺	2.305	0.411	0.138
Cs ⁺ (cn ≤ 12)	1.966	0.561	0.138
Ba ²⁺	2.223	0.406	0.217
Ba ²⁺ (cn ≤ 12)	2.208	0.417	0.215

We may assess whether or not interatomic distances greater than those used for [12] coordination are valid in the following ways: [1] verify if the mean bond-lengths and bond-valence parameters still follow established trends (e.g., with ionization energy) without the longer bonds; [2] verify the valence-sum rule for the bond-valence parameters obtained with and without the cut-off indirectly via the anion bond-valence sums for a set of structures containing these ions; [3] run computational simulations as to whether electron density is observed between the ions at longer distances. Option [3] has no experimental verification and is not considered here.

[1] We plotted mean bond-length as a function of R_o for the 5 alkali-metal ions for the values including and excluding bonds with a hard cut-off of [12]. Including the bonds, $R^2 = 0.94$, whereas excluding these bonds, R^2 drops to 0.79. Plotting $R_o/(\text{mean bond-length})$ against ionization energy (Gagné & Hawthorne, 2015), R^2 (inclusive) = 0.35, whereas R^2 (exclusive) = 0.01.

[2] We compared the bond-valence sums of the anions for 19 structures containing K^+ , Rb^+ , Cs^+ and Ba^{2+} , which we originally described in coordinations greater than [12], for the following two cases: (1) using the parameters of Gagné & Hawthorne (2015) and no cut-off, and (2) using new bond-valence parameters (above) that were derived with a cut-off of coordination [12], and doing the evaluation on the 19 structures using a cut-off of [12]. We find that both sets of parameters, used in the way they were derived, give exactly the same result for the anion bond-valence sums (RMSD = 0.128 v.u., or 6.4% from the nominal oxidation state).

Following [1] and [2], we conclude that the notion of counting bonds up to a maximum of 12 seems unjustified. We can find no strong argument against the occurrence of higher coordination numbers.

4.13 Mean bond-length distributions

Figs. 4.S3 and 4.S4 give all mean bond-length distributions for the alkali-metal and alkaline-earth-metal ions; those with adequate sample sizes (below) are shown in Figs. 4.14 and 4.15. Tables 4.4 and 4.5 give the grand mean bond-length and standard deviation, the minimum and maximum mean bond-length (and range), the skewness and kurtosis of each distribution (where justified by sample size), and the number of coordination polyhedra and coordination numbers for all configurations for the alkali and alkaline-earth metals. A minimum sample size was determined in the same way as above for $^{[6]}\text{Na}^+$, less than which the values of skewness and kurtosis have little significance; this threshold was set to 100 coordination polyhedra, and is relatively high due to the wide range of mean bond-lengths observed for these families.

Table 4.4 Mean-bond-length statistics for the 5 common alkali-metal ions

Ion	Coordination number	Number of coordination polyhedra	Grand mean bond-length (Å)	Standard deviation (Å)	Mean bond-length range (Å)	Maximum mean bond-length (Å)	Minimum mean bond-length (Å)	Skewness	Kurtosis
Li ⁺	3	4	1.913	0.032	0.070	1.958	1.888	--	--
	4	419	1.972	0.039	0.287	2.162	1.875	0.803	2.171
	5	91	2.108	0.050	0.214	2.226	2.012	--	--
	6	173	2.178	0.052	0.311	2.360	2.048	0.886	1.192
	7	2	2.331	0.008	0.012	2.337	2.326	--	--
	8	1	2.513	--	--	2.513	2.513	--	--
Na ⁺	3	7	2.307	0.045	0.112	2.360	2.248	--	--
	4	131	2.359	0.049	0.285	2.537	2.252	0.784	0.937
	5	142	2.413	0.049	0.269	2.561	2.292	0.209	-0.034
	6	920	2.441	0.056	0.466	2.682	2.216	0.295	2.367
	7	193	2.541	0.056	0.313	2.718	2.404	0.423	0.021
	8	201	2.599	0.071	0.458	2.880	2.422	0.574	1.160
	9	50	2.686	0.065	0.382	2.936	2.553	--	--
	10	17	2.741	0.054	0.183	2.830	2.647	--	--
K ⁺	12	21	2.795	0.074	0.254	2.940	2.686	--	--
	4	24	2.708	0.056	0.234	2.852	2.618	--	--

	5	59	2.796	0.078	0.438	3.084	2.646	--	--
	6	119	2.828	0.103	0.652	3.099	2.447	0.022	1.007
	7	67	2.861	0.064	0.295	3.009	2.715	--	--
	8	284	2.894	0.053	0.299	3.081	2.781	0.619	0.462
	9	308	2.955	0.061	0.503	3.174	2.671	-0.003	2.167
	10	243	3.013	0.065	0.382	3.209	2.827	0.384	0.493
	11	87	3.089	0.066	0.306	3.242	2.936	--	--
	12	194	3.095	0.092	0.543	3.337	2.794	-0.708	1.232
	13	35	3.149	0.094	0.327	3.293	2.966	--	--
	14	24	3.239	0.068	0.288	3.374	3.085	--	--
	15	35	3.182	0.064	0.246	3.332	3.086	--	--
Rb ⁺	4	12	2.776	0.634	2.252	3.018	0.765	--	--
	5	3	2.864	0.040	0.078	2.899	2.821	--	--
	6	14	2.989	0.084	0.286	3.122	2.836	--	--
	7	20	3.002	0.083	0.371	3.213	2.842	--	--
	8	60	3.033	0.058	0.260	3.182	2.922	--	--
	9	75	3.079	0.064	0.321	3.287	2.966	--	--
	10	108	3.142	0.064	0.302	3.279	2.977	-0.262	-0.405
	11	44	3.188	0.054	0.226	3.296	3.070	--	--
	12	70	3.228	0.084	0.373	3.410	3.037	--	--

Cs ⁺	13	19	3.293	0.042	0.138	3.350	3.212	--	--
	14	20	3.301	0.061	0.235	3.400	3.164	--	--
	15	13	3.338	0.110	0.337	3.545	3.208	--	--
	17	1	3.456	--	0.000	3.456	3.456	--	--
	18	5	3.478	0.078	0.217	3.582	3.364	--	--
	6	17	3.124	0.032	0.113	3.175	3.062	--	--
	7	10	3.193	0.061	0.206	3.312	3.106	--	--
	8	25	3.244	0.064	0.216	3.359	3.143	--	--
	9	48	3.251	0.054	0.232	3.366	3.134	--	--
	10	93	3.304	0.056	0.348	3.455	3.107	--	--
	11	68	3.333	0.054	0.261	3.479	3.218	--	--
	12	90	3.377	0.072	0.335	3.542	3.207	--	--
	13	40	3.426	0.063	0.267	3.552	3.285	--	--
	14	51	3.444	0.064	0.229	3.539	3.310	--	--
	15	47	3.503	0.066	0.289	3.661	3.372	--	--
	16	14	3.550	0.068	0.230	3.672	3.442	--	--
	17	4	3.530	0.029	0.062	3.549	3.487	--	--
	18	36	3.570	0.062	0.229	3.715	3.487	--	--
	20	1	3.723	--	--	3.723	3.723	--	--

Table 4.5 Mean-bond-length statistics for the 5 common alkaline-earth-metal ions

Ion	Coordination number	Number of coordination polyhedra	Grand mean bond-length (Å)	Standard deviation (Å)	Mean bond-length range (Å)	Maximum mean bond-length (Å)	Minimum mean bond-length (Å)	Skewness	Kurtosis
Be ²⁺	3	8	1.550	0.012	0.031	1.566	1.535	--	--
	4	161	1.637	0.017	0.114	1.719	1.605	1.744	6.011
Mg ²⁺	4	12	1.939	0.017	0.054	1.966	1.912	--	--
	5	24	1.966	0.091	0.309	2.087	1.777	--	--
	6	426	2.089	0.024	0.185	2.223	2.038	1.179	3.051
Ca ²⁺	8	7	2.255	0.035	0.080	2.284	2.203	--	--
	6	211	2.371	0.034	0.217	2.471	2.254	-0.261	0.236
	7	287	2.447	0.038	0.225	2.591	2.366	0.735	0.761
	8	519	2.498	0.048	0.259	2.663	2.404	0.216	-0.238
	9	115	2.559	0.039	0.215	2.694	2.479	0.761	0.927
	10	16	2.632	0.048	0.137	2.686	2.549	--	--
	11	7	2.614	0.060	0.139	2.690	2.551	--	--
Sr ²⁺	12	13	2.668	0.073	0.228	2.777	2.549	--	--
	6	13	2.477	0.034	0.118	2.542	2.424	--	--
	7	38	2.639	0.054	0.188	2.738	2.549	--	--
	8	113	2.658	0.061	0.310	2.871	2.561	1.298	1.633

	9	101	2.703	0.051	0.266	2.871	2.604	1.119	1.523
	10	50	2.769	0.070	0.436	3.053	2.617	--	--
	11	8	2.798	0.027	0.075	2.830	2.755	--	--
	12	53	2.825	0.055	0.213	2.930	2.716	--	--
Ba ²⁺	6	21	2.689	0.054	0.197	2.794	2.597	--	--
	7	21	2.792	0.033	0.121	2.855	2.733	--	--
	8	88	2.816	0.049	0.254	2.952	2.698	--	--
	9	142	2.860	0.055	0.307	3.036	2.729	0.111	0.302
	10	193	2.915	0.053	0.295	3.091	2.796	0.282	-0.022
	11	82	2.944	0.039	0.187	3.035	2.849	--	--
	12	302	2.965	0.058	0.289	3.133	2.845	0.467	-0.299
	13	6	3.010	0.051	0.137	3.070	2.934	--	--
	14	1	3.080	--	--	3.080	3.080	--	--

Figure 4.14 Mean bond-length distributions for the configurations of the alkali-metal ions bonded to O^{2-} with a sample size of 100+ coordination polyhedra: (a) $[4]Li^+$, (b) $[6]Li^+$, (c) $[4]Na^+$, (d) $[5]Na^+$, (e) $[6]Na^+$, (f) $[7]Na^+$, (g) $[8]Na^+$, (h) $[6]K^+$, (i) $[8]K^+$, (j) $[9]K^+$, (k) $[10]K^+$, (l) $[12]K^+$, (m) $[10]Rb^+$.

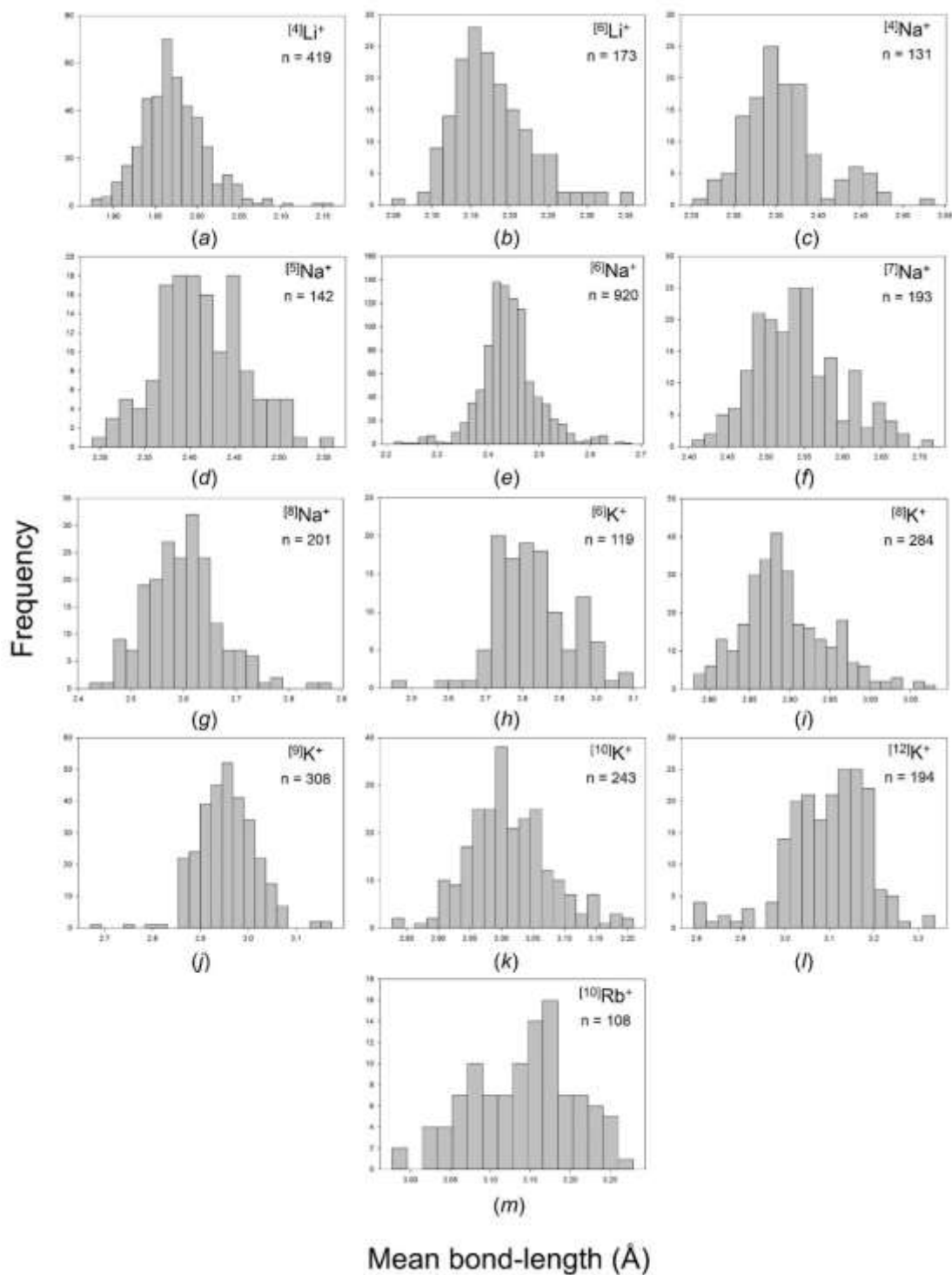
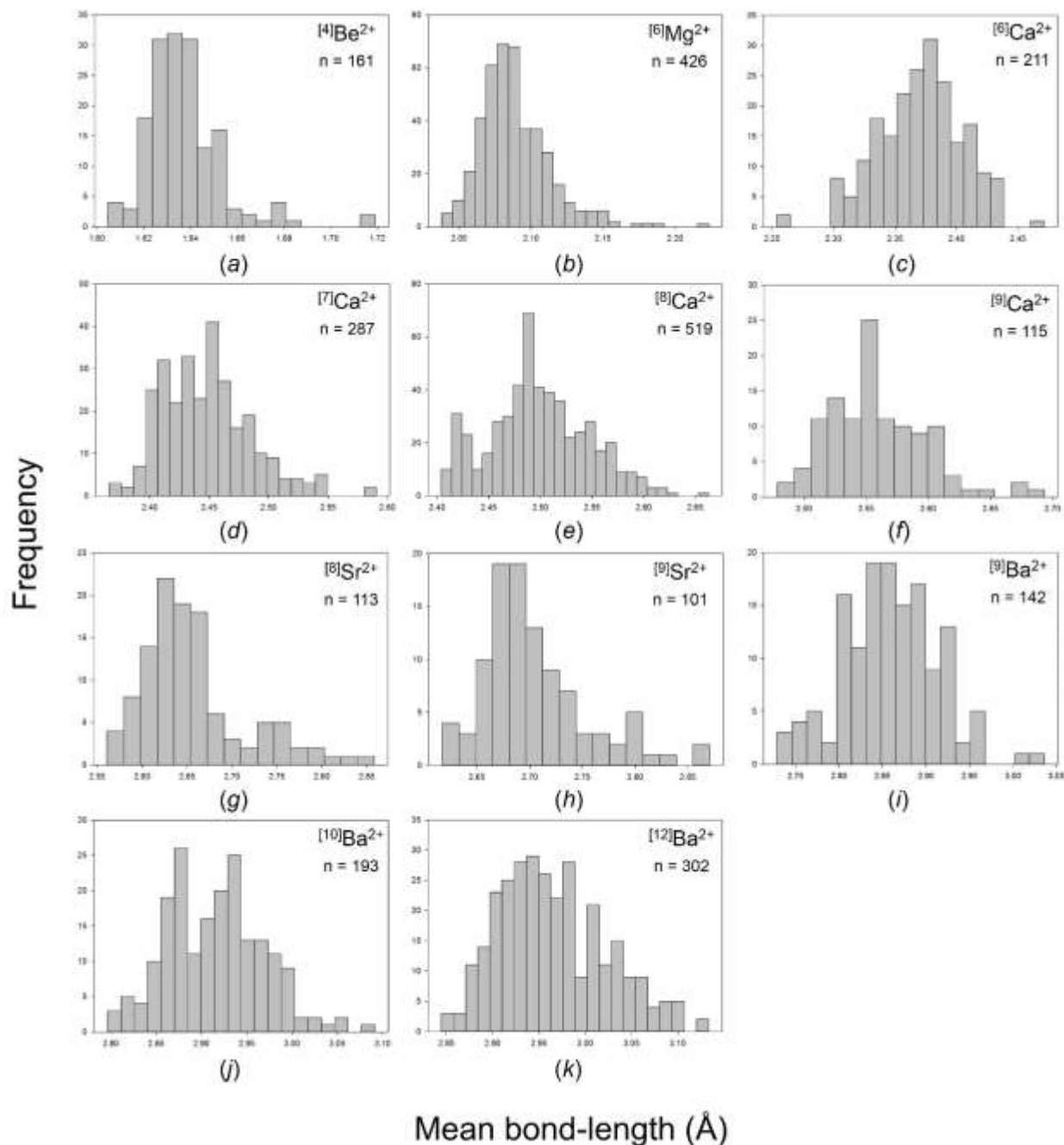


Figure 4.15 Mean bond-length distributions for the configurations of the alkaline-earth-metal ions bonded to O^{2-} with a sample size of 100+ coordination polyhedra: (a) $[4]Be^{2+}$, (b) $[6]Mg^{2+}$, (c) $[6]Ca^{2+}$, (d) $[7]Ca^{2+}$, (e) $[8]Ca^{2+}$, (f) $[9]Ca^{2+}$, (g) $[8]Sr^{2+}$, (h) $[9]Sr^{2+}$, (i) $[9]Ba^{2+}$, (j) $[10]Ba^{2+}$, (k) $[12]Ba^{2+}$.



The average range of mean bond-lengths for the 55 configurations of the alkali metals is 0.308 Å, and is 0.217 Å for the 29 configurations of the alkaline-earth metals. The largest range is observed for $^{[6]}\text{K}^+$, from 2.447 to 3.099 Å. The distribution for $^{[4]}\text{Be}^{2+}$ (Fig. 4.15a) shows a feature that is of importance in examining bond-length distributions: there is a notable outlier with two $\langle ^{[4]}\text{Be}^{2+}\text{-O} \rangle$ distances at ~ 1.717 Å. These values are for sørensenite, ideally $\text{Na}_4\text{Sn}^{4+}[\text{Be}_2\text{Si}_6\text{O}_{18}](\text{H}_2\text{O})_2$ (Metcalf-Johansen & Hazell, 1976), which was assumed to have the ideal composition in the structure study. However, inspection of the chemical analyses listed by Semenov *et al.* (1965) shows that the formulae depart significantly from the ideal stoichiometry used to interpret the structure results. In many pegmatite minerals, Be^{2+} is commonly partly substituted by Li^+ or Al^{3+} , both of which are larger than Be^{2+} (Shannon, 1976) and this may be what has happened here. Of course, this is speculation, but emphasizes the importance of electron- and ion-microprobe analysis of the specific crystal used to collect X-ray intensity data for structure analysis of minerals.

4.13.1 The effect of distortion

4.13.1.1 The distortion theorem

The distortion theorem states that for any ion, lengthening some bonds and shortening others, keeping the bond-valence sum the same, will always increase the mean bond-length due to the exponential nature of the relation (Brown, 2002). Here, we use the following definition of bond-length distortion from the mean value in a polyhedron:

$$\Delta = \frac{1}{n} \sum_{i=1}^n \left[\frac{(R_i - \bar{R})}{\bar{R}} \right]^2 \quad (\text{eq. 4.2})$$

where R_i is the length of bond i , \bar{R} is the mean bond length and the summation is taken over the n bonds of the polyhedron. This expression was designated the quadratic elongation by Robinson et al. (1971) and distortion by Brown & Shannon (1973), and was used by many previous authors as a measure of distortion as it is the standard deviation of the mean bond-length in a specific polyhedron, i.e., the measure of dispersion of the individual bond-lengths. The distortion is shown graphically in Fig. 4.16 with the bond-valence curve for Na^+ . For [4]-coordinated Na^+ , the mean bond-valence is 0.25 v.u., marked by the dashed line intersecting the bond-valence curve at point b (Fig. 4.16). If half the bonds shorten and half the bonds lengthen to a and c, respectively, on the bond-valence curve, the mean bond-length (marked by D1 in Fig. 4.16) increases slightly over the mean bond-length for four equal bonds. For [10]-coordinated Na, the mean bond-valence is 0.10 v.u., marked by the dashed line intersecting the bond-valence curve at point e (Fig. 4.16). If half the bonds shorten and half the bonds lengthen to d and f, respectively, on the bond-valence curve, the mean bond-length (marked by D2 in Fig. 4.16) increases considerably more over the mean bond-length for ten equal bonds.

Secondly, Fig. 4.16 shows that the effect of the distortion theorem is greatly affected by the slope and curvature of the bond-valence—bond-length relation; if we use the same concept for points a, b and c, we see that the mean bond-length changes very little, and much less relative to points d, e and f. Different ions have their mean bond-length at different points (curvature) on this graph, and thus are affected differently by the distortion theorem. The best way to visualize this concept is by making use of a universal curve as described in Brown & Shannon (1973), where the relation for an

isoelectronic series of ions can be described by the same bond-valence curve (with a slight decrease in fit compared to ion-based curves). In Fig. 4.17, we show the bond-valence curve for the Na isoelectronic series ($Ro = 1.630$, $B = 0.438$), and identify the ideal mean bond-valence and associated mean bond-length for the most common coordination number of each ion of the series. We see that ions of lower charge, and with generally higher coordination numbers, occur on part of the bond-valence curve that is much more susceptible to higher bond-length distortion (i.e., with lower bond-valences). Hence, the alkali metals are more strongly affected by distortion than the alkaline-earth metals, and so on. Figs. 4.18a-d show the variation in the range of bond lengths for different coordination numbers as a function of the slope of the bond-valence curve at the mean bond-length corresponding to those coordination numbers for Na^+ , K^+ , Rb^+ and Cs^+ . As predicted above, there is a positive correlation between range and slope for each cation; the trends are well-developed for Na^+ , Rb^+ and Cs^+ , despite a decrease at the highest coordination number for Na^+ and Rb^+ possibly due to fewer data, but is perturbed by considerable scatter for K^+ . As noted above, the distortion will also be correlated with the curvature (as well as the slope) of the bond-valence curve, but the slope and curvature are highly correlated and their effect is well-represented by just the slope of the curve.

Figure 4.16 Bond-valence bond-length curve for Na^+ . The exponential shape leads to the distortion theorem of the bond-valence model.

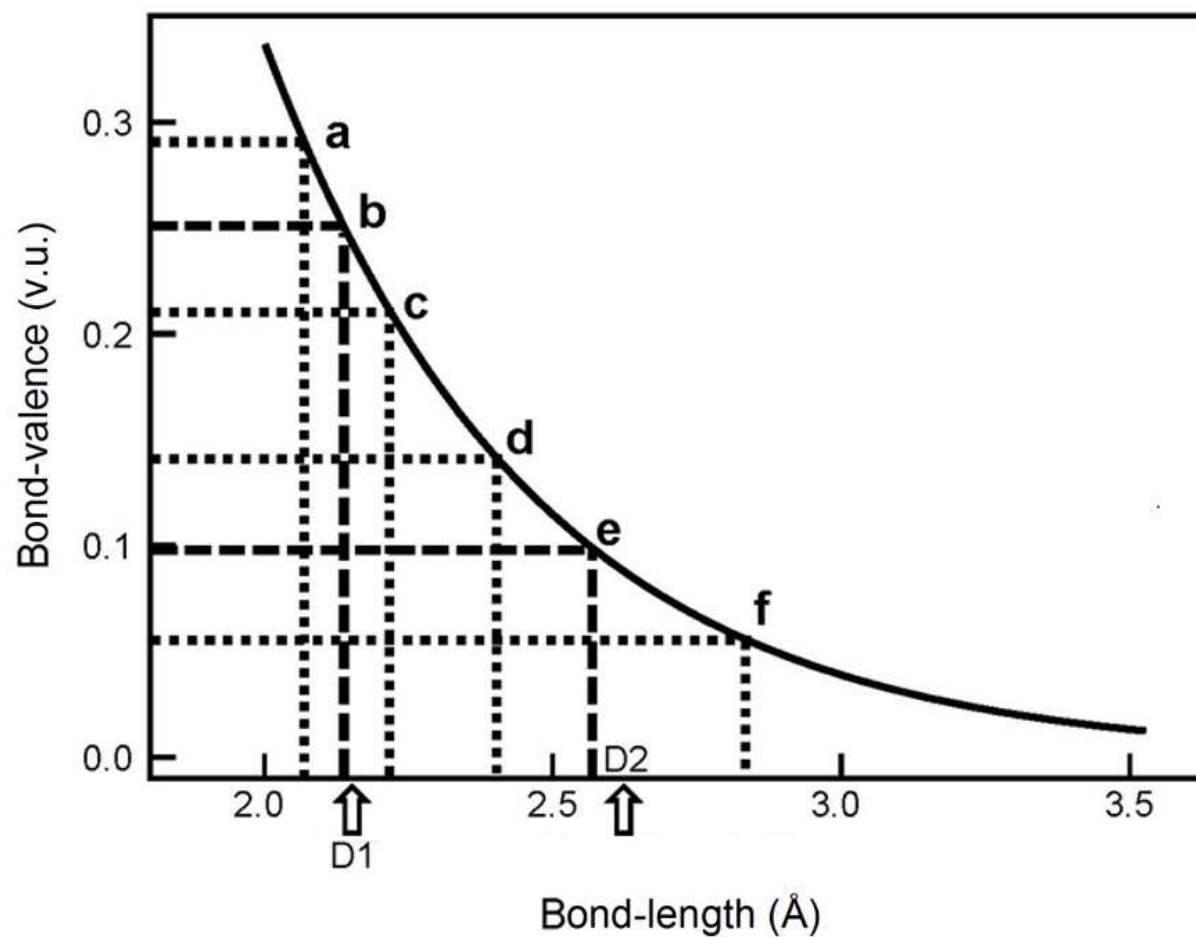


Figure 4.17 Bond-valence curve for the Na isoelectronic series, and ideal mean bond-valence and associated mean bond-length for the most common coordination number of each ion of the series.

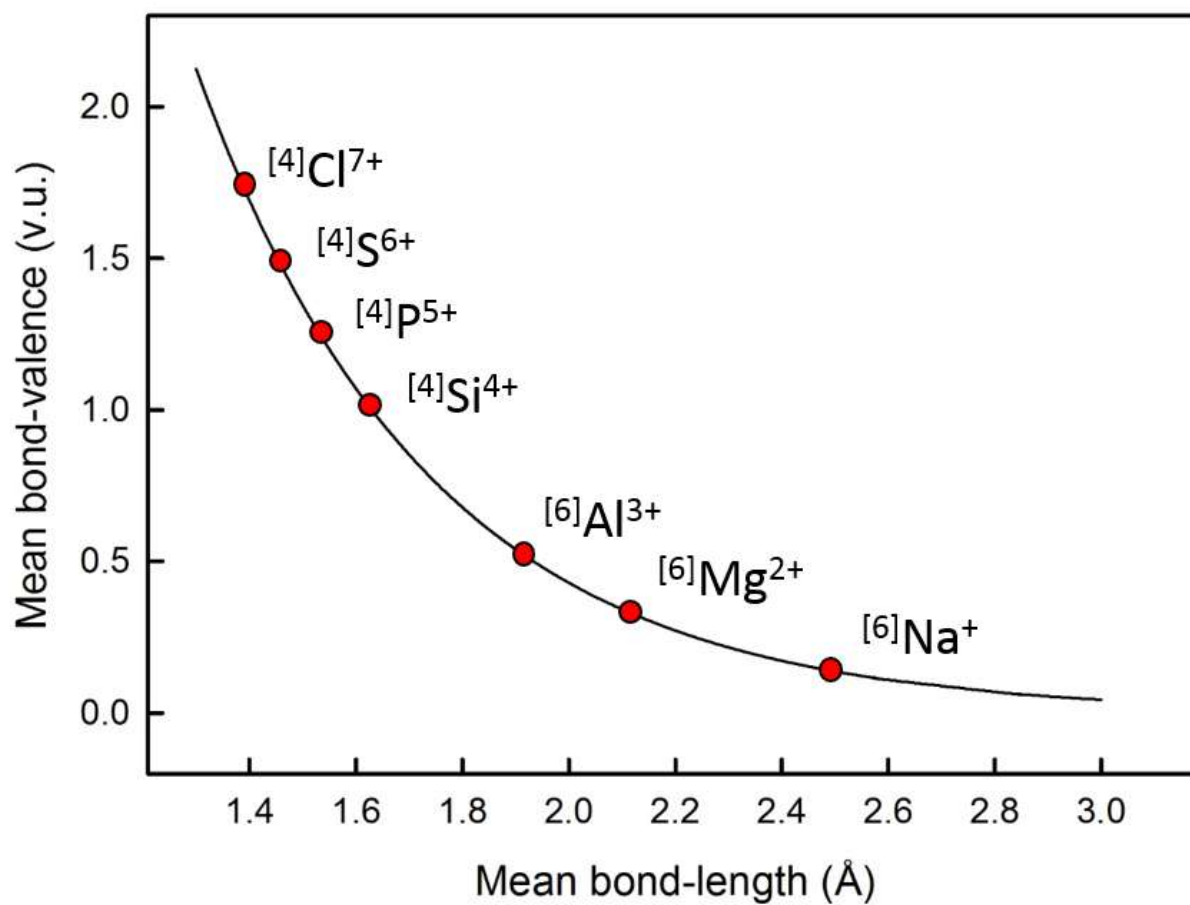


Figure 4.18 Variation in the observed bond-length ranges for the different coordination numbers of (a) Na^+ , (b) K^+ , (c) Rb^+ and (d) Cs^+ bonded to O^{2-} as a function of the slope of the bond-valence curve at the mean bond-length corresponding to those coordinations.

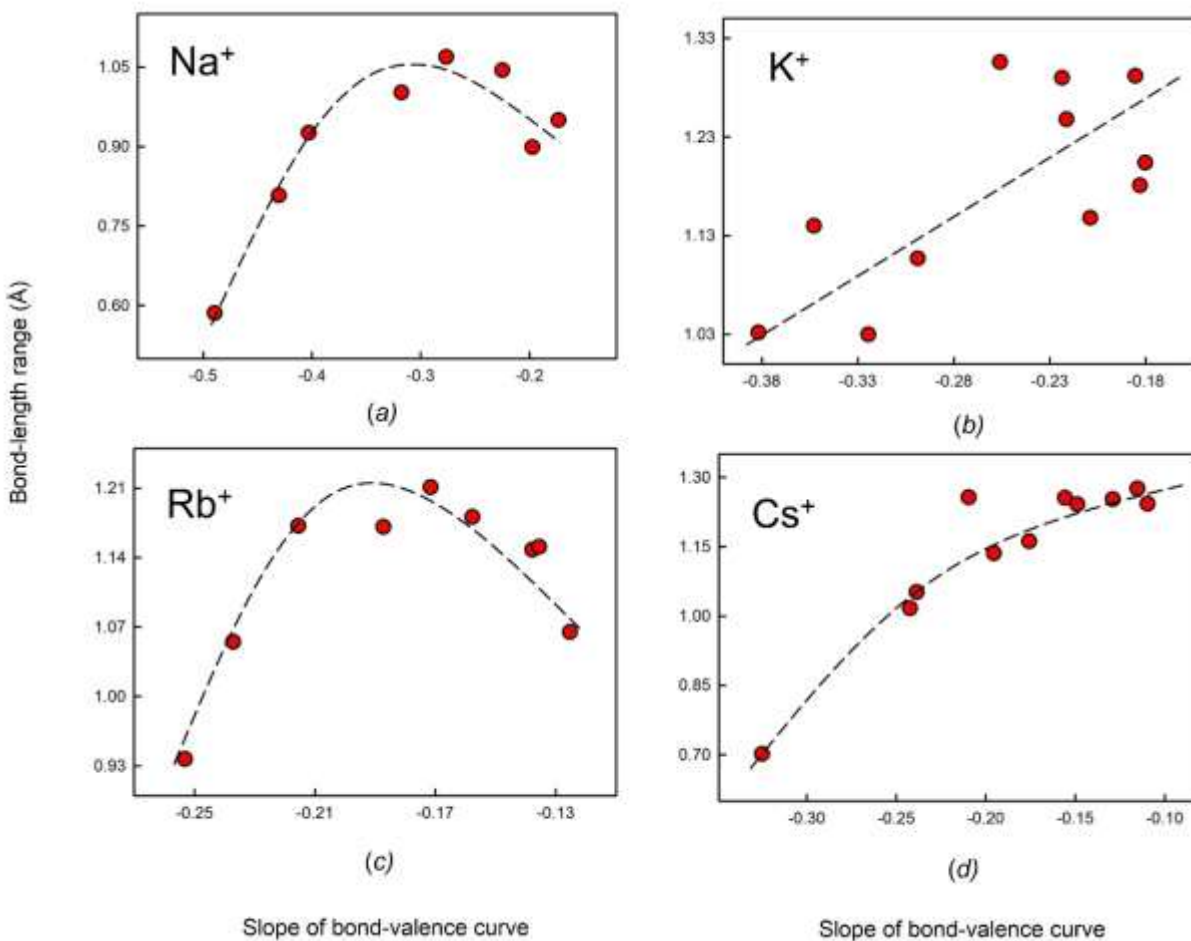
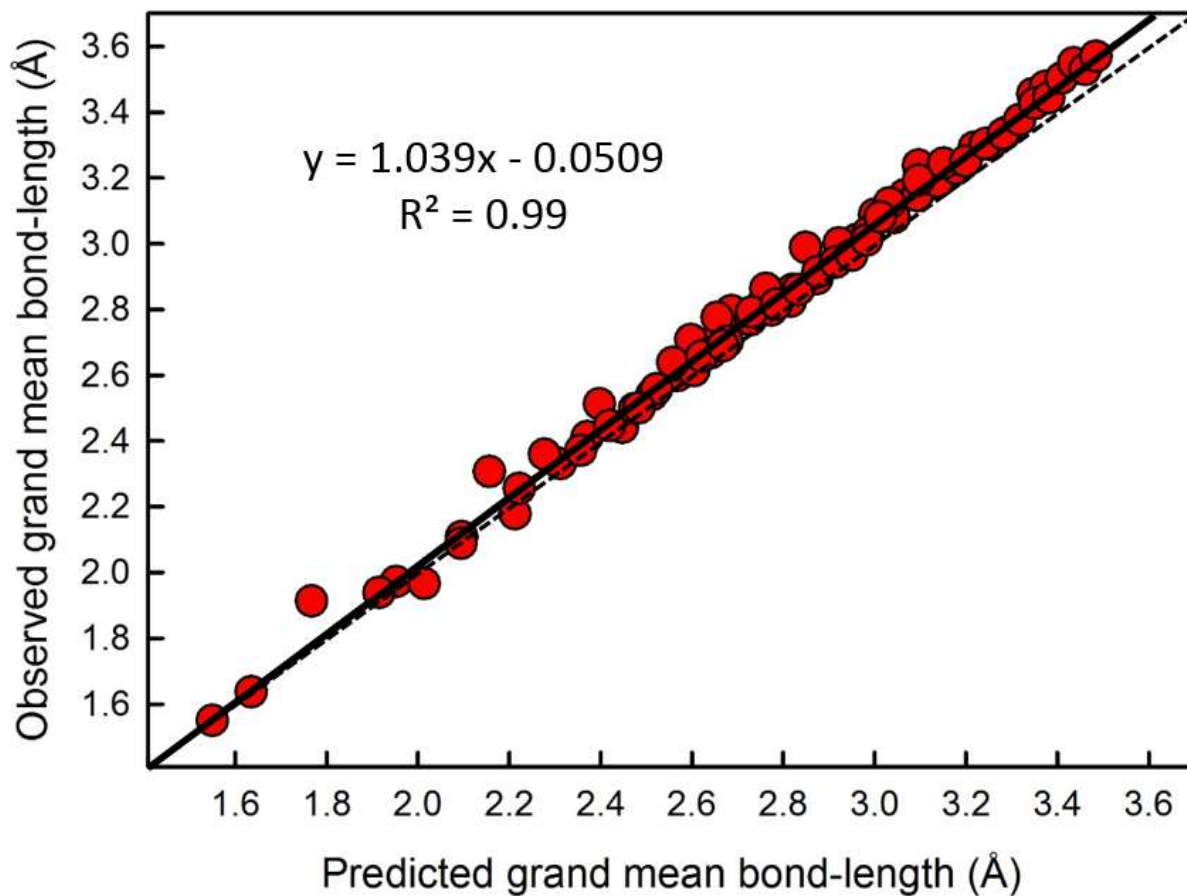


Figure 4.19 Observed vs predicted values of the grand mean bond-length for all observed ion configurations of the alkali-metal and alkaline-earth metal ions. The observed values of mean bond-length are usually larger than the ones predicted by the bond-valence curve for equidistant bonds. The dashed line is for $y = x$.



4.13.1.2 Grand mean bond-length

Using the bond-valence parameters of Gagné & Hawthorne (2015), we calculated the predicted grand mean bond-length for all configurations of the alkali-metal and alkaline-earth-metal ions by converting the mean bond-valence (i.e., the Pauling bond-strength) of the coordination polyhedron into a mean bond-length, where all bonds of the idealized polyhedron have the same length. When comparing the observed grand mean bond-length (Tables 4.4 and 4.5) to the calculated values, we obtain an overall difference of 2.5% for the alkali metals (1.2% when weighted by the number of coordination polyhedra), and 1.0% (0.8% weighted) for the alkaline-earth metals. As shown in Fig. 4.19, the predicted values closely follow the observed values, but are slightly larger and the difference increases with increasing mean bond-length, in accord with the idea that distortion of coordination polyhedra causes an increase in mean bond-length, and that this effect should increase with increasing coordination number.

For any ion configuration, we may calculate the maximum amount of distortion that is compatible with its observed bond-length distribution, using the bond-valence model and the minimum and maximum bond-length observed for that configuration. We have done this for all configurations of the alkali-metal and alkaline-earth-metal ions, by using the minimum and maximum bond-length observed for each configuration and distributing the other bond lengths in a way that maximizes distortion while satisfying the valence-sum rule. This procedure resulted in a mean potential distortion of 3.9% for the 55 alkali-metal configurations (4.6% when weighted by the number of coordination polyhedra), compared to 2.5% (1.2% weighted) for the observed values, and 2.8% (3.4% weighted) for the 29 alkaline-earth-metal configurations, compared to 1.0% (0.8%

weighted) for the observed values. These calculations show that for most ion configurations, the observed ranges of bond-lengths are significantly larger than is compatible with the observed distortions. Thus, in addition to distortion, other factors must also affect mean bond-lengths.

4.13.1.3 Mean bond-length as a function of distortion

Fig. 4.20a shows the mean bond-length for $^{[6]}\text{Na}^+\text{-O}^{2-}$ as a function of distortion ($n = 920$). There is a positive correlation between mean bond-length and distortion, Δ , for reasons discussed above; the inclined solid line shows the result of a linear regression ($R^2 = 0.263$). The calculated curve for the effect that distortion has on mean bond-length for $^{[6]}\text{Na}^+\text{-O}^{2-}$ is shown by the dashed line on Fig. 4.20a. The difference between observed and predicted curve is partly due to the data near $\Delta = 0$ (discussed below) which has a very large scatter. Additionally, we note that highly-distorted configurations generally have poor agreement with the valence-sum rule, which leads to variability in the data above and below the predicted curve. However, highly-distorted polyhedra for $^{[6]}\text{Na}^+$ (with higher mean bond-lengths) tend to have low bond-valence sums ($\sim 0.8\text{-}0.9$ v.u.), indicating that the mean bond-lengths of these polyhedra are larger than predicted from the valence-sum rule and the form of the bond-valence curves.

A very prominent feature of Fig. 4.20a is the fact that the widest range of mean bond-lengths occurs at zero distortion; $\langle^{[6]}\text{Na}^+\text{-O}^{2-}\rangle$ varies from 2.216 to 2.567 Å at $\Delta = 0$ alone, compared to 2.276 to 2.682 Å for all other data with $\Delta \neq 0$, and the range of observed mean bond-lengths decreases as Δ increases. The total range in mean bond-

length is 0.466 Å; this may be compared with the predicted range that may be assigned to the effect of distortion (dashed line), 0.11 Å, as well as the observed range (solid line), 0.21 Å (Fig. 4.20a).

We give the analogous bond-length distortion plots for the 55 configurations of the alkali-metal ions and 29 configurations of the alkaline-earth-metal ions in Figs. 4.S5 and 4.S6, respectively. We note that this concentration of data at $\Delta = 0$ is evident for Li^+ in [4]- and [6]-coordination, Na^+ in [4]- and [6]- coordination and K^+ in [6]-coordination, and occurs more subtly for Na^+ in [5]- and [8]-coordination as well as K^+ in [8]- [9] and [12]-coordination. For the alkaline-earth metals, this concentration of data at $\Delta = 0$ occurs for Be^{2+} [4]-coordinated, Mg^{2+} [4]- and [6]-coordinated, Ca^{2+} [6]- and [12]-coordinated, Sr^{2+} [6]- coordinated and Ba^{2+} [12]-coordinated, and more subtly for Ca^{2+} [7]- and [8]-coordinated, Sr^{2+} [8]-coordinated and Ba^{2+} [8] and [10]-coordinated. In Fig. 4.20b, we show the distortion plot of $^{[10]}\text{K}^+$, which in contrast to that for $^{[6]}\text{Na}^+$ (Fig. 4.20a) shows no preference for $\Delta = 0$. It is therefore interesting to see that the observed mean bond-length values (solid line) are generally lower than what we predict over the whole range of distortion (dashed line) because of the absence of the large scatter and amount of data near $\Delta = 0$ that greatly affects the slope of the observed curve for ion configurations with significant scatter at $\Delta = 0$. Fig. 4.20c shows $^{[8]}\text{Ca}^{2+}$ as an intermediate configuration with some concentration of data near $\Delta = 0$. Some of these differences may be due to the distortion parameter that we use not representing different distributions of bond lengths within a polyhedron, as this does affect somewhat the behaviour of mean bond-length as a function of distortion (Urusov, 2003, 2015). However, this issue does not affect the mean bond-length at zero distortion. Thus it is

apparent from the large amount of scatter in Fig. 4.20 (Figs. 4.S5 and 4.S6) that much of the variation in mean bond-length shown in Figs. 4.14 and 4.15 (Figs. 4.S3 and 4.S4) is not due to distortion, and that one or more other factors must also affect mean bond-length.

Figure 4.20 The effect of bond-length distortion on mean bond-length for (a) $[6]\text{Na}^+$, (b) $[10]\text{K}^+$ and (c) $[8]\text{Ca}^{2+}$. The positive correlation indicates that distortion of the coordination polyhedron has a sizeable effect on the mean bond-length of said polyhedron. The dashed line indicates the predicted effect of distortion on mean bond-length for that ion configuration according to the bond-valence curve of the ion.

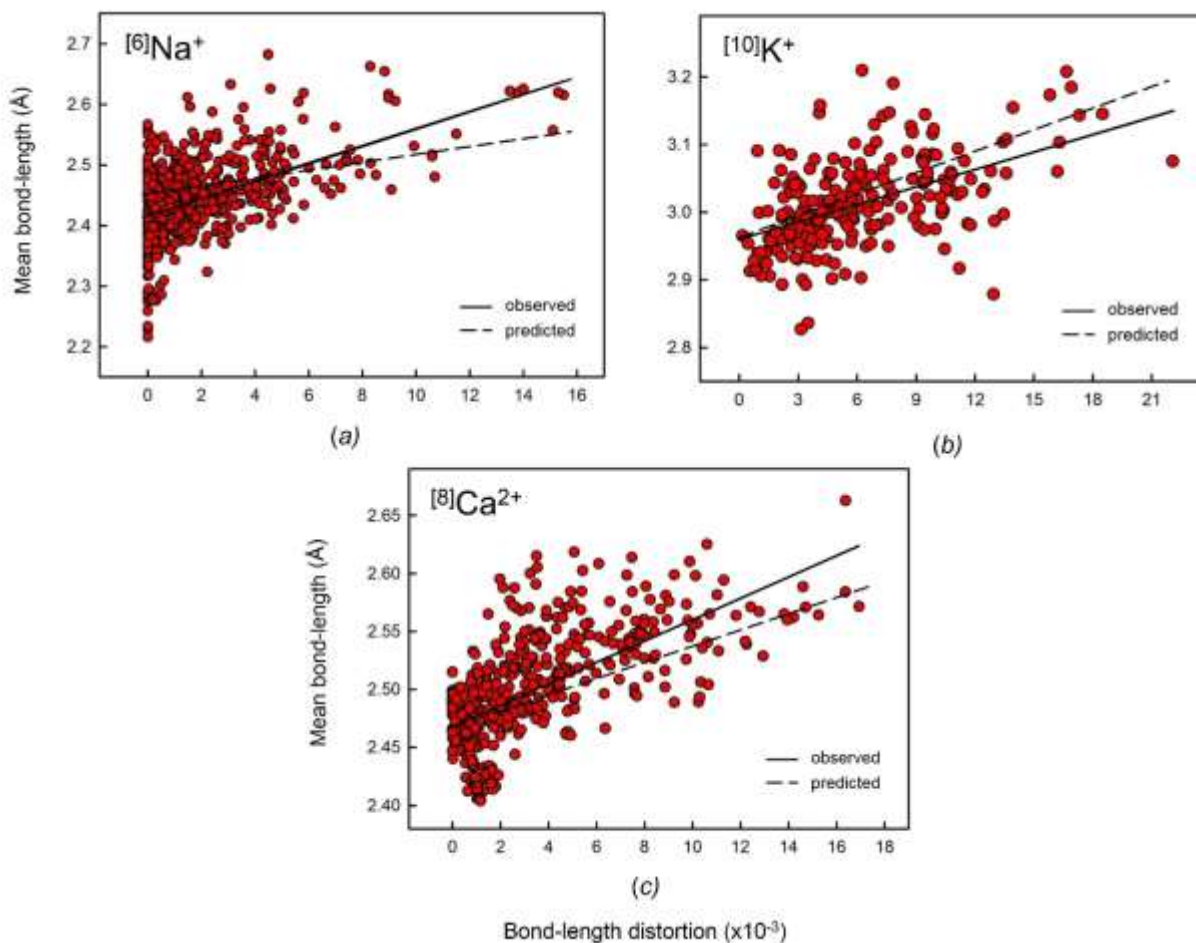
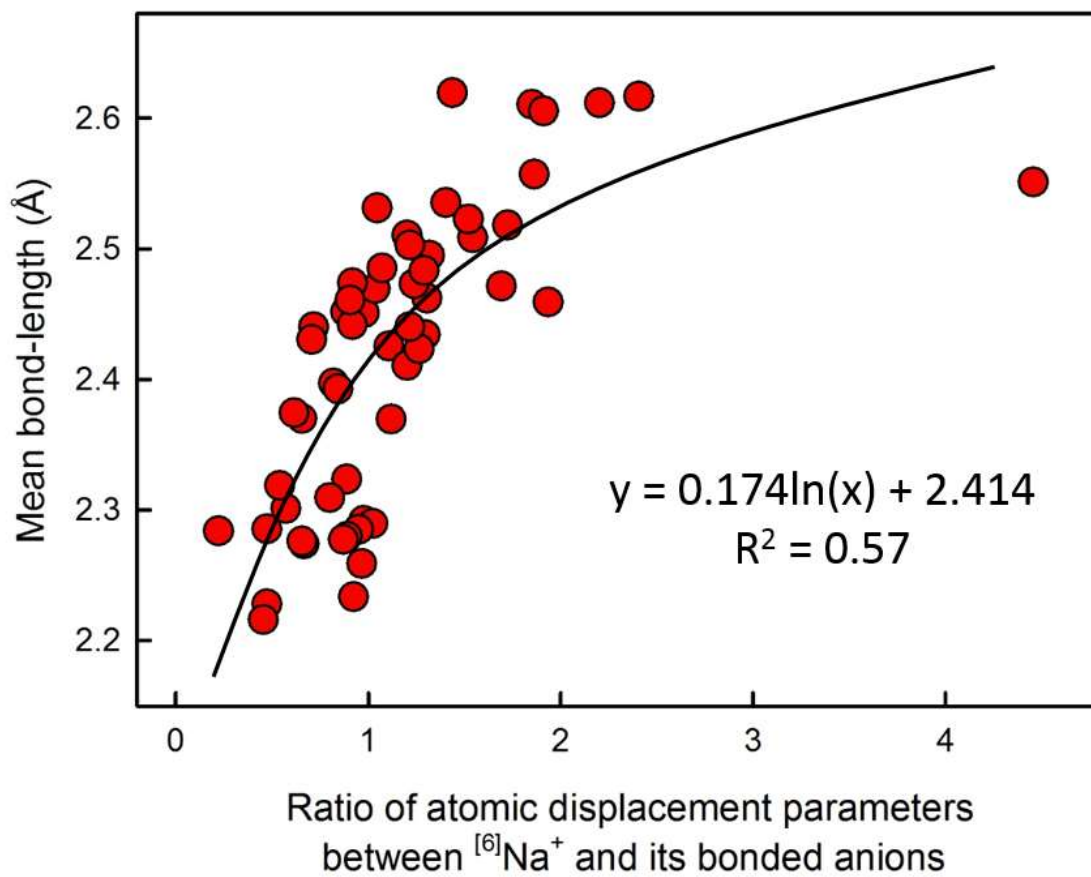


Figure 4.21 The effect of atomic displacement on mean bond-length. Values are for the ratio of the atomic displacement parameters between $^{[6]}\text{Na}^+$ and its bonded anions ($n = 56$).



4.13.2 Atomic displacement

We selected a sample of 56 coordination polyhedra from the parent distribution of $^{[6]}\text{Na}^+$ (920 coordination polyhedra) to examine other possible factors that may correlate with mean bond-length; these samples were selected so that they were representative of all values of distortion.

When examining the data for outliers that were possible erroneous data, we noticed very large relative variations in anisotropic-displacement or equivalent isotropic-displacement parameters in the atoms of the parent structures. cursory examination indicated that the magnitudes of these mean-bond-length outliers often correlated with the atomic displacement of the constituent cations and/or anions, suggesting that the central cation responds to an overly large coordination environment by increasing its dynamic (or static) displacement, while anions respond to an overly small cation-coordination environment by increasing their own displacement. Shannon (1993) and Shannon and Rossman (1992) have commented on the effect of the former when considering the additivity of fictive dielectric constants of ions in crystals, denoting this behaviour as “rattling”. Inspection of many structures eventually showed that the ratio $U_{\text{eq}}(\text{Na})/U_{\text{eq}}(\text{bonded anions})$ was most highly correlated with variation in mean bond-length. This is shown in Fig. 4.21; the observed correlation is logarithmic, with $R^2 = 0.57$. The fit of the correlation is of the same magnitude as that observed for distortion for the same sample of 56 coordination polyhedra ($R^2 = 0.52$). We note that Fig. 4.21 contains an apparent outlier with an atomic displacement ratio of 4.46, and that this single data point has considerable effect on whether the shape of the regression curve is logarithmic or linear. Removing this data point, a linear regression gives $R^2 = 0.62$, while the

logarithmic fit becomes $R^2 = 0.58$. However, we found no justification for the removal of this data point upon examination of the structure.

4.13.3 The relation between mean bond-length and atomic displacement

The correlation of mean bond-length with the atomic-displacement parameter has not been discussed extensively in previous work on variation in mean bond-lengths. In well-ordered crystal structures, there is generally a positive correlation between atomic-displacement parameters and coordination number. As shown above, for $^{[6]}\text{Na}^+$ there is a positive correlation between atomic-displacement parameters and mean bond-length. Taken together, these two observations suggest that the atomic displacements increase as the strength of the constituent chemical bonds decreases, and that such variation in atomic displacement accompanies variation in bond lengths that occur due to other factors such as bond-length distortion.

For a specific cation with a specific coordination number, one expects the following sequence: [1] over a particular range of distances, the atomic displacement increases with increasing distance; [2] with further increase in distance, continuous displacement changes to discontinuous displacement. *i.e.*, hopping of the central cation in an overly large coordination polyhedron; [3] static displacement of the cation away from the centre of the coordination polyhedron; [4] collapse of the anions forming the coordination polyhedron (perhaps via a ferroelastic phase transition), reducing the coordination number and changing the symmetry of the structure. When considering the factors affecting bond length, we need to recognize the relation between the type of

displacement behaviour of the central cation and mean bond-length. In stage [1], there is an increase in mean bond-length due to local differences in structures (together with a monotonic change in vibrational displacement). In stage [2], the question arises as to whether the observed mean distances are comparable with those of stage [1] as they are accompanied by large displacement parameters characteristic of atom hopping. In stage [3], the observed distances are not affected by atom hopping, but a change in coordination number of the central cation may be observed. When examining variation in mean bond-length for a specific ion in a particular coordination, it is important to limit the data to structures at stage [1], as once hopping occurs, an additional component is added to the measured mean bond-length that is not present at smaller distances.

4.14 Summary

[1] We have examined the bond-length distributions for 55 configurations of alkali-metal ions and 29 configurations of alkaline-earth-metal ions, for 4859 coordination polyhedra and 38,594 bond distances (alkali metals) and for 3038 coordination polyhedra and 24,487 bond distances (alkaline-earth metals).

[2] Bond lengths generally show a positively-skewed Gaussian distribution that originates from the variation in Born repulsion and Coulomb attraction as a function of interatomic distance.

[3] The skewness and kurtosis of these distributions generally decrease with increasing coordination number of the central cation, a result of decreasing Born repulsion with increasing coordination number.

[4] We confirm the following minimum coordination numbers: $^{[3]}\text{Li}^+$, $^{[3]}\text{Na}^+$, $^{[4]}\text{K}^+$, $^{[4]}\text{Rb}^+$, $^{[6]}\text{Cs}^+$, $^{[3]}\text{Be}^{2+}$, $^{[4]}\text{Mg}^{2+}$, $^{[6]}\text{Ca}^{2+}$, $^{[6]}\text{Sr}^{2+}$ and $^{[6]}\text{Ba}^{2+}$, but note that some reported examples are the result of extensive dynamic and/or positional short-range disorder and are not ordered arrangements.

[5] Some distributions of bond lengths are distinctly multi-modal (primarily bimodal), but for the alkali-metal and alkaline-earth-metal ions, this is often due to the occurrence of large numbers of structure refinements of a particular structure-type in which a particular cation is always present, *e.g.*, for $^{[8]}\text{Ca}^{2+}$, in which many refinements of garnet and vesuvianite structures lead to an over-representation of specific bond-lengths.

[6] For alkali-metal and alkaline-earth-metal ions, there is a positive correlation between incident bond-valence sum at the central cation and coordination number, the values

varying from 0.84 v.u. for $^{[5]}\text{K}^+$ to 1.06 v.u. for $^{[8]}\text{Li}^+$, and from 1.76 v.u. for $^{[7]}\text{Ba}^{2+}$ to 2.10 v.u. for $^{[12]}\text{Sr}^{2+}$.

[7] Unusually small or large coordination numbers are commonly associated with anomalous values of atomic displacement of the constituent cations and/or anions.

[8] For a sample of $^{[6]}\text{Na}$, the ratio $U_{\text{eq}}(\text{Na})/U_{\text{eq}}(\text{bonded anions})$ is partially correlated with $\langle^{[6]}\text{Na-O}\rangle$ mean bond-length ($R^2 = 0.57$), suggesting that the vibrational/displacement characteristics of the constituent ions are affected by mean bond-length for a fixed coordination number.

[9] Mean bond-lengths show a weak correlation with bond-length distortion from the mean value, but clearly also correlate with one or more other factors, e.g., atomic displacement. In particular, some coordination numbers show the widest variation in mean bond-length for zero distortion, e.g., Li^+ in [4]- and [6]-coordination, Na^+ in [4]- and [6]-coordination and K^+ in [6]-coordination, and for [4]-coordinated Be^{2+} , [4]- and [6]-coordinated Mg^{2+} , [6]- and [12]-coordinated Ca^{2+} , [6]- coordinated Sr^{2+} and [12]-coordinated Ba^{2+} .

[10] Bond-valence parameters for the 4 ions observed in coordinations higher than [12], K^+ , Rb^+ , Cs^+ and Ba^{2+} (Gagné & Hawthorne, 2015) were calculated for a maximum coordination number of [12]. Both sets of parameters give exactly the same result for anion bond-valence sums. However, the bond-valence parameters calculated for a maximum coordination number of [12] show much poorer correlation with mean observed bond-length and no correlation at all with ionization energy of the central cation, in contrast to the bond-valence parameters of Gagné & Hawthorne (2015).

4.15 Acknowledgements

This work was funded by UM Duff Roblin and GETS Fellowships, and an NSERC PGS-D3 Scholarship to OCG, and a Canada Research Chair and a Discovery grant to FCH from the Natural Sciences and Engineering Research Council of Canada, and by Canada Foundation for Innovation grants to FCH.

4.16 References

Baur, W. H. (1971). The prediction of bond length variations in silicon-oxygen bonds.

Am. Mineral. **56**, 1573-1599.

Brown, I.D. (2002). *The Chemical Bond in Inorganic Chemistry*. Oxford University Press.

Brown, I.D. & Altermatt, D. (1985). Bond-valence parameters obtained from a systematic analysis of the Inorganic Crystal-Structure Database. *Acta Cryst.* **B41**, 244-247.

Brown, I.D. & Shannon, R.D. (1973). Empirical bond-strength bond-length curves for oxides. *Acta Cryst.* **A29**, 266-282.

Burns, P.C., Ewing R.C., Hawthorne, F.C. (1997). The crystal chemistry of hexavalent *uranium*: polyhedron geometries, bond-valence parameters, and polymerization of polyhedra, *Can. Mineral.* **35**, 1551-1570

Chaminade, J.-P., Gravereau, P., Jubera, V. and Fouassier, C. (1999). A new family of lithium rare-earth oxyborates, $\text{LiLn}_6\text{O}_5(\text{BO}_3)_3$ ($\text{Ln} = \text{Pr-Tm}$): Crystal structure of the gadolinium phase $\text{LiGd}_6\text{O}_5(\text{BO}_3)_3$. *J.Solid State Chem.* **146**, 189-196.

Chenevas, J., Joubert, J.C. & Marezio, M. (1975) The synthesis and crystal structure of $\text{CaCu}_3\text{Mn}_4\text{O}_{12}$. *J.Solid State Chem.* **14**, 25-32.

Fallon, G.D. & Gatehouse, B.M. (1980). Crystal structures of some niobium and tantalum oxides. VIII. The $5\text{Rb}_2\text{O}:14.6\text{Ta}_2\text{O}_5$ phase—a tunnel structure. *J.Solid State Chem.* **34**, 193-198.

Gagné, O.C. & Hawthorne, F.C. (2015). Comprehensive derivation of bond-valence parameters for ion pairs involving oxygen. *Acta Cryst.* **B71**, 562-578

Gatehouse, B.M. & Grey, I.E. (1983). The crystal structure of $\text{Ca}_3\text{Zn}_4\text{Ti}_{16}\text{O}_{38}$. *J.Solid State Chem.* **46**, 151-155.

Haddad, A. & Jouini, T. (1997). Synthèse et structure cristalline de $\text{Rb}_5\text{VONb}_{14}\text{O}_{38}$. *J.Solid State Chem.* **134**, 10-16.

Hawthorne, F.C., Krivovichev, S.V. and Burns, P.C. (2000). The Crystal Chemistry of Sulfate Minerals. *Rev. Mineral. Geochem.* **40**, 1-112

Hawthorne, F.C and Huminicki, D.M.C (2002). The Crystal Chemistry of Beryllium, *Rev. Mineral. Geochem.* **48**, 333-404

Huminicki, D.M.C and Hawthorne, F.C (2002). The Crystal Chemistry Of The Phosphate Minerals, *Rev. Mineral. Geochem.* **48**, 123-253

- Horiuchi, H., Saito, A., Tachi, T. and Nagasawa, H. (1997). Structure of synthetic $\text{Li}_2(\text{Mg,Cu})\text{Cu}_2[\text{Si}_2\text{O}_6]_2$: A unique chain silicate related to pyroxene. *Am. Mineral.* **82**, 143-148.
- Iyi, N., Gobbels, M. & Matsui, Y. (1995). The Al-rich part of the system $\text{CaO-Al}_2\text{O}_3\text{-MgO}$ Part II. Structure refinement of two new magnetoplumbite-related phases. *J. Solid State Chem.* **120**, 364-371.
- Jahn, H.A. & Teller, E. (1937). Stability of polyatomic molecules in degenerate electronic states. *Proc. Roy. Soc., Ser. A* **161**, 220-235.
- Jubera, V., Graveriau, P., Chaminade, J.P. & Fouassier, C. (2001). A new oxyborate in the ternary phase diagrams $\text{Li}_2\text{O-Ln}_2\text{O}_3\text{-B}_2\text{O}_3$: $\text{Li}_2\text{Ln}_5\text{O}_4(\text{BO}_3)_3$ (Ln = Yb, Lu): Crystal structure of the ytterbium phase. *J. Solid State Chem.* **156**, 161-167.
- Kahlenburg, V. (2002). $\beta\text{-Sr}_{10}\text{Ga}_6\text{O}_{19}$: An oxygen deficient perovskite containing $[\text{Ga}_6\text{O}_{19}]$ -polyanions. *Solid State Sci.* **4**, 183-189.
- Lenaz, D., Skogby, H., Princivalle, F., Halenius, U. (2004). Structural changes and valence states in the $\text{MgCr}_2\text{O}_4\text{ - FeCr}_2\text{O}_4$ solid solution series. *Phys. Chem. Miner.* **31**, 633-642.
- Leoni, S., Niewa, R., Akselrud, L., Prots, Y., Schnelle, W., Göksuc, T., Cetinkol, M., Somer, M. and Kniep, R. (2005). Novel barium beryllates $\text{Ba}[\text{Be}_2\text{N}_2]$ and $\text{Ba}_3[\text{Be}_5\text{O}_8]$: syntheses, crystal structures and bonding properties. *Z. Anorg. Allg. Chem.* **631**, 1818-1824.

Lii, K.H., Wang, Y.P., Chneg, C.Y., Wang, S.L. & Ku, H.C. (1990). Crystal structure and magnetic properties of a vanadium (IV) pyrophosphate: $\text{Rb}_2\text{V}_3\text{P}_4\text{O}_{17}$. *J. Chin. Chem. Soc.* **37**, 141-149.

Lipp, C. & Schleid, T. (2006). $\text{Rb}_6\text{LiPr}_{11}\text{Cl}_{16}[\text{SeO}_3]_{12}$: A chloride-derivatized rubidium lithium praseodymium(III) oxoselenate(IV). *Z.Anorg.Allg.Chem.* **632**, 2226-2231.

Majzlan, J., Drahota, P. and Filippi, M. (2014). Paragenesis and crystal chemistry of arsenic minerals. *Rev. Mineral. Geochem.* **79**, 17-184.

Metcalf-Johansen, J. & Hazell, R.G. (1976). The crystal structure of Sorensenite, $\text{Na}_4\text{SnBe}_2(\text{Si}_3\text{O}_9)_2\text{H}_2\text{O}$. *Acta Cryst.*, **B32**, 2533-2556.

Mills, S.G. & Christy A.G. (2013). Revised values of the bond-valence parameters for Te-IV-O, Te-VI-O and Te-IV-Cl. *Acta Cryst.*, **B69**, 145-149.

Möller, A. (1998). Synthesis, Structures, Magnetic Properties, and Absorption Spectra of the Alkaline Oxocobaltates(II): Li_6CoO_4 , Na_4CoO_3 , and $\text{Na}_{10}\text{Co}_4\text{O}_9$. *Chem. Mater.* **10**, 3196-3201.

Ozaki, Y., Ghedira, M., Chenevas, J., Joubert, J.C. & Marezio, M. (1977). High-pressure synthesis and bond lengths of calcium copper germanium oxide $\text{CaCu}_3\text{Ge}_4\text{O}_{12}$. *Acta Cryst.* **B33**, 3615-3617.

Pushcharovskii, D.Yu., Gobechiya, E.R., Pasero, M., Merlino, S. & Dimitrova, O.V. (2002). Hydrothermal synthesis and crystal structures of (Li, Ba)-nanoborate, $\text{LiBaB}_9\text{O}_{15}$, and Ba-borophosphate, BaBPO_5 . *J. Alloys Compd.* **339**, 70-75.

- Richardson, I.G. (2013). The importance of proper crystal-chemical and geometrical reasoning demonstrated using layered single and double hydroxides, *Acta Cryst.*, **B69**, 150-162.
- Robinson, K., Gibbs, G.V. & Ribbe, P.H. (1971) A quantitative measure of distortion in coordination polyhedra. *Science*, **172**, 567-570.
- Sabrowsky, H. and Vogt, P. (1987). RbLiO: Eine Variante der KNaS-Struktur. *Z. Anorg. Allg. Chem.* **553**, 226-230.
- Sabrowsky, H., Mertens, P. & Thimm, A. (1985b). KLiO: Ein Oxid mit dreifach koordiniertem Lithium. *Z. Kristallogr.* **171**, 1-6.
- Sabrowsky, H. and Schroeer, U. (1982). Darstellung und Kristallstruktur von $K^+ Na^+ O$ und $Rb^+ Na^+ O$. *Z. Naturforsch. B. Anorg. Chem. Org. Chem.* **37**, 818-819.
- Sabrowsky, H., Thimm, A. and Vogt-Mertens, P. (1985a). Kristallstruktur von RbNaO. *Z. Naturforsch. B. Anorg. Chem. Org. Chem.* **40**, 1761-1762.
- Schindler, M., Hawthorne, F.C. and Baur, W. H. (2000). Crystal chemical aspects of vanadium: polyhedral geometries, characteristic bond valences, and polymerization of (VO_n) polyhedra, *Chem. Mater.* **12**, 1248-1259.
- Shannon, R.D. (1976). Revised effective ionic radii and systematic studies of interatomic distances in halides and chalcogenides, *Acta Cryst. A* **32**, 751–767.
- Shannon, R.D. (1993). Dielectric polarizabilities of ions in oxides and fluorides. *J. Appl. Phys.*, **73**, 348-366.

Shannon, R.D. and Rossman, G.R. (1992). Dielectric constants of silicate garnets and the oxide additivity rule. *Am. Mineral.* **77**, 94-10

Semenov, E. I., Gerassimovsky, V., I., Maksimova, N. V., Andersen, S. & Petersen, O. V. (1965) Sorensenite, new sodium-beryllium-tin-silicate from the Ilímaussaq intrusion, South Greenland. *Meddelelser om Grønland*, **181**, 1-19.

Urusov, V.S. (2003) Theoretical analysis and empirical manifestation of the distortion theorem. *Z. Kristallogr.*, **218**, 709-718.

Urusov, V.S. (2015) Terms of parity and distortion of coordination polyhedra in inorganic crystal chemistry. *J. Struct. Chem.*, **55**, 1277-1292.

Wander, C.F.M., Bickmore, B.R., Lind, L., Andros, C., Hunt, J., Checketts, H and Goodell, T. (2015). AIM analysis and the form of the bond-valence equation. *Am. Mineral.* **100**, 160-171.

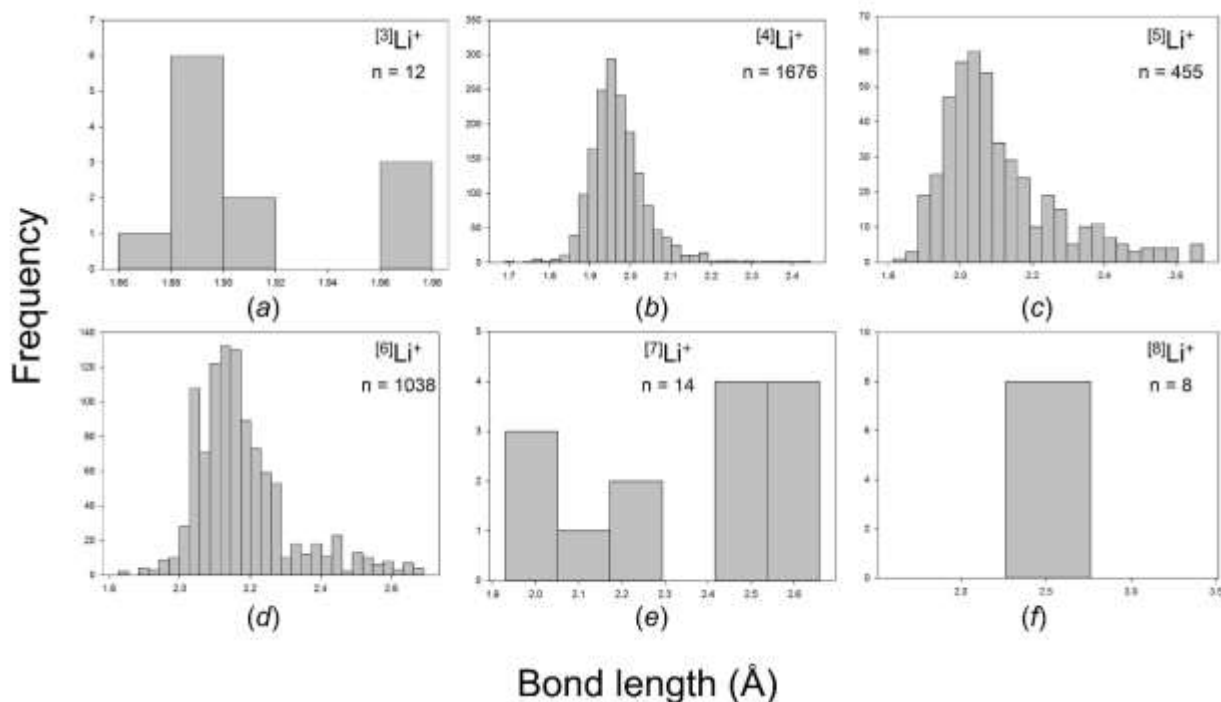
Wilkins, J. and Müller-Buschbaum, Hk. (1991). Einkristalluntersuchung an $\text{Ba}_3\text{CaRu}_2\text{O}_9$. *J. Alloys Compd.* **177**, L31-L33.

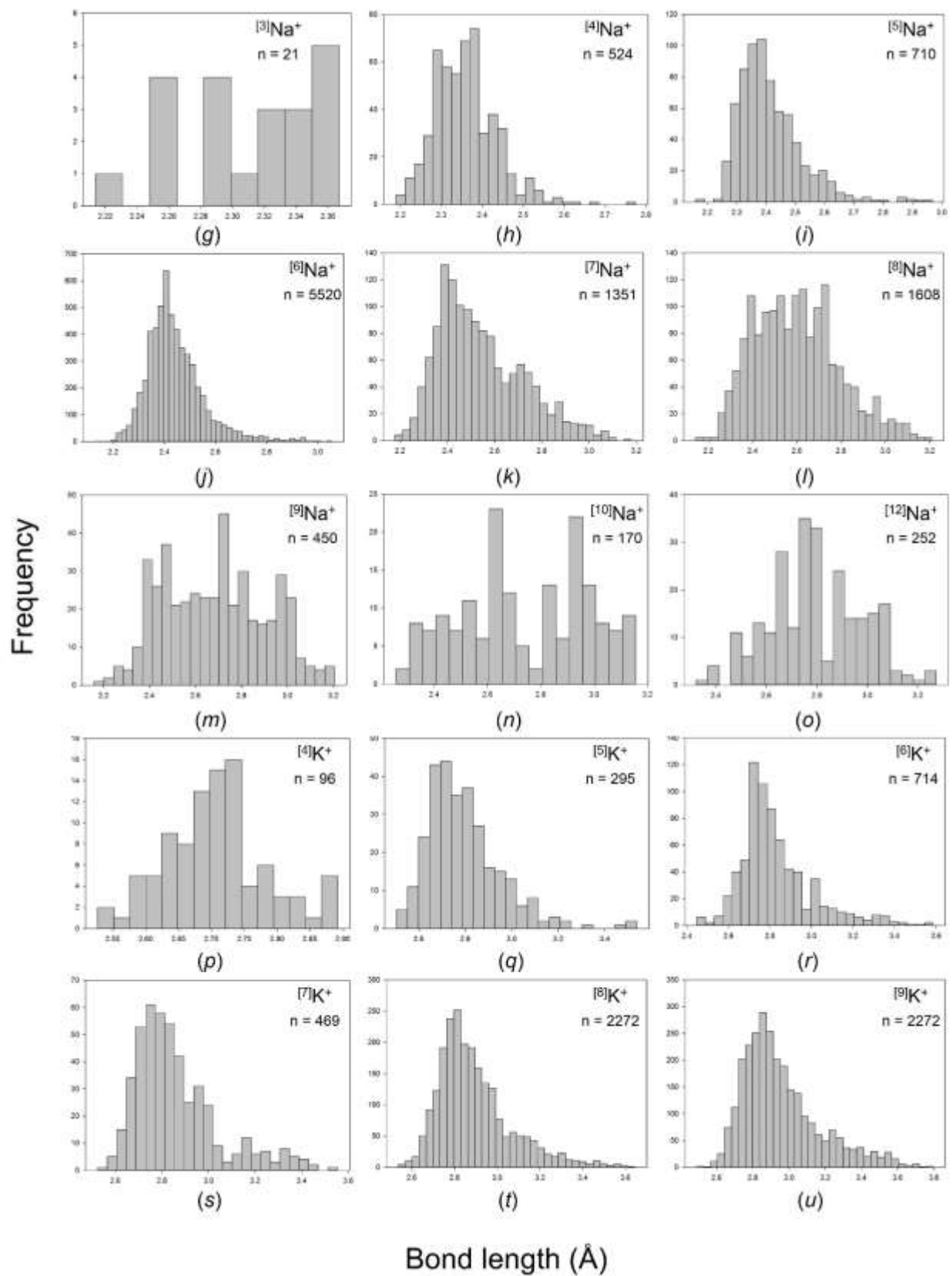
4.17 Appendix A: Supplementary material

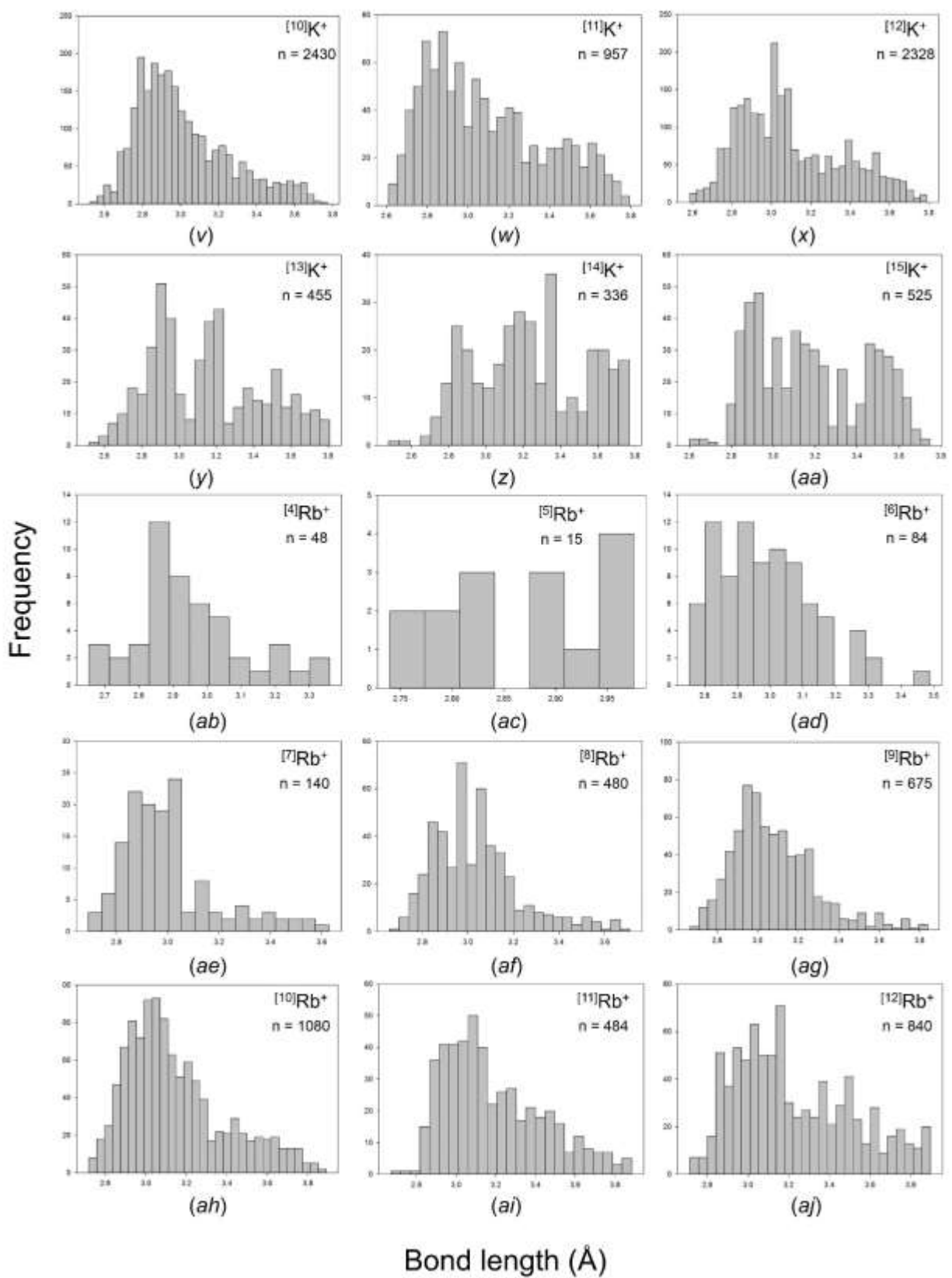
Supplementary material for

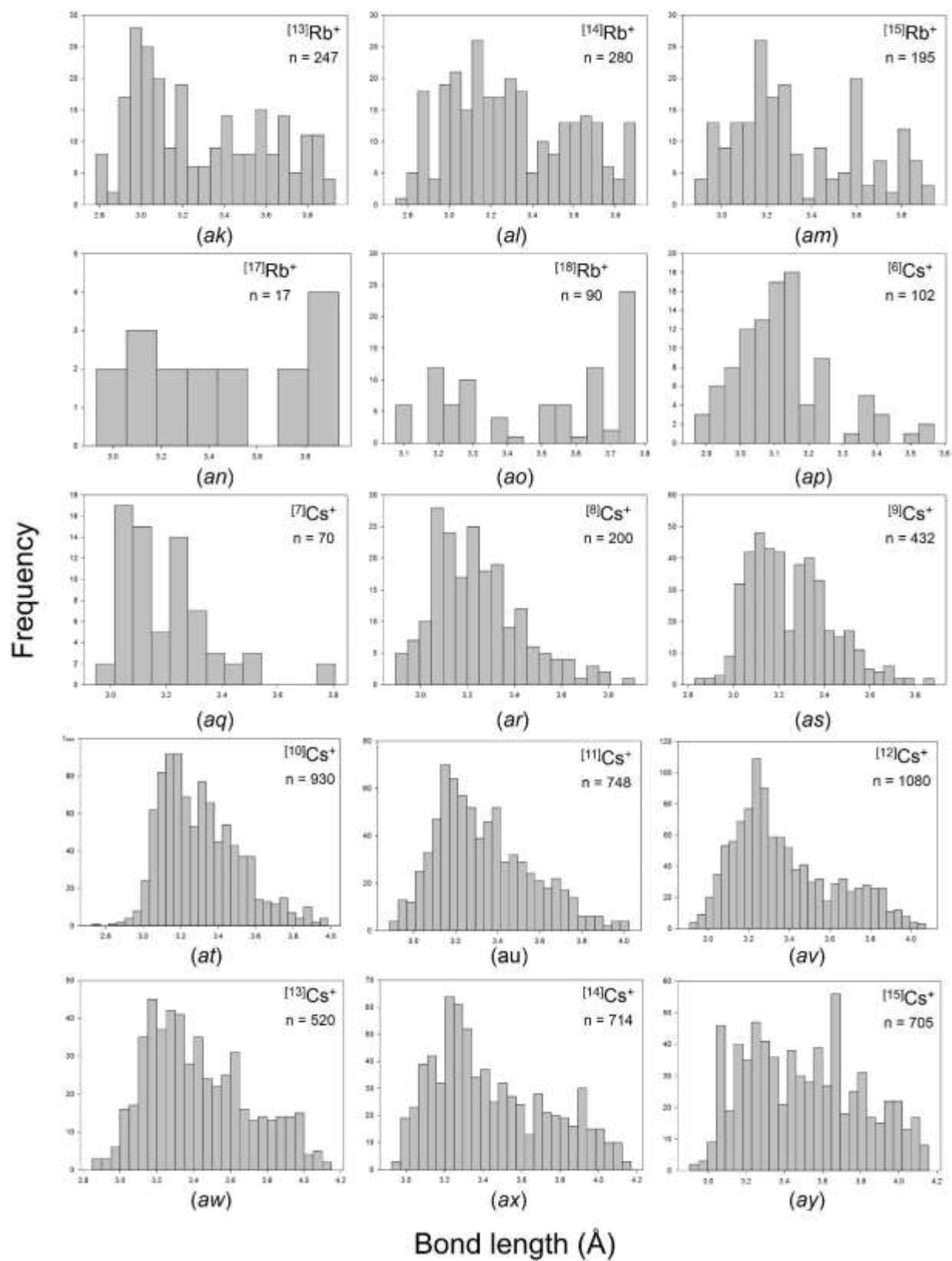
Bond-length distributions for ions bonded to oxygen: Alkali and alkaline-earth metals

Figure 4.S1 Bond-length distributions for all configurations of the alkali-metal ions bonded to O^{2-} : (a) $[^3]Li^+$, (b) $[^4]Li^+$, (c) $[^5]Li^+$, (d) $[^6]Li^+$, (e) $[^7]Li^+$, (f) $[^8]Li^+$, (g) $[^3]Na^+$, (h) $[^4]Na^+$, (i) $[^5]Na^+$, (j) $[^6]Na^+$, (k) $[^7]Na^+$, (l) $[^8]Na^+$, (m) $[^9]Na^+$, (n) $[^{10}]Na^+$, (o) $[^{12}]Na^+$, (p) $[^4]K^+$, (q) $[^5]K^+$, (r) $[^6]K^+$, (s) $[^7]K^+$, (t) $[^8]K^+$, (u) $[^9]K^+$, (v) $[^{10}]K^+$, (w) $[^{11}]K^+$, (x) $[^{12}]K^+$, (y) $[^{13}]K^+$, (z) $[^{14}]K^+$, (aa) $[^{15}]K^+$, (ab) $[^4]Rb^+$, (ac) $[^5]Rb^+$, (ad) $[^6]Rb^+$, (ae) $[^7]Rb^+$, (af) $[^8]Rb^+$, (ag) $[^9]Rb^+$, (ah) $[^{10}]Rb^+$, (ai) $[^{11}]Rb^+$, (aj) $[^{12}]Rb^+$, (ak) $[^{13}]Rb^+$, (al) $[^{14}]Rb^+$, (am) $[^{15}]Rb^+$, (an) $[^{17}]Rb^+$, (ao) $[^{18}]Rb^+$, (ap) $[^6]Cs^+$, (aq) $[^7]Cs^+$, (ar) $[^8]Cs^+$, (as) $[^9]Cs^+$, (at) $[^{10}]Cs^+$, (au) $[^{11}]Cs^+$, (av) $[^{12}]Cs^+$, (aw) $[^{13}]Cs^+$, (ax) $[^{14}]Cs^+$, (ay) $[^{15}]Cs^+$, (az) $[^{16}]Cs^+$, (ba) $[^{17}]Cs^+$, (bb) $[^{18}]Cs^+$, (bc) $[^{20}]Cs^+$.









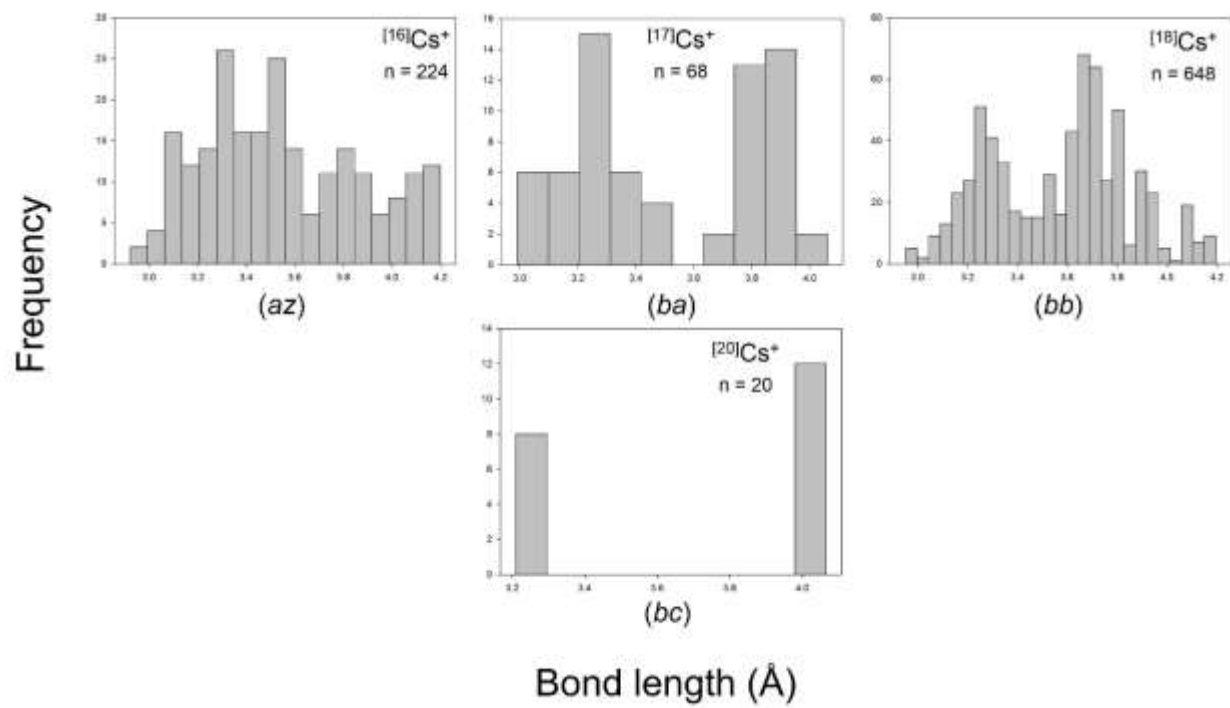
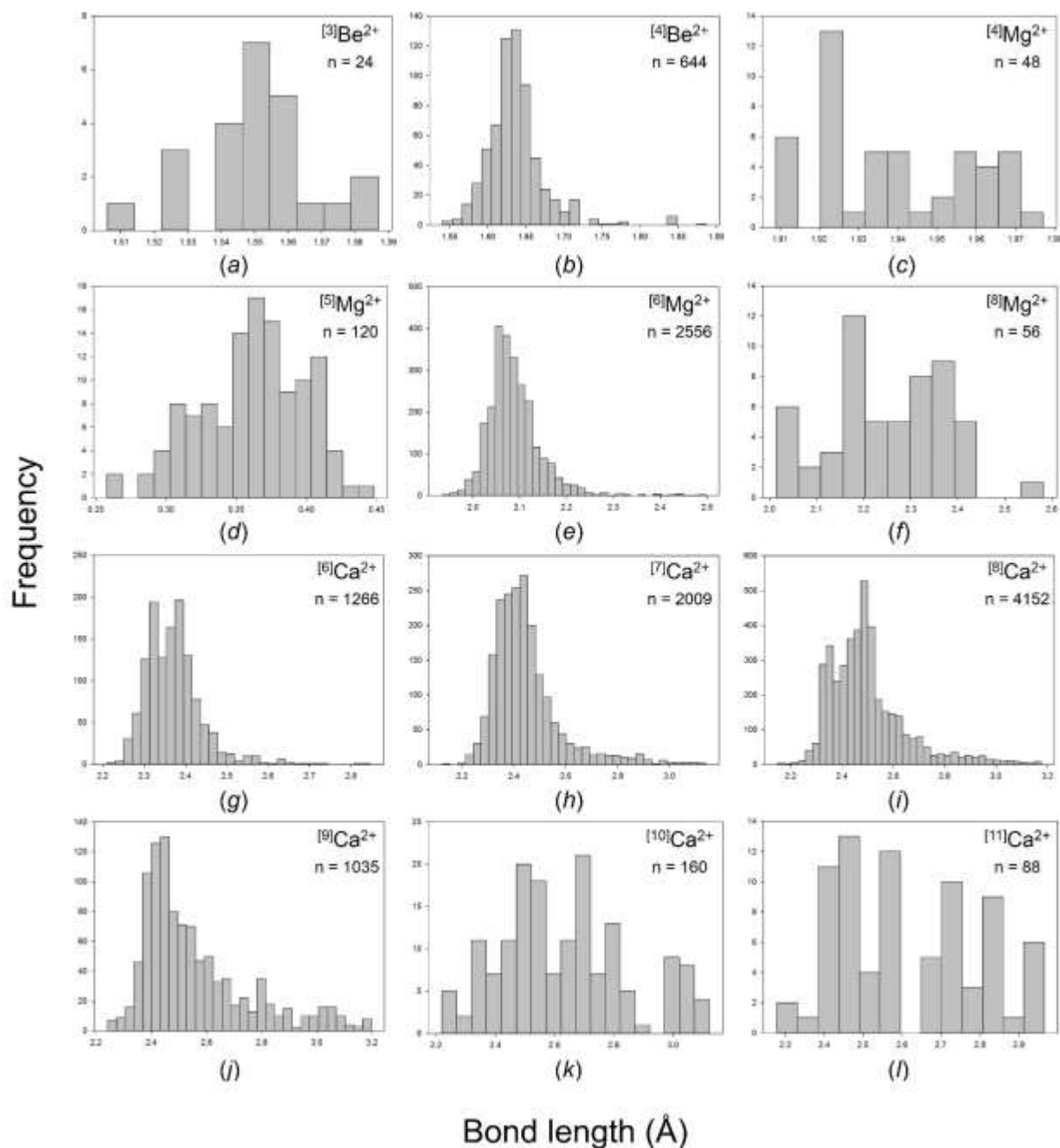
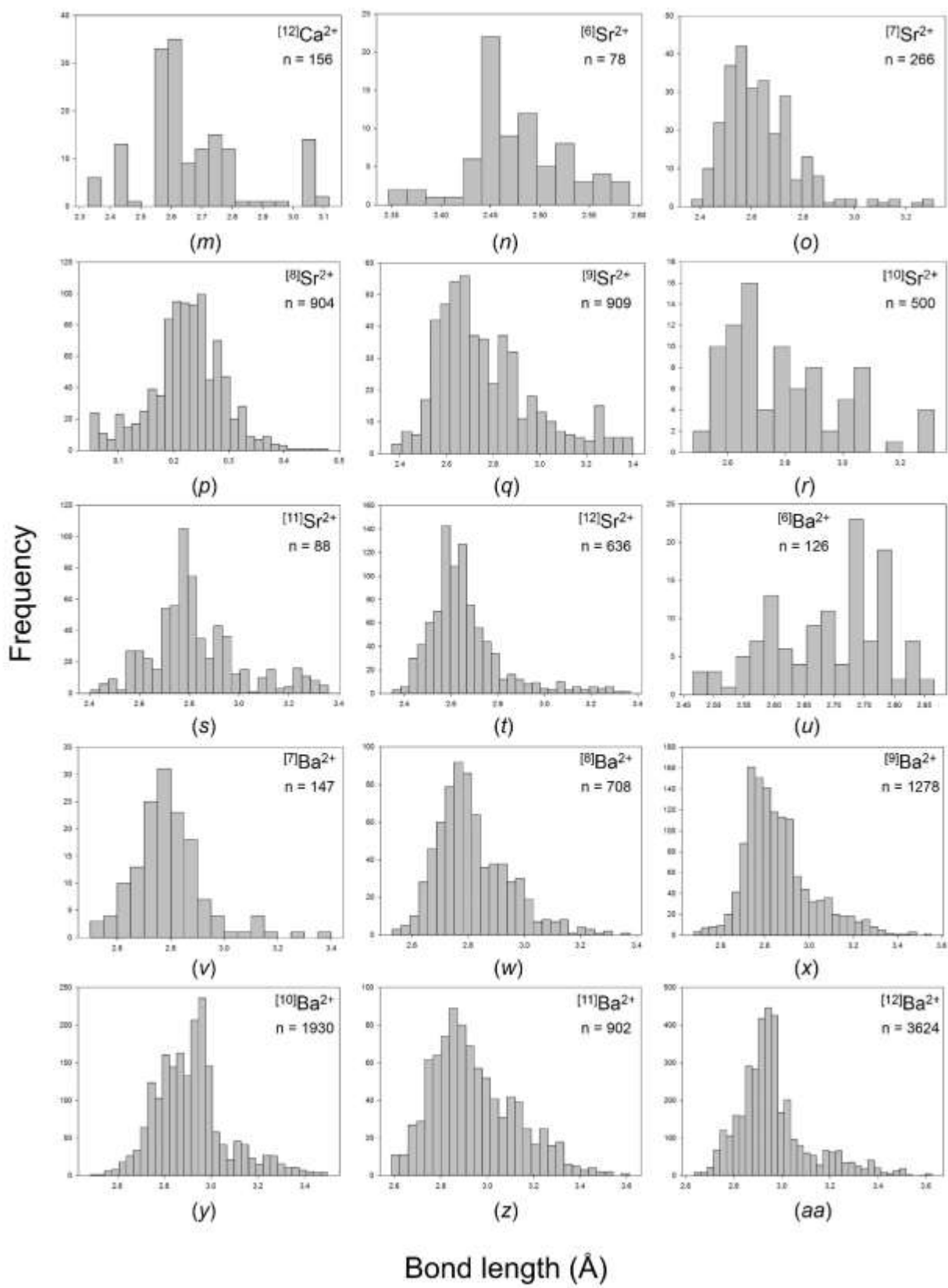


Figure 4.S2 Bond-length distributions for all configurations of the alkaline-earth-metal ions bonded to O^{2-} : (a) $[3]Be^{2+}$, (b) $[4]Be^{2+}$, (c) $[4]Mg^{2+}$, (d) $[5]Mg^{2+}$, (e) $[6]Mg^{2+}$, (f) $[8]Mg^{2+}$, (g) $[6]Ca^{2+}$, (h) $[7]Ca^{2+}$, (i) $[8]Ca^{2+}$, (j) $[9]Ca^{2+}$, (k) $[10]Ca^{2+}$, (l) $[11]Ca^{2+}$, (m) $[12]Ca^{2+}$, (n) $[6]Sr^{2+}$, (o) $[7]Sr^{2+}$, (p) $[8]Sr^{2+}$, (q) $[9]Sr^{2+}$, (r) $[10]Sr^{2+}$, (s) $[11]Sr^{2+}$, (t) $[12]Sr^{2+}$, (u) $[6]Ba^{2+}$, (v) $[7]Ba^{2+}$, (w) $[8]Ba^{2+}$, (x) $[9]Ba^{2+}$, (y) $[10]Ba^{2+}$, (z) $[11]Ba^{2+}$, (aa) $[12]Ba^{2+}$, (ab) $[13]Ba^{2+}$, (ac) $[14]Ba^{2+}$.





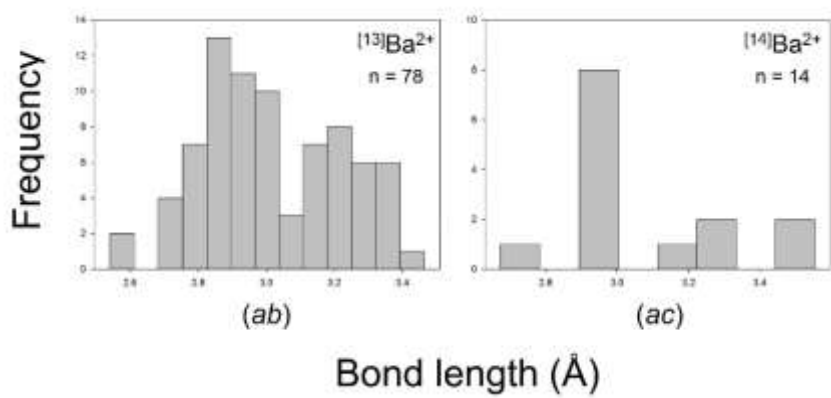
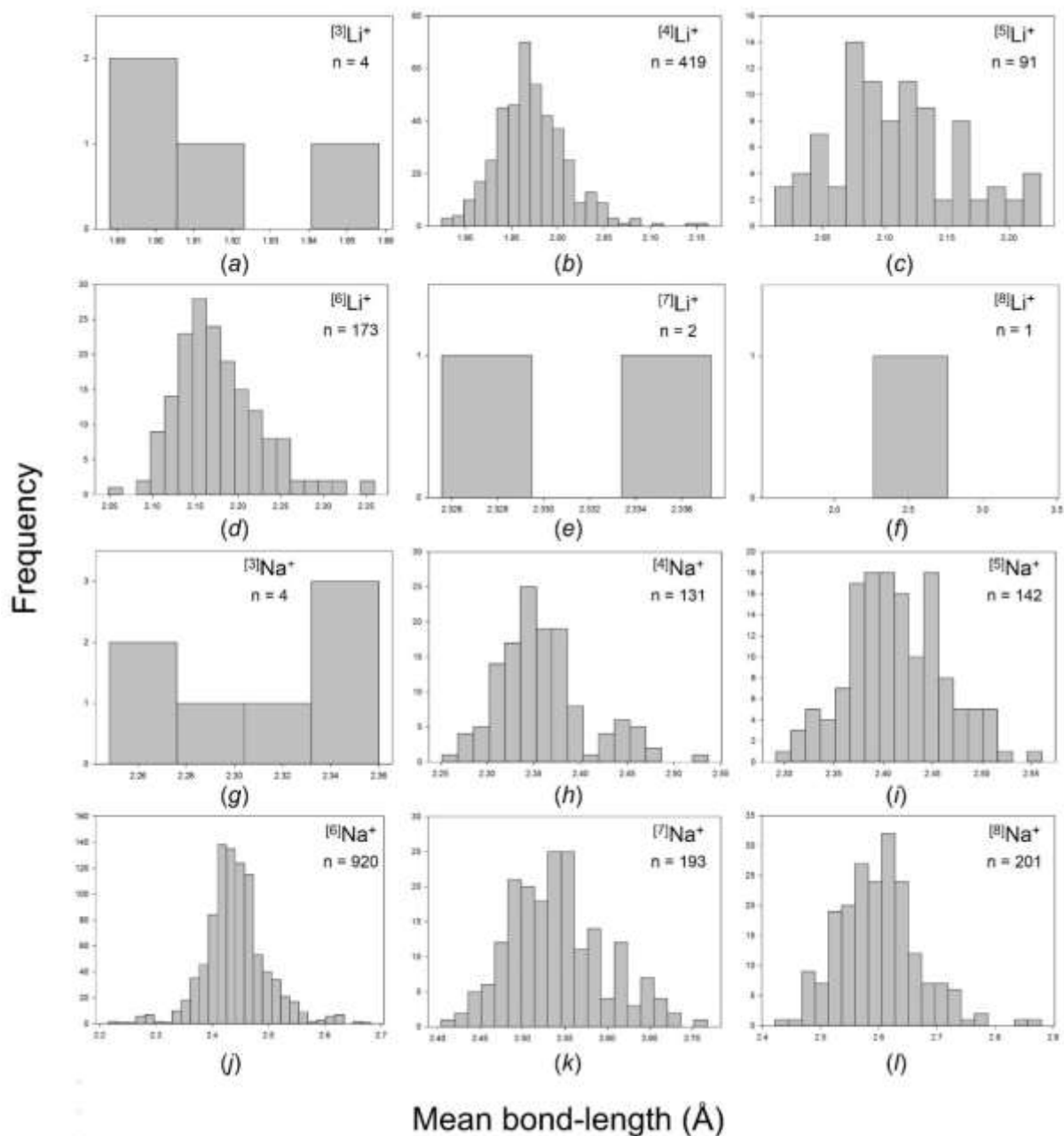
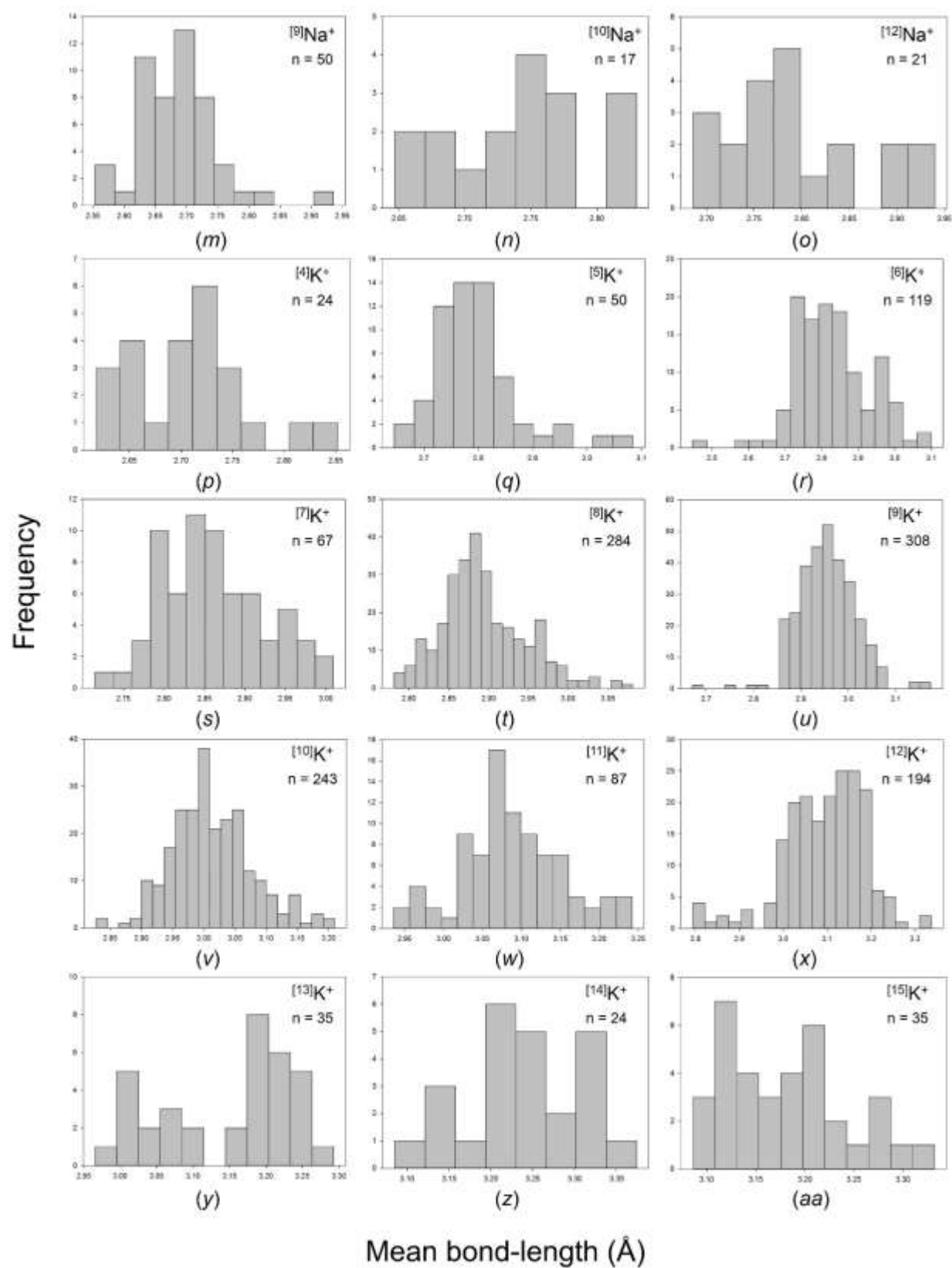
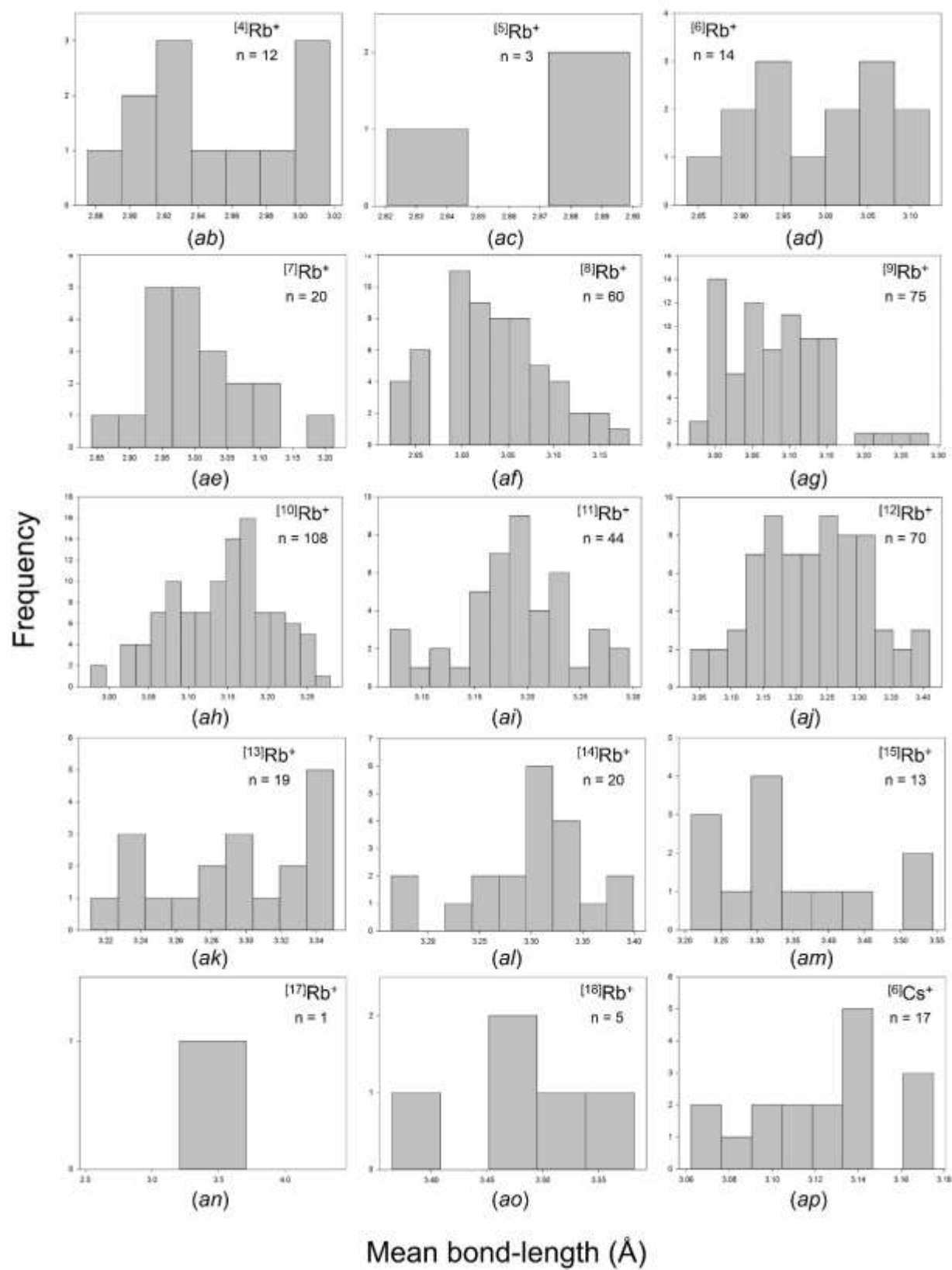


Figure 4.S3 Mean bond-length distributions for all configurations of the alkali-metal ions bonded to O^{2-} : (a) $[^3]Li^+$, (b) $[^4]Li^+$, (c) $[^5]Li^+$, (d) $[^6]Li^+$, (e) $[^7]Li^+$, (f) $[^8]Li^+$, (g) $[^3]Na^+$, (h) $[^4]Na^+$, (i) $[^5]Na^+$, (j) $[^6]Na^+$, (k) $[^7]Na^+$, (l) $[^8]Na^+$, (m) $[^9]Na^+$, (n) $[^{10}]Na^+$, (o) $[^{12}]Na^+$, (p) $[^4]K^+$, (q) $[^5]K^+$, (r) $[^6]K^+$, (s) $[^7]K^+$, (t) $[^8]K^+$, (u) $[^9]K^+$, (v) $[^{10}]K^+$, (w) $[^{11}]K^+$, (x) $[^{12}]K^+$, (y) $[^{13}]K^+$, (z) $[^{14}]K^+$, (aa) $[^{15}]K^+$, (ab) $[^4]Rb^+$, (ac) $[^5]Rb^+$, (ad) $[^6]Rb^+$, (ae) $[^7]Rb^+$, (af) $[^8]Rb^+$, (ag) $[^9]Rb^+$, (ah) $[^{10}]Rb^+$, (ai) $[^{11}]Rb^+$, (aj) $[^{12}]Rb^+$, (ak) $[^{13}]Rb^+$, (al) $[^{14}]Rb^+$, (am) $[^{15}]Rb^+$, (an) $[^{17}]Rb^+$, (ao) $[^{18}]Rb^+$, (ap) $[^6]Cs^+$, (aq) $[^7]Cs^+$, (ar) $[^8]Cs^+$, (as) $[^9]Cs^+$, (at) $[^{10}]Cs^+$, (au) $[^{11}]Cs^+$, (av) $[^{12}]Cs^+$, (aw) $[^{13}]Cs^+$, (ax) $[^{14}]Cs^+$, (ay) $[^{15}]Cs^+$, (az) $[^{16}]Cs^+$, (ba) $[^{17}]Cs^+$, (bb) $[^{18}]Cs^+$, (bc) $[^{20}]Cs^+$.







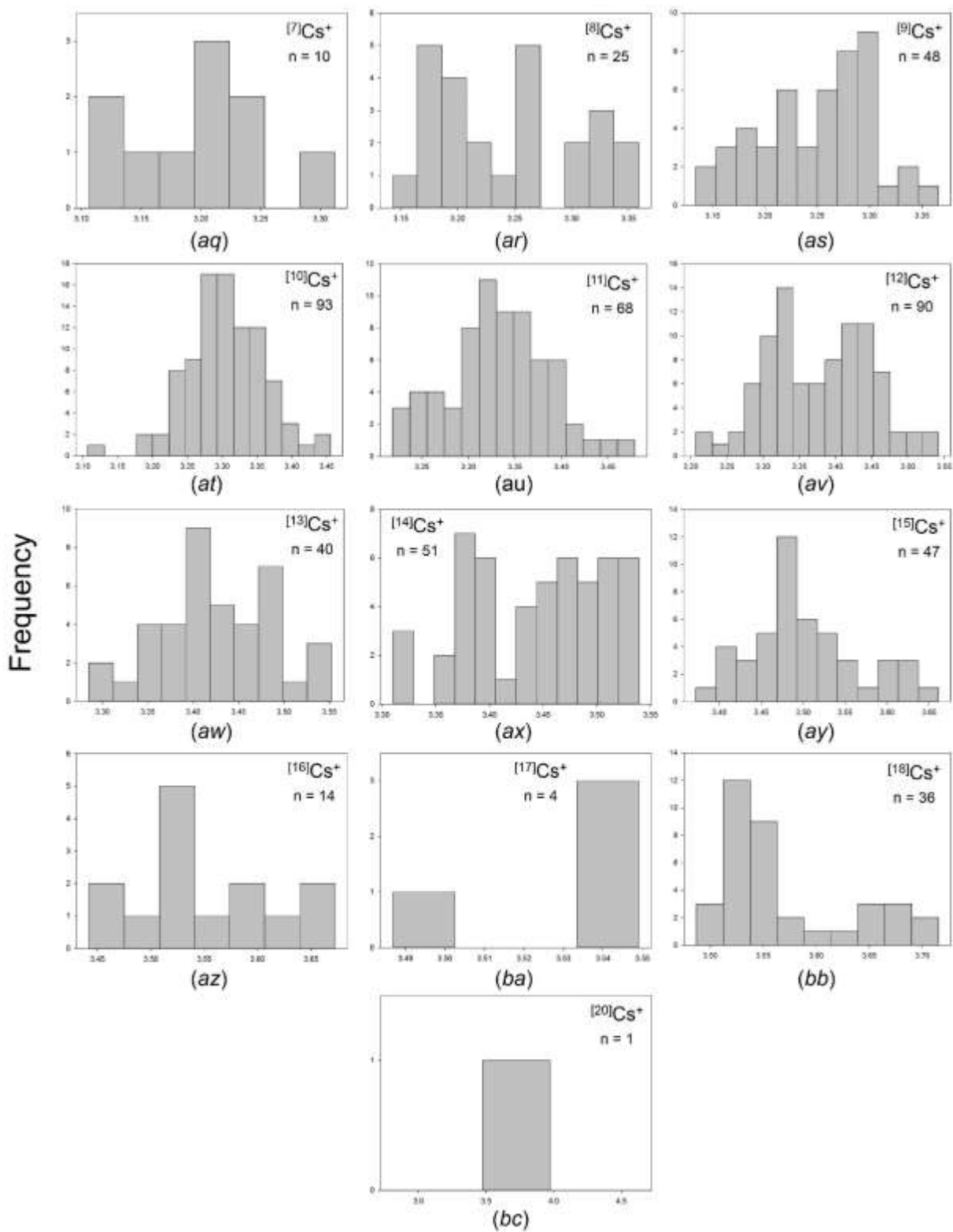
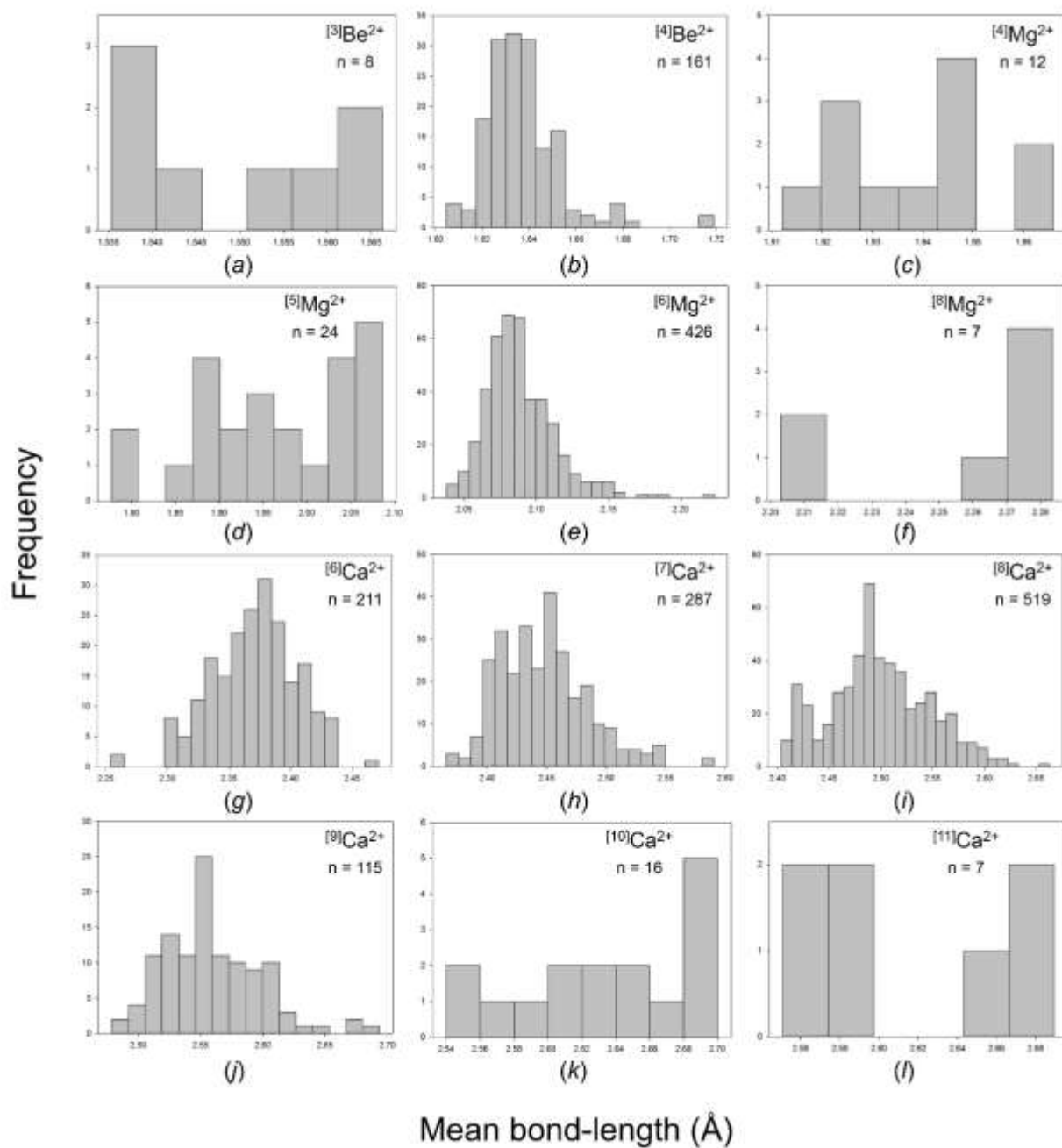
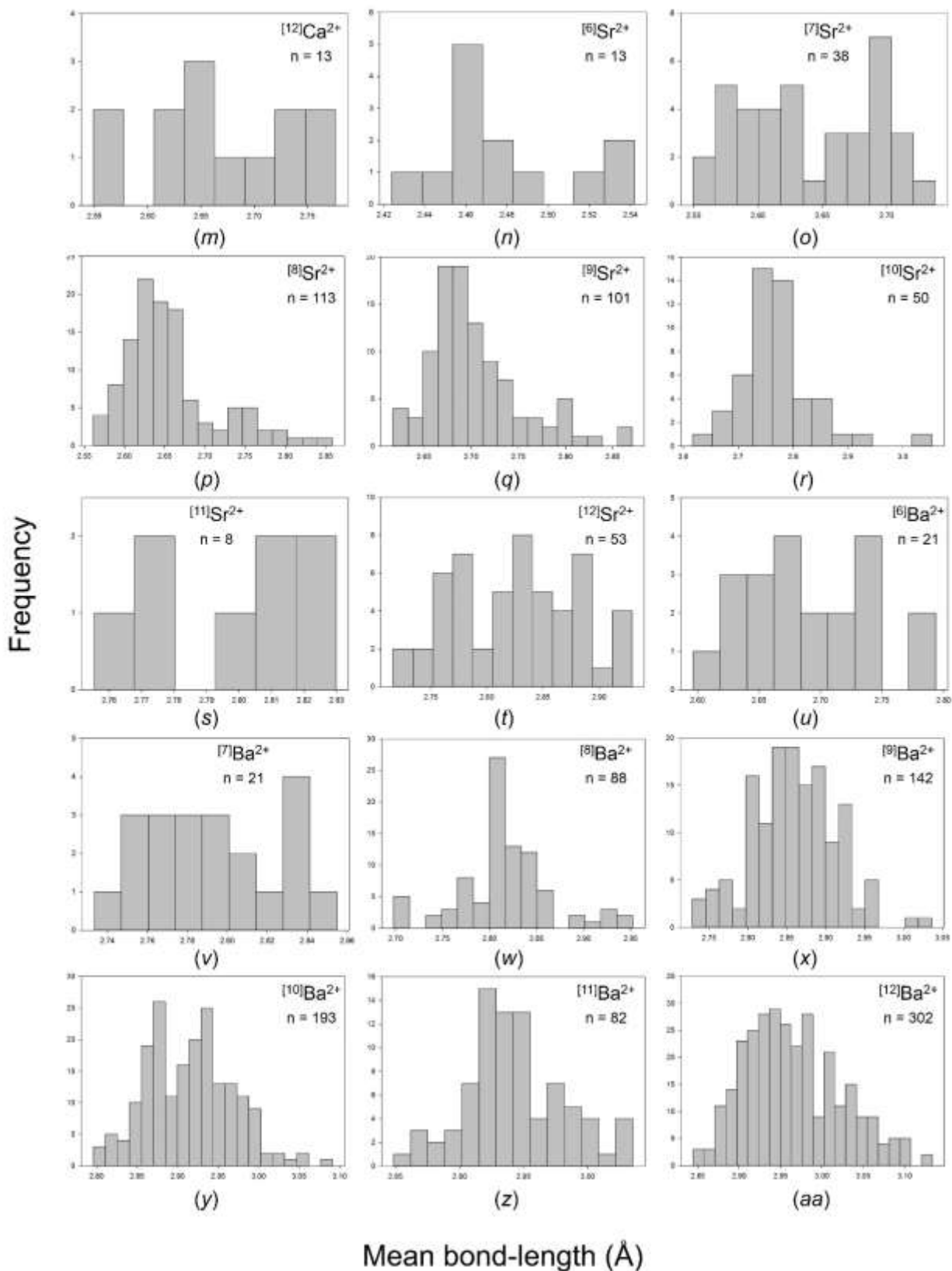


Figure 4.S4 Mean bond-length distributions for all configurations of the alkaline-earth-metal ions bonded to O^{2-} : (a) $[^3]Be^{2+}$, (b) $[^4]Be^{2+}$, (c) $[^4]Mg^{2+}$, (d) $[^5]Mg^{2+}$, (e) $[^6]Mg^{2+}$, (f) $[^8]Mg^{2+}$, (g) $[^6]Ca^{2+}$, (h) $[^7]Ca^{2+}$, (i) $[^8]Ca^{2+}$, (j) $[^9]Ca^{2+}$, (k) $[^{10}]Ca^{2+}$, (l) $[^{11}]Ca^{2+}$, (m) $[^{12}]Ca^{2+}$, (n) $[^6]Sr^{2+}$, (o) $[^7]Sr^{2+}$, (p) $[^8]Sr^{2+}$, (q) $[^9]Sr^{2+}$, (r) $[^{10}]Sr^{2+}$, (s) $[^{11}]Sr^{2+}$, (t) $[^{12}]Sr^{2+}$, (u) $[^6]Ba^{2+}$, (v) $[^7]Ba^{2+}$, (w) $[^8]Ba^{2+}$, (x) $[^9]Ba^{2+}$, (y) $[^{10}]Ba^{2+}$, (z) $[^{11}]Ba^{2+}$, (aa) $[^{12}]Ba^{2+}$, (ab) $[^{13}]Ba^{2+}$, (ac) $[^{14}]Ba^{2+}$.





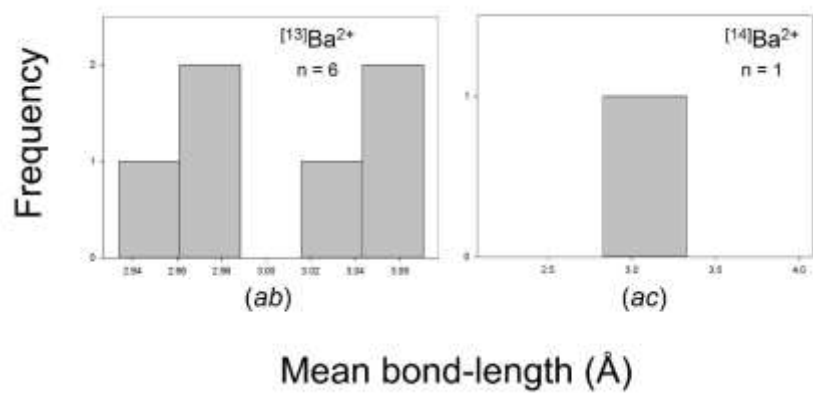
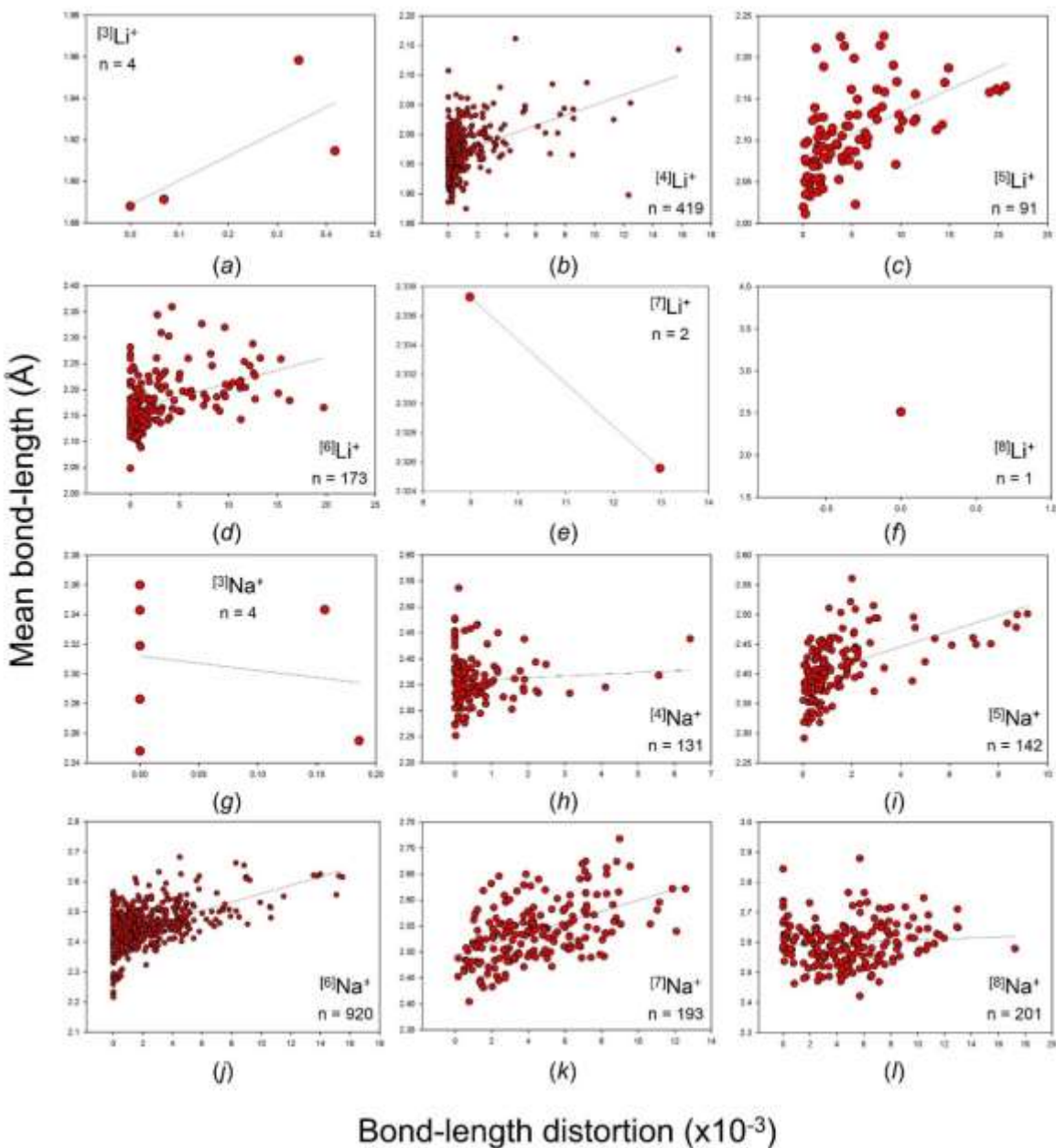
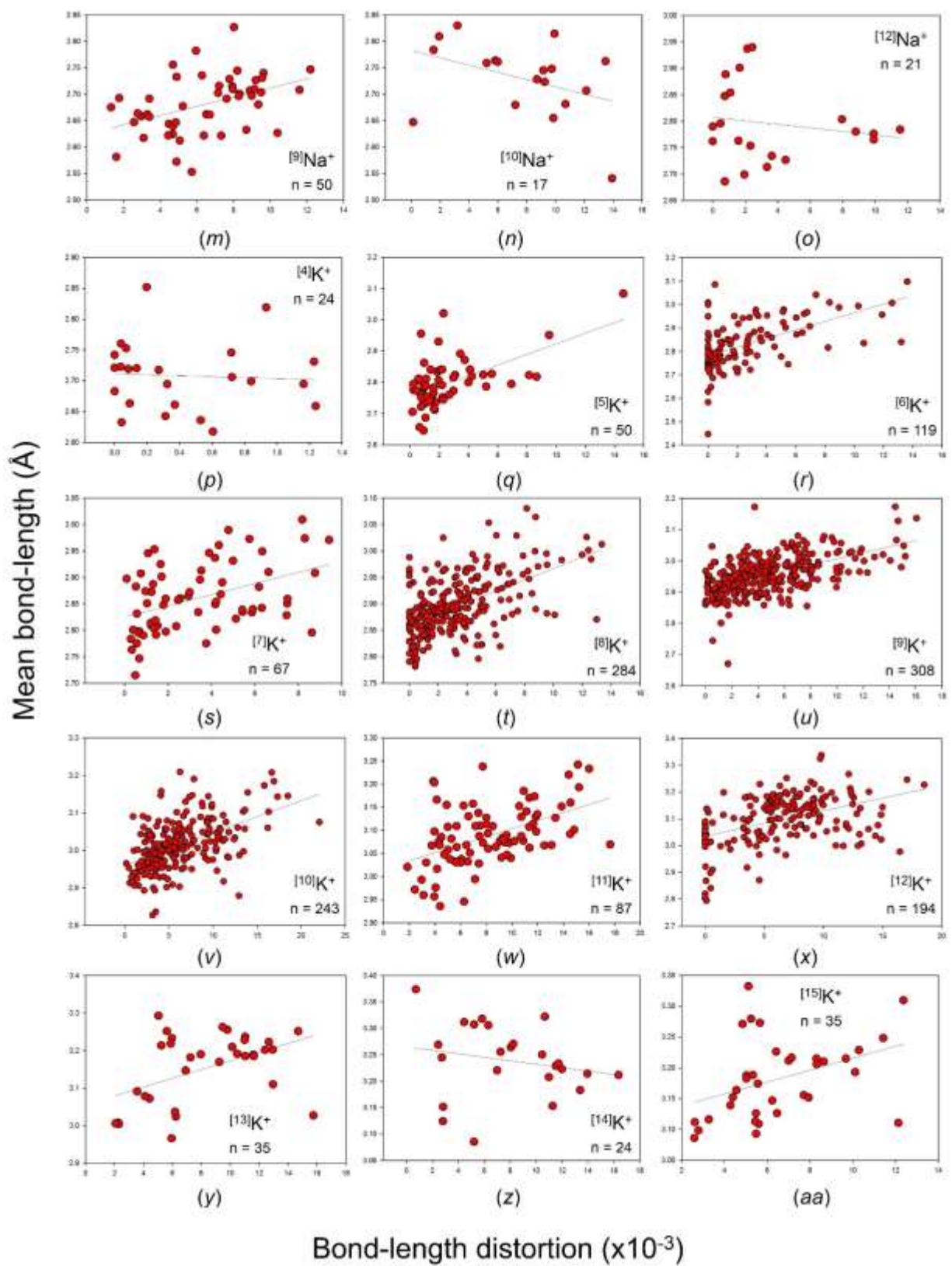
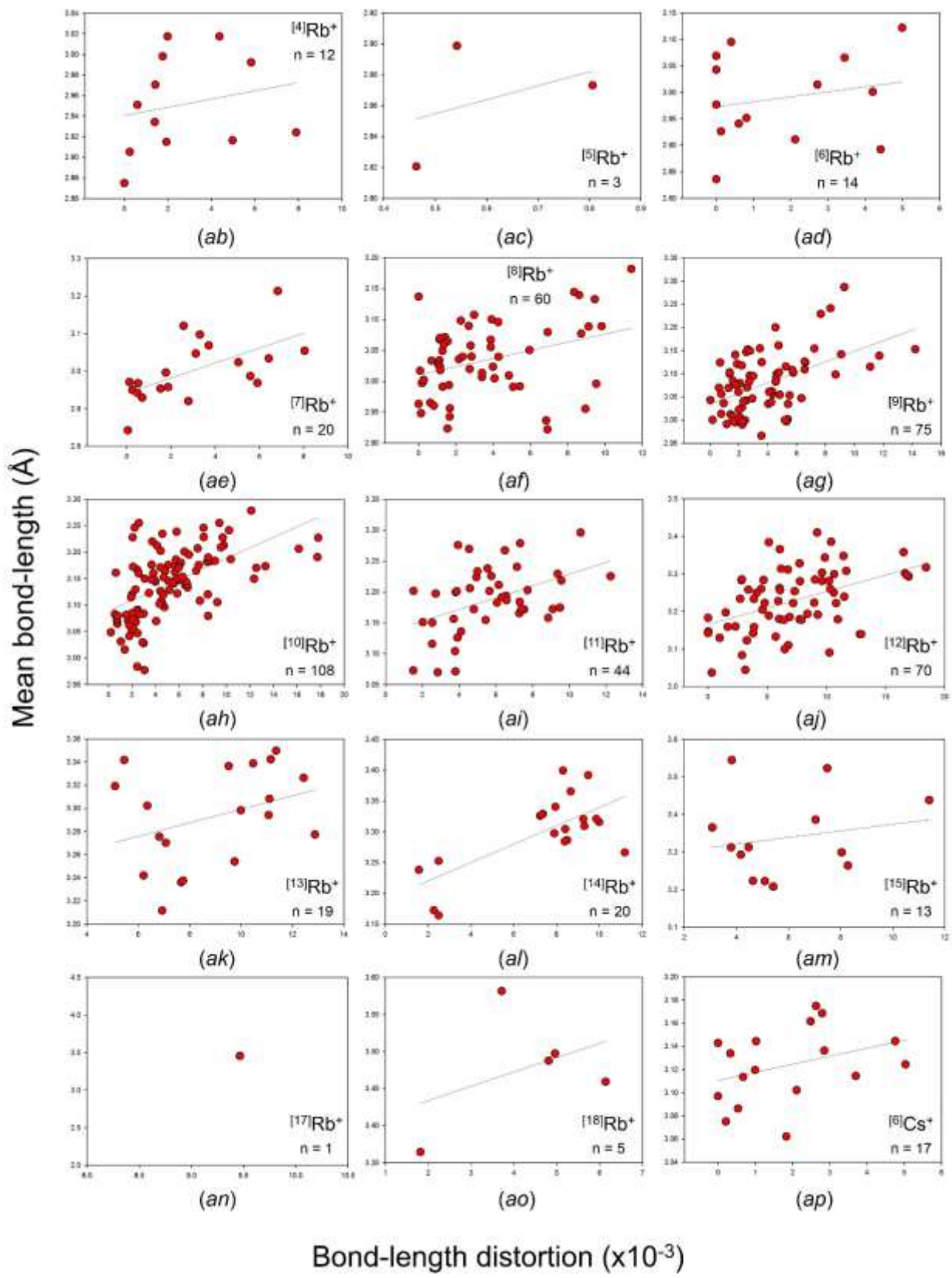


Figure 4.S5 The effect of bond-length distortion on mean bond-length for all configurations of the alkaline-earth-metal ions bonded to O^{2-} : (a) $[^3]Li^+$, (b) $[^4]Li^+$, (c) $[^5]Li^+$, (d) $[^6]Li^+$, (e) $[^7]Li^+$, (f) $[^8]Li^+$, (g) $[^3]Na^+$, (h) $[^4]Na^+$, (i) $[^5]Na^+$, (j) $[^6]Na^+$, (k) $[^7]Na^+$, (l) $[^8]Na^+$, (m) $[^9]Na^+$, (n) $[^{10}]Na^+$, (o) $[^{12}]Na^+$, (p) $[^4]K^+$, (q) $[^5]K^+$, (r) $[^6]K^+$, (s) $[^7]K^+$, (t) $[^8]K^+$, (u) $[^9]K^+$, (v) $[^{10}]K^+$, (w) $[^{11}]K^+$, (x) $[^{12}]K^+$, (y) $[^{13}]K^+$, (z) $[^{14}]K^+$, (aa) $[^{15}]K^+$, (ab) $[^4]Rb^+$, (ac) $[^5]Rb^+$, (ad) $[^6]Rb^+$, (ae) $[^7]Rb^+$, (af) $[^8]Rb^+$, (ag) $[^9]Rb^+$, (ah) $[^{10}]Rb^+$, (ai) $[^{11}]Rb^+$, (aj) $[^{12}]Rb^+$, (ak) $[^{13}]Rb^+$, (al) $[^{14}]Rb^+$, (am) $[^{15}]Rb^+$, (an) $[^{17}]Rb^+$, (ao) $[^{18}]Rb^+$, (ap) $[^6]Cs^+$, (aq) $[^7]Cs^+$, (ar) $[^8]Cs^+$, (as) $[^9]Cs^+$, (at) $[^{10}]Cs^+$, (au) $[^{11}]Cs^+$, (av) $[^{12}]Cs^+$, (aw) $[^{13}]Cs^+$, (ax) $[^{14}]Cs^+$, (ay) $[^{15}]Cs^+$, (az) $[^{16}]Cs^+$, (ba) $[^{17}]Cs^+$, (bb) $[^{18}]Cs^+$, (bc) $[^{20}]Cs^+$.







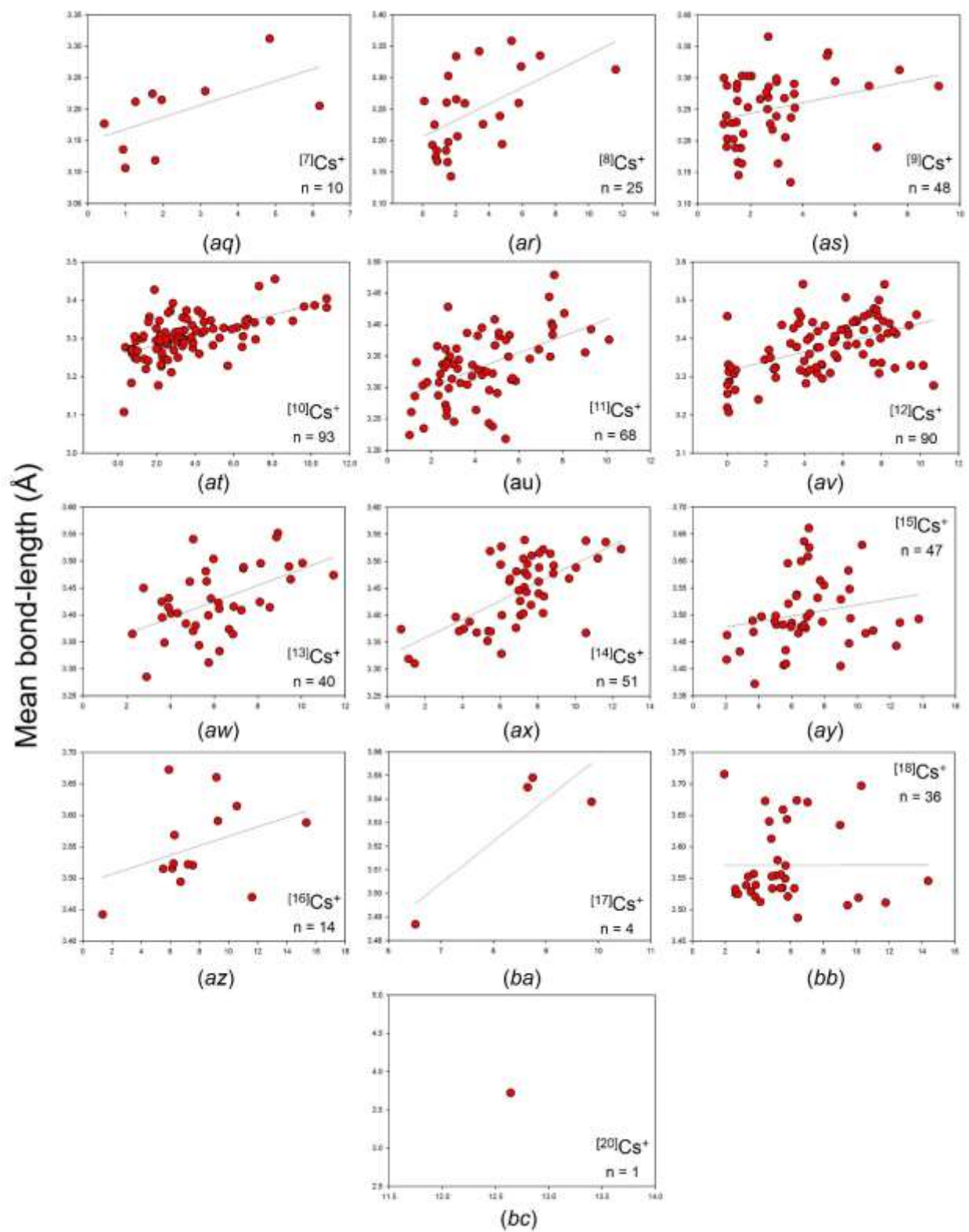
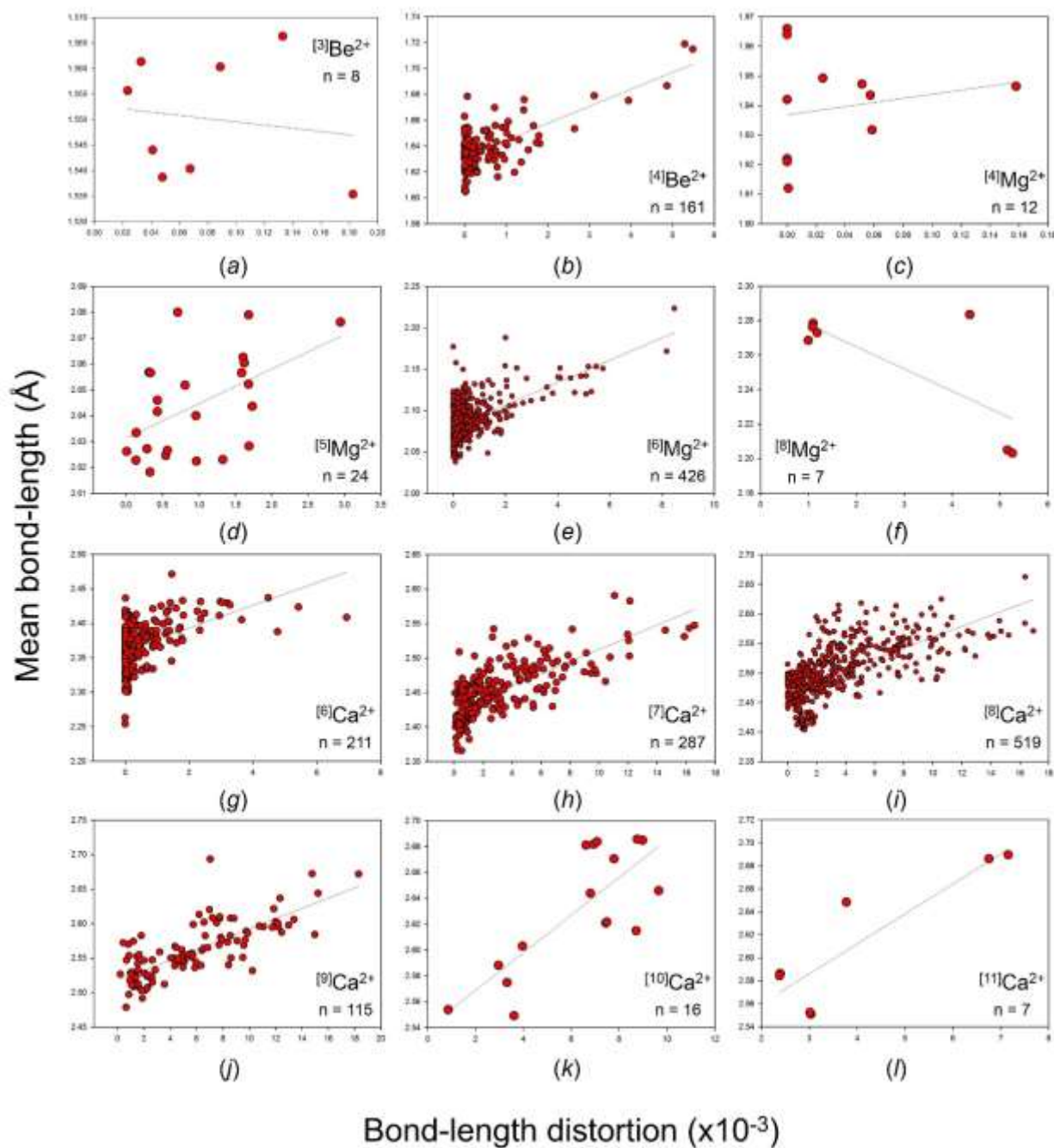
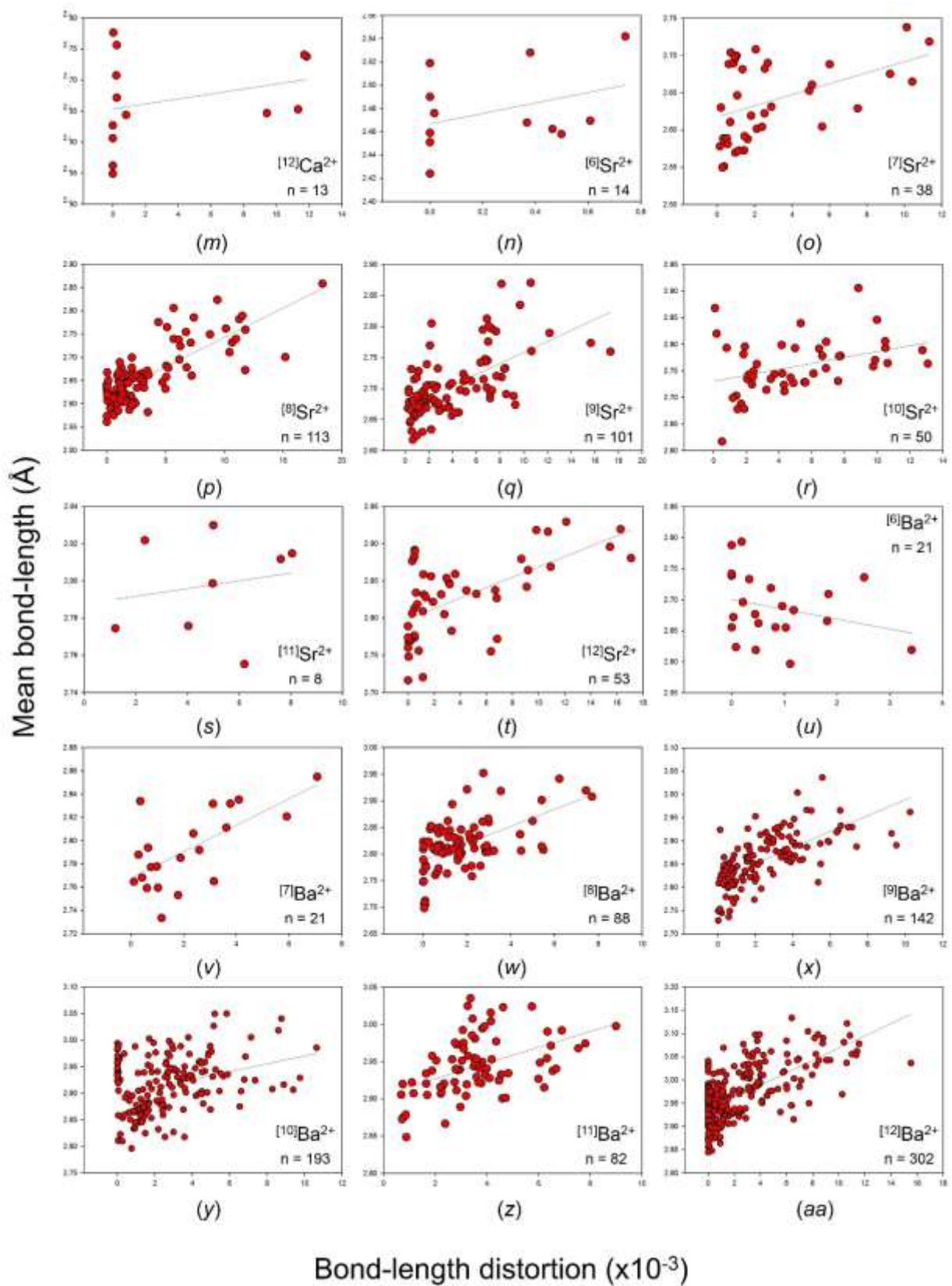
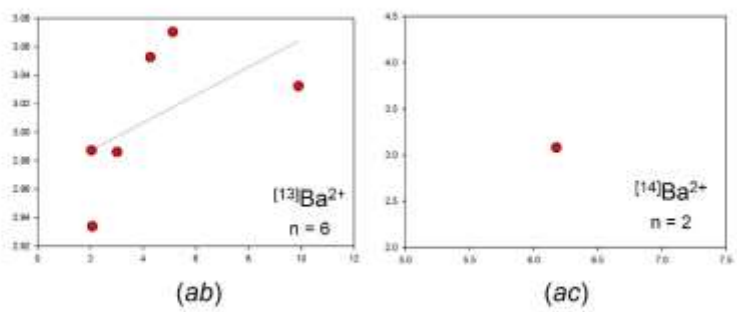


Figure 4.S6 The effect of bond-length distortion on mean bond-length for all configurations of the alkaline-earth-metal ions bonded to O^{2-} : (a) $[3]Be^{2+}$, (b) $[4]Be^{2+}$, (c) $[4]Mg^{2+}$, (d) $[5]Mg^{2+}$, (e) $[6]Mg^{2+}$, (f) $[8]Mg^{2+}$, (g) $[6]Ca^{2+}$, (h) $[7]Ca^{2+}$, (i) $[8]Ca^{2+}$, (j) $[9]Ca^{2+}$, (k) $[10]Ca^{2+}$, (l) $[11]Ca^{2+}$, (m) $[12]Ca^{2+}$, (n) $[6]Sr^{2+}$, (o) $[7]Sr^{2+}$, (p) $[8]Sr^{2+}$, (q) $[9]Sr^{2+}$, (r) $[10]Sr^{2+}$, (s) $[11]Sr^{2+}$, (t) $[12]Sr^{2+}$, (u) $[6]Ba^{2+}$, (v) $[7]Ba^{2+}$, (w) $[8]Ba^{2+}$, (x) $[9]Ba^{2+}$, (y) $[10]Ba^{2+}$, (z) $[11]Ba^{2+}$, (aa) $[12]Ba^{2+}$, (ab) $[13]Ba^{2+}$, (ac) $[14]Ba^{2+}$.





Mean bond-length (Å)



Bond-length distortion ($\times 10^{-3}$)

Chapter 5

Conclusion

5.1 Summary and significance of thesis

Since the determination of the first crystal structures in 1913 and the ensuing development of the fields of Crystallography and Crystal Chemistry, a large amount of information concerning crystal structures and their atomic arrangements has been collected. However, we still only have a limited understanding of the factors that control crystal-structure arrangements and the variation in bond lengths in crystals. Some work has been done on characterizing the variation in bond lengths and mean bond-lengths in crystals, but this has involved only a small number of highly charged ions with low coordination-numbers using only small sets of data. I have begun a much larger-scale investigation of these issues involving bonds to oxygen in inorganic crystal-structures.

[1] I have done a bond-length dispersion analysis of the Inorganic Crystal Structure Database (by far the largest of its kind) involving 180,331 bond lengths from 31,514 coordination polyhedra for 135 ions bonded to oxygen in 462 ion configurations, using 9367 refined crystal-structures. For all ion configurations for which sufficient data exist, I have determined the frequency distributions, their shapes (skewness, kurtosis, range and any multimodal behaviour), and the minimum and maximum bond-lengths. This work has provided the data used in the rest of my thesis. I also intend to make this database generally available to the scientific community, as the work that can be done on understanding the detailed variation of bond lengths and mean bond-lengths in crystals for the listed 462 ion configurations would necessarily involve many scientists for many years. This distillation of crystallographic knowledge will allow experimentalists to cross-reference their results against a database of existing structures, and for computational results to be verified against experimental results (Richardson, 2013).

The consequences of this work extend beyond crystallography, and will provide reference material for understanding the structural arrangements around cations and anions in situations where it is not possible to determine and refine crystal structures by x-ray diffraction (e.g., adsorption sites, local structures in glasses and melts or aqueous fluids).

[2] I have used the results of the bond-length dispersion analysis to assess the published parameterizations of the bond-length—bond-valence relation for cations bonded to oxygen. This evaluation was necessary for a number of reasons:

(1) there is no consistency between bond-valence parameters published from different sources; in particular, the criteria used to select the bond lengths used in the derivation of the bond-valence curves vary widely;

(2) different fitting methods have been used by different authors to derive the bond-valence parameters, and there is no consensus on the best way to derive the bond-valence parameters;

(3) many ion pairs have several different sets of bond-valence parameters available in the literature; at the beginning of my work, there were 1749 sets of parameters for 1350 pairs of ions in the literature (185 ion pairs when bonded to oxygen), and there had been little or no comparative work to guide the general user;

(4) while there has been some criticism of the algebraic form of the bond-valence equation for specific ion-pairs, few alternative forms of the bond-valence—bond-length equation have actually been tested.

I evaluated published bond-valence parameters with regard to their agreement with the valence-sum rule, and identified the “best set” of these parameters that gave the closest agreement with the valence-sum rule for each ion pair for which reliable data was obtained from the bond-length dispersion analysis (*i.e.*, for 135 cations bonded to oxygen). This gave me a baseline set of data to which I could test new bond-valence parameters and equations for the ion pairs.

I then examined a wide variety of algebraic expressions in order to test for the optimal form of the bond-valence equation. I found the following: several equations give very similar agreement with the valence-sum rule, including the widely used equation of Brown & Altermatt (1985); none was conspicuously better than that currently in use, and hence I retained the equation of Brown & Altermatt (1985) for my further work.

Next, I compared the various ways in which bond-valence parameters have been derived. For reasons discussed in Chapter 2, none of these methods was adequate, and I introduced a new method, the GRG (Generalized Reduced Gradient) method, that proved much more robust than previous methods in deriving bond-valence parameters. Using this method, I derived a new set of bond-valence parameters using the data derived from my dispersion analysis for 135 cations bonded to oxygen. I tested these parameters against the set of best published parameters for cations and showed that my new parameters are in better accord with the valence-sum rule. I have also shown that the parameters I derived give better fit to the data for both cations and anions when compared to the parameterizations of Brown & Altermatt (1985) and Brese & O’Keeffe (1991), the two most commonly used sets of bond-valence parameters which account for ~7300 and ~5100 citations today, respectively.

Finally, I showed that there is a consistency in the bond-valence parameters that was lacking from published values, in that they correlate with parameters such as ionization potential, oxidation state and electronegativity.

This in-depth look at the parameterization of the bond-length—bond-valence relation will serve as an unprecedented reference to those who wish to improve this parameterization further, extend it to ion pairs not treated here, or to investigate the physical meaning of the relation.

[3] The new parameterization derived in Chapter 2 was used in Chapter 3 to gain insight into the milarite structure. As I show in this chapter, the bond-valence model may be used beyond structure verification to gain crystal-chemical insight into crystal structures, and as so, an optimal parameterization of the model is critical so that deviations from the valence-sum rule are reflective of the phenomenon investigated rather than being the result of inaccuracies in the bond-valence—bond-length parameterization.

The milarite structure was selected here for the wide compositional variation of its constituent minerals and synthetic phases, which is interesting from the point of view of the factors constraining the possible chemical compositions of crystal structures. First, I did a literature review of all published structural and chemical data on milarite-group minerals and synthetic phases, and examined all compositions for the group in order to clarify end-member compositions. I found that, in addition to the twenty-three approved mineral species for the group, six examples definitely deserve the status of new minerals, and that two additional compositions may also deserve this status pending experimental determination of their patterns of cation order *via* crystal-structure refinement. Moreover, I found that twenty synthetic compounds with the milarite-type

structure have distinct end-member compositions, suggesting that there may be many more undiscovered minerals of the milarite group in nature.

Next, I used the mathematical method of Rutherford (1990) to calculate the *a priori* bond-valences of several minerals with the milarite structure; this has been done only a few times since the initial proposal of Brown (1977) (e.g., Urusov & Orlov 1999, Hawthorne & Sokolova 2008). Here, I show how to determine the *a priori* bond-valence of any crystal structure (no matter how complicated) and the kind of information that can be derived from it. I show how the bond topology of a crystal structure influences its *a priori* bond-valences which in turn affects site occupancy. Comparison of *a priori* and experimental bond-valences for refined crystal structures observed in this group has shown that the agreement between the two is close at all sites except for the *B* site. Parallel to this, I used the *a priori* bond-valences of compositions for which a structure refinement had been done, and evaluated induced strain as a function of chemical composition for the structure. I found that the *B* site has the highest amount of strain in the structure, and in accord with this finding, milarite compositions with a vacant *B* site tend to be more common. The method used is easily transferable to any crystal structure; the calculation of the *a priori* bond-valences of a crystal structure can therefore be used to easily localize strain in a crystal structure, which has otherwise been a difficult phenomenon to study before, and therefore shows great promise in the study of crystal-structure stability. This is in addition to the initial proposal of Brown (1977) of using *a priori* bond-valences to predict the ideal bond-lengths of a crystal structure for a given site occupancy using the appropriate bond-valence curves, which

is a method I have also made more accurate *via* the updated parameterization of the bond-length—bond-valence relation derived in Chapter 2.

[4] Following the bond-length dispersion analysis of the Inorganic Crystal Structure Database (see [1]), I examined the bond-length distributions for 55 configurations of alkali-metal ions and 29 configurations of alkaline-earth-metal ions, for 4859 coordination polyhedra and 38,594 bond distances (alkali metals) and for 3038 coordination polyhedra and 24,487 bond distances (alkaline-earth metals).

I found that bond-lengths generally show a positively-skewed Gaussian distribution that originates from the variation in Born repulsion and Coulomb attraction as a function of interatomic distance, and that the skewness and kurtosis of these distributions generally decrease with increasing coordination number of the central cation, a result I attribute to decreasing Born repulsion with increasing coordination number. I investigated the effect of sample size on the shape of the bond-length and mean bond-length distributions, and note that the occurrence of multi-modal distributions for these ions is often due to sampling issues that lead to an over-representation of specific bond-lengths (*e.g.*, for $^{[8]}\text{Ca}^{2+}$, due to many refinements of garnet and vesuvianite structures).

I found that unusually small or large coordination numbers are commonly associated with anomalous values of atomic displacement of the constituent cations and/or anions.

I examined the validity of less-common configurations of the alkali-metal and alkaline-earth metal ions, such as $^{[3]}\text{Li}^+$, $^{[3]}\text{Na}^+$, $^{[4]}\text{K}^+$, $^{[4]}\text{Rb}^+$, $^{[6]}\text{Cs}^+$, $^{[3]}\text{Be}^{2+}$, $^{[4]}\text{Mg}^{2+}$, $^{[6]}\text{Ca}^{2+}$, $^{[6]}\text{Sr}^{2+}$ and $^{[6]}\text{Ba}^{2+}$, and note that some of these configurations are the result of extensive

dynamic and/or positional short-range disorder and are not ordered arrangements, while others are well-ordered atomic arrangements.

I found a positive correlation between incident bond-valence sum at the central cation and coordination number for the alkali and alkaline-earth metals, with values for these families respectively varying from 0.84 v.u. ($^{[5]}\text{K}^+$) to 1.06 v.u. ($^{[8]}\text{Li}^+$), and from 1.76 v.u. ($^{[7]}\text{Ba}^{2+}$) to 2.10 v.u. ($^{[12]}\text{Sr}^{2+}$).

I examined possible factors that affect variations in bond-length and mean bond-length. Mean bond-lengths show a weak correlation with bond-length distortion from the mean value, but clearly also correlate with other parameters. In particular, some coordination numbers show the widest variation in mean bond-length for zero distortion, and thus the variation in mean bond-length must be caused by factors other than distortion. I found a positive correlation between mean bond-length and atomic displacement for $^{[6]}\text{Na}^+$ bonded to O^{2-} , suggesting that the central cation responds to an overly large coordination environment by increasing its dynamic (or static) displacement, while anions respond to an overly small cation-coordination environment by increasing their own displacement.

Finally, I found that ions may occur in coordination numbers greater than [12]. New bond-valence parameters for the 4 ions observed in coordinations higher than [12], K^+ , Rb^+ , Cs^+ and Ba^{2+} were calculated for a maximum coordination number of [12] and compared to the ones derived without a cut-off. Both sets of parameters give exactly the same result for anion bond-valence sums. However, the bond-valence parameters calculated for a maximum coordination number of [12] show much poorer correlation with mean observed bond-length and no correlation at all with ionization energy of the

central cation. The inclusion of these longer bond distances in routine analysis may therefore increase the fit to the valence-sum rule and to various properties that correlate with bond length.

5.2 Future research opportunities

5.2.1 Bond-length dispersion analysis for all ion pairs

Analysis of the data gathered from the bond-length dispersion analysis of the Inorganic Crystal Structure Database (180,331 individual bond-lengths taken from 31,514 coordination polyhedra in 9367 crystal structures for 135 cations and a total of 462 configurations) goes beyond the scope of this Ph.D. thesis, and examination of this data will take many more years of work.

In Chapters 2 and 3, I showed that these data can be used indirectly to gain insight into the stability of crystal structures by deriving an improved parameterization of the bond-valence model (Chapter 2) and by applying it to the milarite structure (Chapter 3).

Analysis of the raw data begins in Chapter 4, where I did a preliminary examination of this data for the alkali- and alkaline-earth-metal ions. Work done for this thesis has shown that there is a tremendous amount of information available with regard to the positions of atoms in crystal structures, and that we have much to gain from the distillation of this information with regard to the evaluation and improvement of our current understanding of atomic-scale phenomena (e.g., the reasons underlying the arrangements of atoms in crystals). Addressing these questions will require a much closer look at the associated atomic arrangements.

I am currently extending my work on the alkali and alkaline-earth metal families to other families of the periodic table of elements for which I have gathered data for ions bonded to oxygen. These include the metalloids, non-metals, halogens, transition metals, poor metals, lanthanides, actinides, and the hydrogen atom. Their bond-length distributions, bond-length and bond-valence ranges and statistics will be given and analyzed in a similar fashion as was done for the alkali and alkaline-earth metals, and crystal-chemical phenomena of interest that go beyond preliminary examination will be identified as suitable for further work. The bond-length dispersion analysis may also be expanded to include cations bonded to anions other than oxygen.

5.2.2. Reassessment of ionic radii

Landé (1920) published a seminal paper on the estimation of ionic radii in crystals, which Shannon later updated (1969, 1976) to list ionic radii as a function of oxidation state, coordination number, electronic coordination and spin state. In his work, which has been cited ~35,000 times today, Shannon used approximately 900 mean polyhedron bond-distances to determine 497 ionic radii. My work totals 31,521 reliable mean polyhedron bond-distances for a total of 462 ion configurations. Of these 462 ion configurations, 313 may be used to revise radius values given by Shannon (157 of which were only estimated by Shannon), while radii for the other 149 configurations will result in new values of ionic radii that are not listed in Shannon (1976).

5.2.3 Enumeration of all possible end-member compositions of a crystal structure and materials discovery

The results of the bond-length dispersion analysis I have done allow the assignment of a range of bond lengths that the 462 observed configurations of ions can adopt when bonded to oxygen. Using the new parameterization of the relation between bond length and bond valence I derived in Chapter 2, the observed bond-length ranges may be converted to the range of bond valences that these ion configurations can adopt. This allows new *a priori* analysis in crystal structures. I showed in Chapter 3 how the *a priori* bond-valences can be calculated (no matter how complex the structure); the *a priori* bond-valences can then be coupled to the range of bond-valences that ions configuration can adopt as a mean to study and predict site populations in crystal structures. In other words, an ion may occupy the site of a crystal structure if it encompasses all *a priori* bond-valences calculated for that site within its observed range of bond valences derived from the bond-length dispersion analysis. From this, all possible site occupants of a crystal structure may be derived, and all possible end-members of a given crystal structure can be enumerated *via* combinatorial analysis.

Thus, this proposed method sets a limit as to what atoms can occupy the sites of a crystal structure; whether or not an assignment may yield a stable structure is subject to further inspection, as other factors come into play. An important factor consists of whether or not the bond-valence arrangement, once the ions are assigned to the sites of a structure, can lead to reasonable bond lengths (the *a priori* bond-lengths). *A priori* bond-lengths are obtained by converting the *a priori* bond-valences into bond lengths

using the appropriate bond-valence parameters, which were derived in Chapter 2. I am planning to test this method with the milarite structure.

Further development of this approach may be useful in the field of materials discovery by enabling targeted synthesis of new compositions for a given bond topology, whereby the feasibility of proposed combinations of topology and ions with properties of interest may be evaluated before expending effort on synthesis.

From here, the prediction of the connectivity of crystal structures would be the next logical step in realizing crystal-structure prediction from first principles; unfortunately, this remains a largely unresolved issue (*e.g.*, Oganov *et al.* 2010).

5.2.4 Toward a better understanding of crystal-structure stability

The work done in this thesis shows ways in which the study of crystal-structure stability may be approached using transparent arguments based on crystal-chemical grounds. Whereas an important objective of any scientific process is the making of predictions, it is unclear that making accurate predictions using “black-box” methods will enhance our understanding of processes that go on at the atomic scale. Our inability to (for example) predict the structure of crystals from first principles, despite harnessing the tremendous computing power available today, shows that we fall short of a clear understanding of the factors that control crystal-structure stability. Better understanding will emerge from a distillation of crystal-chemical knowledge that allows the isolation and investigation of these factors.

5.3 References

- Brese, N.E. & O'Keeffe, M. (1991). Bond-valence parameters for solids. *Acta Cryst. B* **47**, 192-197.
- Brown, I.D. (1977). Predicting bond lengths in inorganic crystals. *Acta Cryst. B* **33**, 1305-1310.
- Brown, I.D. & Altermatt, D. (1985). Bond-valence parameters obtained from a systematic analysis of the Inorganic Crystal-Structure Database. *Acta Cryst. B* **41**, 244-247.
- Landé A. (1920). Über die Größe der Atome. *Zeitschrift für Physik* **1**, **3**, 191–197.
- Hawthorne, F.C. & Sokolova, E. (2008). The crystal chemistry of the scapolite-group minerals: II. The origin of the $I4/m \rightarrow P4_2/n$ phase transition and the non-linear variations in chemical composition. *Can. Min.* **46**, 1555-1575.
- Oganov, A.R., Yanming, M., Lyakhov, A.O., Valle, M., Gatti, C. (2010). Evolutionary crystal structure prediction as a method for the discovery of minerals and materials. *Rev. Mineral. Geochem.* **71**, 271-298.
- Richardson, I.G. (2013). The importance of proper crystal-chemical and geometrical reasoning demonstrated using layered single and double hydroxides, *Acta Cryst.*, **B69**, 150-162.
- Rutherford, J.S. (1990). Theoretical prediction of bond-valence networks. *Acta Cryst. B* **46**, 289-292.

Shannon, R.D. (1976). Revised effective ionic radii and systematic studies of interatomic distances in halides and chalcogenides. *Acta Cryst. A* **32**, 751–767.

Shannon, R.D. & Prewitt C.T. (1969). Effective ionic radii in oxides and fluorides. *Acta Cryst. B* **25**, 925-946.

Urusov V.S. & Orlov I.P. (1999). State-of-art and perspectives of the bond-valence model in inorganic crystal chemistry, *Crystallogr. rep.* **44**(4), 686-709.